SAPIENZA
UNIVERSITÀ DI ROMA

Dipartimento di Fisica
Scuola di Dottorato "Vito Volterra"
Sapienza – Università di Roma

Spinning compact objects in extreme-mass-ratio inspirals

Gabriel Andres Piovano

Thesis submitted for the degree of
Doctor of Philosophy in Physics (XXXIV cycle)

Advisors:
Prof. Paolo Pani
Prof. Andrea Maselli

Academic Year 2021/2022

Abstract

Since the first landmark observation of gravitational waves (GWs) in 2015, GW astronomy has tremendously impacted fundamental physics and astrophysics. A network of four ground-based detectors (the two LIGOs, Virgo and KAGRA) is now in operation, routinely detecting new events. Future space-based observatories, like the Laser Interferometer Space Antenna (LISA), hold the promise to revolutionize GW astronomy by detecting sources non-observable by current detectors, opening avenues for groundbreaking discoveries.
Among the prime targets of LISA are extreme mass ratio inspirals (EMRIs), which are binaries consisting of a stellar-mass compact object slowly inspiraling into a supermassive black hole. These systems are unique probes of astrophysics and fundamental physics. Motivated by their potential, here we study in detail the EMRI dynamics in the presence of a spinning small compact object.

The tiny mass-ratio in EMRI binaries allows us to treat the smaller companion as a point particle endowed with mass and spin. The latter are free parameters independent of the internal structure of the infalling compact object. The radiation-reaction forces (known as self-force) and equations of motion are typically modeled with perturbative approaches in the mass ratio. At leading order, the dynamics of the particle is governed by the adiabatic emission of energy and angular momentum in gravitational radiation, causing the secular decay of the orbits. All subleading corrections to this general picture are called post-adiabatic terms. The spin of the small compact object starts affecting the GW phase at the first post-adiabatic order (as does the first-order conservative and second-order dissipative self-force).

In this thesis, we focus on the measurability of the smaller companion spin by an EMRI detection with LISA. Using the Teukolsky formalism, we derive the GW fluxes and the adiabatic orbital evolution for a spinning particle in the case of circular, equatorial orbits with (anti-)aligned spins. We provide the spin-induced corrections to GW fluxes (numerically and semi-analytically), along with the corresponding post-adiabatic effects on the GW phase, which are novel results for a Kerr background.
Based on the phase difference between the gravitational signal from a spinning and a non-spinning particle, we develop a criterion to determine the minimum value of the spin resolvable by LISA. Our analysis points out that precise, model-independent tests on the nature of the small compact object could be achieved by measuring its intrinsic angular momentum. We also suggest that LISA could test the so-called Kerr bound that limits the maximum spin of a rotating black hole, allowing for theory-agnostic constraints.

We then perform an accurate Fisher-matrix study of the EMRI parameters using Teukolsky waveforms to leading order in an adiabatic expansion on a Kerr background. Our parameter estimation takes into account the motion of the LISA constellation, higher harmonics, and includes the leading correction from the smaller companion spin in the post-adiabatic approximation. We particularly focus on the measurability of the small body spin, showing that, for spin-aligned EMRIs on quasi-circular orbits, it cannot be measured with sufficient accuracy. However, due to correlations, its inclusion in the waveform model can deteriorate the accuracy on the measurements of other parameters by orders of magnitude, unless a physically-motivated prior on the small compact object spin is imposed.

Contents

Chapter 1

Introduction

1.1 Gravitational wave astronomy

The second "golden age" of general relativity (GR) and gravitational physics has begun, heralded by the detection of gravitational waves (GW) in 2015 by the LIGO observatories [2]. It was undoubtedly a landmark achievement in Science, which has opened up new ways to uncover the mysteries of Nature. Indeed, electromagnetic (EM) waves easily interact with the surrounding matter, resulting in scattering or absorption. By contrast, gravitational radiation reach the detector practically unhampered, carrying pristine information of the sources, which is complementary to that provided by other means. Now we can directly investigate gravity itself and its interaction with matter in conditions of high curvature and relativistic speed, the so-called *strong-gravity regime*.
All the GW events observed so far by the LIGO/Virgo/Kagra (LVK) Collaboration [3–5] originated from the coalescence of stellar-mass compact objects (SCO) in binaries composed of neutron stars (NS) and black holes (BH). Current ground-based observatories are sensitive to GWs in the frequency band $\sim 10\,\mathrm{Hz}$ to $\sim 10^3\,\mathrm{Hz}$, which is dominated by BH binaries with a total mass between $\mathcal{O}(1M_\odot)$ and $\mathcal{O}(100M_\odot)$. Current detectors have shown that SCO binaries can coalesce within the Hubble time by losing energy and angular momentum carried away by GWs. The gravitationally-driven evolution of the binary can be divided into three stages. In the inspiral phase, the two objects are relatively far from each other and slow. As the orbits of the binary shrink, the bodies approaches relativistic speeds, ultimately merging in a highly dynamical and non-linear regime. Subsequently, the remnant of the coalescence, typically described as a perturbed Kerr metric, undergoes a relaxation phase known as ringdown, where it relaxes to a stationary configuration by emitting gravitational radiation.

The gravitational signal emitted during the entire inspiral-merger-ringdown process carries the details of extreme compact objects, providing invaluable data for astrophysics and fundamental physics alike.

From an astrophysical perspective, GW astronomy provides a unique way to observe BH binaries, which are invisible to electromagnetic observations. The signals emitted by these systems allow us to measure the source masses, spins, distance and sky localization, and to constrain the overall parameter distribution of stellar-mass BHs [6]. These observations have major implications for our knowledge of the formation history of binaries, and put constraints on the merger rate of BH binaries in the universe.
Furthermore, we can obtain crucial insights on the NS inner cores, whose physics is still poorly understood. From the observation of gravitational signals emitted by NS-NS and BH-NS binaries, we can infer masses and tidal deformabilities of NS, and constrain their equation of state, which determines their internal composition. The detection of the first NS-NS binary merger, tagged GW170817, already ruled out some of the proposed equations of state [7,8]. When an electromagnetic counterpart to a GW signal can be detected, it is possible to obtain a wealth of information from the combined observations, as shown by GW170817. By observing the electromagentic emission after the merger, we inferred new information on the production mechanism of heavy elements [9], and on the connection between short gamma ray burst and binary NS coalescences [10]. Moreover, coincident observations, as GW170817, provide an independent measurement of the Hubble constant [11]. Additionally, GW170817 also constrained the fractional difference between the speed of light and that of gravity to $\sim 10^{-15}$, excluding some alternative theories of GR [7].

Our current understanding of the gravitational interaction is based on GR, which is capable of explaining all current astronomical and cosmological observations [12,13]. Despite its success, GR is widely considered, at best, incomplete, because of its several theoretical issues. An unavoidable feature is the presence of singularities in physical spacetimes [14–17] such as the BH solutions (Schwarzschild and Kerr) and the Friedman-Lemaître-Robertson-Walker (FLRW) metric. These solutions present pathological regions where the density and curvature of spacetime become infinitely large. Two other fundamental issues of GR include the loss of information in a BH, (which is in contrast with unitary in quantum mechanics), and the presence of a cosmological constant, whose value is in sharp contradiction with the vacuum energy predicted in quantum field theory. Hence, there are very strong motivations to search for discrepancies in observations respect to GR predictions, in the hope to find clues on a, so far

elusive, viable theory of quantum gravity.
There is no shortage of proposed modifications of GR or alternative theories, and we refer the reader to Ref. [18] for a through review. Alternatives to GR typically include additional fields (scalar, vector or tensor fields) or modification to the metric, but all of them must circumvent the Lovelock theorem [19]. Each alternative theory has a different motivation or depart from GR in several possible ways, and most of them are already constrained by tests in the weak field [13,20]. Some of the observational predictions of modified theories of gravity include more than two polarizations in GWs, different dispersion relation than predicted by GR or dipolar radiation, just to mention a few [21].
Possible deviations from GR might also be detectable from tests of the Kerr-paradigm. A striking prediction of GR is the no-hair theorem: all isolated, stationary and asymptotically flat BHs belong to the Kerr family of solutions [22, 23], fully described by just two parameters, mass and angular momentum [24,25]. Some modified theories of gravity predict the existence of "hairy-BHs", i.e. BH metrics that are characterized by other parameters (for instance, a scalar charge). Test of the Kerr paradigm can be performed in the ringdown stage of the signal, described as a superposition of exponentially damped sinusoids or "quasinormal modes" (QNMs) with characteristic frequencies and damping times. Comparing the QNM spectrum predicted by GR with the observed opens to the so called "BH spectroscopy" [26]. Hence, with an accurate spectroscopic analysis of the ringdown we can test the nature of the remnant, verifying if it is compatible with a Kerr BH [27].

To date, all GW observations are entirely consistent with GR to within measurement limits [28]. But the next generation of interferometers planned for the next decade hold the promise to revolutionize GW astronomy. Future third-generation ground-based detectors [29] such as the Einstein Telescope [30] and Cosmic Explorer [31] will provide an order of magnitude upgrade in the sensitivity of second-generation detectors, also widening their frequency range, and allowing to probe the evolution of compact object further in redshift. However, all ground-based detectors can not reach GW frequencies below ~ 10 Hz because of Earth's seismic noise. This intrinsic limit will be overcome by space-borne detectors, which can easily reach lower frequencies band.

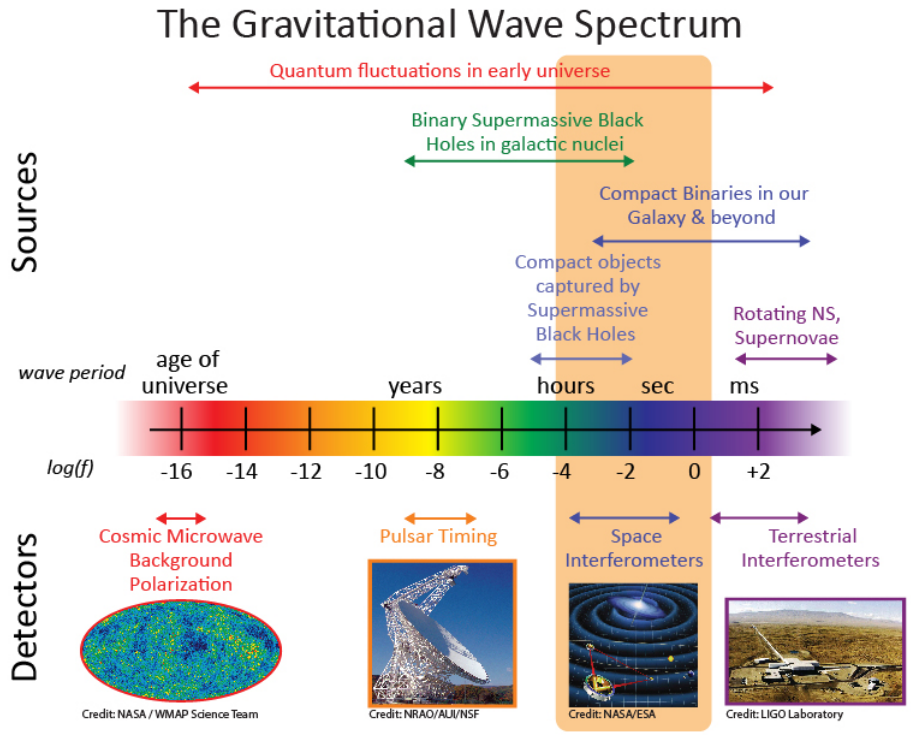

Figure 1.1: Credit: NASA Goddard Space Flight Center

1.1.1 Low-frequency GW astronomy

The Laser Interferometer Space Antenna (LISA) mission [32] is part of the new generation of space observatories, expected to start operating in 2037. With maximum sensitivity in the mHz band (see Fig. 1.1), LISA will detect stellar-mass BH binaries months before entering the ground-based detectors band. Remarkably, LISA will also observe new type of sources, such as the Galactic population of white dwarfs in wide orbits and the coalescence of supermassive BH (SMBH) binaries in the range $10^4 - 10^7 M_\odot$. The latter are expected to be the loudest source of GWs in the mHz band, detectable at redshift $z \lesssim 20$. Observations indicates that many galaxies host in their centers a SMBH, hence the mergers of two galaxies (which is a common event in their evolution) may form SMBH binaries.

Another prime target for LISA is the capture of a SCO with mass $\mu \sim 1 - 100 M_\odot$ (henceforth *secondary*) from a SMBH (henceforth *primary*) with mass $M \sim 10^5 - 10^7 M_\odot$ forming an extreme-mass-ratio system [33]. In fact, SMBHs are surrounded by a dense distribution of stars and SCOs, and the "capture" a SCO could result from several dynamical processes. Detection rates are uncertain due

to the poorly known physics, ranging from just a few events to several thousand over the mission duration out to redshift $z \lesssim 2$. On the bright side, the frequency range of EMRI signals falls around 3 $\sim$ mHz, the most sensitive part of the LISA band.
Modelling the EMRI dynamics is the main topic of this manuscript, and from now we will focus on these sources.

1.1.2 Extreme-mass-ratio inspirals

Due to the small mass ratio $q \ll 1$, the signal emitted by these systems can last months in the LISA band[1], performing up to $O(1/q)$ orbital cycles before the SCO plunges. Combined with the richness of their gravitational waveform, EMRI signals will allow us to measure the physical parameters and to pinpoint the sky position of these sources with extreme precision [33, 34], illuminating how SMBHs and their surrounding galaxies evolved. Furthermore, these precise measurements will allow us to perform stringent tests of gravity [35–40] and of the nature of compact objects [41–46].
However, this huge potential comes with its own burden: data analysis and parameter estimation of EMRIs are challenging and, in many respects, still an open issue [33, 47]. Theoretical waveforms suited for parameter estimation must have an accuracy of 1 rad or better out of $1/q \sim 10^5$, with a computational speed of 1 ms [48, 49]. Indeed, a typical Bayesian Markov Chain Monte Carlo requires more than $10^6 - 10^9$ waveform evaluations to obtain a convergent posterior distribution. Furthermore, it is expected that many events will be detected by LISA at the same time, and a typical EMRI signal will be buried in noise, with a signal-to-noise ratio that builds up only over many months in band. Parameter estimation for LISA will require ad-hoc statistical tools, especially for the case of EMRIs.

The large disparity in scales allows us to consider EMRIs as a point particle (the secondary) orbiting the Kerr background originated by the SMBH. Important corrections to the orbital motion arise from the self-interaction of the secondary with its own gravitational field, known as self-force (SF), which induce perturbations to the primary spacetime [50, 51]. EMRI detection and parameter estimation with LISA requires accurate waveform models that include the relevant SF terms, but not all of the necessary SF contributions have been calculated yet. Numerical computations of the SF are computationally expensive, especially in cases where high accuracy is sought, while analytic calculation are rather complicated.

[1] By comparison, the longest signal from compact binaries observable by the LVK network last few minutes.

One of the crucial missing pieces is a complete model of the spin of the secondary [51–57], which motivates the work behind this thesis. In this manuscript we provide a detailed study of the EMRI dynamics in the presence of a spinning secondary.

In the remainder of this chapter, we will provide a introduction about the theoretical framework typically employed to study the extreme-mass-ratio binaries. As a first step, we present the main approximation schemes used to model compact binaries under gravitational emission. Next, we briefly cover the main features of geodesic motion in Kerr spacetime, which represent the zeroth order approximation of the secondary's motion. The *post-adiabatic* (PA) expansion is then introduced. Together with the two-time scale expansion [58] and perturbation theory, the PA expansion is the typical framework employed to model the evolution of EMRIs and the ensuing gravitational signal. After briefly discussing past work on spinning secondaries, we outline the content of this thesis.

1.2 Modeling extreme-mass-ratio inspirals

1.2.1 Approximated methods for compact binaries

A closed form solution of the two-body problem is well known in Newtonian mechanics for two non-spinning bodies approximated as point-particles. The same problem in GR is way more complicated: the Einstein field equations (EFE)

$$G_{\mu\nu}[g_{\mu\nu}] \coloneqq R_{\mu\nu}[g_{\mu\nu}] - \frac{1}{2} g_{\mu\nu} R[g_{\mu\nu}] = 8\pi T_{\mu\nu} \,, \tag{1.2.1}$$

form a set of 10 coupled, highly non-linear, hyperbolic-elliptic partial differential equations (PDE), which are extremely difficult to solve. Few exact solutions are known, and most of them assume a certain degree of symmetry to simplify the equations. Over the decades, different approximation methods have been employed to model the dynamics of astrophysical binaries in different regimes:

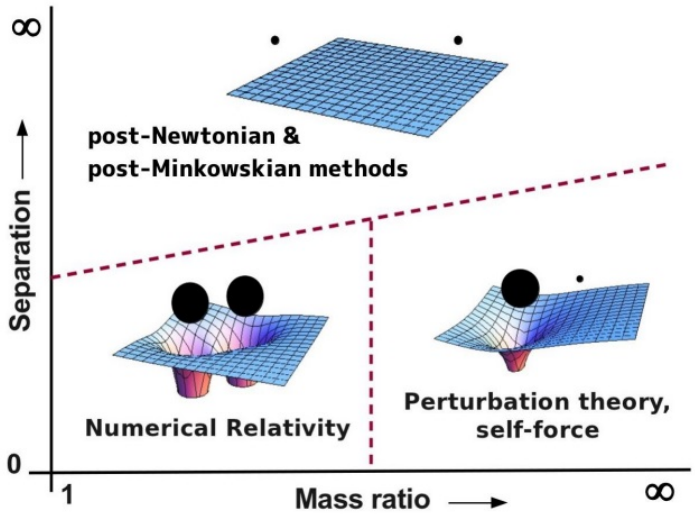

Figure 1.2: Credit: Leor Barack "Lectures on black-hole perturbation theory", Kavli-RISE Summer School on Gravitational Waves, 2019. Note: "Mass ratio" in plot $= 1/q$ in our notation.

Numerical Relativity Tackling the EFE (1.2.1) numerically is a challenging task: the field equations have to be recast in a form more suitable for numerical computations and well-posedness must be carefully assessed. Moreover, highly efficient, specialized algorithms have to be employed to obtain accurate solutions. Nonetheless, numerical relativity (NR) simulations are the only available method to fully address the non-linearities of the field equations during the merger regime [59, 60]. Gravitational waveforms obtained with NR have proved to be invaluable for GW astronomy [61, 62]. To date, thousands of NR simulations of BH and NS binaries have been carried out, but the parameter space is sparsely covered because of the high computational burden. Binaries with mass ratio smaller than $q \sim 1/20$ or when the two objects are far apart are still too costly to simulate. In these two regimes, one can find approximate solutions of the (1.2.1) in terms of a perturbative expansion in a small parameter.

Post-Newtonian theory In the case of small velocities and weak gravitational field, a suitable approximation of the field equations is given by the post-Newtonian (PN) theory [63]. The PN approximation consists in expanding the field equations (1.2.1) in the dimensionless parameter $\epsilon \approx (v/c)^2$, where the v is the velocity scale of the system and c the speed of light in vacuum. At zeroth order, i.e ϵ^0, the binary is simply described by Newtonian mechanics, whereas higher-order terms $(v/c)^{2n}$ introduces relativistic

and curvature corrections. PN theory is particularly useful to model the early stage of the inspiral, when the two objects are relatively far-away from each other and the velocities only mildly relativistic. As the binary orbits shrink, the PN approximation become less accurate, and it eventually breaks down at the merger, where numerical relativity is required to solve the full might of the EFE. Including higher order PN terms improves the accuracy of the PN approximation against numerical simulations, which allows to apply PN series even in strong fields and relatively fast motion. Nevertheless, PN approximations are still not sufficiently accurate in the extreme-mass-ratio regime for orbits close to the last stable orbit before plunge.

Black hole perturbation theory As the name suggest, in BH perturbation theory (BHPT) one seeks for approximate solutions of the field equations by perturbing well known BH metrics [50,51,64]. This approach finds natural applications in the study of the ringdown phase, where the remnant is a slight deformed black hole [26], and for modeling EMRI binaries. In the latter case, the dynamics is solved perturbatively in the mass ratio $q = \mu/M \ll 1$ and the binary spacetime can be treated as being given by the SMBH metric plus small perturbations due to the presence of the smaller companion. The results of this thesis relied on BHPT techniques, which will be thoroughly discussed later on.

Effective one-body formalism In Newtonian gravity the two-body problem can always be reduced to a simpler one-body problem in the center of mass of the system. The Effective one-body (EOB) formalism achieves a similar result in GR by mapping the dynamics of the binary to that a point particle in an effective metric [65,66]. By combining information from the BHPT, PN and numerical relativity results, the EOB provides a complete description of the two-body dynamics as well as the inspiral-merger-ringdown GW signal. This result is achievable at the cost of introducing unknown coefficients to calibrate using other approximation methods. For instance, the EOB Hamiltonian must reduce to the PN Hamiltonian in the weak-field, slow-motion limit, whereas in the test particle limit reduces to the motion of a point-particle in a Kerr spacetime. One additionally requires a smooth transition from the inspiral to the ringdown, which is obtained through calibration to NR simulations [67,68]

The aforementioned approximation methods are not mutually exclusive, and there are regions of the parameter space where two or more methods are equally valid. BHPT computations have allowed to determine unknown coefficients in PN and EOB expansions [69–72], while PN and EOB calculations have been

employed to validate BHPT results [73,74]. Comparison between BHPT and NR have been equally fruitful, showing that the region of validity of BHPT could be remarkably extended to mass ratio as high as $q \sim 1/2$ or even higher [75–77]. Likewise, BHPT results in the conservative sector agree with NR and EOB computations better than previously expected [78].

1.2.2 Geodesic motion in Kerr spacetime

Throughout this thesis, we denote the speed of light in vacuum by c and the gravitational constant by G and adopt the geometric unit system $G = c = 1$. The background spacetime is described by the Kerr metric in Boyer-Lindquist coordinates

$$ds^2 = -dt^2 + \Sigma\left(\frac{dr^2}{\Delta} + d\theta^2\right) + (r^2 + a^2)\sin\theta^2 d\phi^2 + \frac{2Mr}{\Sigma}(a\sin\theta^2 d\theta - dt)^2 \,, \tag{1.2.2}$$

where $\Delta = r^2 - 2Mr + a^2$, $\Sigma = r^2 + a^2\cos^2\theta$, and a is the spin parameter such that $|a| \leq M$. Without loss of generality, we assume that the specific spin a of the primary is aligned to the z-axis, namely $a \geq 0$. From the symmetries of the Kerr space-time, it is possible to identify four integrals of the geodesic equations of motion: the energy, E, the axial angular momentum, L_z, Carter's constant, Q and the mass of the secondary, μ. The latter is the normalization of the the four-momentum $p_\nu p^\nu = -\mu^2$, while the first two are direct consequences of the stationarity and axial symmetry of Kerr space-time. Carter's constant is a conserved quantity associated with a tensorial Killing vector field [79]. As a direct consequence of the four constants of motion (E, L_z, Q, μ), the motion of a non-spinning particle is completely *integrable* [80]. In other words, we can reduce the geodesic equations

$$\frac{\mathrm{d}^2 z^\mu}{\mathrm{d}\tau^2} + \Gamma^\mu_{\alpha\beta}\frac{\mathrm{d}z^\alpha}{\mathrm{d}\tau}\frac{\mathrm{d}z^\beta}{\mathrm{d}\tau} = 0 \,, \tag{1.2.3}$$

from a system of four second-order differential equations to four first-order equations:

$$\Sigma^2\left(\frac{\mathrm{d}r}{\mathrm{d}\tau}\right)^2 = \left[\tilde{E}(r^2+a^2) - a\tilde{L}_z\right]^2 - \Delta\left[r^2 + \left(\tilde{L}_z - a\tilde{E}\right)^2 + \tilde{Q}\right] := R(r)\,, \quad (1.2.4)$$

$$\Sigma^2\left(\frac{\mathrm{d}\theta}{\mathrm{d}\tau}\right)^2 = \tilde{Q} - \cos^2\theta\left[\frac{\tilde{L}_z^2}{\sin^2\theta} + a^2(1-\tilde{E}^2)\right] := \Theta(\theta)\,, \quad (1.2.5)$$

$$\Sigma\frac{\mathrm{d}\phi}{\mathrm{d}\tau} = \frac{\tilde{L}_z^2}{\sin\theta^2} + a\tilde{E}\left(\frac{r^2+a^2}{\Delta} - 1\right) - \frac{a^2\tilde{L}_z}{\Delta} := \Phi(r,\theta)\,, \quad (1.2.6)$$

$$\Sigma\frac{\mathrm{d}t}{\mathrm{d}\tau} = \tilde{E}\left[\frac{(r^2+a^2)^2}{\Delta} - a^2\sin^2\theta\right] + a\tilde{L}_z\left(1 - \frac{r^2+a^2}{\Delta}\right) := T(r,\theta) \quad (1.2.7)$$

where τ is the proper time, $\tilde{E} = E/\mu$, $\tilde{J}_z = J_z/\mu$ and $\tilde{Q} = Q/\mu^2$ [2]. By using the Mino time parameter λ defined via $d\tau/d\lambda = \Sigma$ (see Refs. [79,81]), the equations in r and θ decouple. For equatorial motion, i.e. $\theta = \pi/2$, the system reduces to

$$r^4\left(\frac{\mathrm{d}r}{\mathrm{d}\tau}\right)^2 = \left[\tilde{E}(r^2+a^2) - a\tilde{L}_z\right]^2 - \Delta\left[r^2 + \left(\tilde{L}_z - a\tilde{E}\right)^2\right]\,, \quad (1.2.8)$$

$$r^2\frac{\mathrm{d}\phi}{\mathrm{d}\tau} = \tilde{L}_z^2 + a\tilde{E}\left(\frac{r^2+a^2}{\Delta} - 1\right) - \frac{a^2\tilde{L}_z}{\Delta}\,, \quad (1.2.9)$$

$$r^2\frac{\mathrm{d}t}{\mathrm{d}\tau} = \tilde{E}\left[\frac{(r^2+a^2)^2}{\Delta} - a^2\right] + a\tilde{L}_z\left(1 - \frac{r^2+a^2}{\Delta}\right)\,, \quad (1.2.10)$$

with $\tilde{Q} \equiv 0$ for $\theta = \pi/2$. The above set of equations has the the same structure of the equations of motion for a spinning particle constrained to the equatorial plane Eqs. [(3.3.25)-(3.3.27)] which we shall introduce in chapter 3.
In general, the geodesic motion of a test-particle in Kerr spacetime is multiple periodic, with fundamental frequencies $\Omega_r, \Omega_\theta, \Omega_\phi$ in coordinate time t, and ergodic, i.e. it fills the phase-space densely in a topological sense. The latter is not true when the condition

$$k\Omega_r + n\Omega_\theta + m\Omega_\phi = 0\,, \quad (1.2.11)$$

holds for any $k, n, m \in \mathbb{Z}$. In such situation, the motion is in a resonant orbit. For more details on resonances, see Refs. [56,82–88]. We define the following variables, which we shall prove useful later on: the angles

$$\phi_\alpha = \Omega_\alpha t\,, \qquad \alpha = t, r, \theta, \phi \quad (1.2.12)$$

with $\Omega_t = 1$, and $p^i = (\tilde{E}, \tilde{J}_z, \tilde{Q})$.

[2] Later on in chapter 3 we will use the rescaling $\tilde{J}_z = J_z/\mu M$

1.2.3 Post-adiabatic expansion

Accelerated motion and self-force

In BHPT, an exact solution of the EFE $g_{\mu\nu}^{\rm exact}$ can be expanded in powers of a small dimensionless parameter ϵ, which for us coincides with the mass ratio μ/M, around a known background metric $g_{\mu\nu}$

$$g_{\mu\nu}^{\rm exact} = g_{\mu\nu} + \epsilon h_{\mu\nu}^{(1)} + \epsilon^2 h_{\mu\nu}^{(2)} + O(\epsilon^3) \,, \tag{1.2.13}$$

with $h_{\mu\nu}^{(n)}$ are the n-order metric perturbation due to the presence of the SCO. We assume that $g_{\mu\nu}$ is a vacuum metric. The biggest conceptual issue in BHPT is the divergence of the field $h_{\mu\nu}^{(n)}$ at the wordline of the point-particle. Mino, Sasaki and Tanaka [89], and later Quinn and Wald [90] found the correct regularisation procedure to remove the singular terms, which leads to the MiSaTaQuWa field equations. Building upon these works, Ref. [91] introduced a convenient way to overcome the problem of the singularities. The approach consists in splitting the metric into two parts - a regular part $h_{\mu\nu}^{S(n)}$ and a singular part $h_{\mu\nu}^{R(n)}$:

$$h_{\mu\nu}^{(n)} = h_{\mu\nu}^{S(n)} + h_{\mu\nu}^{R(n)} \,. \tag{1.2.14}$$

The split is made in such way that $g_{\mu\nu} + \sum_n \epsilon^n h_{\mu\nu}^{R(n)}$ solved the vacuum EFE:

$$G_{\mu\nu}[g_{\mu\nu} + \sum_n \epsilon^n h_{\mu\nu}^{R(n)}] = 0 \,. \tag{1.2.15}$$

In particular, $h_{\mu\nu}^{R(1)}$ satisfies the first-order homogeneous field equations, while $h_{\mu\nu}^{S(1)}$ solved the inhomogeneous first-order field equations, as $h_{\mu\nu}^{(1)}$. By design, the singular field does not affect the motion of the particle but completely contains the singular structure of $h_{\mu\nu}^{(n)}$, whereas the regular field is a smooth on wordline of the particle [89,91–93]. To study radiation-reaction effects on the SCO in EMRI, it is convenient to treat the dynamics as that of a point-particle pushed away by forces from a geodesic path. In other words, given f^μ a small force per unit mass μ, we can write

$$\frac{D^2 z^\mu}{d\tau^2} = f^\mu = \epsilon f_{(1)}^\mu(z^\mu, \dot{z}^\mu) + \epsilon^2 f_{(2)}^\mu(z^\mu, \dot{z}^\mu) + \mathcal{O}(\epsilon^3) \,, \tag{1.2.16}$$

with $\dot{z}^\mu \equiv dz^\mu/d\tau$ and $D^2 z^\mu = \dot{z}^\rho \nabla_\rho \dot{z}^\mu$ with the covariant derivative compatible with the metric background $g_{\mu\nu}$. In this context, $f^\mu$is the *self-force*, which result from the metric pertubations on the background. The terms $f_{(1)}^\mu$ and $f_{(2)}^\mu$ are

caused by different part of the regular metric perturbations $h^{R(1)}_{\mu\nu}$ and $h^{R(2)}_{\mu\nu}$. At each order in the pertubative expansion, the metric perturbations $h^{R(n)}_{\mu\nu}$ can be further splitted as

$$h^{R(n)}_{\mu\nu} = h^{\mathrm{rad}(n)}_{\mu\nu} + h^{\mathrm{con}(n)}_{\mu\nu} \,, \tag{1.2.17}$$

where $h^{\mathrm{rad}(n)}_{\mu\nu}$ is the time-asymmetric part and $h^{\mathrm{cons}(n)}_{\mu\nu}$ is the time-symmetric part. The self-force can be divided in two parts as well

$$f^{\mu}_{(n)} = f^{\mu}_{(n)\mathrm{dis}} + f^{\mu}_{(n)\mathrm{con}} \,, \tag{1.2.18}$$

where $f^{\mu}_{(n)\mathrm{dis}}$ is the dissipative component of the self-force, which is generated by $h^{\mathrm{rad}(n)}_{\mu\nu}$, whereas $f^{\mu}_{(n)\mathrm{con}}$ consists in the conservative component of the self-force, which is sourced by $h^{\mathrm{con}(n)}_{\mu\nu}$. As we shall see in a moment, the two terms have a drastically different impact on the dynamics.

Adiabatic and post-adiabatic approximation

Due to the self-force, the first integrals p^i and frequencies Ω_α are no longer constant, but they evolve slowly with time over the radiation-reaction timescale $T_{\mathrm{rad}} \sim M/\epsilon$. For small mass-ratios, the latter is much longer than the orbital timescale $T_\alpha = 2\pi/\Omega_\alpha \sim M$ over which the angle variables ϕ_α changes. This separation of scales allow us to expand the equations of motion in the *two-time scale expansion*, a systematic method for studying the cumulative effect of a small disturbance on a dynamical system that is active over a long time. Schematically, at first order in q we can write [50, 58]

$$\frac{\mathrm{d}\phi_\alpha}{\mathrm{d}\tau} = \Omega_\alpha(p_i) + q g^{(1)}_\alpha(\phi_r, \phi_\theta, p_i) + \mathcal{O}(q^2) \,, \tag{1.2.19}$$

$$\frac{\mathrm{d}p_i}{\mathrm{d}\tau} = q G^{(1)}_i(\phi_r, \phi_\theta, p_k) + \mathcal{O}(q^2) \,, \tag{1.2.20}$$

which is valid for a non-spinning particle and we neglected the evolution equations for the central black hole parameters (M, a), which also evolve due to absorption of energy and angular momentum from incoming radiation. The corrections due to the SF are encoded in G_i and g_α. At "zeroth" order in q the motion is geodesic i.e. the free-falling of a test-particle. Given a function $F(\phi_r, \phi_\theta)$, it is possible to expand in Fourier series

$$F(\phi_r, \phi_\theta) = \sum_{nk} F_{kn} e^{i(n\phi_r + k\phi_\theta)} \,, \tag{1.2.21}$$

$$F_{kn} = \frac{1}{(2\pi)^2} \int_0^{2\pi} \mathrm{d}\phi_r \int_0^{2\pi} \mathrm{d}\phi_\theta F(\phi_r, \phi_\theta) e^{-i(n\phi_r + k\phi_\theta)} \,. \tag{1.2.22}$$

For non-resonant orbits, we can split a function $F(\phi_r, \phi_\theta)$ in a term that accumulate secularly over many orbits and a term that oscillate on short timescales:

$$F(\phi_r, \phi_\theta) = \langle F \rangle + \delta F(\phi_r, \phi_\theta) \,, \tag{1.2.23}$$

where $\langle F \rangle$ is the *torus average* and $\delta F(\phi_r, \phi_\theta)$ the oscillatory component define as

$$\delta F(\phi_r, \phi_\theta) := \sum_{nk \neq 0} F_{kn} e^{i(n\phi_r + k\phi_\theta)} \,, \tag{1.2.24}$$

$$\langle F \rangle := \frac{1}{(2\pi)^2} \int_0^{2\pi} \mathrm{d}\phi_r \int_0^{2\pi} \mathrm{d}\phi_\theta F(\phi_r, \phi_\theta) \equiv F_{00} \,. \tag{1.2.25}$$

By construction, $\langle \delta F \rangle = 0$ for ergodic trajectories, i.e., phase-space filling trajectories, but not for resonant orbits. The equations of motion then become [50, 58]

$$\frac{\mathrm{d}\phi_\alpha}{\mathrm{d}\tau} = \Omega_\alpha(p_i) + q \left\langle g_\alpha^{(1)}(p_k) \right\rangle + q \delta g_\alpha^{(1)}(\phi_r, \phi_\theta, p_i) + \mathcal{O}(q^2) \,, \tag{1.2.26}$$

$$\frac{\mathrm{d}p_i}{\mathrm{d}\tau} = q \left\langle G_i^{(1)}(p_k) \right\rangle + \delta G_i^{(1)}(\phi_r, \phi_\theta, p_i) + \mathcal{O}(q^2) \,. \tag{1.2.27}$$

The average of $G_i^{(1)}(\phi_r, \phi_\theta, p_k)$ describes the leading evolution of the would-be integrals of motion:

$$\left\langle G_i^{(1)}(p_k) \right\rangle = \left(\left\langle \frac{\mathrm{d}\tilde{E}}{\mathrm{d}\lambda} \right\rangle, \left\langle \frac{\mathrm{d}\tilde{J}_z}{\mathrm{d}\lambda} \right\rangle, \left\langle \frac{\mathrm{d}\tilde{Q}}{\mathrm{d}\lambda} \right\rangle \right) \,. \tag{1.2.28}$$

The *adiabatic approximation* consists of neglecting all forcing terms except the average $\left\langle G_i^{(1)}(p_k) \right\rangle$ [3]

$$\frac{\mathrm{d}\phi_\alpha}{\mathrm{d}\tau} = \Omega_\alpha(p_i) \,, \tag{1.2.29}$$

$$\frac{\mathrm{d}p_i}{\mathrm{d}\tau} = q \langle G_i^{(1)}(p_k) \rangle + \mathcal{O}(q^2) \,. \tag{1.2.30}$$

Since the waveform phase in a binary is directly related to the orbital phase, the two-time scale expansion provides a simple means of assessing the level of accuracy of a given approximation. Ref. [58] determined what inputs are required in a 1PA approximation, which is necessary for waveform models

[3] It can be shown that $\langle G_i(p_k) \rangle$ do not depend on the shift δM and δa induce by the slow evolution of the mass and spin of the SMBH.

accurate enough for data analysis with LISA. At 1PA order, the GW phase has the following contributions

$$\Phi_{\rm GW} = \underbrace{q^{-1}\mathcal{C}^{(0)}}_{\text{adiabatic}} + \underbrace{q^{-1/2}\mathcal{C}^{(1/2)}}_{\text{resonances}} + \underbrace{q^{0}\mathcal{C}^{(1)}}_{\text{post-1-adiabatic}} + \mathcal{O}(q)\,,$$

where

- $\mathcal{C}^0$ is only due to $f^{\mu}_{(1)\rm dis}$ effects, which sourced the average forcing terms $\left\langle G^{(1)}_i(p_k)\right\rangle$
- $\mathcal{C}^{(1/2)}$ includes the secular terms due to resonances (see also [50, 56] and references therein)
- $\mathcal{C}^1$ contains contributions from $f^{\mu}_{(2)\rm dis}$, $f^{\mu}_{(1)\rm con}$ and the secondary spin force $f^{\mu}_{\text{small-spin}}$ (see [52, 53, 55, 94, 95])

The force induces by the secondary spin $f^{\mu}_{\text{small-spin}}$ comprise the spin-curvature coupling term (i.e the right hand side of Eq. (3.2.2)) and the linear in spin, linear in mass ratio dissipative self-force and self-torque (the latter is the torque impress on the spin by the self-force) [53, 54]. We will see in the next chapter how to obtained the averaged rate-of changes $\left\langle G^{(1)}_i(p_k)\right\rangle$ without computing $h^{{\rm rad}(n)}_{\mu\nu}$ and $f^{\mu}_{(1)\rm dis}$. Moreover, we will estimate the dissipative effects of $f^{\mu}_{\text{small-spin}}$ and their contribution at 1PA order by modeling the inspiral at adiabatic order.

1.2.4 Secondary spin effects on EMRIs

A considerable body of work is present in literature concerning the dynamics of a spinning point-particle in curved spacetime. However, the vast majority of studies on the subject do not treat the radiation-driven inspiral of a spinning SCO in the extreme-mass-ratio binaries. In the following, we summarize some of the relevant work on gravitation emission by a secondary endowed with spin in EMRIs, referring the reader to later chapters for more references.

Earlier work in perturbation theory mostly focused on the effect of the spin on unbound orbits [96–98], and the spin of the secondary was taken to be unrealistically large in order to maximize its effect and compensate for the mass-ratio suppression. One of the first work to consider dissipative spin effects on bound orbits is Ref. [99], which estimated post-Newtonian terms for the

fluxes by expanding the GW fluxes computed with BHPT (see also Ref. [100] for a more recent analysis). A more recent work [94] considered the precession of a gyroscope in Schwarzschild spacetime induced by the conservative self-torque of the particle. Subsequent works [101–103] extended this computation to a Kerr background.
The effects of conservative spin-curvature coupling and self-force were studied in Ref. [95, 104] for circular orbits in Schwarzschild, and later on in Ref. [55] for generic orbits (the latter neglected the spin contribution to the GW fluxes) while Ref. [105] calculated the gravitational fluxes including the spin-induced quadrupole in the case of a near extremal Kerr BH. GW fluxes and waveforms for a spinning secondary have also been computed using EOB models in the test-mass limit [106–108]. For instance, an estimate of the conservative contributions on the dynamics induced by the secondary spin was computed in Ref. [109].
The GW fluxes for circular orbits in Schwarzschild and Kerr spacetimes were computed accurately using a time-domain code [101, 110, 111], comparing also some of the most used choices for the supplementary spin conditions discussed in chapter 3. Ref. [53] considered spin dissipative effects with a spinning test particle and derived new flux-balance laws relating the asymptotic fluxes of energy and angular momentum to the adiabatic changes of the orbital parameters, focusing on the case of circular orbits around a Schwarzschild and secondary spin perpendicular to the orbital plane.

None of the previous work went on to compute explicitly the adiabatic evolution to the leading order and the corresponding spin-corrections to the GW phase in a Kerr spacetime, which is crucial to estimate the detectability of the secondary spin. Furthermore, only a handful of works performed a parameter estimation in EMRIs for the spin of a SCO [112, 113], but all of them resorted to approximated and semi-relativistic - but computationally efficient - waveforms commonly known as “kludge” waveforms. It is known that using these models may lead to large systematic errors when performing parameter estimation (see, for instance [48]). Nevertheless, due to the complexity and the slow generation of EMRI waveforms computed using BHPT, almost all parameter-estimation studies done so far made use of kludge models [33, 114–117].

1.3 Thesis outline

In this thesis I studied the evolution of a spinning compact object moving in a Kerr background under gravitational radiation-reaction forces. My investigation proceeded in two closely related directions: modeling the inspiral of a spinning SCO and the corresponding gravitational signal; performing a forecast of the

constraints on the binary parameters expected by LISA, with emphasis on the secondary spin. In my work I made use of BHPT methods, which provide fully-relativistic waveform models.

On the source-modeling front, I first obtained new relations for the orbital dynamics of a spinning SCO in Kerr background. Furthermore, I computed the GW fluxes for a spinning secondary in EMRI in spin (anti-)aligned equatorial motion. As a by product of this calculation, I obtained several technical results useful for solving the ordinary differential equations for the radiative part of the metric pertubations. Since the spin of a SCO is of the same order of the mass ratio, the orbital dynamics and the GW fluxes can be fully linearized in the spin. I calculated the first order spin-induced corrections to the GW fluxes, both numerically and with semianalytic approaches, which are novel. These corrections allow to significantly improve the efficiency of numerical calculations, improving accuracy and computational time. The methods developed in this thesis lie the foundation for studying radiation emission of a spinning body for more generic orbits.

Regarding the detectability of the smaller companion spin in EMRIs, I first performed a back-on-the-enveloped calculation based only on the phase of the gravitational signal. Using the fluxes computed in my previous work, I model the adiabatic inspiral of a spinning SCO, extracting the post-adiabatic corrections due the secondary spin. These corrections allowed me to estimate the minimum detectable spin by LISA, providing a criterion that depend solely on the primary spin and the expected dephasing by neglecting the small spin. My simplistic analysis showed that the SCO spin might be detectable by LISA with 10% relative accuracy for sufficiently fast spinning SMBH. Furthermore, I pointed out that model-independent tests of the Kerr bound[4] could be performed by measuring the spin of the small companion. In the extreme mass ratio limit, the dynamics of the SCO depends only on its mass and spin, which are free parameters, and its completely oblivious of the secondary's internal structure.
Lastly, I performed a parameter estimation on the secondary spin with a Fisher matrix approach. My statistical analysis is the first to include full-relativistic waveform models along with the antenna pattern functions of LISA and higher order modes, providing benchmarks for studies with "kludge" waveforms. I showed that the secondary spin is not measurable because of statistical correlations, which spoil the accuracy on the other parameters unless a physically motivated prior is introduced. My work represents a first step in the analysis of

[4]The angular momentum S of an isolated BH with mass μ is limited by the Kerr bound, $S \leq G\mu 2/c$.

the impact of the secondary spin on EMRI's evolution, in parallel with recent work along related directions.

The content of this thesis is based on the following research papers published in refereed journals:

- G. A. Piovano, A. Maselli, and P. Pani, "Model independent tests of the Kerr bound with extreme mass ratio inspirals," *Phys. Lett. B* **811** (2020) 135860, arXiv:2003.08448 [gr-qc].
- G. A. Piovano, A. Maselli, and P. Pani, "Extreme mass ratio inspirals with spinning secondary: a detailed study of equatorial circular motion," *Phys. Rev. D* **102** no. 2, (2020) 024041, arXiv:2004.02654 [gr-qc].
- G. A. Piovano, R. Brito, A. Maselli, and P. Pani, "Assessing the detectability of the secondary spin in extreme mass-ratio inspirals with fully relativistic numerical waveforms," *Phys. Rev. D* **104** no. 12, (2021) 124019, arXiv:2105.07083 [gr-qc]

The results of [118] contributed to the BH Perturbation Toolkit project [119], a collection of state-of-the-art numerical algorithms for BHPT and numerical data.

The structure of the manuscript is the following. In chapter 2, I present the main aspects of BHPT, followed by an introduction on metric perturbation with the Newman–Penrose formalism and the Teukolsky equation. Chapter 3 describes the dynamics of spinning test-particles in curved spacetime, focusing on the case of motion in Kerr background. In chapter 4, I present the computation of GW fluxes for EMRI with spinning SCO using BHPT. Chapter 5 illustrate my analysis on the detectability of the secondary spin in EMRIs by LISA. Finally, in "Conclusions and outlook", I draw my conclusions and present possible extensions of my work. Furthermore, there are 6 appendices with the more technical results of my work. In each chapter will refer the reader to the proper appendix for more details on specific calculations.

1.3.1 Notation and abbreviations

In this section we summarize the main conventions adopted in this thesis.

We denote the speed of light in vacuum by c and the gravitational constant by G. We use the spacetime metric with signature $(-,+,+,+)$. Throughout this work we use geometric units, $G = c = 1$ unless otherwise stated. Hatted

variables denote dimensionless quantities rescaled by the primary mass, i.e. $\hat{r} \equiv r/M$ and so on. We adopt the Einstein convention, i.e., repeated indices are implicitly summed over.
Round ( ) and square [ ] brackets in the indices indicate symmetrization and antisymmetrization, respectively. For instance,

$$T^{(ab)} = \frac{1}{2}\left(T^{ab} + T^{ba}\right) \qquad T^{[ab]} = \frac{1}{2}\left(T^{ab} - T^{ba}\right) .$$

Given ω_δ an arbitrary 1-form, we define the Riemann tensor as

$$R_{\mu\nu\sigma}{}^{\delta}\omega_\delta = 2\nabla_{[\mu}\nabla_{\nu]}\omega_\sigma , \tag{1.3.1}$$

and the Ricci tensor by $R_{\mu\nu} = R^{\alpha}{}_{\mu\alpha\nu}$. The scalar is curvature is denoted by $R = R^{\alpha}{}_{\alpha}$.

Chapter 2

Black hole perturbation theory

In this chapter we give a brief overview of perturbation theory applied to BH metrics, with an emphasis on first-order corrections. First, we present the expansion of the EFE (1.2.1) in the mass-ratio, covering the main techniques typically employed to simplify the linearized field equations. The second half of the chapter illustrates the Newman-Penrose (NP) formalism, a tetrad basis approach particularly suited to study GWs. In fact, the gravitational waveforms and fluxes can be computed efficiently from the linear perturbations of Weyl scalars, defined in NP formalism, avoiding the direct computation of $h^{\mathrm{rad}(1)}_{\mu\nu}$.

2.1 Metric expansion of the field equations

2.1.1 Expansion Einstein field equations in the small mass ratio

We start with the metric expansion (1.2.13) of an exact metric $g^{\mathrm{exact}}_{\mu\nu}$ around a vacuum metric $g_{\mu\nu}$, with the assumption that also $T_{\mu\nu}$ depends smoothly on the small dimensionless parameter ϵ as

$$T_{\mu\nu} = \epsilon T^{(1)}_{\mu\nu} + \epsilon^2 T^{(2)}_{\mu\nu} + O(\epsilon^3)\,. \tag{2.1.1}$$

For later convenience, we define the total metric perturbation

$$h_{\mu\nu} = \sum_{n>0} \epsilon^n h^{(n)}_{\mu\nu}\,, \tag{2.1.2}$$

By convention, all indices are raised and lowered using the background metric $g_{\mu\nu}$. Given that $g^{\mathrm{exact}}_{\mu\rho} g^{\rho\nu}_{\mathrm{exact}} = \delta_\mu{}^\nu$, it is easy to show that

$$g^{\mu\nu}_{\mathrm{exact}} = g^{\mu\nu} - \epsilon h^{\mu\nu}_{(1)} - \epsilon^2 \left(h^{(2)}_{\mu\nu} - g_{\rho\lambda} h^{\mu\rho}_{(1)} h^{\lambda\nu}_{(1)} \right) + O(\epsilon^3)\,, \tag{2.1.3}$$

Before expanding Eqs. (1.2.1) in powers of ϵ, we first expand the EFE in powers of the exact perturbation $h_{\mu\nu}$

$$G_{\mu\nu}[g_{\rho\sigma}+h_{\rho\sigma}] = G_{\mu\nu}[g_{\rho\sigma}] + G^{(1)}_{\mu\nu}[h_{\rho\sigma}] + G^{(2)}_{\mu\nu}[h_{\rho\sigma},h_{\rho\sigma}] + O(|h_{\rho\sigma}|^3)\,. \tag{2.1.4}$$

For a vacuum background, the first two terms are

$$G^{(1)}_{\mu\nu}[h] = \left(\delta_\mu{}^\alpha\delta_\nu{}^\beta - \tfrac{1}{2}g_{\mu\nu}g^{\alpha\beta}\right)R^{(1)}_{\alpha\beta}\,, \tag{2.1.5}$$

$$G^{(2)}_{\mu\nu}[h,h] = \left(\delta_\mu{}^\alpha\delta_\nu{}^\beta - \tfrac{1}{2}g_{\mu\nu}g^{\alpha\beta}\right)R^{(2)}_{\alpha\beta} - \frac{1}{2}\left(h_{\mu\nu}g^{\alpha\beta} - g_{\mu\nu}h^{\alpha\beta}\right)R^{(1)}_{\alpha\beta}\,, \tag{2.1.6}$$

where the linear and quadratic terms in the Ricci tensor are

$$R^{(1)}_{\alpha\beta}[h] = -\frac{1}{2}\left(\Box h_{\alpha\beta} + 2R_\alpha{}^\mu{}_\beta{}^\nu h_{\mu\nu} - 2\bar{h}_{\mu(\alpha}{}^{;\mu}{}_{\beta)}\right), \tag{2.1.7}$$

$$\begin{aligned} R^{(2)}_{\alpha\beta}[h,h] = {}& \frac{1}{4}h^{\mu\nu}{}_{;\alpha}h_{\mu\nu;\beta} + \frac{1}{2}h^\mu{}_\beta{}^{;\nu}\left(h_{\mu\alpha;\nu} - h_{\nu\alpha;\mu}\right) - \frac{1}{2}\bar{h}^{\mu\nu}{}_{;\nu}\left(2h_{\mu(\alpha;\beta)} - h_{\alpha\beta;\mu}\right) \\ & - \frac{1}{2}h^{\mu\nu}\left(2h_{\mu(\alpha;\beta)\nu} - h_{\alpha\beta;\mu\nu} - h_{\mu\nu;\alpha\beta}\right). \end{aligned} \tag{2.1.8}$$

$R_{\alpha\mu\beta\nu}$ is the Riemann tensor for the background $g_{\mu\nu}$, while $\bar{h}_{\mu\nu}$ the trace-reversed perturbation defined as

$$\bar{h}_{\mu\nu} := h_{\mu\nu} - \frac{1}{2}g_{\mu\nu}h \tag{2.1.9}$$

where $h := g^{\alpha\beta}h_{\alpha\beta}$ is the trace. We also defined the d'Alembertian $\Box := g^{\mu\nu}\nabla_\mu\nabla_\nu$. A semicolon and ∇ both denote the covariant derivative compatible with $g_{\mu\nu}$. After substituting the expansions (1.2.13) and (2.1.1) into the Einstein equations and equating powers of ϵ, we obtain

$$G^{(1)}_{\mu\nu}[h^{(1)}_{\rho\sigma}] = 8\pi T^{(1)}_{\mu\nu}, \tag{2.1.10}$$

$$G^{(1)}_{\mu\nu}[h^{(2)}_{\rho\sigma}] = 8\pi T^{(2)}_{\mu\nu} - G^{(2)}_{\mu\nu}[h^{(1)}_{\rho\sigma},h^{(1)}_{\rho\sigma}]\,. \tag{2.1.11}$$

Explicitly, Eq.(2.1.10) is given as

$$-\frac{1}{2}\Box\bar{h}^{(1)}_{\alpha\beta} - R_\alpha{}^\mu{}_\beta{}^\nu\bar{h}^{(1)}_{\mu\nu} + \bar{h}^{(1)}_{\mu(\alpha}{}^{;\mu}{}_{\beta)} - \frac{1}{2}g^{\alpha\beta}\bar{h}^{(1)}{}_{\mu(\alpha}{}^{;\mu}{}_{\beta)} = 8\pi T^{(1)}_{\mu\nu}\,. \tag{2.1.12}$$

2.1.2 Gauge freedom

The fields $h^{(n)}_{\alpha\beta}$ can be changed arbitrarily by a small coordinate transformation:

$$x^\alpha \to x^\alpha + \epsilon\xi^\alpha_{(1)} + \frac{1}{2}\epsilon^2\xi^\alpha_{(2)} + \mathcal{O}(\epsilon^3) \tag{2.1.13}$$

with $\xi^\alpha_{(n)}$ arbitrary vector fields. Under the coordinate transformation (2.1.13), the first and and second-order metric perturbations transform as

$$h^{(1)}_{\mu\nu} \to h^{(1)}_{\mu\nu} + \pounds_{\xi_{(1)}} g_{\mu\nu} \,, \tag{2.1.14}$$

$$h^{(2)}_{\mu\nu} \to h^{(2)}_{\mu\nu} + \pounds_{\xi_{(2)}} g_{\mu\nu} + \frac{1}{2}\pounds^2_{\xi_{(1)}} g_{\mu\nu} + \pounds_{\xi_{(1)}} h^{(1)}_{\mu\nu}, \tag{2.1.15}$$

where $\pounds_\xi$ is a Lie derivative. The above local diffeomorphisms are also called *gauge transformations*. Their main effect consists in changing the split between "background" and "perturbations" or, in other words, different $h^{(1)}_{\alpha\beta}$ may correspond to the same physical effects. A similar situation occurs in classical electrodynamics, where the vector potentials A^μ and its gauge-transformed counterpart A'^μ

$$A^\mu \to A'^\mu = A^\mu + \chi_{,\mu} \tag{2.1.16}$$

correspond to the same magnetic vector B^μ for some gauge potential χ. It can be shown that $G^{(1)}_{\mu\nu}[h^{(1)}_{\rho\sigma}]$ is invariant under the transformation (2.1.14). The freedom to perform gauge transformations is used in BHPT to simplify Eqs. (2.1.12). One of the most employed condition is the Lorenz gauge

$$\nabla_\mu \bar{h}^{\mu\nu} = 0, \tag{2.1.17}$$

in which case the linearized field equations (2.1.12) reduce to

$$\Box \bar{h}^{(1)}_{\mu\nu} + 2R_\alpha{}^\mu{}_\beta{}^\nu \bar{h}^{(1)}_{\mu\nu} = -16\pi T^{(1)}_{\mu\nu} \,. \tag{2.1.18}$$

Both $h^{(1)}_{\mu\nu}$ and $h^{(2)}_{\mu\nu}$ are needed to model the dynamics of an EMRI binary with sufficient accuracy. Solving the second order field equations (2.1.11) is a formidable task, but much progress has been recently made [76, 77]. Hereafter we only consider first-order metric perturbations.

2.1.3 Solving the first-order perturbative field equations

The field equations (2.1.18) are a system of 10 linear, hyperbolic, partial differential equations (PDE). Being coupled, these equations are computationally expensive to solve, especially when high precision is sought. Furthermore, one needs to solve Eqs. (2.1.18) and (1.2.16) together: the metric perturbations depend on the position and velocity of the particle, whose motion evolves under the action of the SF computed from $h^{(1)}_{\mu\nu}$ [89, 90]. On top of that, a fundamental issue arise from the divergences of the field $h^{(1)}_{\mu\nu}$ at the worldline of the particle,

which requires a careful treatment of the singularities [120]. We refer the reader to Refs. [50, 51] for an introduction to the topic and Refs. [52, 64] for a more in depth review. Here we just briefly present the main methods that have been employed in the literature to recast Eqs. (2.1.18) in a more tractable form. The following short presentation is adapted from the notes of the lectures given by Leor Barack at the Kavli Rise Summer school in Cambridge [121]. For more details, see also Refs. [122–125].

Schwarzschild background - Lorenz gauge

In Schwarzschild spacetime, the $3+1$D PDE can be reduced to $1+1$D or even ODEs using a multipole decomposition in *tensor harmonic*. Such result is achievable with the following ansatz [126–128]

$$h_{\mu\nu} = \sum_{\ell m} \sum_{i=0}^{10} h^{(i)\ell m}(t,r) Y^{(i)\ell m}_{\mu\nu}(\theta,\phi) \,, \tag{2.1.19}$$

$Y^{(i)\ell m}_{\mu\nu}(\theta,\phi)$ are 10 orthornormal tensor-harmonic basic functions given as linear combination of spherical harmonics $Y^{\ell m}$, vector and tensor harmonics. $Y^{(i)\ell m}_{\mu\nu}(\theta,\phi)$ are divided in two groups: there are 7 tensor harmonics corresponding to even-parity modes and 3 for odd-parity modes. As a result, for each given ℓ, m mode the above ansatz separate the field equations in two sets of coupled hyperbolic equations, with the following structure:

$$\Box^{(2)} h^{(i)\ell m}(t,r) + D^{(i)}{}_{(j)} h^{(j)\ell m}(t,r) = T^{(i)\ell m} \,, \tag{2.1.20}$$

where $\Box^{(2)}$ is the 2D wave operatorm and $D^{(i)}{}_{(j)}$ a first-order differential operator that couple different $i-$ modes of the same parity. There are 7 coupled equations for the 7 even-parity modes and 3 odd-parity equations for the odd-parity modes. Also the Lorenz gauge condition separates, taking the form

$$D^{(i)}{}_{(j)} h^{(i)\ell m}(t,r) = 0 \,, \tag{2.1.21}$$

with $\tilde{D}^{(i)}{}_{(j)}$ another first-order operator. The above equation separates in 3 coupled equations for the even-parity sector and only one for the odd-parity sector.
The field equations can be further reduced from $1+1$D PDEs to ordinary ODEs in the frequency domains:

$$h_{\mu\nu} = \sum_{\ell m} \sum_{i=0}^{10} \int_{-\infty}^{\infty} \mathrm{d}\omega h^{(i)\ell m\omega}(r) Y^{(i)\ell m}_{\mu\nu}(\theta,\phi) e^{-i\omega t} \tag{2.1.22}$$

with $h^{(i)\ell m\omega}(r)$ obeying ODEs in the radial variable.

Schwarzschild background - Regge-Wheeler gauge

An alternative of the Lorenz gauge is the Regge-Wheeler (RW) gauge, which drastically simplifies the expansion of metric perturbation in tensor harmonics. This simplification allow to define two scalar-like variables $\Psi^{\ell m}_{\rm even}$ and $\Psi^{\ell m}_{\rm odd}$ in terms of even and odd modes, respectively. These quantities obeys two master equations, the celebrated RW equation [129] (for the odd sector) and Zerilli equation [130] (for the even sector)

$$(\partial_{tt} - \partial_{r^* r^*} + V_{\rm even/odd})\Psi^{\ell m}_{\rm even/odd} = S_{\rm even/odd}[T_{\mu\nu}] \,, \tag{2.1.23}$$

where $V_{\rm even/odd}$ effective potentials depending on ℓ, while $S_{\rm even/odd}[T_{\mu\nu}]$ are the source terms written in terms of the stress-energy tensor $T_{\mu\nu}$. Finally, r^* is defined as $r^* = r + 2M\ln(r/2M-1)$. From $\Psi^{\ell m}_{\rm even}$ and $\Psi^{\ell m}_{\rm odd}$ we can directly write the gravitational waveforms as sum over the ℓ, m modes, and compute the GW fluxes without needing $h^{{\rm rad}(1)}_{\mu\nu}$. Moreover, we can recover the metric perturbations $\bar{h}^{(1)}_{\mu\nu}$ from $\Psi^{\ell m}_{\rm even/odd}$ using "reconstruction techniques". For more details, see Ref. [50].

Kerr background

Unlike the Schwarzschild metric, no methods have been found to date to fully separate Eqs. (2.1.18) in the presence of source, although significant progress has been recently made in the $T_{\mu\nu} = 0$ case [131]. It is still possible to use the ansatz Eq. (2.1.19), but modes of different parity and different ℓ, m are coupled in the Kerr background. By exploiting the axial symmetry of the metric, it is still possible to reduce the dimensions of the PDEs with the ansatz:

$$h_{\mu\nu} = \sum_{i=0}^{\infty} h^m_{\mu\nu}(t, r, \theta) e^{im\phi} \,. \tag{2.1.24}$$

The resulting equations for $h^m_{\mu\nu}(t, r, \theta)$ are $2+1$D hyperbolic equations. One can further reduces the field equations by passing to the frequency domain

$$h_{\mu\nu} = \sum_{i=0}^{\infty} \int_{-\infty}^{\infty} {\rm d}\omega h^{m\omega}_{\mu\nu}(t, r, \theta) e^{i(m\phi - \omega t)} \,, \tag{2.1.25}$$

with $h^{m\omega}_{\mu\nu}(r, \theta)$ obeying elliptic equations in 2D.

2.2 NP formalism and Teukolsky master equation

2.2.1 Weyl tensor and Petrov classification

The Weyl tensor is particularly useful for studying the perturbations of vacuum solutions of the EFE. It is defined in four dimensions as:

$$C_{\mu\nu\rho\sigma} := R_{\mu\nu\rho\sigma} + \frac{1}{2}(R_{\mu\sigma}g_{\nu\rho} - R_{\mu\rho}g_{\nu\sigma} + R_{\nu\rho}g_{\mu\sigma} - R_{\nu\sigma}g_{\mu\rho}) + \\ + \frac{1}{6}R(g_{\mu\rho}g_{\nu\sigma} - g_{\mu\sigma}g_{\nu\rho}) \,, \tag{2.2.1}$$

which implies that $C_{\mu\nu\rho\sigma}$ is traceless (contracting any pair of indices gives zero) and has the same symmetries of the Riemann tensor $R_{\mu\nu\rho\sigma}$. For Ricci-flat manifolds, i.e spacetimes where $R_{\mu\nu} = 0$, the Weyl tensor coincides with the Riemann tensor. This is the case of any vacuum solutions of the EFE. A special property of $C_{\mu\nu\rho\sigma}$ is its invariance under conformal transformations of the metric, i.e. if

$$g_{\mu\nu} \to g'_{\mu\nu} = f g_{\mu\nu} \,, \tag{2.2.2}$$

for a positive scalar function f, then $C'_{\mu\nu\rho\sigma} = C_{\mu\nu\rho\sigma}$. In four dimensions, a metric is conformally flat if and only if the Weyl tensor vanishes. We can obtain crucial insights on the properties of spacetimes by studying the algebraic symmetries of the Weyl tensor, which depend on the multiplicities of the roots of a quartic characteristic equation [132, 133]:

$$\Psi_0 + 4\lambda\Psi_1 + 6\Psi_2\lambda^2 + 4\Psi_3\lambda^3 + \lambda^4\Psi_4 = 0 \,, \tag{2.2.3}$$

where $\Psi_0, \Psi_1, \Psi_2, \Psi_3, \Psi_4$ are complex scalar function, which we will defined later on. The number of simple roots of Eq.(2.2.3) determine how many distinct *principal null-directions* (PND), a special class of null-geodesics, the spacetime admits at a given position. According to the *Petrov classification* [134, 135], the Weyl tensor admit six possible classes of algebraic symmetries known as *Petrov types*

- Type I: four simple roots (four distinct PND)
- Type II: one double root and two simple roots (three distinct PND)
- Type D: two double roots (two distinct PND)
- Type III: one triple and one simple root (two distinct PND)
- Type N: one quadruple root (one distinct PND)

- Type O: the Weyl tensor vanishes

A type I Weyl tensor is called algebraically general; otherwise it is known as algebraically special. The Petrov classification provides a frame independent way to classify spacetimes, and in some cases there is a close correspondence between the Petrov type and symmetries of a metric. For instance, the Kerr and Schwarzschild metrics are everywhere type D, while FLRW models are type O for every event. BH solutions in GR admits two distinct PRD, which describe ingoing and outgoing null geodesics. These null-vectors are particularly useful to described metric perturbations of BHs in combination with the NP formalism.

2.2.2 Newman-Penrose formalism

The NP formalism [136] is a special case of the tetrad formalism, where the relevant tensors are projected onto a complete vector fields basis called tetrad. In this case, the tetrad is given by four null vectors:

$$\{e^{\mu}_{(a)}\} = \{l^{\mu}, n^{\nu}, m^{\mu}\bar{m}^{\mu}\} \tag{2.2.4}$$

where l^{μ} and n^{μ} are real and $m^{\mu}, \bar{m}^{\mu}$ are a complex-conjugate pair, which satisfy the condition

$$g_{\mu\nu}e^{\mu}_{(a)}e^{\mu}_{(a)} \equiv \eta_{(a)(b)} \begin{pmatrix} 0 & -1 & 0 & 0 \\ -1 & 0 & 0 & 0 \\ 0 & 0 & 0 & 1 \\ 0 & 1 & 0 & 0 \end{pmatrix} \tag{2.2.5}$$

and the Latin indices $a = 0, 1, 2, 3$. In terms of the null-tetrad, the metric can be written as

$$g_{\mu\nu} = -l_{\mu}n_{\nu} - l_{\nu}n_{\mu} + m_{\mu}\bar{m}_{\nu} + m_{\nu}\bar{m}_{\mu} \tag{2.2.6}$$

In the NP formalism, the components of tensors and other quantities are typically expressed with separate symbols. For instance, there are four covariant derivatives $(D, \Diamond, \delta, \bar{\delta})$ [1]

$$D := l^{\mu}\nabla_{\mu} \qquad \Diamond := n^{\mu}\nabla_{\mu} \qquad \delta := m^{\mu}\nabla_{\mu} \qquad \bar{\delta} := \bar{m}^{\mu}\nabla_{\mu} \tag{2.2.7}$$

In the same fashion, all the components of the Ricci rotation coefficients are denoted with lower-case Greek letters, which constitute 12 complex *spin coefficients* [132].

[1] It is standard to use Δ to denote $n^{\mu}\nabla_{\mu}$, but we choose $\Diamond$ to avoid confusion with our previous notation.

Of the 20 non-trivial degrees of freedom (DoF) of the Riemann tensor, 10 are encoded in the Ricci tensor and 10 in the Weyl tensor. The 10 independent components of the latter are described by 5 complex *Weyl scalars* $\Psi_0, \Psi_1, \Psi_2, \Psi_3, \Psi_4$

$$\begin{aligned} \Psi_0 &= C_{\mu\nu\rho\sigma} l^\mu m^\nu l^\rho m^\sigma \qquad \Psi_1 = C_{\mu\nu\rho\sigma} l^\mu n^\nu l^\rho m^\sigma \,, \\ \Psi_2 &= C_{\mu\nu\rho\sigma} l^\mu m^\nu \bar{m}^\rho n^\sigma \qquad \Psi_3 = C_{\mu\nu\rho\sigma} l^\mu n^\nu \bar{m}^\rho n^\sigma \,, \\ \Psi_4 &= C_{\mu\nu\rho\sigma} n^\mu \bar{m}^\nu n^\rho \bar{m}^\sigma \,. \end{aligned} \tag{2.2.8}$$

The above quantities are the coefficients of the characteristic equation (2.2.3). The 10 independent components of the Ricci tensor are encoded into 4 real $(\Phi_{00}, \Phi_{11}, \Phi_{12}, \Lambda)$ and 3 complex scalars $(\Phi_{20}, \Phi_{21}, \Phi_{22})$

$$\begin{aligned} &\Lambda := \frac{R}{24} \quad \Phi_{00} := \frac{1}{2} R_{\mu\nu} l^\mu l^\nu \quad \Phi_{11} := \frac{1}{4} R_{\mu\nu} (l^\mu n^\nu + m^\mu \bar{m}^\nu) \quad \Phi_{22} := \frac{1}{2} R_{\mu\nu} n^\mu n^\nu \,, \\ &\Phi_{01} := \frac{1}{2} R_{\mu\nu} l^\mu m^\nu \quad \Phi_{02} := \frac{1}{2} R_{\mu\nu} m^\mu m^\nu \quad \Phi_{12} := \frac{1}{2} R_{\mu\nu} m^\mu n^\nu \,. \end{aligned} \tag{2.2.9}$$

For vacuum metrics, the Ricci tensor vanishes hence only the Weyl scalars are in general different from zero.
We can recast the EFE in terms of the NP scalars, the covariant derivatives $(D, \Diamond, \delta, \bar{\delta})$ and the spin-coefficients, giving the NP equations. For the explicit form of the NP equations, see Ref. [132]. The NP formalism is particularly suited to algebraically special spacetimes, which are endowed with symmetries. We shall consider from now Petrov type D spacetimes, (like the Schwarzschild and Kerr metrics), for which the Riemann tensor has only 2 out of 20 non-trivial DoF encoded in Ψ_2. For these metrics, it is convenient to choose the vectors l^μ and n^ν as the ingoing and the outgoing PND, respectively.

2.2.3 Teukolsky master equation

Let us now consider small perturbations of the Weyl scalars:

$$\Psi_{\hat{k}} = \Psi^a_{\hat{k}} + \epsilon \Psi^b_{\hat{k}} \,, \qquad \hat{k} = 0, 1, \cdots, 4 \tag{2.2.10}$$

where $\Psi^a_{\hat{k}}$ denote the Weyl scalar for the metric background and $\Psi^b_{\hat{k}}$ its linear perturbations. All $\Psi^a_{\hat{k}}$ are zero expect for Ψ^a_2. The quantities Ψ^b_1 and Ψ^b_3 can be set to zero through infinitesimal rotation of the tetrad basis, whereas Ψ^b_0 and Ψ^b_4 are invariant under such rotations [137]. Furthermore, Ψ^b_0 and Ψ^b_4 are gauge invariant. Being scalars, $\Psi_{\hat{k}}$ transforms under gauge transformation $x^\mu \to x^\mu + \xi^\mu$ with ξ^μ infinitesimal as

$$\Psi_{\hat{k}} \to \Psi_{\hat{k}} - \xi^\mu \partial_\mu \Psi_{\hat{k}} \,, \tag{2.2.11}$$

Therefore, at linear order in ξ^μ, $\Psi^b_{\hat{k}}$ transforms as

$$\Psi^b_{\hat{k}} \to \Psi^b_{\hat{k}} - \xi^\mu \partial_\mu \Psi^a_{\hat{k}} \,, \tag{2.2.12}$$

and $\xi^\mu \partial_\mu \Psi^a_{\hat{k}} = 0$ for all $\hat{k}$ except for $\hat{k} = 2$.
Ψ^b_0 and Ψ^b_4 encode all the information on ingoing and outgoing gravitational radiation, respectively. As we shall see in the next chapters, the GW waveforms and fluxes can written in terms of Ψ^b_4.
In the seminal paper [137], it was shown that the first-order perturbative NP equations for Ψ^b_0 and Ψ^b_4 are separable. Moreover, for a Kerr background, all scalar, electromagnetic and gravitational perturbations given by NP scalars are solutions of the master equation

$$\begin{aligned}
&\left[\left(\frac{(r^2+a^2)^2}{\Delta} - a^2\sin^2\theta\right)\frac{\partial^2}{\partial t^2} + \frac{4Mar}{\Delta}\frac{\partial^2}{\partial t\partial\phi} + \left(\frac{a^2}{\Delta} - \frac{1}{\sin^2\theta}\right)\frac{\partial^2}{\partial\phi^2} + \right. \\
&- \Delta^{-s}\frac{\partial}{\partial r}\left(\Delta^{s+1}\frac{\partial}{\partial r}\right) - \frac{1}{\sin\theta}\frac{\partial}{\partial\theta}\left(\sin\theta\frac{\partial}{\partial\theta}\right) - 2s\left(\frac{M(r^2-a^2)}{\Delta} - r - ia\cos\theta\right)\frac{\partial}{\partial t} + \\
&\left. - 2s\left(\frac{a(r-M)}{\Delta} + \frac{i\cos\theta}{\sin^2\theta}\right)\frac{\partial}{\partial\phi} + (s^2\cot^2\theta - s)\right]\psi_s = -4\pi\Sigma T_s \,,
\end{aligned} \tag{2.2.13}$$

which is the celebrated Teukolsky's master equation, with $\psi_2 = \Psi^b_0$ and $\psi_{-2} = \rho^{-4}\Psi^b_4$ with $\rho = (r - ia\cos\theta)^{-1}$. T_s is a differential operator acting on the stress-energy tensor $T^{\mu\nu}$. The index s denotes the helicity of the perturbed field: $s = 0, s = \pm 1, s \pm 2$ for scalar, vector and rank 2 tensor, respectively. For $s = -2$, the source term is given in appendix C.

To conclude this chapter, we just mention that the metric perturbations $h^{(1)}_{\mu\nu}$ can be recovered with reconstruction methods from Ψ^b_0 and Ψ^b_4 (see for instance, Refs. [138–140]).

Chapter 3

Spinning bodies in curved spacetime

In this chapter we present a detailed description of the dynamics of a spinning, relativistic test-particle, moving on a curved background. We discuss how the stress energy tensor of an extended object in GR can be analysed in terms of a multipolar expansion, in which the first two moments, corresponding to the mass and spin of the body, provide the leading contribution. We then introduce the so called *Mathisson Papapetrou-Dixon* equations for the motion of a spinning test-particle, and discuss their main properties. We show in particular how the spin of an extended body interacts with the background spacetime, leading to a net spin-curvature force that pushes the center of mass of the object away from a geodetic path.
Finally, in the last section we consider the case of a spinning point-particle in the Kerr spacetime. We focus in particular on binaries on circular orbits, assuming aligned and anti-aligned spin configurations. In various sections of this chapter we discuss novel results, originally derived in Ref. [118], which provide new constraints on the orbital motion derived from the 4-velocity norm, as well as new analytical formulas for the energy and angular momentum of circular, equatorial motion in terms of the orbital parameters.

3.1 Multipolar expansion in general relativity

Various physical problems, both related to electromagnetic and gravitational phenomena, can be studied by considering sources localized in a small region of space, located far away from the observer. In this case, a suitable representation of the electromagnetic or of the gravitational fields at distant points from the source is provided by an expansion in terms of angular moments called multipoles. Most of the information on the charges, current or matter distributions are typically contained in the first few terms of such series. For more details on the

multipolar expansion we refer the reader to Refs. [141, 142].

Hereafter we briefly outline the expansion in multipoles of the stress-energy tensor of an extended body in curved space-time. In general relativity this approximation is accurate as long as the size of the object is considerably smaller than the spacetime curvature. This condition is always satisfied by the EMRI secondary, since its size is much smaller than the typical scale of the binary, which is set by the curvature radius of the primary. In this framework the stress-energy tensor of the secondary $T^{\mu\nu}$, admits a multipolar expansion within the so-called *gravitational skeletonization* [143–146].
Given a worldline $z^\alpha(\tau)$, specified by the extended object proper time τ, the multipole moments in general relativity have the following structure [147]

$$\int_{x^0=const} \sqrt{-g}\mathrm{d}^3x\, T^{\mu\nu}\delta x^{\alpha_1}\cdots\delta x^{\alpha_n}\,, \tag{3.1.1}$$

where $\delta x^\alpha = x^\alpha - z^\alpha$ is the deviation from $z^\alpha(\tau)$, defined inside the world-tube of the body, and $g = \det(g_{\mu\nu})$ is the determinant of the metric $g_{\mu\nu}$. Neglecting all moments but the first two yields the so called *pole-dipole* approximation, which is equivalent to consider an extended body as a spinning test particle. All details on the internal structure are neglected, being encoded within the quadrupole and higher multipoles.
The first two moments are the linear momentum p^μ, and the spin-dipole described by the skew-symmetric tensor $S^{\mu\nu}$:

$$p^\alpha(z^\alpha) = \int_{x^0=const} \sqrt{-g}\mathrm{d}^3x T^{\alpha 0}\,, \tag{3.1.2}$$

$$S^{\alpha\beta}(z^\alpha) = \int_{x^0=const} \sqrt{-g}\mathrm{d}^3x(\delta x^\alpha T^{\beta 0} - \delta x^\beta T^{\alpha 0})\,. \tag{3.1.3}$$

The integrals (3.1.2)-(3.1.3) are computed choosing a coordinate frame such that $\delta x^0 = 0$ while δx^i lie inside the integration region. An equivalent covariant representation is provided by

$$p^\alpha(z^\alpha) = \int_\Sigma \mathrm{d}\Sigma_\beta T^{\alpha\beta}\,, \tag{3.1.4}$$

$$S^{\alpha\beta}(z^\alpha,\Sigma) = 2\int_\Sigma \mathrm{d}\Sigma_\gamma \delta x^{[\alpha}T^{\beta]\gamma}\,. \tag{3.1.5}$$

where Σ is an arbitrary space-like hypersurface. In terms of the first two moments, the multipolar expansion of the stress-energy tensor $T^{\mu\nu}$ reads

$$T^{\mu\nu}(x) = \int \mathrm{d}\tau\left[\frac{\delta^{(4)}(x,z(\tau))}{\sqrt{-g}}p^{(\mu}(\tau)v^{\nu)}(\tau) - \nabla_\sigma\left(S^{\sigma(\mu}(\tau)v^{\nu)}(\tau)\frac{\delta^{(4)}(x,z(\tau))}{\sqrt{-g}}\right)\right], \tag{3.1.6}$$

where

$$\delta^{(4)}(x, z(\tau)) \equiv \delta^{(4)}(x - z(\tau)) := \prod_{\nu=1}^{4} \delta(x^\nu - z^\nu(\tau))$$

We refer the reader to Refs. [99, 144, 148] for a covariant representation of the multipole moments and for a detailed discussion on their properties. A more rigorous representation of the stress-energy tensor in terms of multipole moments would require the use of "bitensors", introduced by Synge in Ref. [149], but for our purposes Eq. (3.1.6) is sufficient.

3.2 Mathisson- Papapetrou-Dixon equations

The covariant conservation of the energy-momentum tensor, $\nabla_\mu T^{\mu\nu} = 0$, leads to the Mathisson- Papapetrou-Dixon (MPD) equations of motion for the spinning test body. These equations were first obtained by Mathisson in linearized theory of gravity [150], and then by Papapetrou in full general relativity [151, 152]. A covariant formulation was obtained by Tulczyjew [143] and Dixon [144–146], who also included the higher-order multipole moments of a test-body. A modern derivation is given in Ref. [153]. The MPD equations of motion read:

$$\frac{\mathrm{d}X^\mu}{\mathrm{d}\zeta} = v^\mu \,, \tag{3.2.1}$$

$$\nabla_{\vec{v}} p^\mu = -\frac{1}{2} R^\mu{}_{\nu\alpha\beta} v^\nu S^{\alpha\beta} \,, \tag{3.2.2}$$

$$\nabla_{\vec{v}} S^{\mu\nu} = 2 p^{[\mu} v^{\nu]} \,, \tag{3.2.3}$$

$$\mathfrak{m} \equiv -p_\mu v^\mu \,, \tag{3.2.4}$$

where $\nabla_{\vec{v}} \equiv v^\mu \nabla_\mu$, v^μ is the tangent vector to the representative worldline, and ζ is an affine parameter that can be different from the proper time τ. Thus, the tangent vector v^μ does not need to be the 4-velocity of a physical observer. The timelike condition $v^2 \equiv v^\mu v_\mu < 0$ is not a priori guaranteed by the MPD equations, i.e., v^2 is not necessarily conserved. The mass $\mathfrak{m}$ is the so-called monopole rest-mass, which is related to the energy of the particle as measured in the center of mass frame. The total or dynamical rest mass of the object is given by

$$\mu^2 = -p^\sigma p_\sigma \,, \tag{3.2.5}$$

and represents the mass measured in a reference frame where the spatial components of p^μ vanish. Neither $\mathfrak{m}$ nor μ are necessarily constants of motion [154] and it can be shown as follows. By multiplying the third MPD equations for p_ν

we get the identity

$$p^\mu = \frac{1}{\mathfrak{m}}(\mu^2 v^\mu - p_\sigma \nabla_{\vec{v}} S^{\mu\sigma}) \,. \tag{3.2.6}$$

It then follows that

$$\frac{\mathrm{d}\mathfrak{m}}{\mathrm{d}\tau} = \nabla_{\vec{v}} m = -(\nabla_{\vec{v}} v_\rho) p^\rho \,, \tag{3.2.7}$$

$$\frac{\mathrm{d}\mu}{\mathrm{d}\tau} = \nabla_{\vec{v}} \mu = -\frac{p_\sigma}{\mu} \nabla_{\vec{v}} p_\sigma = -\frac{(\nabla_{\vec{v}} p_\rho)}{\mathfrak{m}\mu}(\mu^2 v^\mu - p_\sigma \nabla_{\vec{v}} S^{\rho\sigma}) = \frac{(\nabla_{\vec{v}} p_\rho)}{\mathfrak{m}\mu} p_\sigma \nabla_{\vec{v}} S^{\rho\sigma} \,, \tag{3.2.8}$$

and in general $\mathrm{d}\mathfrak{m}/\mathrm{d}\tau$ and $\mathrm{d}\mu/\mathrm{d}\tau$ are different from zero.
Moreover, the 4-velocity and the linear momentum are not aligned since

$$p^\mu = -\frac{1}{v^2}(\mathfrak{m} v^\mu - v_\sigma \nabla_{\vec{v}} S^{\mu\sigma}) \,, \tag{3.2.9}$$

which can be obtained by multiplying the third MPD equations for v_ν.
The spin parameter S is defined as

$$S^2 \equiv \frac{1}{2} S^{\mu\nu} S_{\mu\nu} \,, \tag{3.2.10}$$

which is also not a priori conserved. In fact,

$$\frac{\mathrm{d}}{\mathrm{d}\tau}(S^2) = S_{\mu\nu} \nabla_{\vec{v}} S^{\mu\nu} = 2 S_{\mu\nu} p^\mu v^\nu \,, \tag{3.2.11}$$

If the background features spacetime symmetries associated with a Killing vector κ^μ, there exist first integrals of motion

$$C_\kappa = p_\mu \kappa^\mu - \frac{1}{2} \nabla_\nu \kappa_\mu S^{\mu\nu} \,, \tag{3.2.12}$$

which are conserved also when higher multipoles are included [155].

The system of MPD equations is undetermined, since there are 18 dynamical variables $\{X^\mu, v^\mu, p^\mu, S^{\mu\nu}\}$ (note that $S^{\mu\nu}$ is skew-symmetric) and only 15 equations of motion. One therefore needs to specify 3 additional constraints to close the system of equations. These constraints are given by choosing a spin-supplementary condition, which fixes the reference worldline with respect to which the moments are computed. We choose as a reference worldline the body's center of mass. However, in general relativity the center of mass of a

spinning body is observer-dependent, thus it is necessary to specify a reference frame by fixing, for example, the spin-supplementary condition covariantly as[1]

$$S^{\mu\nu}V_\nu = 0\,, \tag{3.2.13}$$

and by choosing V^ν as the 4-velocity of a physical observer. The representative worldline $X^\mu(\zeta)$ identifies then the center of mass measured by an observer with timelike 4-velocity V^ν (for more details see [156, 157]). Hereafter we choose the Tulczyjew-Dixon condition:

$$S^{\mu\nu}p_\nu = 0\,, \tag{3.2.14}$$

which corresponds to $V^\mu \equiv p^\mu$, i.e. we require that the center of mass is measured in the frame where $p^i = 0$. This spin condition fixes a unique worldline (see Ref. [147]), and gives a relation between the 4-velocity v^μ and the linear momentum p^μ:

$$v^\mu = \frac{\mathfrak{m}}{\mu^2}\left(p^\mu + \frac{2S^{\mu\nu}R_{\nu\rho\sigma\lambda}p^\rho S^{\sigma\lambda}}{4\mu^2 + R_{\alpha\beta\gamma\delta}S^{\alpha\beta}S^{\gamma\delta}}\right). \tag{3.2.15}$$

Moreover, as a consequence of the Tulczyjew-Dixon spin-supplementary condition, the mass μ and the spin S become constants of motion, unlike the mass term $\mathfrak{m}$. In fact

$$p_\mu S^{\mu\nu} = 0 \implies \begin{cases} \dfrac{\mathrm{d}\mu}{\mathrm{d}\tau} = \dfrac{1}{\mathfrak{m}\mu}(\nabla_{\vec{v}}p_\rho)p_\sigma\nabla_{\vec{v}}S^{\rho\sigma} = -\dfrac{1}{\mathfrak{m}\mu}(\nabla_{\vec{v}}p_\rho)(\nabla_{\vec{v}}p_\sigma)S^{\rho\sigma} = 0 \\ \dfrac{\mathrm{d}}{\mathrm{d}\tau}(S^2) = 2S_{\mu\nu}p^\mu v^\nu = 0 \end{cases}$$

To fix $\mathfrak{m}$, we first need to choose an affine parameter ζ for the MPD equations. One possible choice is setting ζ equal to the proper time τ, which guarantees that $v^\mu v_\mu = -1$ throughout the dynamics. Imposing $v^\mu v_\mu = -1$ automatically fixes $\mathfrak{m}$. Another possibility, first proposed in [155], (see also [158, 159]) consists in rescaling ζ such that

$$p^\mu v_\mu = -\mu \implies \mu = \mathfrak{m} = const\,, \tag{3.2.16}$$

which makes $\mathfrak{m}$ constant. In this case however we need to check that $v^\mu v_\mu < 0$ during the orbital evolution. This choice of the affine parameter will be labeled with $\zeta \equiv \lambda$, to differentiate it from the generic affine parameter ζ. It has been numerically shown that, by imposing the same initial conditions, λ and τ are equivalent and lead to the same worldline [158]. In the next section we will

[1] There are several possible physical spin-supplementary conditions, at least in the pole-dipole approximation. See for example Ref. [147] for a summary of the most common choices used in the literature.

also check that the condition $v^\mu v_\mu < 0$ is always satisfied for all configurations, and that it is equivalent to impose $v^\mu v_\mu = -1$ and to require that $\mathfrak{m} \in \mathbb{R}$. Finally, the conservation of the mass parameter μ in the Tulczyjew-Dixon spin-supplementary condition guarantees that the normalization $\mu^2 = -p^\mu p_\mu$ holds during the dynamical evolution.

The freedom in the choice of the spin-supplementary condition reflects the physical requirement that in classical theories particles with intrinsic angular momentum must have a finite size, and that any point of the body can be used to fix the representative worldline. Given R the size of the rotating object, it has been shown that $R \geq S/\mu$ where S/μ is the Møller radius [160]. Hence, assuming $R = S/\mu$ and denoting with $\left|R_{\mu\nu\rho\sigma}\right|$ the magnitude of the Riemann tensor, the MPD equations are valid as long as the condition $\left|R_{\mu\nu\rho\sigma}\right|^{-1} \gg (S/\mu)^2$ is satisfied, i.e if the size of the spinning secondary is much smaller than the curvature radius of the primary. For a Kerr spacetime, the Kretschmann scalar is $48M^2/r^6$ on the equatorial plane, so $\left|R_{\mu\nu\rho\sigma}\right| \approx M/r^3$. Thus, the validity condition of the MPD equations for a Kerr background becomes

$$\left(\frac{r}{M}\right)^3 \gg \left(\frac{S}{\mu M}\right)^2 . \tag{3.2.17}$$

In the following it will be useful to define the dimensionless spin parameter σ as

$$\sigma := \frac{S}{\mu M} = \chi q \,, \tag{3.2.18}$$

where $\chi = S/\mu^2$ is the reduced spin of the secondary. Regardless of the nature of the secondary, in EMRIs it is expected $|\chi| \ll 1/q$, which implies $|\sigma| \ll 1$. This also shows that Eq. (3.2.17) is always satisfied in the EMRI limit. Finally, plugging Eq. (3.2.15) into Eq. (3.2.3), it is easy to see that

$$\nabla_{\vec{v}} S^{\mu\nu} = \mathcal{O}(q) \,. \tag{3.2.19}$$

Thus, the spin tensor is parallel-transported along the worldline to leading order in the mass ratio.

3.3 Orbital motion in Kerr spacetime

In this section we review the dynamics of a spinning test particle in the Kerr spacetime, with a particular emphasis on equatorial orbits with (anti-)aligned spins, discussing new relations between orbital elements obtained in Ref. [118].

The computations in this section are valid for a generic spin parameter σ, although in the next chapters we will mostly be interested in the case $\sigma \ll 1$ which is relevant for EMRIs.

3.3.1 Field equations in the tetrad formalism and constants of motion

To describe the orbital motion in Kerr spacetime, it is convenient to introduce the following orthonormal tetrad frame (in Boyer-Lindquist coordinates)

$$e^{(0)}_\mu = \left(\sqrt{\frac{\Delta}{\Sigma}}, 0, 0, -a\sin^2\theta\sqrt{\frac{\Delta}{\Sigma}}\right) , \tag{3.3.1}$$

$$e^{(1)}_\mu = \left(0, \sqrt{\frac{\Sigma}{\Delta}}, 0, 0\right) , \tag{3.3.2}$$

$$e^{(2)}_\mu = \left(0, 0, \sqrt{\Sigma}, 0\right) , \tag{3.3.3}$$

$$e^{(3)}_\mu = \left(-\frac{a}{\sqrt{\Sigma}}\sin\theta, 0, 0, \frac{r^2+a^2}{\sqrt{\Sigma}}\sin\theta\right) . \tag{3.3.4}$$

We use the notation $e^{(a)}_\mu = (e^{(a)}_t, e^{(a)}_r, e^{(a)}_\theta, e^{(a)}_\phi)$, with the Latin indices for the tetrad components, which are raised/lowered using the flat metric

$$\eta^{ab} = \mathrm{diag}(-1,1,1,1) . \tag{3.3.5}$$

The MPD equations in the tetrad frame read

$$\frac{\mathrm{d}}{\mathrm{d}\lambda}p^{(a)} = \omega_{(b)(c)}{}^{(a)}v^{(b)}p^{(c)} - \frac{1}{2}R^{(a)}{}_{(b)(c)(d)}v^{(b)}S^{(c)(d)} , \tag{3.3.6}$$

$$\frac{\mathrm{d}}{\mathrm{d}\lambda}S^{(a)(b)} = -2v^{(e)}\omega_{(e)(c)}{}^{[(a}S^{(b)]c)} + 2p^{[(a}v^{(b)]} , \tag{3.3.7}$$

where $p^{(a)} = p^\mu e^{(a)}_\mu$ and so on, whereas $\omega_{(a)(b)}{}^{(c)} \equiv e^\mu_{(a)}e^\nu_{(b)}\nabla_\mu e^{(c)}_\nu$ are the Ricci rotation coefficients [96].
The timelike and spacelike Killing vector fields of the Kerr spacetime ($\xi^\mu = (1,0,0,0)$ and $\Xi^\mu = (0,0,0,1)$, respectively), can be written as

$$\xi^\mu = \sqrt{\frac{\Delta}{\Sigma}}\,e^\mu_{(0)} - \frac{a\sin\theta}{\sqrt{\Sigma}}\,e^\mu_{(3)} , \tag{3.3.8}$$

$$\Xi^\mu = -a\sin^2\theta\sqrt{\frac{\Delta}{\Sigma}}\,e^\mu_{(0)} + \frac{(r^2+a^2)\sin\theta}{\sqrt{\Sigma}}\,e^\mu_{(3)} . \tag{3.3.9}$$

The conserved quantities $C_\xi \equiv E$ and $C_\Xi \equiv J_z$, given by Eq. (3.2.12), are associated with ξ^μ and Ξ^μ, respectively [97]. It is important to notice that the Carter constant is no longer a first integral of motion, although an approximated, conserved quantity at $\mathcal{O}(\sigma)$ can still be found [161, 162].
It is convenient to introduce the spin vector

$$s^{(a)} \equiv -\frac{1}{2}\epsilon^{(a)(b)(c)(d)} u_{(b)} S_{(c)(d)} \,, \tag{3.3.10}$$

where $u^{(a)} = p^{(a)}/\mu$ and $\epsilon_{(a)(b)(c)(d)}$ the antisymmetric Levi-Civita tensor ($\epsilon_{(0)(1)(2)(3)} = 1$) . The spin tensor can be recast in the following form

$$S^{(a)(b)} \equiv \epsilon^{(a)(b)(c)(d)} u_{(c)} s_{(d)} \,. \tag{3.3.11}$$

Finally, we mention that the motion of a spinning particle in Kerr is generally non-integrable in the Liouville sense, unlike the non-spinning case [56, 57]. As shown in Ref. [163], chaotic motion appears even in the EMRI regime for values of the secondary spin relevant in astrophysical scenarios.

3.3.2 Equations of motion on the equatorial plane

For equatorial orbits, it can be shown that if the spin vector is parallel to the z-axis, i.e. $s^\mu = s^\theta \delta^\mu_\theta$, the spinning particle is constrained on the equatorial plane. In fact, suppose we set $s^\mu = s^\theta \delta^\mu_\theta$ as initial condition. By construction, $s^\mu p_\mu = 0$, which implies $p^\theta = 0$ and $S^{\mu\theta} = 0$. Thus, using the equations of motion (3.2.3):

$$\nabla_{\vec{v}} S^{\mu\theta} = 0 \implies p^\mu v^\theta - p^\theta v^\mu = 0 \implies p^\mu v^\theta = 0 \,, \tag{3.3.12}$$

which implies the only nontrivial solution $v^\theta = 0$. From Eq. (3.2.2), we have

$$\nabla_{\vec{v}} p^\theta = 0 \implies 0 = -\frac{1}{2} R^\theta{}_{\nu\alpha\beta} v^\nu S^{\alpha\beta} \propto \cos\theta \,, \tag{3.3.13}$$

which shows that $\theta = \pi/2$ is a solution of the equations of motion. Finally, if $\theta = \pi/2$ at $\lambda = 0$, then the initial condition $s^\mu = s^\theta \delta^\mu_\theta$ guarantees that $\theta = \pi/2$ for any value of the evolution parameter λ. Note that this property does not depend on the spin-supplementary condition.

Without loss of generality, we assume that the specific spin a of the primary is aligned to the z-axis, namely $a \geq 0$. We focus on equatorial orbits with the spin of the secondary aligned (anti-aligned) to a, i.e. $S > 0$ ($S < 0$). Hereafter, in order to simplify the notation, we introduce the hatted dimensionless quantities as

$\hat{a} = a/M$ and $\hat{r} = r/M$. We also set $s^{(2)} \equiv -S$, such that for $S > 0$ (resp. $S < 0$) the spin is parallel (resp. antiparallel) to the z-axis[2].
Using Eqs. (3.2.15),(3.2.16) and the normalization $u^{(a)}u_{(a)} = -1$, it is possible to write the velocities $v^{(a)}$ in terms of the normalized momenta $u^{(a)}$

$$v^{(0)} = \frac{1}{N}\left(1 - \frac{\sigma^2}{\hat{r}^3}\right)u^{(0)}\,, \tag{3.3.14}$$

$$v^{(1)} = \frac{1}{N}\left(1 - \frac{\sigma^2}{\hat{r}^3}\right)u^{(1)}\,, \tag{3.3.15}$$

$$v^{(3)} = \frac{1}{N}\left(1 + \frac{2\sigma^2}{\hat{r}^3}\right)u^{(3)}\,, \tag{3.3.16}$$

with $N = 1 - \frac{\sigma^2}{\hat{r}^3}\left[1 + 3\left(u^{(3)}\right)^2\right]$. Likewise, the conserved quantities can be written as [97]

$$\tilde{E} = \frac{\sqrt{\Delta}}{\hat{r}}u^{(0)} + \frac{\hat{a}\hat{r} + \sigma}{\hat{r}^2}u^{(3)}\,, \tag{3.3.17}$$

$$\tilde{J}_z = \frac{\sqrt{\Delta}}{\hat{r}}(\hat{a} + \sigma)u^{(0)} + \left[\frac{\hat{r}^2 + \hat{a}^2}{\hat{r}} + \frac{\hat{a}\sigma}{\hat{r}^2}(1 + \hat{r})\right]u^{(3)}\,, \tag{3.3.18}$$

where $\tilde{E} = E/\mu$ and $\tilde{J}_z = J_z/(\mu M)$. Since we assumed $a \geq 0$, the orbit is prograde and retrograde for $\tilde{J}_z > 0$ and $\tilde{J}_z < 0$, respectively. At infinity[3] the constant of motion J_z can be interpreted as the total angular momentum on the z-axis, i.e. the sum $J_z \approx L_z + S$ of the orbital angular momentum L_z and of the spin S of the secondary.
The above relations can be inverted to obtain $u^{(0)}$ and $u^{(3)}$ in terms of $\tilde{E}$ and $\tilde{J}_z$:

$$u^{(0)} = -\frac{\tilde{E}\hat{r}^3 + (\tilde{E}\hat{a} - \tilde{J}_z)\sigma + \hat{r}\hat{a}[\tilde{J}_z - \tilde{E}(\hat{a} + \sigma)]}{\Sigma_\sigma\sqrt{\Delta}}\,, \tag{3.3.19}$$

$$u^{(3)} = \frac{\hat{r}[\tilde{J}_z - \tilde{E}(\hat{a} + \sigma)]}{\Sigma_\sigma}\,, \tag{3.3.20}$$

where

$$\Sigma_\sigma = \hat{r}^2\left(1 - \frac{\sigma^2}{\hat{r}^3}\right) > 0\,, \tag{3.3.21}$$

[2] In spherical coordinates on the equatorial plane, ∂_θ and ∂_z are anti-aligned, therefore $s^{(2)} = rs^\theta < 0$ means that the spin is aligned to ∂_z, and so to the spin of the primary.

[3] Or, equivalently, in the weak-field and slow-motion regime (see Appendix B of Ref. [164] for details).

which is positive due to the constraint (3.2.17). Using Eqs. (3.3.19)-(3.3.20) and the relations between the velocities $v^{(a)}$ and the normalized momenta $u^{(a)}$ [Eqs. (3.3.14)-(3.3.16)], we can write the equations of motion in Boyer-Lindquist coordinates as (see also Ref. [97])

$$\Sigma_\sigma \Lambda_\sigma \frac{\mathrm{d}\hat{t}}{\mathrm{d}\hat{\lambda}} = \hat{a}\left(1+\frac{3\sigma^2}{\hat{r}\Sigma_\sigma}\right)[\tilde{J}_z - \tilde{E}(\hat{a}+\sigma)] + \frac{\hat{r}^2+\hat{a}^2}{\Delta}P_\sigma \,, \tag{3.3.22}$$

$$(\Sigma_\sigma \Lambda_\sigma)^2 \left(\frac{\mathrm{d}\hat{r}}{\mathrm{d}\hat{\lambda}}\right)^2 = R_\sigma^2 \,, \tag{3.3.23}$$

$$\Sigma_\sigma \Lambda_\sigma \frac{\mathrm{d}\phi}{\mathrm{d}\hat{\lambda}} = \left(1+\frac{3\sigma^2}{\hat{r}\Sigma_\sigma}\right)[\tilde{J}_z - \tilde{E}(\hat{a}+\sigma)] + \frac{\hat{a}}{\Delta}P_\sigma \,, \tag{3.3.24}$$

where

$$\Lambda_\sigma = 1 - \frac{3\sigma^2\hat{r}[-(\hat{a}+\sigma)\tilde{E}+\tilde{J}_z]^2}{\Sigma_\sigma^3} \,, \tag{3.3.25}$$

$$R_\sigma = P_\sigma^2 - \Delta\left(\frac{\Sigma_\sigma^2}{\hat{r}^2} + [-(\hat{a}+\sigma)\tilde{E}+\tilde{J}_z]^2\right) \,, \tag{3.3.26}$$

$$P_\sigma = \left[(\hat{r}^2+\hat{a}^2) + \frac{\hat{a}\sigma}{\hat{r}}(\hat{r}+1)\right]\tilde{E} - \left[\hat{a}+\frac{\sigma}{\hat{r}}\right]\tilde{J}_z \,, \tag{3.3.27}$$

and $\frac{1}{\hat{r}^2}\Sigma_\sigma\Lambda_\sigma = N$. A study of eccentric solutions of the above equations of motion can be found in Ref. [165]. Note that Eqs. (3.3.25)-(3.3.27) have the same structure of the equations of motion for a non-spinning particle in equatorial motion [(1.2.8)-(1.2.10)]. In the case of spin (anti)-aligned, equatorial motion, the system is sufficiently constrained to be integrable in the Liouville sense, at least with the Tulczyjew-Dixon supplementary spin-condition [165].

As previously discussed, condition (3.2.16) does not necessarily imply $v^{(a)}v_{(a)} < 0$ and the latter condition must be checked during the dynamics. We now show that the norm of the four velocity $v^{(a)}$ is always negative in EMRIs for realistic values of the secondary spin [118]. The norm of $v^{(a)}$ reads

$$v^{(a)}v_{(a)} = \frac{-\hat{r}^6 + 3\sigma^2(u^{(3)})^2(2\hat{r}^3+\sigma^2) + 2\sigma^2\hat{r}^3 - \sigma^4}{(\hat{r}^3 N)^2} \,,$$

and the constraint $v^{(a)}v_{(a)} < 0$ leads to

$$\Lambda_\sigma > \frac{\hat{r}^3+2\sigma^2}{2\hat{r}^3+\sigma^2} \,. \tag{3.3.28}$$

Equation (3.3.28) shows that Λ_σ must be positive definite, which implies $N > 0$. Moreover, for realistic values of σ (recall that $|\sigma| \ll 1$ when $|\chi| \ll 1/q$, see Eq. (3.2.18)) the constraint (3.3.28) reduces to

$$\Lambda_\sigma \gtrsim \frac{1}{2} \quad \text{for} \quad \sigma \ll 1 \tag{3.3.29}$$

and, since $\hat{E}$ and $\hat{J}_z$ are usually $\mathcal{O}(1)$ during the dynamics, $\Lambda_\sigma \approx 1$ for $\sigma \ll 1$. Thus Eq. (3.3.28) is always satisfied for bound equatorial EMRIs. Finally, we note that choosing the proper time of the object as evolution parameter, the condition $v^{(a)}v_{(a)} = -1$ fixes the kinematical mass $\mathfrak{m}$ as

$$\mathfrak{m}(\hat{r}) = \frac{\hat{r}^3 N}{\sqrt{\hat{r}^6 - 3\sigma^2 (u^{(3)})^2 (2\hat{r}^3 + \sigma^2) - 2\sigma^2 \hat{r}^3 + \sigma^4}} \,. \tag{3.3.30}$$

Imposing that $\mathfrak{m}(\hat{r})$ is a real number gives again the constraint (3.3.28).

3.3.3 Effective potential, ISCO, and orbital frequency

We now consider the case of circular, equatorial motion. For circular orbits, there are two additional constraints on the motion: one enforces zero radial velocity, the other requires zero radial acceleration. The condition $v^r = 0$ implies $v^{(1)} = 0$ and, together with Eq. (3.3.15) yields $p^{(1)} = 0$, whereas zero radial acceleration requires $\frac{\mathrm{d}}{\mathrm{d}\lambda} p^{(1)} = 0$. Imposing these constraints is equivalent to ask the orbital radius to be the local minimum of an effective potential. For a spinning particle moving on the equatorial plane of a Kerr BH, the effective potential depends on the spin-supplementary condition (see Refs. [101, 111] for the form of the effective potentials for some common choices of the spin-supplementary conditions). Following Ref. [166] we use

$$V_\sigma(\hat{r}) = \frac{1}{\hat{r}^4}(\alpha_\sigma \tilde{E}^2 - 2\beta_\sigma \tilde{E} + \gamma_\sigma) \,, \tag{3.3.31}$$

where

$$\alpha_\sigma = \left[\hat{r}^2 + \hat{a}^2 + \frac{\hat{a}\sigma(\hat{r}+1)}{\hat{r}}\right]^2 - \Delta(\hat{a}+\sigma)^2 \,, \tag{3.3.32}$$

$$\beta_\sigma = \left[\left(\hat{a} + \frac{\sigma}{\hat{r}}\right)\left(\hat{r}^2 + \hat{a}^2 + \frac{\hat{a}\sigma(\hat{r}+1)}{\hat{r}}\right) - \Delta(\hat{a}+\sigma)\right]\tilde{J}_z \,, \tag{3.3.33}$$

$$\gamma_\sigma = \left(\hat{a} + \frac{\sigma}{\hat{r}}\right)^2 \tilde{J}_z^2 - \Delta\left[\hat{r}^2\left(1 - \frac{\sigma^2}{\hat{r}^3}\right)^2 + \tilde{J}_z^2\right] . \tag{3.3.34}$$

The effective potential reduces to the standard one for a nonspinning particle in Kerr when $\sigma = 0$. The condition for a circular orbit with radius $\hat{r}_0$ translates to

$$V_\sigma(\hat{r}_0) = 0\,, \qquad \left.\frac{\mathrm{d}V_\sigma}{\mathrm{d}\hat{r}}\right|_{\hat{r}=\hat{r}_0} = 0\,,$$

and stability of such orbits against radial perturbations requires $\left.\frac{\mathrm{d}^2V_\sigma}{\mathrm{d}\hat{r}^2}\right|_{\hat{r}=\hat{r}_0} < 0$, although the orbit might still be unstable under perturbation in the θ direction [167]. The innermost stable circular orbit (ISCO) is obtained by imposing $\left.\frac{\mathrm{d}^2V_\sigma}{\mathrm{d}\hat{r}^2}\right|_{\hat{r}=\hat{r}_0} = 0$.

The orbital frequency of a circular equatorial orbit as measured by an observer located at infinity,

$$\widehat{\Omega} = M\Omega = \frac{\mathrm{d}\phi}{\mathrm{d}\hat{t}} = \frac{\hat{a}v^{(0)} + \sqrt{\Delta}v^{(3)}}{(\hat{r}^2+\hat{a}^2)v^{(0)} + \hat{a}\sqrt{\Delta}v^{(3)}}\,.$$

In terms of the momenta, $\widehat{\Omega}$ is given by

$$\widehat{\Omega} = \frac{\hat{a}(\hat{r}^3-\sigma^2)u^{(0)} + \sqrt{\Delta}(\hat{r}^3+2\sigma^2)u^{(3)}}{(\hat{r}^2+\hat{a}^2)(\hat{r}^3-\sigma^2)u^{(0)} + \hat{a}\sqrt{\Delta}(\hat{r}^3+2\sigma^2)u^{(3)}}\,, \tag{3.3.35}$$

where $u^{(0)}$ and $u^{(3)}$ are given in terms of $\hat{r}$ by solving $\frac{\mathrm{d}}{\mathrm{d}\lambda}p^{(1)} = 0$:

$$u^{(0)} = \frac{1}{\sqrt{1-U_\mp^2}}\,, \qquad u^{(3)} = \frac{U_\mp}{\sqrt{1-U_\mp^2}}\,, \tag{3.3.36}$$

where [99]

$$U_\mp = \frac{u^{(3)}}{u^{(0)}} = -\frac{2\hat{a}\hat{r}^3 + 3\sigma\hat{r}^2 + \hat{a}\sigma^2 \mp \mathcal{D}}{2\sqrt{\Delta}(\hat{r}^3+2\sigma^2)}\,, \tag{3.3.37}$$

with

$$\mathcal{D} = \sqrt{4\hat{r}^7 + 12\hat{a}\sigma\hat{r}^5 + 13\sigma^2\hat{r}^4 + 6\hat{a}\sigma^3\hat{r}^2 - 8\sigma^4\hat{r} + 9\hat{a}^2\sigma^4}\,, \tag{3.3.38}$$

and the $\mp$ sign corresponding to co-rotating and counter-rotating orbits, respectively. Note that the argument of the square root is not positive definitive for generic values of σ. Nevertheless, for $\sigma \ll 1$, it is easy to see that Eq. (3.3.37) is always real. Using Eq. (3.3.36), the orbital frequency $\widehat{\Omega}$ can be recast as

$$\widehat{\Omega} = \frac{(2\hat{a}+3\sigma)\hat{r}^3 + 3(2\hat{a}^2\sigma + \hat{a}\sigma^2)\hat{r} + 4\hat{a}\sigma^2 \mp \hat{r}\mathcal{D}}{2(\hat{a}^2+3\hat{a}\sigma+\sigma^2)\hat{r}^3 + 6\sigma(\hat{a}+\sigma)\hat{a}^2\hat{r} + 4\hat{a}^2\sigma^2 - 2\hat{r}^6}\,. \tag{3.3.39}$$

This formula agrees with the one shown in Ref. [110].
Plugging Eq. (3.3.36) into Eqs. (3.3.17)-(3.3.18) finally yields the first integrals $\tilde{E}$ and $\tilde{J}_z$ for a spinning object in circular equatorial orbit in the Kerr spacetime:

$$\tilde{E} = \frac{\hat{r}\sqrt{\Delta} + (\hat{a}\hat{r} + \sigma)U_{\mp}}{\hat{r}^2\sqrt{1 - U_{\mp}^2}}\,, \tag{3.3.40}$$

$$\tilde{J}_z = \frac{\hat{r}\sqrt{\Delta}(\hat{a} + \sigma) + [\hat{r}^3 + \hat{r}\hat{a}(\hat{a} + \sigma) + \hat{a}\sigma]U_{\mp}}{\hat{r}^2\sqrt{1 - U_{\mp}^2}}\,. \tag{3.3.41}$$

The minus and plus sign in Eq. (3.3.39)-(3.3.41) correspond to prograde and retrograde orbits, respectively. To be the best of our knowledge, expressions (3.3.40) and (3.3.41) were shown for the first time in [118].
Since for EMRIs $|\sigma| \ll 1$, it is convenient to expand $\tilde{E}$, $\tilde{J}_z$ and $\widehat{\Omega}$ in terms of the spin parameters, considering linear corrections only, such that at first order in σ:

$$\tilde{E} = \tilde{E}^0 + \sigma\tilde{E}^1 \quad , \quad \tilde{J}_z = \tilde{J}_z^0 + \sigma\tilde{J}_z^1\,, \tag{3.3.42}$$

with

$$\tilde{E}^0 = \frac{\pm\hat{a} + (\hat{r} - 2)\hat{r}^{1/2}}{\hat{r}^{3/4}\Delta_{\pm}}\,, \tag{3.3.43}$$

$$\tilde{E}^1 = \frac{(\hat{a} \mp \sqrt{\hat{r}})(3\hat{a}^2 \mp 4\sqrt{\hat{r}} + \hat{r}^2)}{2\hat{r}^{11/4}\Delta_{\pm}^3}\,, \tag{3.3.44}$$

$$\tilde{J}_z^0 = \pm\frac{\hat{r}^2 + \hat{a}^2 \mp 2\hat{a}\sqrt{\hat{r}}}{\hat{r}^{3/4}\Delta_{\pm}}\,, \tag{3.3.45}$$

$$\tilde{J}_z^1 = \frac{1}{2\hat{r}^{11/4}\Delta_{\pm}^3}\Big(3\hat{a}^4 \pm \sqrt{\hat{r}}(3\hat{r} - 7)(\hat{a}^3 + 3\hat{a}\hat{r}^2) + \\ + 2\hat{a}^2\hat{r}(\hat{r} + 2) + \hat{r}^3(\hat{r} - 2)(2\hat{r} - 9)\Big)\,, \tag{3.3.46}$$

where $\Delta_{\pm} = \sqrt{\pm 2\hat{a} + (\hat{r} - 3)\sqrt{\hat{r}}}$, and the upper (lower) sign corresponds to prograde (retrograde) orbits [166]. The orbital frequency can be written as

$$\widehat{\Omega}(\hat{r}) = \widehat{\Omega}^0(\hat{r}) + \sigma\widehat{\Omega}^1(\hat{r}) + \mathcal{O}(\sigma^2)\,, \tag{3.3.47}$$

where $\widehat{\Omega}^0(\hat{r}) = 1/(\hat{a} \pm \hat{r}^{3/2})$ is the orbital frequency of a nonspinning particle around Kerr, and

$$\widehat{\Omega}^1(\hat{r}) = -\frac{3}{2}\frac{\sqrt{\hat{r}} \mp \hat{a}}{\sqrt{\hat{r}}(\hat{r}^{3/2} \pm a)^2}\,. \tag{3.3.48}$$

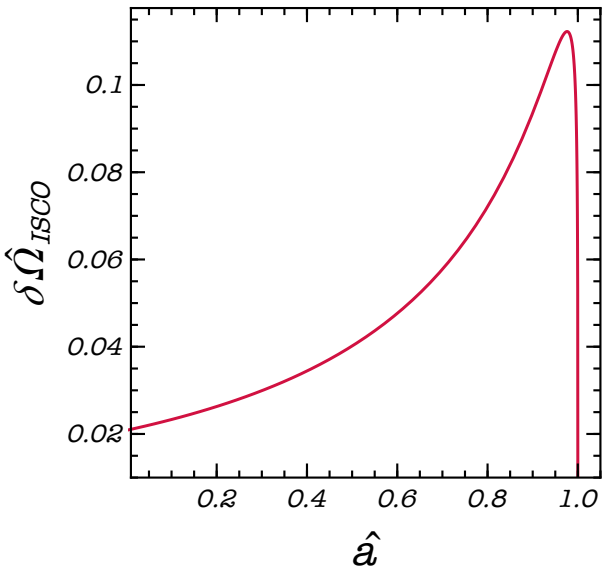

Figure 3.1: Spin correction to the orbital frequency at the ISCO as a function of $\hat{a}$ for prograde orbits (upper sign Eq. (3.3.50))

In the next chapter we will exploit the linear expansions for $\tilde{E}$, $\tilde{J}$ and $\widehat{\Omega}$ to compute the GW fluxes and the waveforms at $\mathcal{O}(\sigma)$ order.
The ISCO location can be expanded in the same way and its leading-order spin correction reads

$$\delta\hat{r}_{\rm ISCO} = \frac{4\hat{a}}{\hat{r}^0_{\rm ISCO}} \mp \frac{4}{\sqrt{\hat{r}^0_{\rm ISCO}}}\,, \tag{3.3.49}$$

where $\hat{r}^0_{\rm ISCO}$ is the (normalized) ISCO location of the Kerr metric for a nonspinning secondary, which is solution to $\hat{r}^2 - 6\hat{r} + 8\hat{a}\hat{r}^{1/2} - 3\hat{a}^2 = 0$ (its analytical expression as a function of $\hat{a}$ can be found in Ref. [168]). Using the above results, the leading-order spin correction to the ISCO orbital frequency is

$$\delta\widehat{\Omega}_{\rm ISCO} = \frac{9}{2}\left(\frac{\sqrt{\hat{r}^0_{\rm ISCO}} \mp \hat{a}}{\sqrt{\hat{r}^0_{\rm ISCO}}\left((\hat{r}^0_{\rm ISCO})^{3/2} \pm \hat{a}\right)^2}\right)\,. \tag{3.3.50}$$

This quantity is shown in Fig. 3.1 as a function of $\hat{a}$ for prograde orbits (upper sign Eq. (3.3.50)). Note that $\delta\widehat{\Omega}_{\rm ISCO} > 0$ for any $\hat{a}$ (being zero in the extremal case), i.e., if the spin of the secondary is aligned to that of the primary the orbital frequency at the ISCO is higher.

Chapter 4

GW fluxes in EMRIs with spinning secondaries

The last ingredient needed to study the orbital evolution of EMRI with spinning particles is given by the emission of gravitational radiation, which drives the binary coalescence. Key to this chapter is the so-called *Teukolsky formalism*, which allows to derive the scalar, vector and metric wave perturbations of the Kerr spacetime from the solutions ψ_s of the Teukolsky master equation (2.2.3). As seen in chapter 2, ψ_s are the linear order perturbations of geometrical scalars defined in the Newman-Penrose formalism. All nontrivial degrees of freedom of outgoing gravitational radiation are encoded in Ψ_4^b. From the latter, one can determine the waveform observed far away from the source as well as the fluxes of energy and angular momentum carried away by GW. Instead of solving directly the partial differential equation (2.2.3), we consider an equivalent system of two decoupled ordinary differential equations, known as the *Teukolsky equations*, obtained from a suitable ansatz for Ψ_4^b. The gravitational signal is then given as a mode of sum in the frequency domain of functions that obey the Teukolsky equations.

Since for EMRIs $\sigma \sim q \ll 1$ (see chapter 3), the GW flux receives a subleading contribution from the smaller companion spin, which is $\mathcal{O}(\sigma)$ compared to leading order. Nonetheless, the spin-induced dissipative term give rise to relevant effects on the GW phase (see chapters 1 and 5) which accumulates during the long EMRI inspiral. To obtain waveforms accurate at 1st post-adiabatic level, it is sufficient to compute the corrections to the fluxes at linear order in σ [54].

We present in this chapter our work on the asymptotic GW fluxes from spinning secondaries in the case of circular equatorial motion with aligned spins, published in Piovano et *al* [118] and Piovano et *al* [169]. In the former we solved

the Teukolsky equations in the frequency domain to compute the exact fluxes at all orders in the secondary spin. Then, we extracted the corrections at $\mathcal{O}(\sigma)$ order to the fluxes $\delta\mathcal{F}^{\sigma}(\hat{r})$. In the follow-up work [169] we expanded the Teukolsky equations in terms of σ, obtaining semi-analytic expressions $\mathcal{F}^{1}(\hat{r})$ for the leading order corrections to the gravitational fluxes. This formulation represents a novel result, and provides a major improvement upon our previous works and approaches known in literature so far. Indeed, the corrections $\mathcal{F}^{1}(\hat{r})$ are crucial to develop fast and accurate EMRI waveforms to be used to perform parameter estimations of the secondary spin with a Fisher matrix approach. We refer the reader to the next chapter for more information.
The Teukolsky formalism for metric perturbations is illustrated in Section 4.1, with the original work on the spin-dependent fluxes presented in Sec. 4.2. All technical details are available in appendices A, C and E. In Section 4.3 we outline the computation of $\mathcal{F}^{1}(\hat{r})$, whereas a thorough derivation of the corrections and of the linear expansion in σ of Teukolsky equations are shown in the appendices B and D.
For sake of clarity, we summarize here the content of all the appendices mentioned above:

- Appendices A and B introduce two of three approaches employed to solve the homogeneous radial Teukolsky equation, the Sasaki-Nakamura and the hyperboloidal slicing coordinates methods. For both methods, we derived novel, accurate boundary conditions in terms of recursion relations.
- Appendix. C provides a detailed computation of the generic source term of the Teukolsky equation for spinning test-particles in bound motion.
- The thorough derivation of the linear expansion in σ of the Teukolsky equations and GW fluxes is showed in appendix D.
- Finally, appendix E provides a comparison of the GW fluxes with results previously obtained in literature.

4.1 GW fluxes in the Teukolsky formalism

From the partial differential equation (2.2.3), we can be obtained a set of two decoupled ordinary differential equations by means of separation of variables in Fourier space

$$\psi_s = \sum_{\ell=2}^{\infty} \sum_{m=-\ell}^{\ell} \int_{-\infty}^{\infty} \mathrm{d}\hat{\omega}\, {}_sR_{\ell m\hat{\omega}}(\hat{r})\, {}_sS^{\hat{a}\hat{\omega}}_{\ell m}(\theta) e^{i(m\phi-\hat{\omega}\hat{t})} \,. \tag{4.1.1}$$

The functions ${}_sS^{\hat{a}\hat{\omega}}_{\ell m}(\theta)$ and ${}_sR_{\ell m\hat{\omega}}(\hat{r})$ are the angular and radial components of ψ_s respectively, in the frequency domain. We keep the helicity of the pertubation s general, and we will specialize later on to outgoing gravitational radiation, i.e with $s=-2$.
${}_sS^{\hat{a}\hat{\omega}}_{\ell m}$ are the spin-weighted spheroidal harmonics[1], which obey the angular Teukolsky equation

$$\left[\frac{1}{\sin\theta}\frac{\mathrm{d}}{\mathrm{d}\theta}\left(\sin\theta\frac{\mathrm{d}}{\mathrm{d}\theta}\right)-c^2\sin^2\theta-\left(\frac{m+s\cos\theta}{\sin\theta}\right)^2+\right.$$
$$\left.-2cs\cos\theta+s+2mc\right]{}_sS^c_{\ell m}=-{}_s\lambda_{\ell m\hat{\omega}}{}_sS^c_{\ell m}\,, \tag{4.1.2}$$

with $c\equiv\hat{a}\hat{\omega}$ and ${}_s\lambda_{\ell m\hat{\omega}}={}_sE_{\ell m\hat{\omega}}-2mc+c^2-s(s+1)$ with ${}_sE_{\ell m\hat{\omega}}$ the separation constant. The eigenvalues and the eigenfunctions satisfy the following identities:

$$\begin{aligned}{}_s\lambda_{\ell m-\hat{\omega}}&={}_s\lambda_{\ell-m\hat{\omega}}\,,\\ {}_s\lambda_{\ell m\hat{\omega}}&={}_{-s}\lambda_{\ell m\hat{\omega}}-2s\,,\end{aligned}$$

and

$$\begin{aligned}{}_{-2}S^{-c}_{\ell-m}(\theta)&=(-1)^{\ell+s}{}_sS^c_{\ell m}(\pi-\theta)\,,\\ {}_sS^c_{\ell m}(\theta)&=(-1)^{\ell+m}{}_{-s}S^c_{\ell m}(\pi-\theta)\,,\end{aligned}$$

For specific values of $\hat{a},\hat{\omega}$ and s, the spin-weighted spheroidal harmonics and their eigenvalues reduce to known functions:

- for either $\hat{a}=0$ or $\hat{\omega}=0$, ${}_sS^{\hat{a}\hat{\omega}}_{\ell m}(\theta)e^{im\phi}$ reduces to the spin-weighted spherical harmonics with ${}_s\lambda_{\ell m\hat{\omega}}\equiv\ell(\ell+1)-s(s+1)$
- for $s=0$, ${}_sS^{\hat{a}\hat{\omega}}_{\ell m}(\theta)e^{im\phi}$ reduces to the spheroidal harmonics [170]
- finally, for either $\hat{a}=0$ or $\hat{\omega}=0$ and $s=0$, ${}_sS^{\hat{a}\hat{\omega}}_{\ell m}(\theta)e^{im\phi}$ reduces to the well known spherical harmonics with ${}_0\lambda_{\ell m\hat{\omega}}\equiv\ell(\ell+1)$

The functions ${}_sS^c_{\ell m}(\theta)e^{im\phi}$ are orthonormal and form complete set [171]

$$\int\sin\theta\mathrm{d}\theta\mathrm{d}\phi\,{}_sS^c_{\ell m}(\theta)\,{}_sS^c_{\ell'm'}(\theta)e^{i\phi(m-m')}=\delta_{\ell\ell'}\delta_{mm'}\,, \tag{4.1.3}$$

[1] Here the term "spin" refer to the helicity of the perturbation.

The radial function ${}_sR_{\ell m\hat{\omega}}(\hat{r})$ obeys the radial Teukolsky equation

$$\left[\Delta^{-s}\frac{\mathrm{d}}{\mathrm{d}\hat{r}}\left(\Delta^{s+1}\frac{\mathrm{d}}{\mathrm{d}\hat{r}}\right)-V(\hat{r})\right]{}_sR_{\ell m\hat{\omega}}(\hat{r})={}_s\mathcal{T}_{\ell m\hat{\omega}}\,, \tag{4.1.4}$$

where the source term ${}_s\mathcal{T}_{\ell m\hat{\omega}}$ is discussed below and the potential $V(\hat{r})$ reads

$$V(\hat{r})=-\frac{K^2-2is(\hat{r}-1)K}{\Delta}-4is\hat{\omega}\hat{r}+{}_s\lambda_{\ell m\hat{\omega}}\,, \tag{4.1.5}$$

$$K=(\hat{r}^2+\hat{a}^2)\hat{\omega}-\hat{a}m\,. \tag{4.1.6}$$

The homogeneous radial Teukolsky equation admits two linearly independent solutions, ${}_sR^{\rm in}_{\ell m\hat{\omega}}$ and ${}_sR^{\rm up}_{\ell m\hat{\omega}}$, with the following asymptotic values at horizon $\hat{r}_+$ and at infinity:

$${}_sR^{\rm in}_{\ell m\hat{\omega}}\sim\begin{cases}B^{\rm tran}_{\ell m\hat{\omega}}\Delta^{-s}e^{-i\hat{\kappa}\hat{r}^*} & \hat{r}\to\hat{r}_+\,,\\ B^{\rm out}_{\ell m\hat{\omega}}\hat{r}^{-1-2s}e^{i\hat{\omega}\hat{r}^*}+B^{\rm in}_{\ell m\hat{\omega}}\hat{r}^{-1}e^{-i\hat{\omega}\hat{r}^*} & \hat{r}\to\infty\,,\end{cases} \tag{4.1.7}$$

$${}_sR^{\rm up}_{\ell m\hat{\omega}}\sim\begin{cases}D^{\rm out}_{\ell m\hat{\omega}}e^{i\hat{\kappa}\hat{r}^*}+D^{\rm in}_{\ell m\hat{\omega}}\Delta^{-s}e^{-i\hat{\kappa}\hat{r}^*} & \hat{r}\to\hat{r}_+\,,\\ D^{\rm tran}_{\ell m\hat{\omega}}\hat{r}^{-1-2s}e^{i\omega\hat{r}^*} & \hat{r}\to\infty\,,\end{cases} \tag{4.1.8}$$

where $\hat{\kappa}=\hat{\omega}-m\hat{\omega}_+$, $\hat{r}_\pm=1\pm\sqrt{1-\hat{a}^2}$, $\hat{\omega}_+=\hat{a}/(2\hat{r}_+)$, and being $\hat{r}^*$ the tortoise coordinate of the Kerr metric,

$$\hat{r}^*=\hat{r}+\frac{2\hat{r}_+}{\hat{r}_+-\hat{r}_-}\ln\left(\frac{\hat{r}-\hat{r}_+}{2}\right)-\frac{2r_-}{r_+-\hat{r}_-}\ln\left(\frac{\hat{r}-\hat{r}_-}{2}\right). \tag{4.1.9}$$

Through the Green function method [172], we can write the inhomogeneous solution of radial Teukolsky equation with the correct asymptotics

$$\begin{aligned}{}_sR_{\ell m\hat{\omega}}(\hat{r})=&{}_sR^{\rm up}_{\ell m\hat{\omega}}(\hat{r})\int_{\hat{r}_+}^{\hat{r}}\mathrm{d}\hat{r}'\,\frac{{}_sR^{\rm in}_{\ell m\hat{\omega}}(\hat{r}')\,{}_s\mathcal{T}_{\ell m\hat{\omega}}(\hat{r}')}{\Delta^2W_{\hat{r}}}\\&+{}_sR^{\rm in}_{\ell m\hat{\omega}}(\hat{r})\int_{\hat{r}}^{\infty}\mathrm{d}\hat{r}'\,\frac{{}_sR^{\rm up}_{\ell m\hat{\omega}}(\hat{r}')\,{}_s\mathcal{T}_{\ell m\hat{\omega}}(\hat{r}')}{\Delta^2W_{\hat{r}}}\,,\end{aligned} \tag{4.1.10}$$

with the constant Wronskian given by

$$W_{\hat{r}}\equiv\Delta^{s+1}\left({}_sR^{\rm in}_{\ell m\hat{\omega}}\frac{\mathrm{d}\,{}_sR^{\rm up}_{\ell m\hat{\omega}}}{\mathrm{d}\hat{r}^*}-{}_sR^{\rm up}_{\ell m\hat{\omega}}\frac{\mathrm{d}\,{}_sR^{\rm in}_{\ell m\hat{\omega}}}{\mathrm{d}\hat{r}^*}\right)=2i\hat{\omega}B^{\rm in}_{\ell m\hat{\omega}}D^{\rm tran}_{\ell m\hat{\omega}}\,. \tag{4.1.11}$$

The solution is purely outgoing at infinity and purely ingoing at the horizon:

$$ {}_sR_{\ell m\hat{\omega}}(\hat{r}\to\hat{r}_+) = {}_sZ^{\infty}_{\ell m\hat{\omega}}\Delta^{-s}e^{-i\hat{\kappa}\hat{r}^*}\,, \tag{4.1.12} $$

$$ {}_sR_{\ell m\hat{\omega}}(\hat{r}\to\infty) = {}_sZ^{H}_{\ell m\hat{\omega}}\hat{r}^{-1-2s}e^{i\hat{\omega}\hat{r}^*}\,, \tag{4.1.13} $$

with

$$ {}_sZ^{\infty}_{\ell m\hat{\omega}} = C^{\infty}_{\ell m\hat{\omega}}\int_{\hat{r}_+}^{\infty}\mathrm{d}\hat{r}'\,\frac{{}_sR^{\rm up}_{\ell m\hat{\omega}}(\hat{r}')}{\Delta^2}\,{}_s\mathcal{T}_{\ell m\hat{\omega}}(\hat{r}')\,, \tag{4.1.14} $$

$$ {}_sZ^{H}_{\ell m\hat{\omega}} = C^{H}_{\ell m\hat{\omega}}\int_{\hat{r}_+}^{\infty}\mathrm{d}\hat{r}'\,\frac{{}_sR^{\rm in}_{\ell m\hat{\omega}}(\hat{r}')}{\Delta^2}\,{}_s\mathcal{T}_{\ell m\hat{\omega}}(\hat{r}')\,, \tag{4.1.15} $$

and

$$ C^{H}_{\ell m\hat{\omega}} \equiv \frac{D^{\rm tran}_{\ell m\hat{\omega}}}{W_{\hat{r}}} = \frac{1}{2i\hat{\omega}B^{\rm in}_{\ell m\omega}}\,, \qquad C^{\infty}_{\ell m\hat{\omega}} \equiv \frac{B^{\rm tran}_{\ell m\hat{\omega}}}{W_{\hat{r}}} = \frac{B^{\rm tran}_{\ell m\hat{\omega}}}{2i\hat{\omega}B^{\rm in}_{\ell m\hat{\omega}}D^{\rm tran}_{\ell m\hat{\omega}}}\,. \tag{4.1.16} $$

The amplitudes ${}_sZ^{H}_{\ell m\hat{\omega}}$ and ${}_sZ^{\infty}_{\ell m\hat{\omega}}$ fully determine the asymptotic GW fluxes at infinity and at the horizon. The factors $B^{\rm tran}_{\ell m\hat{\omega}}$ and $D^{\rm tran}_{\ell m\hat{\omega}}$ are arbitrary, but there are two convenient ways to fix their values, shown in sections 4.2 and 4.3. The source term ${}_s\mathcal{T}_{\ell m\hat{\omega}}$ of the radial Teukolsky equation is rather cumbersome, even for nonspinning bodies. For generic bound orbits, the source term is given by

$$ {}_sZ^{H,\infty}_{\ell m\hat{\omega}} = C^{H,\infty}_{\ell m\hat{\omega}}\int_{-\infty}^{\infty}\mathrm{d}\hat{t}\,e^{i(\hat{\omega}\hat{t}-m\phi(\hat{t}))}\,{}_s\mathcal{I}^{H,\infty}\left[\hat{r}(\hat{t}),\theta(\hat{t})\right]\,, \tag{4.1.17} $$

where ${}_s\mathcal{I}^{H,\infty}\left[\hat{r}(\hat{t}),\theta(\hat{t})\right]$ is

$$ \begin{aligned} {}_s\mathcal{I}^{H,\infty}\left[\hat{r}(\hat{t}),\theta(\hat{t})\right] = \Bigg[&A_0 - (A_1+B_1)\frac{\mathrm{d}}{\mathrm{d}\hat{r}} + (A_2+B_2)\frac{\mathrm{d}^2}{\mathrm{d}\hat{r}^2} - B_3\frac{\mathrm{d}^3}{\mathrm{d}\hat{r}^3} \\ &+ (A_2+B_2)\frac{\mathrm{d}^2}{\mathrm{d}\hat{r}^2} - B_3\frac{\mathrm{d}^3}{\mathrm{d}\hat{r}^3}\Bigg]\,{}_sR^{\rm in,up}_{\ell m\hat{\omega}}\Big|_{\theta=\theta(\hat{t}),\hat{r}=\hat{r}(\hat{t})}\,. \end{aligned} \tag{4.1.18} $$

The terms B_1, B_2 and B_3 are due to the secondary spin components of the stress-energy tensor. Such terms are zero for a spinless particle and highly non-linear in σ. For the case of gravitational perturbations, the explicit form of (4.1.18) together with related technical details are given in Appendix (C) [e.g., Eq. (C.1.51)].

We now focus on gravitational radiation, fixing $s = -2$ and show how to compute the GW fluxes at infinity and the horizon of the primary. At infinity, the

two GW polarizations are both encoded in the linear perturbation of the Weyl scalar Ψ_4^b:

$$\Psi_4^b = (\hat{r} - i\hat{a}\cos\theta)^{-4}\psi_{-2} \sim \frac{1}{2}\frac{\partial^2}{\partial \hat{t}^2}(h_+ - ih_\times) \qquad \text{for } \hat{r} \to \infty\,. \tag{4.1.19}$$

Equations. (4.1.1) and (4.1.15) with $s = -2$ lead to the gravitational-wave signal at $\hat{r} \to \infty$

$$h_+ - ih_\times \sim -\frac{2}{\hat{r}}\sum_{\ell m}\int_{-\infty}^{\infty}\frac{\mathrm{d}\hat{\omega}}{\hat{\omega}^2}\,{}_{-2}Z^H_{\ell m\hat{\omega}}e^{i\hat{\omega}(\hat{r}^*-\hat{t})}\,{}_{-2}S^{\hat{a}\hat{\omega}}_{\ell m}(\vartheta)e^{im\varphi}\,, \tag{4.1.20}$$

where ϑ is the angle between the observer's line of sight and the spin axis of the primary (here aligned with the z-axis), while $\varphi \equiv \phi(\hat{t} = 0)$.
For a circular equatorial orbit, the form of the source term greatly simplifies and, since $\phi(\hat{t}) = \widehat{\Omega}\hat{t}$, Eq. (4.1.17) reduces to

$${}_{-2}Z^{H,\infty}_{\ell m\hat{\omega}} = 2\pi\delta(\hat{\omega} - m\widehat{\Omega})C^{H,\infty}_{\ell m\hat{\omega}}\,{}_{-2}\mathcal{I}^{H,\infty}(\hat{r}_0, \pi/2)\,, \tag{4.1.21}$$

computed for a specific orbital radius $\hat{r}_0$. In this case the waveform (4.1.20) reduces to

$$h_+ - ih_\times \sim -\frac{2}{\hat{r}}\sum_{\ell m}\frac{{}_{-2}Z^H_{\ell m\hat{\omega}}}{(m\widehat{\Omega})^2}e^{im\widehat{\Omega}(\hat{r}^*-\hat{t})}\,{}_{-2}S^c_{\ell m}(\vartheta)e^{im\varphi}\,, \tag{4.1.22}$$

where for simplicity, we have redefined

$${}_{-2}Z^{H,\infty}_{\ell m\hat{\omega}} \equiv 2\pi C^{H,\infty}_{\ell m\hat{\omega}}\,{}_{-2}\mathcal{I}^{H,\infty}(\hat{r}_0, \pi/2)\,, \tag{4.1.23}$$

The GW energy fluxes are given by

$$\left(\frac{\mathrm{d}\tilde{E}}{\mathrm{d}\hat{A}\mathrm{d}\hat{t}}\right)^{\infty}_{\mathrm{GW}} = \frac{1}{16\pi}\left\langle(\dot{h}_+)^2 + (\dot{h}_\times)^2\right\rangle_{\mathrm{GW}} \tag{4.1.24}$$

$$= \frac{1}{4\pi\hat{r}^2}\sum_{\ell m}\frac{\left|{}_{-2}Z^{H,\infty}_{\ell m\hat{\omega}}\right|^2}{(m\widehat{\Omega})^2}\left|{}_{-2}S^{\hat{a}\hat{\omega}}_{\ell m}(\vartheta)\right|^2\,, \tag{4.1.25}$$

where the angle brackets here denote averaging over several wavelengths. Using the normalization condition of the spin-weighted spheroidal harmonics (4.1.3), the gravitational fluxes [2] are obtained by integrating the fluxes over the solid

[2] It is a slightly abuse of terminology common in the literature, since the correct term is luminosities.

angle, which yields:

$$\left(\frac{\mathrm{d}\tilde{E}}{\mathrm{d}\hat{t}}\right)^{\infty}_{\mathrm{GW}} = \sum_{\ell=2}^{\infty}\sum_{m=1}^{\ell}\frac{\left|{}_{-2}Z^{H}_{\ell m\hat{\omega}}\right|^2}{2\pi\hat{\omega}^2} = \sum_{\ell=2}^{\infty}\sum_{m=1}^{\ell} I_{\ell m}\,, \tag{4.1.26}$$

$$\left(\frac{\mathrm{d}\tilde{J}_z}{\mathrm{d}\hat{t}}\right)^{\infty}_{\mathrm{GW}} = \sum_{\ell=2}^{\infty}\sum_{m=1}^{\ell}\frac{m\left|{}_{-2}Z^{H}_{\ell m\hat{\omega}}\right|^2}{2\pi\hat{\omega}^3} = \sum_{\ell=2}^{\infty}\sum_{m=1}^{\ell}\frac{m}{\hat{\omega}} I_{\ell m}\,, \tag{4.1.27}$$

while at the horizon:

$$\left(\frac{\mathrm{d}\tilde{E}}{\mathrm{d}\hat{t}}\right)^{H}_{\mathrm{GW}} = \sum_{\ell=2}^{\infty}\sum_{m=1}^{\ell}\alpha_{\ell m}\frac{\left|{}_{-2}Z^{\infty}_{\ell m\hat{\omega}}\right|^2}{2\pi\hat{\omega}^2} = \sum_{\ell=2}^{\infty}\sum_{m=1}^{\ell} H_{\ell m}\,, \tag{4.1.28}$$

$$\left(\frac{\mathrm{d}\tilde{J}_z}{\mathrm{d}\hat{t}}\right)^{H}_{\mathrm{GW}} = \sum_{\ell=2}^{\infty}\sum_{m=1}^{\ell}\alpha_{\ell m}\frac{m\left|{}_{-2}Z^{\infty}_{\ell m\hat{\omega}}\right|^2}{2\pi\hat{\omega}^3} = \sum_{\ell=2}^{\infty}\sum_{m=1}^{\ell}\frac{m}{\hat{\omega}} H_{\ell m}\,, \tag{4.1.29}$$

where the sum over m goes for $m = 1,\dots,\ell$ since ${}_{-2}Z^{H,\infty}_{\ell -m-\hat{\omega}} = (-1)^{\ell}\,{}_{-2}\bar{Z}^{H,\infty}_{\ell m\hat{\omega}}$ and the bar denotes complex conjugation. Note that, for circular orbits, the gravitational frequency ω is related to the orbital frequency $\widehat{\Omega}$ as $\hat{\omega} = m\widehat{\Omega}$. The coefficient $\alpha_{\ell m}$ are explicitly given in [173]

$$\alpha_{\ell m} = \frac{256(2\hat{r}_+)^5\hat{\kappa}(\hat{\kappa}^2+4\epsilon^2)(\hat{\kappa}^2+16\epsilon^2)\hat{\omega}^3}{\left|C_{\ell m}\right|^2}$$

with $\epsilon = \sqrt{1-\hat{a}^2}/(4\hat{r}_+)$, and

$$\begin{aligned}\left|C_{\ell m}\right|^2 = {}&[({}_{-2}\lambda_{\ell m\hat{\omega}}+2)^2 + 4\hat{a}\hat{\omega} - 4\hat{a}^2\hat{\omega}^2][{}_{-2}\lambda^2_{\ell m\hat{\omega}} + 36m\hat{a}\hat{\omega} - 36\hat{a}^2\hat{\omega}^2] + \\ &+ (2\,{}_{-2}\lambda_{\ell m\hat{\omega}}+3)[96\hat{a}^2\hat{\omega}^2 - 48m\hat{a}\hat{\omega}] + 144\hat{\omega}^2(1-\hat{a}^2)\,.\end{aligned} \tag{4.1.30}$$

4.2 Exact GW fluxes at all orders in the secondary spin

We now present the results of the code developed in Ref. [118] to compute the fluxes for a spinning body at all orders in σ. The code provide the normalized fluxes $\mathcal{F}$, defined as:

$$\mathcal{F} = \frac{1}{q}\left[\left(\frac{\mathrm{d}\tilde{E}}{\mathrm{d}\hat{t}}\right)^{H}_{\mathrm{GW}} + \left(\frac{\mathrm{d}\tilde{E}}{\mathrm{d}\hat{t}}\right)^{\infty}_{\mathrm{GW}}\right]. \tag{4.2.1}$$

All fluxes were calculated in normalized units, and they were rescaled by the mass ratio q. $\mathcal{F}_{\ell m}$ denotes the flux for the harmonic indexes l and m. We remind

that $\tilde{E} = E/\mu$. Since $\dot{E} \propto q^2$ to the leading order, the normalized flux $\mathcal{F}$ does not depend on q. In our numerical calculations we only considered prograde orbits, i.e. orbits for which the initial z-component of the angular momentum L_z is positive. Once the orbital radius $\hat{r}$ and the parameters $\hat{a}$ and σ are specified, the orbital dynamics is completely determined by the energy $\tilde{E}$, angular momentum $\tilde{J}_z$, and frequency $\widehat{\Omega}$ given by Eqs. (3.3.40), (3.3.41) and (3.3.39) respectively.

4.2.1 Numerical methods

We employed the numerical routines provided by the Black Hole Perturbation Toolkit [119] to compute ${}_{-2}\lambda_{\ell m\hat{\omega}}$, the spin-weighted spheroidal harmonics, and their derivatives. The solutions ${}_{-2}R^{\rm in}_{\ell m\hat{\omega}}$ and ${}_{-2}R^{\rm up}_{\ell m\hat{\omega}}$ to the homogeneous Teukolsky equation were calculated in two different ways:

- through the MST method [174–176], as implemented in the MATHEMATICA packages of the Black Hole Perturbation Toolkit [119] (see their documentation for the values of the constants $B^{\rm tran}_{\ell m\hat{\omega}}$ and $D^{\rm tran}_{\ell m\hat{\omega}}$)).
- by first solving the Sasaki-Nakamura (SN) equation and then transforming the obtained solution to ${}_{-2}R^{\rm in}_{\ell m\hat{\omega}}$ and ${}_{-2}R^{\rm up}_{\ell m\hat{\omega}}$ (see appendix A, which also shows how to fix the constants $B^{\rm tran}_{\ell m\hat{\omega}}$ and $D^{\rm tran}_{\ell m\hat{\omega}}$).

Both methods require arbitrary precision arithmetic, and the MST method is usually faster and more accurate than solving directly the SN equation. Unfortunately, the implementation of the MST method of [119] has one limitation: the precision of ${}_{-2}R^{\rm in}_{\ell m\hat{\omega}}$ and ${}_{-2}R^{\rm up}_{\ell m\hat{\omega}}$ crucially depends on the gravitational frequency $m\widehat{\Omega}$. As $m\widehat{\Omega}$ increases, the precision of the input parameters should drastically increase as well, in order for the computed ${}_{-2}R^{\rm in}_{\ell m\hat{\omega}}$ and ${}_{-2}R^{\rm up}_{\ell m\hat{\omega}}$ to have enough significant figures. Thus, the MST method tends to become slower for large values of ℓ and when $\hat{r}$ approaches the ISCO[3] [4]. We, therefore, took the best of the two methods and implemented both of them in a MATHEMATICA code. We have checked that the methods agree with each other within numerical accuracy in the entire parameter space considered in our analysis.
The algorithm we devised works according to the following procedure:

[3] For instance, let us consider a nonspinning particle at the ISCO for a Kerr BH with $\hat{a} = 0.9$: for $\ell = m = 2$, with 35 figures in input, $\mathcal{F}$ is returned with 18 figures, while for $\ell = m = 20$, using 90 figures in input returns fluxes with only 9 figures of precision. The SN method, albeit generally slower, does not have the same issue; the precision of the fluxes in output is not affected by the gravitational frequency.

[4] At the time we used version 0.2.0 of the *Teukolsky* package, which implement the MST method.

- Choose the parameters $\hat{a}$ and χ;
- Loop on the harmonic index ℓ, starting with $\ell = 2$ until $\ell_{\rm max}$. We typically used $\ell_{\rm max} = 20$, see discussion below;
- If $\ell \leq 8$, loop on the index $m = 1, \ldots, \ell$ starting with $m = 1$. For larger values of ℓ, we only considered the $m = \ell$ and $m = \ell - 1$, since the others are negligibly small[5];
- Loop on the values of an array of orbital radii $\hat{r}$, starting from $\hat{r}_{\rm start}$. The starting point $\hat{r}_{\rm start}$ is calculated in such a way that all the spinning test objects start the inspiral with the same frequency of a nonspinning object (i.e $\chi = 0$) at the reference value $\hat{r} = 10.1$;
- Compute the energy fluxes $\mathcal{F}$, using the MST method as implemented in [119] to obtain ${}_{-2}R^{\rm in}_{\ell m\hat{\omega}}$ and ${}_{-2}R^{\rm up}_{\ell m\hat{\omega}}$.
- The above point is performed within a certain precision threshold. If the MST method fails to give the fluxes with prescribed precision (for increasing number of figures in the input parameters; the number depends on ℓ), switch to the SN method. To solve the SN equation, we employed the boundary conditions described in Appendix A.1, keeping 10 and 13 terms for the series at the horizon and infinity, respectively.
- Stop the $\hat{r}$ loop at the ISCO. Interpolate the fluxes in the range $\hat{r} \in (\hat{r}_{\rm ISCO}, \hat{r}_{\rm start})$;

The parameters chosen for the numerical simulations are the following:

- $\hat{a} = (0,\, 0.1,\, 0.2, \ldots\, 0.9,\, 0.95,\, 0.97,\, 0.990,\, 0.995)$;
- $\chi \in (-2, 2)$ with steps $\delta\chi = 0.2$;
- $\mu = 30 M_\odot$ and $M = 10^6 M_\odot$, hence $q = 3 \times 10^{-5}$.

To estimate the maximum truncation errors of our code, we computed the fluxes at the ISCO for a spinning particle with $\chi = 2$ for $\ell = 21$ and $\ell = 22$ and compared with the corresponding fluxes summed up to $\ell_{\rm max} = 20$. Choosing $\chi = 2$ as a reference is just for convenience: the truncation error is practically independent of the spin of the secondary, but it is greatly affected by $\hat{a}$ and

[5] When $\ell > 8$, we compare the flux for $m = \ell$ with the flux for $m = \ell - i$ at the ISCO. When

$$\frac{\mathcal{F}_{\ell\ell-i}}{|\mathcal{F}_{\ell\ell} - \mathcal{F}_{\ell\ell-i}|} < 10^{-6}$$

for a certain $i = 1, \ldots, \ell - 1$, we truncate the m series.

by the orbital radius. In Table 4.1 we report the fractional truncation error $\Delta^{\rm tr}(\mathcal{F})$ obtained by comparing, for $\chi = 2$ and $q = 3 \times 10^{-5}$, the fluxes at the ISCO truncated at $\ell = 20$ with the fluxes including the $\ell = 21$ and $\ell = 22$ contributions.

$\hat{a}$	$\Delta^{\rm tr}(\mathcal{F})$
0	3.5×10^{-11}
0.3	4.5×10^{-10}
0.5	3.7×10^{-9}
0.8	3.4×10^{-7}
0.9	3.8×10^{-6}
0.97	6.1×10^{-5}
0.995	5.0×10^{-4}

Table 4.1: Fractional truncation error $\Delta^{\rm tr}(\mathcal{F})$, obtained by taking $\chi = 2$ and $q = 3 \times 10^{-5}$ as reference. The error were estimated at the ISCO by comparing the fluxes truncated at $\ell_{\rm max} = 20$ with the ones truncated at $\ell_{\rm max} = 22$.

In appendix E, we compare our results for the fluxes with previous work, overall finding excellent agreement. Data for $\delta\mathcal{F}^\sigma$ are available online [177] and on the Black Hole Perturbation Toolkit webpage [119].

4.2.2 Spin corrections to the fluxes - polynomial interpolation

The GW fluxes $\mathcal{F}$ can be expanded at fixed orbital radius $\hat{r}$ as

$$\mathcal{F}(\hat{r}, \sigma) = \mathcal{F}^0(\hat{r}) + \sigma \delta\mathcal{F}^\sigma(\hat{r}) + \mathcal{O}(\sigma^2) \,, \tag{4.2.2}$$

where $\mathcal{F}^0$ are the fluxes for a nonspinning secondary around a Kerr primary and $\delta\mathcal{F}^\sigma$ are the linear spin corrections. The coefficients $\delta\mathcal{F}^\sigma$ were obtained by fitting the fluxes $\mathcal{F}$ with a cubic polynomial in σ and then retaining only the linear terms. Such fitting procedure was repeated for each value of $\hat{r}$ at which we computed the fluxes.
The top panels of Fig. 4.1 show the linear spin corrections

$$\delta\mathcal{F}^\sigma_\ell = \sum_{m=-\ell}^{\ell} \delta\mathcal{F}^\sigma_{\ell m} \,, \tag{4.2.3}$$

for $\ell = 2, 3, 4$ and summing up to all values of m such that $|m| \leq \ell$. An analogous plot for the total flux, $\delta\mathcal{F}^\sigma = \sum_{\ell=2} \delta\mathcal{F}^\sigma_\ell$ (summing up to $\ell = 20$) is presented in

Fig. 4.2. In the bottom panels of Fig. 4.1 we also show $\delta\mathcal{F}^\sigma$ for fixed values of the orbital frequency instead of $\hat{r}$, since the latter is a gauge dependent quantity. To this aim, for a given primary spin $\hat{a}$, we considered an evenly spaced grid of frequencies, with the same number of points for all the values of σ, such that

$$\widehat{\Omega}(i) = \widehat{\Omega}_{\rm start} + (i-1)\delta\widehat{\Omega}\,, \quad i = 1, ...100\,, \tag{4.2.4}$$

where $\delta\widehat{\Omega} = (\widehat{\Omega}_{\rm ISCO} - \widehat{\Omega}_{\rm start})/100$. $\widehat{\Omega}_{\rm ISCO}$ and $\widehat{\Omega}_{\rm start}$ are the orbital frequencies at the ISCO and at $\hat{r}_{\rm start} = 10.1$ for a nonspinning particle, respectively. To compare the fluxes at equal frequencies, $\widehat{\Omega}_{\rm ISCO}$ was not included in the grid. At fixed spins, it is then possible to find a map between $\widehat{\Omega}$ and the orbital radius $\hat{r}$, which allows to recast Eq. (4.2.2) as

$$\mathcal{F}(\widehat{\Omega}, \sigma) = \mathcal{F}^0(\widehat{\Omega}) + \sigma\delta\mathcal{F}^\sigma(\widehat{\Omega}) + \mathcal{O}(\sigma^2)\,. \tag{4.2.5}$$

Note that the fluxes corrections shown in Figs. 4.1 and 4.2 are always negative both at fixes orbital radius and frequency. Thus, a point-particle with spin aligned to the primary spin emits less radiation compare to a spin-less point-particle or the anti-aligned case. Moreover, the total fluxes $\delta\mathcal{F}^\sigma$ are always monotonic, whereas the partial fluxes $\delta\mathcal{F}^\sigma_\ell$, shown in Fig. 4.1, have a nonmonothonic behaviour for nearly-extremal primary ($\hat{a} \gtrsim 0.99$) in the proximity of the ISCO. Indeed, near extremality, $\ell = 2$ is not the dominant spin correction to the flux [178].

Comparison with Akcay *et al.*

A new flux balance law relating the local changes of energy and angular momentum of a spinning particle in Kerr spacetime with the asymptotic fluxes was recently obtained in Ref. [53]. This procedure has been applied to particles with spin perpendicular to the orbital plane on circular orbits in the Schwarzschild spacetime, computing the linear spin corrections to the fluxes. Table 4.2 provides our spin corrections to the flux and the fractional difference with respect to the sum of the spin's contributions at horizon and infinity given in Table I of Ref. [53]. The errors show a very good agreement between the two results.

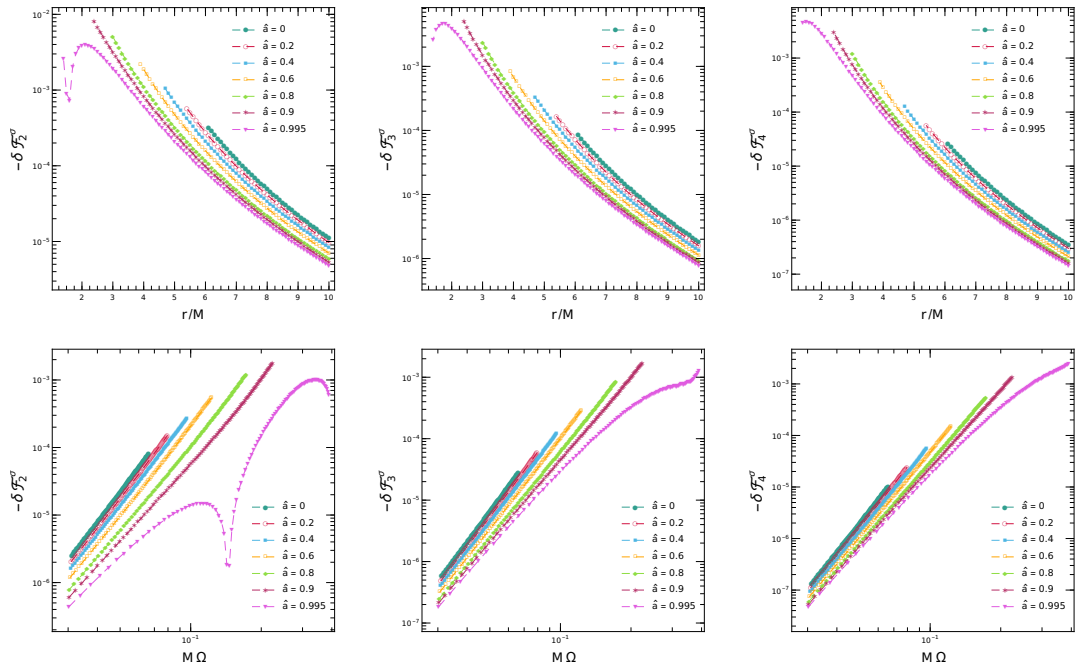

Figure 4.1: Top panels: The spin-correction coefficient $\delta\mathcal{F}^{\sigma}_{\ell}$ (see Eqs. (4.2.2) and (4.2.3)) as a function of the orbital radius (up to the ISCO) for different values of the spin $\hat{a}$ of the primary and for $\ell = 2, 3, 4$ (from left to right), summing up to all values of m such that $|m| \leq \ell$. Bottom panels: same as top row but for the fluxes as a function of the orbital frequency. Note that, for nearly-extremal primary ($\hat{a} \gtrsim 0.99$), $\delta\mathcal{F}^{\sigma}_{2}$ is nonmonotonic near the ISCO, although near extremality $\ell = 2$ is not the dominant spin correction to the flux [178] and the total correction $\delta\mathcal{F}^{\sigma}$ is monotonic 4.2.

$\hat{r}$	$\delta\mathcal{F}^{\sigma}$	$\Delta^{\rm rel}(\delta\mathcal{F}^{\sigma})$
10	$-1.35324081460517 \times 10^{-5}$	3.0×10^{-14}
8	$-6.28540371972 \times 10^{-5}$	1.9×10^{-13}
6	$-5.074933017 \times 10^{-4}$	2.5×10^{-11}

Table 4.2: Linear spin correction to the GW flux $\delta\mathcal{F}^{\sigma}$ and fractional differences $\Delta^{\rm rel}(\delta\mathcal{F}^{\sigma})$ with respect to the fluxes shown in Table I of Ref. [53] for $\hat{a} = 0$.

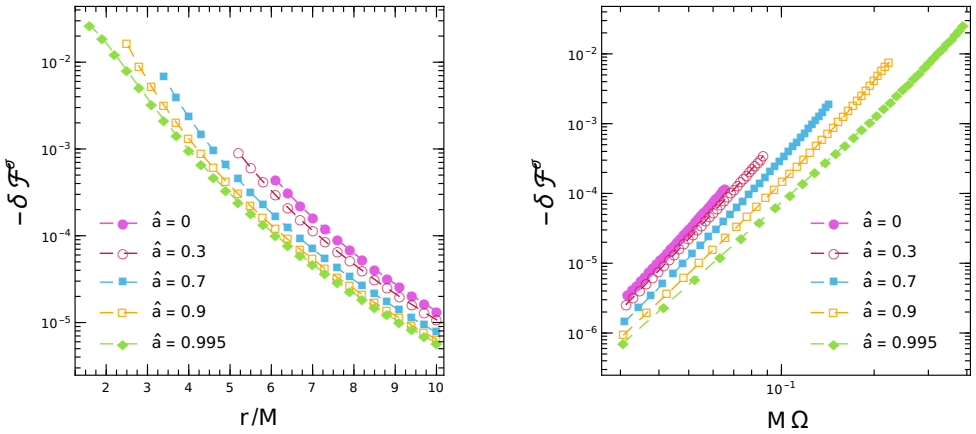

Figure 4.2: Left panel: The total spin-correction coefficient $\delta\mathcal{F}^\sigma$ [see Eqs. (4.2.2) and (4.2.3)] as a function of the orbital radius (up to the ISCO) for different values of the spin $\hat{a}$ of the primary, summing up $\ell_{\rm max} = 20$. Right panel: the same but for the fluxes as a function of the orbital frequency.

4.3 Linear expansion in the secondary spin

Extracting the linear corrections to the fluxes as shown in section 4.2 is time-consuming, because of the additional computational cost of repeating the calculation of the exact fluxes for different values of σ. This numerical procedure is likely to be too expensive for eccentric or off-equatorial orbits. Moreover, it was shown in [53] that the GW fluxes for spinning secondaries in EMRI are valid only at $\mathcal{O}(\sigma)$ order. Motivated by these reasons, we fully expanded the fluxes in σ, deriving the semi-analytic expressions for first order corrections $\mathcal{F}^1(\hat{r})$ for spins-aligned, circular equatorial motion. We outline here the expansion carried out in [169] , whereas the appendices present more information on technical aspects and the in-depth derivation of certain relations.
We fully expanded the fluxes by keeping the orbital radius $\hat{r}$ fixed. An alternative method, developed in Refs. [54, 179], consists in expanding the fluxes at fixed orbital frequencies. The two methods are equivalent, and there is a unique map between the corrections computed at fixed frequency and those computed at fixed orbital radius.
To compute the amplitudes $I_{\ell m}$ (4.1.26) and $H_{\ell m}$ (4.1.28) to linear order in σ we need to expand the complex amplitudes

$$ {}_sZ^{H,\infty}_{\ell m\hat{\omega}} = {}_sZ^{H,\infty}_{\ell m\hat{\omega}}({}_s\lambda_{\ell m\hat{\omega}}, {}_sS^c_{\ell m}, {}_sR^{\rm in}_{\ell m\hat{\omega}}, {}_sR^{\rm up}_{\ell m\hat{\omega}}) \,, \tag{4.3.1} $$

which depend on the solutions of the Teukolsky equations. To this aim, we first

expand the solutions of the Teukolsky angular and radial equations, i.e.

$$
\begin{aligned}
{}_s\lambda_{\ell m\hat{\omega}} &= {}_s\lambda^0_{\ell m}(c^0) + \sigma\, {}_s\lambda^1_{\ell m}(c^0, c^1)\,, && (4.3.2)\\
{}_sS^c_{\ell m}(\theta) &= {}_sS^0_{\ell m}(\theta, c^0) + \sigma\, {}_sS^1_{\ell m}(\theta, c^0, c^1)\,, && (4.3.3)\\
{}_sR^{\rm in}_{\ell m\hat{\omega}}(\hat{r}) &= {}_sR^{{\rm in},0}_{\ell m}(\hat{r}, \omega^0) + \sigma\, {}_sR^{{\rm in},1}_{\ell m}(\hat{r}, \hat{\omega}^0, \hat{\omega}^1)\,, && (4.3.4)\\
{}_sR^{\rm up}_{\ell m\hat{\omega}}(\hat{r}) &= {}_sR^{{\rm up},0}_{\ell m}(\hat{r}, \omega^0) + \sigma\, {}_sR^{{\rm up},1}_{\ell m}(\hat{r}, \hat{\omega}^0, \hat{\omega}^1)\,, && (4.3.5)
\end{aligned}
$$

where $\hat{\omega}^i = m\widehat{\Omega}^i$, and we expanded $c = c^0 + \sigma c^1 + \mathcal{O}(\sigma^2)$, where $c^i = \hat{a}\hat{\omega}^i$ with $i = 0, 1$. We shall now describe the procedure we adopted to compute all the components of Eqs. (4.3.2)-(4.3.5) as well as of Eqs. (4.1.26)-(4.1.28). All terms in (4.3.2)-(4.3.5) were derived for generic helicity perturbation s, whereas the linear corrections to the amplitudes ${}_sZ^{H,\infty}_{\ell m\hat{\omega}}$ were computed only for gravitational radiation, i.e $s = -2$.
We expanded $\tilde{E}$, $\tilde{J}_z$ and the orbital frequency $\widehat{\Omega}$ in terms of the spin parameter, considering linear corrections only, such that that at first order in σ:

$$
\tilde{E} = \tilde{E}^0 + \sigma\tilde{E}^1\,, \quad \tilde{J}_z = \tilde{J}^0_z + \sigma\tilde{J}^1_z\,, \quad \widehat{\Omega} = \widehat{\Omega}^0 + \sigma\widehat{\Omega}^1\,.
$$

See Eqs. (3.3.43), (3.3.44) for the zeroth and first order corrections of $\tilde{E}$, respectively. The terms $\tilde{J}^0_z$ and $\tilde{J}^1_z$ are given by Eqs. (3.3.45), (3.3.46) respectively, while $\widehat{\Omega}^0 = 1/(\hat{a} \pm \hat{r}^{3/2})$ and see Eq. 3.3.48 for $\widehat{\Omega}^1$.

4.3.1 Linearization in the secondary spin: Angular solutions

If we impose regularity of the solutions at the boundaries $\theta = 0$ and $\theta = \pi$, which are regular singular points, Eq. (4.1.2) defines a Sturm-Liouville eigenvalue problem. Despite being a singular Sturm-Liouville problem (see Appendix D.1), for real frequencies, Eq. (4.1.2) retains much of the properties of a regular one. In particular, it can be seen as an eigenvalue problem for a Hermitian operator $\mathcal{H}$:

$$
\mathcal{H}|S\rangle = -\,{}_s\lambda_{\ell m\hat{\omega}}|S\rangle\,, \tag{4.3.6}
$$

where $|S\rangle \equiv {}_sS^c_{\ell m}(\theta)$ and $\mathcal{H}$ is the left-hand side of Eq. (4.1.2). If we expand $\mathcal{H}$, ${}_s\lambda_{\ell m\hat{\omega}}$, and $|S\rangle$ to linear order in σ, we obtain:

$$
\begin{aligned}
\mathcal{H}^0|S^0\rangle &= -\,{}_s\lambda^0_{\ell m}(c^0)|S^0\rangle\,, && (4.3.7)\\
\mathcal{H}^0|S^1\rangle + \mathcal{V}^1|S^0\rangle &= -\,{}_s\lambda^0_{\ell m}(c^0)|S^1\rangle - {}_s\lambda^1_{\ell m}(c^0, c^1)|S^0\rangle\,, && (4.3.8)
\end{aligned}
$$

where ${}_sS^0_{\ell m}(\theta, c^0) \equiv |S^0\rangle$ and ${}_sS^1_{\ell m}(\theta, c^0, c^1) \equiv |S^1\rangle$. The functional form of $\mathcal{V}^1$ is given in the Appendix D, while $\mathcal{H}^0$ is simply given by $\mathcal{H}$ with $c \leftrightarrow c^0$. In

this fashion, we can consider $\mathcal{V}^1$ as a perturbation of an Hermitian operator $\mathcal{H}^0$, and the corrections ${}_s\lambda^1_{\ell m}(c^0, c^1)$ induced by the spin σ can be obtained using the same techniques of time-independent perturbation theory for a (nondegenerate) quantum mechanical system, i.e

$$ {}_s\lambda^1_{\ell m}(c^0, c^1) = \langle S^0|\mathcal{V}^1|S^0\rangle \equiv \int_0^\pi {}_sS^0_{\ell m}\mathcal{V}^1\,{}_sS^0_{\ell m}\sin\theta \mathrm{d}\theta\,. \tag{4.3.9} $$

Once the corrections to the eigenvalues ${}_s\lambda^1_{\ell m}(c^0, c^1)$ are known, we can compute the corrections to the eigenfunctions ${}_sS^1_{\ell m}(\theta, c^0, c^1)$ by expanding in σ the series coefficients of the solution obtained with Leaver's method (see Appendix D.1 for more details). To compute the 0-th order eigenvalues ${}_s\lambda^0_{\ell m}(c^0)$ and eigenfunctions ${}_sS^0_{\ell m}(\theta, c^0)$ of Eq. (4.1.2) we used Leaver's method implemented in the Black Hole Perturbation Toolkit [119].
It is worth to remark that we can always find the exact solutions of Eq. (4.1.2) for any value of σ, and then interpolate to extract the first order correction in the spin. However, the semi-analytic linearization approach described above provides a powerful and fast method to avoid such numerical procedure. It may happen, though, that in some regions of the parameter space, the input parameters require higher precision than expected due to large numerical cancellations in the algorithm. When the precision of the corrections obtained with the semi-analytic method dropped below a certain threshold, we used as a "backup" approach a simple interpolation from the exact solutions, i.e.

$$ {}_s\lambda^1_{\ell m} = \frac{{}_s\lambda_{\ell m\hat{\omega}}(c^0 + \epsilon c^1) - {}_s\lambda_{\ell m\hat{\omega}}(c^0 - \epsilon c^1)}{\epsilon}\,, \tag{4.3.10} $$

$$ {}_sS^1_{\ell m} = \frac{{}_sS^{(c^0+\epsilon c^1)}_{\ell m} - {}_sS^{(c^0-\epsilon c^1)}_{\ell m}}{\epsilon}\,, \tag{4.3.11} $$

where the exact eigenvalues ${}_s\lambda_{\ell m\hat{\omega}}(c^0 + \epsilon c^1)$, ${}_s\lambda_{\ell m\hat{\omega}}(c^0 - \epsilon c^1)$ and eigenfunctions ${}_sS^{(c^0+\epsilon c^1)}_{\ell m}$, ${}_sS^{(c^0-\epsilon c^1)}_{\ell m}$ of Eq. (4.1.2) were computed using the Leaver method of the Black Hole Perturbation Toolkit with $\epsilon = 10^{-6}$. We have checked that the corrections obtained with the semi-analytic method and with the numerical interpolation agree in all the parameter space under investigation.

4.3.2 Linearization in the secondary spin: Radial solutions

Equation (4.1.4) is a stiff differential equation, i.e. the solutions of physical interest are fast oscillating functions with amplitudes increasing as $\hat{r}^3$ at infinity. The stiffness is caused by the long range of the potential, which makes it challenging to obtain accurate solution in the domain of integration. Two workarounds of

this issue are the semi-analytic Mano-Suzuki-Takasugi method [175,176] and the numerical Sasaki-Nakamura method [180]. Here we employed a third method, which consists in considering a particular ansatz of the solutions of Eq. (4.1.4) based on hyperboloidal-slicing coordinates [181] (see also Ref. [182,183] for more details). Such ansatz is[6]

$$ {}_sR_{\ell m\hat{\omega}}(\hat{r}) = \hat{r}^{-1}\Delta^{-s}e^{\mp i\hat{\omega}\hat{r}^*}e^{im\tilde{\phi}}\,{}_s\psi_{\ell m}(\hat{r})\,, \tag{4.3.12} $$

when the minus (plus) sign refers to ${}_sR^{\rm in}_{\ell m\hat{\omega}}$ (${}_sR^{\rm up}_{\ell m\hat{\omega}}$),

$$ \tilde{\phi} = \frac{\hat{a}}{\hat{r}_+ - \hat{r}_-}\ln\left(\frac{\hat{r}-\hat{r}_+}{\hat{r}-\hat{r}_-}\right). \tag{4.3.13} $$

By plugging the ansatz (4.3.12) in Eq. (4.1.4), we obtain an ordinary differential equation for ${}_s\psi_{\ell m}$:

$$ \Delta^2\frac{\mathrm{d}^2\,{}_s\psi_{\ell m\omega}}{\mathrm{d}\hat{r}^2} + \Delta\tilde{F}(\hat{r};H)\frac{\mathrm{d}\,{}_s\psi_{\ell m\omega}}{\mathrm{d}\hat{r}} + \tilde{U}(\hat{r};H)\,{}_s\psi_{\ell m\omega} = 0\,, \tag{4.3.14} $$

where the functions $\tilde{F}(\hat{r};H)$ and $\tilde{U}(\hat{r};H)$ are given in Appendix B. Solving Eq. (4.3.14) numerically is much easier than solving Eq. (4.1.4) because the potential $\tilde{U}(\hat{r};H)/\Delta^2$ is short ranged and the oscillating behavior at the horizon and infinity is already factored out in the ansatz (4.3.12). It is worth noticing that the oscillating term $e^{\mp i\hat{\omega}\hat{r}^*}$ does not enter in the Wronskian $W_{\hat{r}}$. We found exact boundary conditions for Eq. (4.3.14), which allowed us to find the radial solutions ${}_sR^{\rm in}_{\ell m\hat{\omega}}$ and ${}_sR^{\rm up}_{\ell m\hat{\omega}}$ quickly and accurately. Such boundary conditions are provided in Appendix B.1.
After expanding the ansatz (4.3.12) as shown in Appendix D.1.1,we obtained some algebraic formulas for ${}_sR^{\rm in,1}_{\ell m}$ and ${}_sR^{\rm up,1}_{\ell m}$ that depend on the linear corrections ${}_s\psi^{\rm in,0}_{\ell m}$, ${}_s\psi^{\rm in,1}_{\ell m}$ and ${}_s\psi^{\rm up,0}_{\ell m}$, ${}_s\psi^{\rm up,1}_{\ell m}$. We computed such solutions by solving a system of ordinary differential equations derived by expanding Eq. (4.3.14) and the related boundary conditions to $\mathcal{O}(\sigma)$. See Appendix D.1.1 for more details.

4.3.3 Linearization in the secondary spin: GW fluxes

Once the zeroth- and first-order corrections to the Teukolski variables are known, it is then possible to expand the complex amplitudes ${}_{-2}Z^{H,\infty}_{\ell m\hat{\omega}}$ as

$$ {}_{-2}Z^{H}_{\ell m\hat{\omega}}(\hat{r}) = {}_{-2}Z^{H,0}_{\ell m}(\hat{r},\omega^0) + \sigma\,{}_{-2}Z^{\rm H,1}_{\ell m}(\hat{r},\hat{\omega}^0,\hat{\omega}^1)\,, \tag{4.3.15} $$

$$ {}_{-2}Z^{\infty}_{\ell m\hat{\omega}}(\hat{r}) = {}_{-2}Z^{\infty,0}_{\ell m}(\hat{r},\omega^0) + \sigma\,{}_{-2}Z^{\infty,1}_{\ell m}(\hat{r},\hat{\omega}^0,\hat{\omega}^1)\,, \tag{4.3.16} $$

[6] The original ansatz used in [181] [their Eq. (13)] has wrong signs in some factors.

and finally obtain the correction to the fluxes at the horizon and infinity for each ℓ, m as follows:

$$I_{\ell m}(\hat{r}) = I^0_{\ell m}(\hat{r}, \omega^0) + \sigma I^1_{\ell m}(\hat{r}, \hat{\omega}^0, \hat{\omega}^1)\,, \tag{4.3.17}$$

$$H_{\ell m}(\hat{r}) = H^0_{\ell m}(\hat{r}, \omega^0) + \sigma H^1_{\ell m}(\hat{r}, \hat{\omega}^0, \hat{\omega}^1)\,, \tag{4.3.18}$$

where $I_{\ell m}$ and $H_{\ell m}$ have been defined in Eqs. (4.1.26) and (4.1.28), respectively. The coefficients $I^0_{\ell m}$, $I^1_{\ell m}$ and $H^0_{\ell m}$, $H^1_{\ell m}$ are given in Appendix D.1.2.

4.3.4 Numerical methods

To compute the fluxes, we constructed a nonuniform grid in the orbital radius $\hat{r}$ defined as follows: given $v(\hat{r}) \equiv (\widehat{\Omega}^0)^{1/3} = (\hat{r}^{3/2} + \hat{a})^{-1/3}$, we considered 180 points for $a < 0.99$ and 200 points for $a = 0.99$ evenly spaced in v, starting from $v_{\rm start} = v(14)$ and ending at $v_{\rm end} = v(\hat{r}_{\rm ISCO})$, with $\hat{r}_{\rm ISCO}$ being the ISCO for a nonspinning test particle. The radiation reaction grid in $\hat{r}$ was then obtained as the solution of $\hat{r}_i = (1/v_i^3 - \hat{a})^{-2/3}$ for $i = 1, \ldots 180\,(200)$ for $\hat{a} < 0.99$ ($\hat{a} = 0.99$). In the computation of the fluxes, we summed over all multipoles ℓ up to $\ell_{\rm max} = 20$ ($\ell_{\rm max} = 24$) for $a < 0.99$ ($a = 0.99$), summing over the index $m = 1, \ldots, \ell$ for each harmonic index ℓ. As shown in Table 4.1, the fractional error in truncating the multipole sum at $\ell_{\rm max}$ is no larger than $\sim 10^{-5}$. All the fluxes were calculated for prograde stable orbits.

4.3.5 Results

As seen in section 4.2, the linear corrections $\delta\mathcal{F}^\sigma$ to the fluxes in a Kerr spacetime were computed through a cubic interpolation of the exact fluxes in σ. In order to compare with the semianalytic linear corrections $\mathcal{F}^1$, we recomputed $\delta\mathcal{F}^\sigma$ as done in Ref. [118] with the following differences:

- we solved the radial Teukolsky equation in hyperboloidal slicing coordinates, using the same radiation-reaction grid adopted here;
- for each ℓ, we summed over all azimuthal indexes $m = 1, \ldots, \ell$.

The fractional difference between $\delta\mathcal{F}^\sigma$ and $\mathcal{F}^1$ is, at most, $10^{-10}\%$ ($10^{-4}\%$) for $\hat{a} = 0.9$ ($\hat{a} = 0.99$) (the largest differences occurring at the ISCO), as also shown in Fig. 4.3 for $\hat{a} = 0.99$. Finally, we compared the linearized fluxes with the results available in the literature. In the case of a Schwarzschild spacetime, our results are in perfect agreement with those of Ref. [53] (they agree within all the digits shown in Table I of [53]).

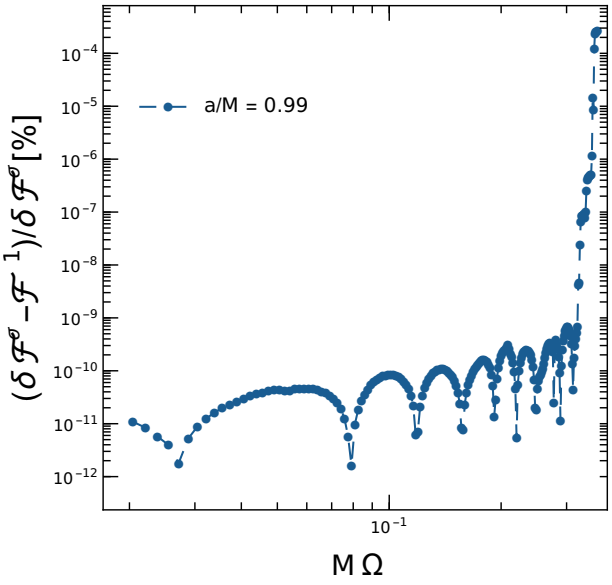

Figure 4.3: Percentage fractional difference between $\delta\mathcal{F}^{\sigma}$ and $\mathcal{F}^{1}$ for a primary with spin $\hat{a} = 0.99$.

Chapter 5

Parameter estimation of the secondary spin with fully-relativistic waveforms

Our goal in this chapter is to quantify the impact of the secondary spin on the gravitational wave signal and assess its detectability though LISA observations. As done in the previous chapters, we consider spin (anti-)aligned and quasi circular equatorial motion. We use the term "quasi" since the motion of the spinning particle evolve through a sequence of circular orbits. In the adiabatic approximation, the evolution of the orbital elements caused by radiation emission depends solely on the asymptotic fluxes, which are related to the local rate of change of the would-be constants of motion by flux-balance laws. We can compute the asymptotic fluxes with the Teukolsky formalism (which from now on we refer to as Teukolsky fluxes), while the gravitational waveform emitted by a test-particle is given by Eq. (4.1.22). This dissipative approach to the inspiral based on the Teukolsky formalism is computationally efficient compared to the calculation of the local self-force and it avoids altogether all related issues with the divergences at the worldline of the particle [50, 120].

Modeling the inspiral adiabatically is sufficient for our purposes, due to the dissipative nature of the leading order contribution of the secondary spin to the GW phase. However, it is worth to remark that the adiabatic approximation completely ignores conservative effects, which may accumulate during the EMRI inspiral providing significant changes to the signal. Moreover, we neglect dissipative terms due to second order metric perturbations, which may also play an important role to avoid systematic effects for realistic parameter estimations, especially for EMRIs detected with large signal to noise ratios.

A precise assessment of the detectability of the secondary spin by future interferometers would require a statistical analysis based on Bayesian inference. However, parameter estimation for EMRIs is a challenging and still open problem [33,47], due to the complexity and the slow generation of EMRI waveforms computed using BH perturbation theory. Moreover, the parameter space for EMRIs is rather large [114]: even assuming the system can be modeled within GR already yields seventeen parameters to be constrained. Markov Chain Monte Carlo (MCMC) algorithms are the standard approach to reconstruct the posterior probability of such parameters, but they require waveforms to be generated in few milliseconds to cover the entire parameter space in a reasonable time. A single Teukolsky waveform for the Kerr spacetime take from several minutes to many hours to be computed, depending on the orbital configuration considered. In practice, almost all parameter-estimation studies done so far made use of approximated – but fast to generate – kludge waveforms [33,112–117]. In fact, techniques to generate fast and fully relativistic EMRI waveforms have started to be developed only recently [48,49,184,185], but so far fully Bayesian studies with these waveforms have only been done for a nonspinning secondary in eccentric orbits around a Schwarzschild SMBH [48].

We can get a crude estimate on the impact of systematic errors on gravitational signals by looking at the phase difference between two waveforms, which we refer to as "dephasing". This method provides a "quick and dirty" way to evaluate the detectability of certain parametesr before performing an accurate but time-consuming analysis. In Refs. [118,186], we estimated the measurability of χ by using as a requirement that the total dephasing is $\gtrsim 1$ rad. Such threshold in considered large enough to substantially impact a matched-filter search, leading to a significant loss of detected events [187].
An analysis based on the dephasing is simplistic, and must be validated by a more careful study, which includes accurate waveform models and a statistical analysis that can account for correlations among the parameters. In this regard, an alternative strategy to full MCMC methods to compute the posterior of the EMRI parameters consists in using a Fisher matrix approach, which is valid for sufficiently high signal-to-noise ratios [188]. In this framework, the probability distribution of the binary parameters is approximated by a multivariate Gaussian distribution, whose covariance is given as the inverse of the Fisher matrix. The latter in turn depends on the derivatives of the GW template with respect to the source parameters, e.g. masses, spins, distance.

Previous work [112, 113] computed Fisher-matrix errors using numerical kludge waveforms including corrections due to the spin of the SCO. Their results

suggest that LISA will be unable to constrain the magnitude of the secondary spin for systems with mass ratios $q \lesssim 10^{-4}$. Since the SCO spin introduces a nonnegligible dephasing [118, 186], its unmeasurability can be probably related to correlations with the rest of the waveform parameters.
The main purpose of our work [169] was to study whether these conclusions hold when considering more accurate (albeit much slower to generate) Teukolsky waveforms. Indeed, it is known that using kludge waveforms may lead to large systematic errors when performing parameter estimation [48].

This chapter is structured as follows: section 5.1 illustrates the flux balance laws and evolution equations for a quasi-circular, equatorial inspiral. Some technical issues related to the secondary spin are discussed, together with the linearized in σ set of equations for the evolution of the orbital radius $\hat{r}$ and azimuthal phase ϕ. In section 5.2, we present our analysis on the measurability of the secondary spin based on dephasing, carried out in our work Piovano *et al.* [118] and Piovano *et al.* [186]. We first computed the GW phase at all order in σ, extracting the linear-in-spin contribution to the GW phase $\delta\Phi^{\sigma}_{\rm GW}$, which represent a novel result. Using these corrections, we provided a criterion, based on the dephasing, for the minimal value for the secondary spin, resolvable by LISA. We then discussed in detail how this approach can foster theory-agnostic tests on the Kerr bound and constraints on superspinar based on EMRI detections. Finally, in section 5.3, we present our parameter estimation based on the Fisher matrix approach, supplied by fully-relativistic Teukolsky waveforms, originally shown in Piovano *et al.* [169]. Appendix F provides a technical discussion on the numerical stability and convergence of the Fisher and covariance matrices.

5.1 Quasi-circular, equatorial inspiral

5.1.1 Radiation-reaction effects and balance laws

We study radiation-reaction effects within the adiabatic approximation, already described in chapter 1. For circular, equatorial orbits, this approximation holds as long as

$$\frac{2\pi}{\widehat{\Omega}} \ll \hat{r} \left| \frac{\mathrm{d}\hat{r}}{\mathrm{d}\hat{t}} \right|^{-1} . \tag{5.1.1}$$

At the adiabatic order, changes to the mass terms μ and M and to the spin $\hat{a}$ are smaller than the leading-order dissipative terms [58]. The change to the primary mass and spin due to GW absorption at the horizon formally enter at the next-to-leading order, although with a small coefficient [189].

Thus, for a *nonspinning* object on an equatorial orbit around a Kerr BH

$$\frac{\mathrm{d}E}{\mathrm{d}t} = \Omega \frac{\mathrm{d}L_z}{\mathrm{d}t} \,. \tag{5.1.2}$$

In the adiabatic approximation, the following balance equations hold:

$$\left(\frac{\mathrm{d}E}{\mathrm{d}t}\right)_{\rm GW} = -\left\langle \frac{\mathrm{d}E}{\mathrm{d}t} \right\rangle \,, \qquad \left(\frac{\mathrm{d}L_z}{\mathrm{d}t}\right)_{\rm GW} = -\left\langle \frac{\mathrm{d}L_z}{\mathrm{d}t} \right\rangle \,, \tag{5.1.3}$$

where the brackets denote time-averaging over a time length much longer than the time evolution of the orbital parameters but shorter than the radiation time scales. The gravitational energy and angular momentum fluxes include both the contribution at infinity and at the event horizon, and are calculated by averaging over several wavelengths. Equation (5.1.1) breaks down at the onset of the inspiral/plunge transition region, where the adiabatic approximation is no longer valid (see Ref. [190] and Refs. [191, 192] for a discussion on this topic). Nonetheless, the difference between the ISCO frequency and the transition frequency scales as $q^{2/5} \ll 1$. Thus, for a typical EMRI, Eq. (5.1.1) is valid for almost all the inspiral prior to plunge.

For a spinning particle in Kerr, there is an extra degree of freedom related to the spin of the small object. In general, the evolution of the constants of motion can also depend on the secondary spin evolution. However, it was recently shown that the evolution of the E and J_z are formally the same as those above to first order in σ [53]. On the other hand, the evolution of the spin tensor $S_{\mu\nu}$ depends on *local* metric perturbations and not only on asymptotic fluxes [53]. This evolution determines that of the particle 4-velocity through Eq. (3.2.12). However, as shown in Eq. (3.2.19), the spin tensor evolves at $\mathcal{O}(q)$ and it affects the particle acceleration to higher order in the mass ratio. Likewise, the effect of the secondary spin on the adiabatic changes to M and $\hat{a}$ is subleading. Thus – for what concerns the leading-order spin corrections to the dynamics – the evolution of the binary masses and spins can be neglected.

It remains to prove that the equation

$$\frac{\mathrm{d}\tilde{E}}{\mathrm{d}\hat{t}} = \widehat{\Omega} \frac{\mathrm{d}\tilde{J}_z}{\mathrm{d}\hat{t}} \,, \tag{5.1.4}$$

holds for a spinning object with the above assumptions. Using the chain rule, Eq. (5.1.4) is equivalent to

$$\widehat{\Omega} = \frac{\partial \tilde{E}}{\partial \hat{r}} \left(\frac{\partial \tilde{J}_z}{\partial \hat{r}}\right)^{-1} \,. \tag{5.1.5}$$

and by plugging into this Eqs. (3.3.39)–(3.3.41), it is straightforward to see that the previous relation is satisfied in our case at all order in σ. This is the generalization of Eq. (20) in Ref. [193], which derived an equivalent formula in the case of a non-spinning SCO. In Ref. [99], the authors considered circular orbits for a spinning particle moving slightly off the equatorial plane by a quantity $\mathcal{O}(\sigma)$, and they showed in a similar manner that Eq. (5.1.4) is valid to $\mathcal{O}(\sigma)$.
Noteworthy, the above argument assumes that circular orbits for a spinning particle remains circular under radiation reaction, i.e. that Eq. (5.1.4) remains valid throughout the adiabatic inspiral. In other words, one needs to prove that an initial circular orbit for a spinning particle does not become slightly eccentric during inspiral due to backreaction effects, following the same procedure of Refs. [193, 194] in the case of a nonspinning secondary. In principle, given a circular geodesic, small perturbations induced by the spin can induce eccentricity [195] or push the orbit off the equatorial plane for not aligned spins [196, 197]. Nevertheless, we shall assume that a circular orbit remains circular under radiation-reaction effects even when the SCO is spinning. Here we just note that, under the assumption that the secondary spin remains constant, it is self-consistent to use Eq. (5.1.4), as also shown in Ref. [99].
Let us now consider the normalized fluxes (4.2.1). It is possible to calculate the adiabatic evolution of the orbital radius $\hat{r}(\hat{t})$ and phase $\Phi(\hat{t})$ due to radiation losses as follows (see also Eq. (1.2.30)):

$$\frac{\mathrm{d}\hat{r}}{\mathrm{d}\hat{t}} = -q\mathcal{F}(\hat{r})\left(\frac{\mathrm{d}\tilde{E}}{\mathrm{d}\hat{r}}\right)^{-1} \qquad \frac{\mathrm{d}\Phi}{\mathrm{d}\hat{t}} = \widehat{\Omega}(\hat{r}(\hat{t}))\,, \tag{5.1.6}$$

with $\tilde{E}$ given by Eq. (3.3.40). In Ref. [118, 186], we employed Eq. (5.1.6) to model the adiabatic inspiral using the exact fluxes $\mathcal{F}$ at linear order in the spin. For our Fisher matrix analysis, we adopted a different approach. In the framework of [169] (shown in the previous chapter), the energy fluxes are expanded in σ at fixed spins $\hat{a}$ and orbital radius $\hat{r}$, with

$$\mathcal{F}(\hat{r}, \widehat{\Omega}) = \mathcal{F}^0(\hat{r}, \widehat{\Omega}^0) + \sigma\mathcal{F}^1(\hat{r}, \widehat{\Omega}^0, \widehat{\Omega}^1)\,, \tag{5.1.7}$$

Let us define

$$\mathcal{G}(\hat{r}, \widehat{\Omega}) := \left(\frac{\mathrm{d}\tilde{E}}{\mathrm{d}\hat{r}}\right)^{-1} \mathcal{F}(\hat{r}, \widehat{\Omega})\,, \tag{5.1.8}$$

then, at first order in σ

$$\mathcal{G}(\hat{r},\widehat{\Omega}) = \mathcal{G}^0(\hat{r},\widehat{\Omega}^0) + \sigma\mathcal{G}^1(\hat{r},\widehat{\Omega}^0,\widehat{\Omega}^1)\,, \tag{5.1.9}$$

$$\mathcal{G}^0 = \left(\frac{\mathrm{d}\tilde{E}^0}{\mathrm{d}\hat{r}}\right)^{-1}\mathcal{F}^0\,, \tag{5.1.10}$$

$$\mathcal{G}^1 = \left(\frac{\mathrm{d}\tilde{E}^0}{\mathrm{d}\hat{r}}\right)^{-1}\mathcal{F}^1 - \left(\frac{\mathrm{d}\tilde{E}^0}{\mathrm{d}\hat{r}}\right)^{-2}\left(\frac{\mathrm{d}\tilde{E}^1}{\mathrm{d}\hat{r}}\right)\mathcal{F}^0\,, \tag{5.1.11}$$

which yield for the time evolution of the orbital radius

$$\frac{\mathrm{d}\hat{r}}{\mathrm{d}\hat{t}} = -\mathcal{G}^0(\hat{r},\widehat{\Omega}^0) - \sigma\mathcal{G}^1(\hat{r},\widehat{\Omega}^0,\widehat{\Omega}^1)\,. \tag{5.1.12}$$

Finally, at first order in σ the orbital phase is given by

$$\frac{\mathrm{d}\phi}{\mathrm{d}\hat{t}} = \widehat{\Omega}^0(\hat{r}) + \sigma\widehat{\Omega}^1(\hat{r})\,. \tag{5.1.13}$$

Solving Eqs. (5.1.12) and (5.1.13) and linearizing them in σ one can obtain $\hat{r}(\hat{t})$ and $\phi(\hat{t})$ to $\mathcal{O}(\sigma)$.

5.2 Detectability of the secondary spin based on dephasing

We saw in chapter 3 that in the extreme-mass-ratio limit, an extended body can be approximated as a point-particle endowed with multipoles. Only the first two multipoles are needed to model EMRIs within first-post adiabatic accuracy. In the pole-dipole approximation, all extended bodies are treated as spinning point-particle regardless of their internal structure, shape and size. Hence, all objects with the same mass and spin evolve in the same way. An EMRI detection would allow to place constraint on the spin of the secondary in a model-independent fashion, without assuming any property of the secondary other than its mass and spin. This feature offers the unique opportunity to perform theory-agnostic tests of the Kerr bound (5.2.6) $|\chi| \leq 1$ and, in particular, to probe the existence of more exotic families of compact objects like superspinars [198], which exceed the Kerr bound, and were suggested to arise generically in high-energy modifications to GR such as string theories [198].

As we mention earlier, measuring the binary parameters from an EMRI signal is challenging and rather computationally expensive, especially when employing

Teukolsky waveforms. We will illustrate in the next section our parameter estimation of the secondary spin with a Fisher matrix approach, carried out in Ref. [169]. As we shall see later on, a Fisher matrix analysis for EMRIs is plagued by several numerical and computational issues, despite being much easier compared to a full-fledged Bayesian analysis with MCMC. It is then useful to have a crude estimate of the detectability of a certain physical effect before performing an in-depth but time-consuming analysis.
In this section we present a back-on-the-envelop calculation of the minimum resolvable χ, shown in Refs. [118, 186]. We first cover our original results for the computation of linear-spin contribution to the GW phase $\delta\Phi^{\sigma}$. Using these corrections, we obtained a crude estimate of the resolution on χ achievable by LISA by computing the uncertainty on χ which would lead to a total GW dephasing ≈ 1 rad. A larger dephasing would substantially impact a matched-filter search, leading to a significant loss of detected events and potentially to systematics in the parameter estimation [187]. Finally, we illustrate how a measurement of the secondary spin by LISA could potentially put model-independent constraints on superspinars.

Before presenting our results, we remind here that the specific spin of the secondary, defined as $\chi = S/\mu^2$, with S the secondary spin and μ its mass, is analog to the specific spin of the primary $\hat{a} = S_{\rm prim}/M^2$, with $S_{\rm prim}$ the primary spin. If the secondary is a Kerr BH, then $|\chi| \leq 1$. For the fastest millisecond pulsars, $\chi \approx 0.3$. However, χ can be much larger than unity for other objects. For example, a ball of radius 1 cm and mass 1 kg making one rotation per second has $\chi \approx 1 \times 10^{17}$. Astrophysical objects do not reach such extreme values, but can have $\chi \gg 1$ [199]. For example, $\chi \approx 140$ for Earth, and $\chi \approx 10$ for the fastest white dwarfs in accreting binary systems. The above reference values are shown in Fig. 5.3 by horizontal lines. Owing to the mass ratio dependence, for an EMRI $|\sigma| \ll 1$ even when χ is very large, since it is sufficient that $|\chi| \ll 1/q \sim (10^4 - 10^7)$. Therefore, it is possible to linearize the dynamics to $\mathcal{O}(\sigma)$ even when χ is large.

5.2.1 Spin corrections to GW phase

Having computed the fluxes, we can now proceed to determine the adiabatic orbital evolution and the orbital phase by solving Eqs. (5.1.6). We considered an inspiral starting at $\hat{r} = \hat{r}_{\rm start}$. We remind that the starting point $r_{\rm start}$ was chosen such that the initial orbital frequency is the same as in the case of a nonspinning particle at the reference value $r = 10.1M$. Ideally, one would like to evolve the inspiral up to the ISCO. However, since the latter depends on

σ, so it does the duration of the inspiral, also for a fixed value of $\hat{a}$. It would therefore be complicated to compare the phase evolution for different spins of the secondary. Thus, we chose[1] to evolve the inspiral up to a reference end time $t_{\rm ref} = t_{\rm end} - 1/2$ day, where $t_{\rm end}$ is the time to reach the ISCO for a nonspinning secondary for a given value of $\hat{a}$. The offset of $1/2$ day is chosen so that the evolution stops before the ISCO for any value of $\hat{a}$ and χ. By integrating the system (5.1.6), we can obtain the *instantaneous* orbital phase $\Phi(t)$, which can be expanded as

$$\Phi(t) = \Phi^0(t) + \frac{\sigma}{q}\delta\Phi^\sigma(t) + \mathcal{O}(\sigma^2/q)\,, \tag{5.2.1}$$

where $\Phi^0(t)$ is the phase for a nonspinning secondary and $\delta\Phi^\sigma(t)$ is the change due to the $\mathcal{O}(\sigma)$ contribution. Note that, since $\sigma = q\chi$, the linear spin correction is independent of q to the leading order, and it is therefore suppressed by a factor q relative to $\Phi^0(t) = \mathcal{O}(1/q)$. The coefficients $\delta\Phi^\sigma(t)$ were obtained by interpolating $\Phi(t) - \Phi^0(t)$ with a cubic polynomial in χ as follows

$$\Phi(t) - \Phi^0(t) = a_0 + \chi a_1 + q\chi^2 a_2 + q^2\chi^3 a_3\,, \tag{5.2.2}$$

where a_i are the fit coefficients, with $a_0 \approx 0$. The reported values of $a_1 \equiv \delta\Phi^\sigma(t)$ are robust against the truncation order of the fit. The orbital phase $\Phi(t)$ is then related to the GW phase of the dominant mode by $\Phi_{\rm GW}(t) = 2\Phi(t)$. The GW phase as a function of time is shown in Fig. 5.1 for various values of $\hat{a}$. Figure 5.2 also shows the phase difference $\Phi_{\rm GW}(t_{\rm ref}) - \Phi^0_{\rm GW}(t_{\rm ref})$ computed at $t_{\rm ref}$ as a function of the spin χ, showing that it is linear to excellent accuracy. Although we only present the range $|\chi| \leq 2$, the phase difference is linear provided $|\sigma| \ll 1$, i.e. $|\chi| \ll 1/q$, as expected.

The values of $\delta\Phi^\sigma_{\rm GW}(t_{\rm ref})$ (i.e., the slope of the lines shown in Fig. 5.2) for different values of $\hat{a}$ are given in Table 5.1. We fitted these data with two different fits. The first one is

$$\delta\Phi^\sigma_{\rm GW}(t_{\rm ref}) = \sum_{i=0}^{3} b_i(1-\hat{a}^2)^{i/2} + b_4\hat{a}\,, \tag{5.2.3}$$

where $b_0 = 38.44, b_1 = -90.36, b_2 = 99.43, b_3 = -44.95, b_4 = 1.91$. This fit is accurate within 5% in the whole range $\hat{a} \in [0, 0.995]$, with better accuracy at large $\hat{a}$. The second fit is

$$\delta\Phi^\sigma_{\rm GW}(t_{\rm ref}) = \begin{cases} \sum_{i=0}^{3} d_i\hat{a}^i & \hat{a} \leq 0.7 \\ \sum_{i=0}^{3} e_i(1-\hat{a}^2)^{i/2} & 0.7 \leq \hat{a} < 0.995 \end{cases}\,, \tag{5.2.4}$$

[1] A more rigorous choice is to determine the end of the evolution for each binary as the onset of the transition region where the adiabatic approximation breaks down [190–192]. However, since the latter depends on the secondary spin, a choice of a reference time $t_{\rm ref}$ equal for all values of σ would still be required. In our parameter estimation shown in the next section, we stopped the inspiral at the onset of the transition region for non-spinning test-particles.

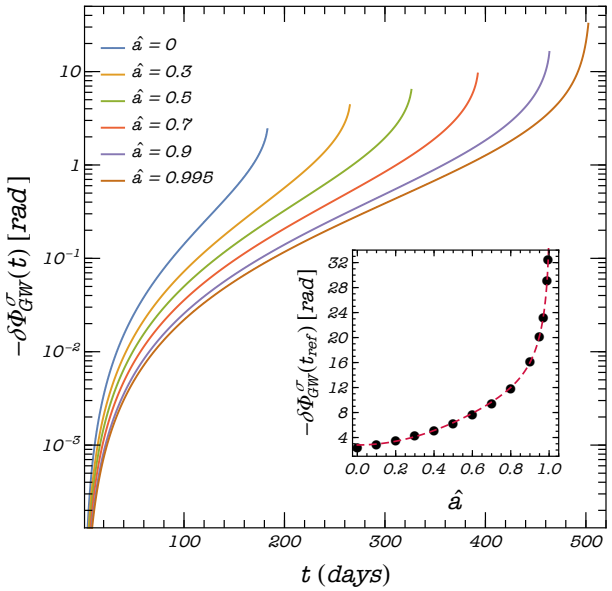

Figure 5.1: Spin correction, $\delta\Phi^{\sigma}_{\rm GW}(t)$, to the instantaneous GW phase [cf. Eq. (5.2.1)] as a function of time up to the ISCO for different values of the spin $\hat{a}$ of the primary. The inset shows the spin correction, $\delta\Phi^{\sigma}_{\rm GW}(t_{\rm ref})$, to the total accumulated phase. The dashed colored curve shows the fit (5.2.3). We assumed $\mu = 30M_{\odot}$ and $M = 10^6 M_{\odot}$ as reference values. Note that in general $\delta\Phi^{\sigma}_{\rm GW}(t_{\rm ref}) < 0$, i.e. when $\chi > 0$ the inspiral lasts longer.

$\hat{a}$	$\delta\Phi^{\sigma}_{\rm GW}(t_{\rm ref})$[rad]	$\Delta\chi$
0	-2.416	-0.414
0.1	-2.962	-0.338
0.2	-3.606	-0.277
0.3	-4.367	-0.229
0.4	-5.277	-0.189
0.5	-6.379	-0.157
0.6	-7.748	-0.129
0.7	-9.522	-0.105
0.8	-12.013	-0.0832
0.9	-16.215	-0.0617
0.95	-20.328	-0.0492
0.97	-23.271	-0.0430
0.990	-29.201	-0.0342
0.995	-32.570	-0.0307

Table 5.1: Spin corrections to the phase $\delta\Phi^{\sigma}_{\rm GW}(t_{\rm ref})$ and its inverse (which gives the resolution on a measurement of χ according to criterion (5.2.5) with $\alpha = 1$) for different values of $\hat{a}$.

where $d_0 = -2.40$, $d_1 = -5.70$, $d_2 = 0.13$, $d_3 = -9.25$, and $e_0 = -41.42$, $e_1/e_0 = -2.49$, $e_2/e_0 = 3.30$, $e_3/e_0 = -2.47$. This piecewise fit is accurate within 1% in the whole range $\hat{a} \in [0, 0.995]$.

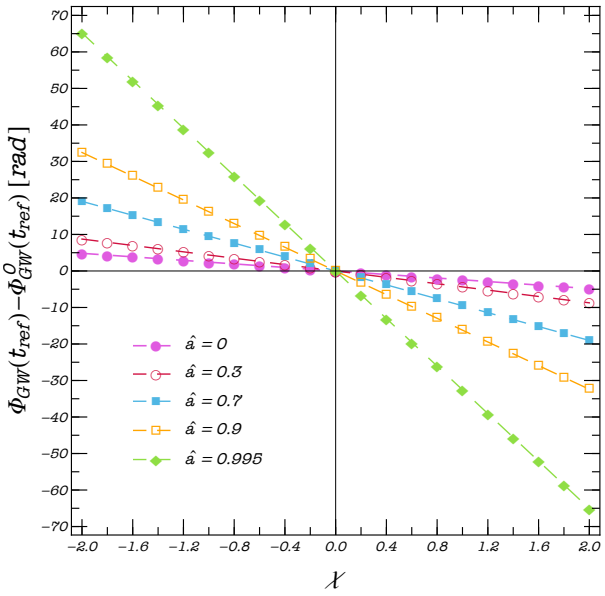

Figure 5.2: Phase difference $\Phi_{\rm GW}(t_{\rm ref}) - \Phi^0_{\rm GW}(t_{\rm ref})$ between a spinning and nonspinning secondary as a function of χ, calculated at $t_{\rm ref} = t_{\rm end} - 1/2$ day, where $t_{\rm end}$ is the time to reach the ISCO for a nonspinning secondary. Note that the curves are linear to an excellent accuracy, showing that $\Phi_{\rm GW}(t_{\rm ref}) - \Phi^0_{\rm GW}(t_{\rm ref}) \propto \chi$.

Finally, we note that the order of magnitude of our dephasing is consistent with previous results that used approximated waveforms. In particular, our dephasing is compatible with the results of Refs. [41, 112] that used "kludge" waveforms, and it agrees within a factor ≈ 2, with the results of Ref. [109], which used effective-one-body waveforms to model the EMRI signal.

5.2.2 Minimum resolvable spin of the secondary

Let us now suppose that the EMRI masses, the spin of the primary BH $\hat{a}$, and the other waveform parameters except χ are known[2], i.e we consider two waveforms which differ only by the value of the spin of the secondary, χ_A and χ_B, respectively. The minimum difference $\Delta\chi = \chi_B - \chi_A$ which would lead to a

[2] As we shall see later on, the primary mass and spin and the secondary mass are the parameters that can be constrained with the tightest accuracy by EMRI observations. See also Refs. [33, 41, 112]

difference in phase larger than α radiant is

$$|\Delta\chi| > \frac{\alpha}{|\delta\Phi^{\sigma}_{\rm GW}|} \,. \tag{5.2.5}$$

The critical value is shown in the last column of Table 5.1 as a function of the primary spin $\hat{a}$ and assuming the 1-radiant condition, i.e. $\alpha = 1$. For a reference value $\hat{a} = 0.7$ ($\hat{a} = 0.9$) with $\alpha = 1$ [187], we obtain $|\Delta\chi| > 0.1$ ($|\Delta\chi| > 0.05$). Thus, our simplified analysis shows that EMRIs can provide a measurement of the spin of the secondary at the level of $5 - 10\%$ for fast spinning primaries.

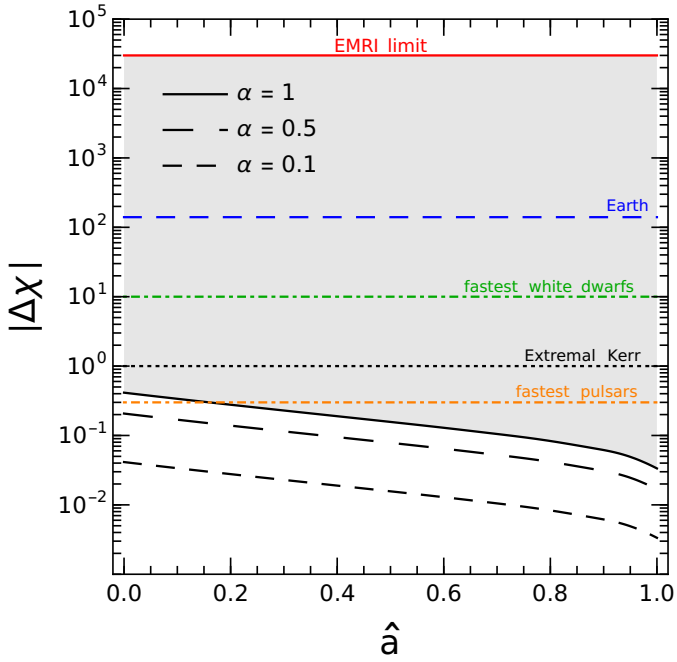

Figure 5.3: Resolution $|\Delta\chi|$ on a GW measurement of the spin of the EMRI secondary obtained saturating the criterion (5.2.5). A measured GW dephasing at the level of α rad would probe the region above each curve. As a reference, we mark with horizontal lines some typical values of χ for astrophysical objects. Our analysis is valid for $\chi \ll 1/q \approx 3 \times 10^4$ (continuous horizontal red line).

Figure 5.3 shows the minimum resolution $|\Delta\chi|$ [obtained saturating Eq. (5.2.5)] as a function of the primary spin. For each chosen value of α, the area above the corresponding curve identifies binary configurations producing a measurable dephasing according to our simplified analysis. In other words, the spin χ of a secondary can be measured with a relative error $|\Delta\chi|/\chi$.

5.2.3 Model-independent constraints on"superspinars"

Some basic relativistic effects associated with BHs remain elusive and have not been yet tested directly. Arguably the most striking one is the fact that, within GR, a BH with mass μ can spin only below a critical value of the angular momentum S,

$$|S| \leq S_{\rm max} \equiv \frac{G\mu^2}{c} \approx 2\times 10^{44}\left(\frac{\mu}{15M_\odot}\right)^2 \,{\rm kg\,m^2/s}\,, \tag{5.2.6}$$

above which a naked singularity would appear. Indeed, the unique stationary solution to GR in vacuum is the Kerr metric, which is regular outside an event horizon only if the above "Kerr bound" is fulfilled. Therefore, any evidence of $|S| > S_{\rm max}$ in a compact object would imply either the presence of matter fields (e.g., compact stars can theoretical exceed the Kerr bound) or a departure from GR. High-energy modifications to GR such as string theories can resolve curvature singularities, making the Kerr bound superfluous. Indeed, in these theories compact objects violating the bound (5.2.6) – so-called *superspinars* – arise generically [198]. A representative example is the large class of regular microstate geometries in supergravity theories (e.g. [200–204]). These solutions have the same asymptotic metric of a Kerr BH, and their deviations in the near-horizon region are suppressed by powers of $M_P/\mu \ll 1$, where M_P is the Planck mass. Therefore, besides the possible violation of the Kerr bound and its consequences (e.g. for the accretion efficiency of compact objects [198]), these solutions are practically indistinguishable from a BH (see Ref. [205] for a review). In this context, testing the bound (5.2.6) provides a *model-independent* way to test GR and high-energy extensions thereof.

However, testing the Kerr bound is very challenging [21, 205–208]. The standard route is to interpret observations in various contexts *assuming* the Kerr metric and look for inconsistencies in explaining the data. This strategy is not optimal as one would wish to compare the Kerr case with some alternative and perform Bayesian model selection. The latter option is however hampered by the fact that the geometry of spinning BHs beyond GR [207] – or of spinning extreme compact objects without a horizon [205] (such as boson stars) – is known only perturbatively or numerically [209–218]. Furthermore, regardless of the technical difficulties, any analysis based on a specific model or theory would be limited to that specific case, whereas performing a model-independent test of the Kerr bound (5.2.6) would be much more profitable.

In this section, we show that many of the above issues can be resolved with tests based on EMRIs, which are also model independent to a large extend.

Remarkably, EMRIs allow to devise tests which do not require any assumption on the specific properties of the secondary other than specifying its multipole moments. This is a great advantage to study generic (and arguably vague) proposals such as the superspinar one. In order to test the Kerr bound (5.2.6) we studied the EMRI evolution in which the secondary is assumed to be either a Kerr BH, which fulfills the constraint $|\chi| \leq 1$, or an extreme compact object [205] that can violate such a bounde.
Our results of Fig. 5.3 and Table 5.1 show that the typical resolution on χ achievable with an EMRI detection can be used to rule out (or detect) superspinars in a large region of the parameter space [186]. For reference values $\chi \approx \hat{a} \approx 0.7$, the accuracy is approximately 15%, which would exclude $\chi > 1$ at 3σ confidence level. Indeed, since $|\chi_A| \leq 1$ for a Kerr BH, an accuracy at the level of (say) $|\Delta\chi| > 0.1$ allows us to distinguish a Kerr BH from another fast spinning object provided the spin of the latter is $|\chi_B| \gtrsim 1 + |\Delta\chi| \approx 1.1$. In Fig. 5.3 we show the exclusion plot for the spin of a superspinar obtained using the criterion (5.2.5) and under the most conservative assumption, $\chi_A = 1$, as a function of the spin $\hat{a}$ of the primary. We consider different values for the dephasing threshold α. For the standard choice of $\alpha = 1\,\text{rad}$, our results suggest that it should be possible to exclude/probe the range $|\chi_B| > 1.4$ ($|\chi_B| > 1.05$) for nonspinning (highly-spinning) primaries. Since no theoretical upper bound is expected for superspinars (other, possibly, than those coming from the ergoregion instability [219–222]) a spin measurement at this level can potentially probe a vast region of the parameter space for these objects.

One might argue that, while clearly incompatible with the secondary being a Kerr BH, a putative EMRI measurement of $|\chi| > 1$ could still be compatible with the secondary being a neutron star or a white dwarf. Given that neutron stars and white dwarfs have masses in the narrow range $\mu \sim (1-2)M_\odot$, an EMRI measurement of μ larger than $3M_\odot$ (resp. $\sim 1.4M_\odot$) would exclude a standard origin for the superspinar, as a neutron star (resp. a white dwarf). Similarly, no compact object spinning above the Kerr bound is know with $\mu \ll M_\odot$. Furthermore, even in the case in which $\mu \in (1,2)M_\odot$, the spin of an isolated compact star is expected to be significantly smaller than the Kerr bound. As a reference, the spin of the fastest pulsar known to date is $\chi \approx 0.3$ [223]. Out of 340 observations of millisecond pulsars in the ATNF Pulsar Database [224], $\langle\chi\rangle = 0.11 \pm 0.04$, suggesting that $|\chi| > 1$ would be very unlikely. Isolated white dwarfs have comparable values of χ. The fastest spinning white dwarf to date has $\chi \approx 10$, but it is strongly accreting from a binary companion [225]. Less compact objects, such as brown dwarfs, might also have spin larger then the Kerr bound, but can be easily distinguishable from exotic superspinars, as they

are tidally disrupted much before reaching the ISCO[3].

Finally, in the context of our analysis one could wonder whether it is theoretically consistent to study a secondary superspinar around a primary Kerr BH. This is indeed the case in two scenarios (see Ref. [205] for a review): a) if superspinars arise within GR in the presence of exotic matter fields, in such case both Kerr BHs and superspinars can co-exist in the spectrum of solutions of the theory; b) if superspinars arise in high-energy modified theories of gravity such as string theories, as originally proposed [198]. In the latter case it is natural to expect that high-energy corrections which are relevant for the secondary might be negligible for the primary. Indeed, in an effective-field-theory approach high-energy corrections to GR modify the Einstein-Hilbert action with the inclusion of higher-order curvature terms of the form [21,207]

$$R + ... + \beta (R_{abcd})^n + ... \,, \quad n > 1 \tag{5.2.7}$$

where R is the Ricci scalar, R_{abcd} schematically denotes terms that depend on the Riemann tensor, and β is a coupling constant with dimensions of a $(\text{length})^{2(n-1)}$. In these theories relative corrections to the metric of a compact object of size $\sim L$ are of the order of [226]

$$\frac{\beta}{L^{2(n-1)}} \,, \tag{5.2.8}$$

or some power thereof. Thus, the difference between the high-curvature corrections of the secondary relative to those of the primary scales as

$$\sim \frac{M^{2(n-1)}}{\mu^{2(n-1)}} = q^{2(1-n)} \gg 1 \,. \tag{5.2.9}$$

This heuristically shows the obvious fact that in an EMRI the SCO is much more affected by the high-curvature corrections than the primary, especially for high-order terms (i.e., higher values of n).
In certain high-curvature modifications to GR, the secondary might also be charged under new fundamental fields, in which case there is also extra emission (in particular there could be dipolar, $\ell = 1$, fluxes) [37,40,227]. We neglected extra radiation channels and considered only the standard GW emission in GR. The motivation for this choice is twofold: (i) superspinars can also arise within GR in the presence of exotic matter fields, in which case our analysis is exact; (ii) in the

[3] As a reference, the critical tidal-disruption radius is of the order $R_t \sim M q^{2/3}/C$, where $C = \mu/R$ is the compactness of the secondary with radius R. For a typical brown dwarf $C \sim 10^{-6}$, and $R_t \sim 100M$ for $q \sim 10^{-6}$. In general, objects less compact than white dwarfs are tidally disrupted at low frequency and can be distinguished on this ground.

context of supergravity and string theories, putative extra degrees of freedom are expected to be extremely heavy and therefore do not propagate at the frequency of an EMRI. Thus, corrections to the dissipative sector are also negligible. At any rate, extra putative dissipative channels (e.g. due to massless degrees of freedom) can be straightforwardly accommodated within our framework.

5.3 Parameter estimation analysis

In section 5.2, we showed that the effect of the secondary spin can contribute to more than 1 rad dephasing, therefore suggesting that it could provide detectable effects. However, such a simplified analysis neglects possible correlations between the waveform parameters that might hamper their measurability, especially for subleading terms. In order to gain a deeper insight on the detectability of the SCO spin we performed a Fisher matrix analysis. As a first step, we illustrate the gravitational waveform emitted by an EMRI and the corresponding response of the LISA detector to such signal. Then, we briefly introduce the Fisher information matrix, along with the numerical setup adopted. Finally, we present the results of our parameter estimation analysis.
Throughout the remaining of the chapter, repeated indices does not intend summation.

5.3.1 Waveform computation

The emitted waveform in the Teukolsky formalism is given by (see Eq. (4.1.22))

$$h_+ - ih_\times = 2\frac{\mu}{D}\sum_{\ell,m}\mathcal{A}_{\ell m\hat{\omega}}(t)\,{}_sS^c_{\ell m}(\vartheta,t)e^{-i\Phi(t)}\,, \tag{5.3.1}$$

$$\Phi(t) = m\phi(t) + m(\varphi+\phi_0)\,, \tag{5.3.2}$$

where ϕ_0 is the initial orbital phase, $\mathcal{A}_{\ell m\hat{\omega}} \equiv \hat{Z}^H_{\ell m\hat{\omega}}/\hat{\omega}^2$, and $\hat{Z}^H_{\ell m\hat{\omega}} = M^2 Z^H_{\ell m\hat{\omega}}$. D is the source's luminosity distance from the detector[4], and (ϑ,φ) identify the direction, in Boyer-Lindquist coordinates, of the latter in a reference frame centered at the source. Since ϕ_0 in Eq. (5.3.1) is degenerate with the azimuth direction φ, from now on we will identify the initial phase as $\phi_0 \to \varphi + \phi_0$. From

[4]In this detector frame configuration, the component masses in Eq. (5.3.1) are rescaled with respect to the source-frame quantities by the redshift factor $(1+z)$.

Eq. (5.3.1) it is straightforward to get the two waveform polarizations

$$h^{+}_{\ell m} = 2\frac{\mu}{D}{}_{s}S^{c}_{\ell m}(\mathrm{Re}\,\mathcal{A}_{\ell m\hat{\omega}}\cos\Phi + \mathrm{Im}\,\mathcal{A}_{\ell m\hat{\omega}}\sin\Phi)\,, \tag{5.3.3}$$

$$h^{\times}_{\ell m} = 2\frac{\mu}{D}{}_{s}S^{c}_{\ell m}(\mathrm{Re}\,\mathcal{A}_{\ell m\hat{\omega}}\sin\Phi - \mathrm{Im}\,\mathcal{A}_{\ell m\hat{\omega}}\cos\Phi)\,, \tag{5.3.4}$$

being $\mathrm{Re}\,\mathcal{A}_{\ell m\hat{\omega}}$ and $\mathrm{Im}\,\mathcal{A}_{\ell m\hat{\omega}}$ the real and imaginary parts of $\mathcal{A}_{\ell m\hat{\omega}}$. In the presence of the secondary spin, we expand the amplitudes $\mathcal{A}_{\ell m\hat{\omega}} = \mathcal{A}^{0}_{\ell m}(\hat{\omega}^{0}) + \sigma\mathcal{A}^{1}_{\ell m}(\hat{\omega}^{0},\hat{\omega}^{1}) + \mathcal{O}(\sigma^{2})$, where

$$\mathcal{A}^{0}_{\ell m} = \frac{\hat{Z}^{H,0}_{\ell m\hat{\omega}}}{(\hat{\omega}^{0})^{2}}\,, \tag{5.3.5}$$

$$\mathcal{A}^{1}_{\ell m} = -2\frac{\hat{\omega}^{1}}{\hat{\omega}^{0}}\mathcal{A}^{0}_{\ell m} + \frac{\hat{Z}^{H,1}_{\ell m\hat{\omega}}}{(\hat{\omega}^{0})^{2}}\,. \tag{5.3.6}$$

Therefore, we recast the two polarizations as:

$$h^{+}_{\ell m} = 2\frac{\mu}{D}({}_{-2}S^{0}_{\ell m} + \sigma\,{}_{-2}S^{1}_{\ell m})\,A^{+}_{\ell m}\,, \tag{5.3.7}$$

$$h^{\times}_{\ell m} = 2\frac{\mu}{D}({}_{-2}S^{0}_{\ell m} + \sigma\,{}_{-2}S^{1}_{\ell m})\,A^{\times}_{\ell m}\,, \tag{5.3.8}$$

with

$$A^{+}_{\ell m} = \mathrm{Re}(\mathcal{A}^{0}_{\ell m} + \sigma\mathcal{A}^{1}_{\ell m})\cos\Phi + \mathrm{Im}(\mathcal{A}^{0}_{\ell m} + \sigma\mathcal{A}^{1}_{\ell m})\sin\Phi\,, \tag{5.3.9}$$

$$A^{\times}_{\ell m} = \mathrm{Re}(\mathcal{A}^{0}_{\ell m} + \sigma\mathcal{A}^{1}_{\ell m})\sin\Phi - \mathrm{Im}(\mathcal{A}^{0}_{\ell m} + \sigma\mathcal{A}^{1}_{\ell m})\cos\Phi\,. \tag{5.3.10}$$

The LISA response to the GW signal emitted by an EMRI can be written in terms of the $+,\times$ polarizations as

$$h_{\alpha}(t) = F^{+}_{\alpha}(\vartheta_{D},\varphi_{D},\Psi)h_{+}(t,D,\vartheta,\varphi) + F^{\times}_{\alpha}(\vartheta_{D},\varphi_{D},\Psi)h_{\times}(t,D,\vartheta,\varphi)\,, \tag{5.3.11}$$

where $\alpha = I, II$ refers to the two independent Michelson-like detectors that constitute the LISA response [228]. The antenna pattern functions[5] F^{+}_{α} and $F^{\times}_{\alpha}$ depend on the direction $(\vartheta_{D},\varphi_{D})$ of the source with respect to the detector's frame and on the polarization angle Ψ [112]:

$$F^{+}_{I} = \frac{1}{2}(1+\cos^{2}\vartheta_{D})\cos(2\varphi_{D})\cos(2\Psi) - \cos\vartheta_{D}\sin(2\varphi_{D})\sin(2\Psi)\,, \tag{5.3.12}$$

$$F^{\times}_{I} = \frac{1}{2}(1+\cos^{2}\vartheta_{D})\cos(2\varphi_{D})\sin(2\Psi) + \cos\vartheta_{D}\sin(2\varphi_{D})\cos(2\Psi)\,, \tag{5.3.13}$$

[5] For simplicity, we assume that $F_{+,\times}$ are constant within the frequency range sampled by the binary configurations considered. However, for values of f larger than $f_{*} = 19.1\,\mathrm{mHz}$, LISA's antenna pattern functions also depend on the GW frequency [229].

where $F_{II}^{+,\times}$ can be obtained by rotating φ_D in the previous expressions by $-\pi/4$, i.e. $F_{II}^{+,\times}(\vartheta_D, \varphi_D, \psi) = F_I^{+,\times}(\vartheta_D, \varphi_D - \pi/4, \psi)$.
Given the LISA satellite motion, such angles are not constant but vary with time. However it is possible to recast $(\vartheta_D, \varphi_D, \Psi)$ in terms of fixed angles (ϑ_S, φ_S) and (ϑ_K, φ_K) which provide the direction of the source and of the orbital angular momentum (which for equatorial orbits coincides with the direction of the primary spin) in a heliocentric reference frame attached with the ecliptic [41]. The same applies to the polar angle ϑ in the signal (5.3.1):

$$\cos\vartheta = \cos\vartheta_S \cos\vartheta_K + \sin\vartheta_S \sin\vartheta_K \cos(\varphi_S - \varphi_K)\,. \tag{5.3.14}$$

Finally, we also include the effect of the Doppler modulation by introducing an offset in the phase

$$\Phi(t) \to \Phi(t) + \frac{\hat{\omega} R}{M} \sin\vartheta_S \cos[2\pi(t/T_{\rm LISA}) - \varphi_S]\,, \tag{5.3.15}$$

where $R = 1\text{AU}$ and $T_{\rm LISA} = 1\,\text{yr}$ is LISA's orbital period [112].
We have considered $T = 1\,\text{yr}$ observation time, ending the orbital evolution at the onset of the transition region as defined in [190], i.e. at $\hat{r}_{\rm ISCO} + \delta\hat{r}$ with $\delta\hat{r} = 4q^{2/5}$. We have chosen $\delta\hat{r}$ by setting $X = 1$ and $R_0 = 4$ in Eq. (3.20) of [190] for all the configurations analysed. In general, $\delta\hat{r} \sim \gamma q^{2/5}$ with $\gamma \sim O(1)$, and we checked that the Fisher matrices computed below are unaffected by the specific value of γ, since the signal-to-noise ratio (SNR) accumulated around the transition region is negligible.

5.3.2 Fisher matrix analysis for EMRI waveforms

The GW signal emitted by an EMRI with a spinning secondary, moving on the equatorial plane with spin (anti-)aligned to the z-axis, is completely specified by eleven parameters $\vec{x} = \{\vec{x}_{\rm I}, \vec{x}_{\rm E}\}$: (i) five intrinsic parameters $\vec{x}_{\rm I} = (\ln\mu, \ln M, \hat{a}, \chi,$ and $\hat{r}_0)$ and (ii) six extrinsic parameters$\vec{x}_{\rm E} = (\phi_0, \vartheta_S, \varphi_S, \vartheta_K, \varphi_K, \ln D)$, where we remind that: (M, μ) are the mass components, $(\hat{a}, \chi)$ are the primary and secondary spin parameters, $(\phi_0, \hat{r}_0)$ define the binary initial phase and orbital radius, and D is the source luminosity distance. The four angles (ϑ_S, φ_S) and (ϑ_K, φ_K) correspond to the colatitude and the azimuth of the source sky position and of the orbital angular momentum, respectively [41]. Since the orbit is circular and equatorial, the orbital angular momentum has no precession around the primary spin, and the orbital and primary angular momenta are parallel to each other.

In the limit of large SNR, the errors on the source parameters inferred by a given EMRI observation can be determined using the Fisher information matrix:

$$\Gamma_{ij} = \sum_{\alpha=I,II} \left(\frac{d\tilde{h}_\alpha}{dx^i} \middle| \frac{d\tilde{h}_\alpha}{dx^j} \right)_{\vec{x}=\vec{x}_0} , \tag{5.3.16}$$

where $\vec{x}_0$ corresponds to the true set of binary parameters, and we have introduced the noise-weighted scalar product between two waveforms p_α and q_α in the frequency domain:

$$(p_\alpha|q_\alpha) = 2 \int_{f_{\rm min}}^{f_{\rm max}} \frac{df}{S_n(f)} [\tilde{p}^*_\alpha(f)\tilde{q}_\alpha(f) + \tilde{p}_\alpha(f)\tilde{q}^*_\alpha(f)] . \tag{5.3.17}$$

Here the tilded quantities correspond to the Fourier transform of the time-domain waveforms, and a star identifies complex conjugation. We used Simpson's integration rule to compute the scalar product. As discussed in the previous section, the index α runs over the two independent channels of the LISA interferometer. In our computations we set $f_{\rm min} = 10^{-4}$ Hz, while we choose $f_{\rm max}$ as

$$f_{\rm max} = \frac{\ell_{\rm max}}{2\pi} \frac{1}{M} \left[\widehat{\Omega}^0(\hat{r}_{\rm ISCO}) + \sigma \widehat{\Omega}^1(\hat{r}_{\rm ISCO}) \right] , \tag{5.3.18}$$

where $\hat{r}_{\rm ISCO}$ is the ISCO for a nonspinning test particle and $\ell_{\rm max}$ the maximum harmonic index ℓ considered for a given system. Following the Shannon theorem, for the sampling time we used $\Delta t_s = \lfloor 1/(2f_{\rm max}) - 1 \rfloor$ while the number of samples $n_s = T/\Delta t_s$ is adjusted to be an even number for a more efficient computation of the fast Fourier transform. As discussed before, for all systems the binary evolves for $T = 1$ yr before the plunge, so the frequency content of the signal is smaller than the range $[f_{\rm min}, f_{\rm max}]$.

The waveform scalar product also allows us to define the optimal SNR for a given signal h as

$$\text{SNR} = (h|h)^{1/2} , \tag{5.3.19}$$

which scales linearly with the inverse of the luminosity distance. Furthermore, in the large-SNR limit the covariance matrix scales inversely with the SNR so, for a given set of parameters, it is straightforward to rescale the errors by changing the distance D (and hence the SNR).

The inverse of Γ_{ij} yields the covariance matrix, Σ_{ij}, whose diagonal elements correspond to the statistical uncertainties of the waveform parameters,

$$\sigma^2_{x_i} = \Sigma_{ii} \geq (\Gamma^{-1})_{ii} , \tag{5.3.20}$$

whereas the off-diagonal elements correspond to the correlation coefficients,

$$c_{x_i x_j} = \Sigma_{ij} / \sqrt{\Sigma_{ii}\Sigma_{jj}} . \tag{5.3.21}$$

Hereafter we consider two data-analysis scenarios, depending on whether we also include a prior probability functions on the spin of the SCO or not. We follow the approach described in [230], assuming for the prior a Gaussian distribution $p_0(\chi)$ with standard deviation $\sigma_\chi = 1$. Given Γ_0 the Fisher matrix of the prior (which in our case has all vanishing elements except for the diagonal term corresponding to the secondary spin, with $(\Gamma_0)_{\chi\chi} = 1/\sigma_\chi$), the new errors on the source parameters are obtained by modifying Eq. (5.3.20) as

$$\sigma^2_{x_i} = [(\Gamma + \Gamma_0)^{-1}]_{ii} \,. \tag{5.3.22}$$

We notice that the matrix Γ_0 is independent of the distance D, therefore when including a prior, the error on χ does not, in general, scale inversely with the SNR.
In addition to the standard deviations on the eleven parameters defined above, we also analyze the error box on the solid angle spanned by the unit vector associated to (ϑ_S, φ_S) and (ϑ_K, φ_K):

$$\Delta\Omega_i = 2\pi |\sin\vartheta_i| \sqrt{\sigma^2_{\vartheta_i}\sigma^2_{\varphi_i} - \Sigma^2_{\vartheta_i\varphi_i}} \,. \tag{5.3.23}$$

where $i = (S, K)$.
From a technical point of view, the fact that the EMRI waveform is known numerically implies that, to compute the Fisher matrix, one needs to evaluate numerical derivatives. Apart from the derivative with respect to the luminosity distance D (which can be obtained analytically since the waveform scales as $h \sim 1/D$), we have computed the derivatives of the other ten parameters using the five-points stencil formula, namely:

$$\frac{dh}{dx} = \frac{1}{12\epsilon}[h(x-2\epsilon) - h(x+2\epsilon) + 8h(x+\epsilon) - 8h(x-\epsilon)] + \mathcal{O}(\epsilon^4) \,. \tag{5.3.24}$$

The numerical derivative is sensitive to the value of the shift ϵ chosen to compute the finite differences. We have explored various combinations of ϵ for each parameter, finding in general a range of at least two orders of magnitude in which the Fisher (and the covariance) matrices show convergence in the small-ϵ limit (see Appendix F for a detailed analysis).
It is well known that the Fisher matrices used for the data-analysis of EMRIs are badly ill-conditioned [188], which means that a small perturbation in the matrix (due to numerical or systematic errors) is greatly amplified after computing the inverse. As a rule of thumb, for a condition number[6] $\kappa = 10^k$, one may lose up to k digits of accuracy, which should be added to the numerical errors.

[6] For a symmetric, positive-definite matrix, the condition number κ is given by the ratio between the largest and the smallest of the matrix eigenvalues.

In our setup, an accurate inversion of the Fisher matrix requires at least 60-digit precision in the waveform in most of the configurations, and in the worst case (namely $\hat{a} = 0.9, \chi = 1, \mu = 10, 100 M_\odot$), up to 90-digit precision.
To achieve such precision in the waveform, we have computed the GW fluxes with 70-digit precision (100-digit precision in the most demanding case), which allowed us to derive the Fisher matrices with no less than 38-digit precision. In Appendix F we provide a detailed analysis of the stability of the Fisher matrices for the problem at hand.

5.3.3 Settings

We have computed the numerical integral in Eq. (5.3.17) using the LISA noise spectral density curve (PSD) of Ref. [229], including the contribution of the confusion noise from the unresolved Galactic binaries assuming $T = 1\,\mathrm{yr}$ of observation time. The PSD analytic fit for the detector noise consists of two parts: the instrumental and the confusion noise produced by unresolved galactic binaries, i.e.

$$S_n(f) = S_n^{\rm Ins}(f) + S_n^{\rm WDN}(f)\,. \tag{5.3.25}$$

where

$$S_n^{\rm Ins}(f) = A_1 \left[P_{\rm OMS} + 2(1+\cos^2(f/f_\star))\frac{P_{\rm acc}}{(2\pi f)^4}\right]\left(1+\frac{6}{10}\frac{f^2}{f_\star^2}\right)\,,$$

$A_1 = \frac{10}{3L^2}$, $L = 2.5\mathrm{Gm}$, $f_\star = 19.09\mathrm{mHz}$, while

$$P_{\rm OMS} = (1.5\times 10^{-11}\mathrm{m}^2\left[1+\left(\frac{2\mathrm{mHz}}{f}\right)^4\right]\ \mathrm{Hz}^{-1}\,,$$
$$P_{\rm ACC} = (3\times 10^{-15}\mathrm{ms}^{-2})^2\left[1+\left(\frac{0.4\mathrm{mHz}}{f}\right)^2\right]\left[1+\left(\frac{f}{8\mathrm{mHz}}\right)^4\right]\ \mathrm{Hz}^{-1}\,.$$

For the white dwarf contribution

$$S_n^{\rm WDN} = A_2 f^{-7/3} e^{-f^\alpha+\beta f\sin(\kappa f)}[1+\tanh(\gamma(f_k-f))]\ \mathrm{Hz}^{-1}\,,$$

with the amplitude $A_2 = 9\times 10^{-45}$, and the coefficients

$$(\alpha,\beta,\kappa,\gamma,f_k) = (0.171, 292, 1020, 1680, 0.00215)\,.$$

The PSD, taken from Ref. [231], is shown in Fig. 5.4.

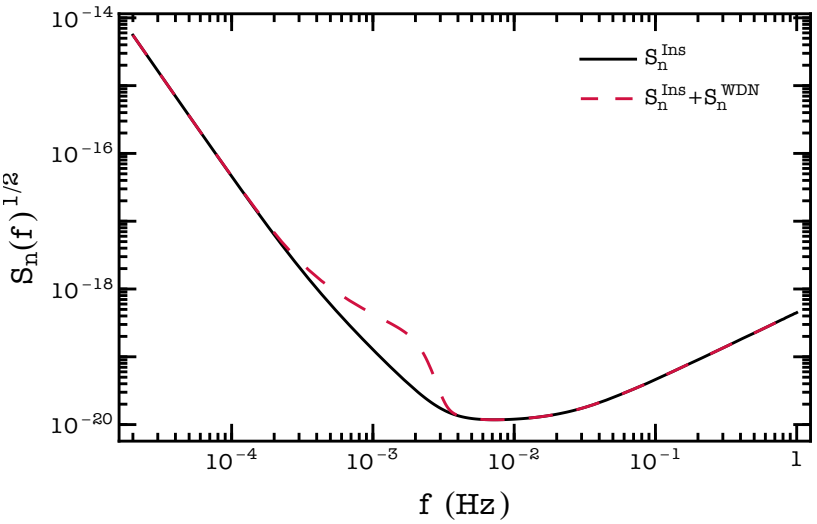

Figure 5.4: Noise spectral density for LISA as a function of the frequency, with and without the confusion noise produced by unresolved galactic white dwarf binaries (WDN). Picture taken from Ref. [231]

In order to reduce the spectral leakage in the frequency domain due to the Fourier transform, we have tapered the time-domain waveforms $h(t = i\Delta t)$ for $i = 0, \dots n_s - 1$ with a Tukey window $w[n]$ with window size $\beta = 0.05$.

$$w[n] = \begin{cases} \sin\left[\frac{n\pi}{\beta(1-N)}\right]^2 & 0 \leq n \leq \frac{\beta(N-1)}{2}\,, \\ 1 & \frac{\beta(N-1)}{2} \leq n \leq (N-1)(1-\frac{\beta}{2})\,, \\ \sin\left[\frac{(1+n-N)\pi}{\beta(1-N)}\right]^2 & (N-1)(1-\frac{\beta}{2}) \leq n \leq N-1\,. \end{cases}$$

We checked that our results do not change noticeably when varying β around this fiducial value.

For simplicity, in our analysis we fix the injected angles to the fiducial values $\vartheta_S = \pi/4, \phi_S = 0, \vartheta_K = \pi/8, \phi_K = 0$. Moreover, we consider a primary mass $M = 10^6 M_\odot$, and two choices of the secondary mass: $\mu = (10, 100) M_\odot$. We compute the Fisher matrices for sources at fixed luminosity distance $D = 1\,\text{Gpc}$, but renormalize the results to a fixed fiducial SNR such that SNR $= 30$ and SNR $= 150$, for the two choices of μ, respectively.

In order to analyze how the inclusion of higher-order ($\ell \geq 2$) multipoles in the signal (5.3.11) may affect the measurement of the source parameters, in the following we consider the purely quadrupolar case ($\ell = 2$), and the cases in which the octupole ($\ell = 3$) and the hexadecapole ($\ell = 4$) are included.

Finally, we shall discuss two cases separately: (i) in Sec. 5.3.4 we neglect the spin of the secondary (i.e., removing χ from the waveform parameters); (ii) in

Sec. 5.3.5 we perform a more comprehensive analysis by including also the SCO spin.
Before presenting our results for the parameter estimation with the Fisher matrix, we report as reference in Tab. 5.2 the GW dephasing $\delta\phi_{\rm GW}$ between a spinning particle with $\chi = 1$ and a non-spinning particle for the cases considered in section 5.3.5, Tables 5.5 and 5.7.

$\mu/M_\odot$	$\hat{a}$	$\delta\phi_{\rm GW}$[rad]
10	0	1.06
	0.9	2.38
	0.99	3.48
100	0.9	5.48
	0.99	6.47

Table 5.2: GW dephasing $\delta\phi_{\rm GW}$ between a spinning particle with $\chi = 1$ and a non-spinning particle for the cases considered in Tables 5.5 and 5.7. The GW phase difference is computed for the dominant $\ell = 2$ mode, i.e $\phi_{\rm GW}(t) = 2\phi(t)$ at $\hat{r}_{\rm ISCO} + \delta\hat{r}$.

5.3.4 Results: Neglecting the spin of the secondary

We start by neglecting the secondary spin χ from the waveform parameters. Our results are summarized in Table 5.3 and Table 5.4. The former shows results when the spin $\hat{a}$ is removed from the waveform parameters, and assume that both the primary and the secondary are nonspinning. In Table 5.4 instead, we include the spin of the primary as a parameter, injecting $\hat{a} = 0.9$ but keeping all other parameters unchanged with respect to the injection of Table 5.3 (except for $\hat{r}_0$, since the latter changes in order for the binary to take exactly $T = 1\,$yr to reach the ISCO).
For $\ell = 2$, our results are in very good agreement with the analysis of [112,113] which used approximated kludge waveforms. Being the latter analytical, the Fisher-matrix analysis is significantly faster than in our case. It is therefore reassuring that a fully-relativistic, numerical waveform provides the same results.
Furthermore, we find that including the octupole ($\ell = 3$) contribution to the signal does not affect the measurement errors on the intrinsic parameters, but it improves the errors on the luminosity distance and on the solid angle which defines the orbital angular momentum ($\Delta\Omega_K$) by one order and two orders of magnitude, respectively. Adding the $\ell = 4$ multipole does not improve such errors significantly, suggesting that $\ell > 4$ multipoles are negligible for this purpose.

As expected, increasing the dimensionality of the waveform parameter space by including the primary spin, reduces the accuracy on the intrinsic parameters, especially the masses. This happens despite the fact that the ISCO frequency is higher for a rapidly-spinning BH, since we chose to normalize the results to the same SNR. For sources at a fixed distance, the SNR in the $\hat{a} = 0.9$ case is four times larger than in the nonspinning case, almost compensating the higher dimensionality of the parameter space.
Overall, all parameters are measured with exquisite accuracy, confirming previous analyses that used approximated semi-relativistic waveforms [33,41,112,113].

ℓ	$\ln M$	$\ln \mu$	$\hat{r}_0$	ϕ_0	$\ln D$	$\Delta\Omega_S$	$\Delta\Omega_K$
2	-4.62	-4.19	-4.96	0.54	-0.27	3.1×10^{-3}	1.5
2+3	-4.64	-4.22	-4.97	-0.66	-1.46	2.4×10^{-3}	7.9×10^{-3}
2+3+4	-4.64	-4.22	-4.97	-0.67	-1.46	2.4×10^{-3}	7.3×10^{-3}

Table 5.3: Errors on the intrinsic source parameters, on the luminosity distance, and on the solid angles which define the orientation and the orbital angular momentum of the binary, for various choices of the multipoles included in the waveform. Both EMRI components are nonspinning ($\hat{a} = \chi = 0$), with $M = 10^6 M_\odot$ and $\mu = 10 M_\odot$. We neglect the spin parameters of both binary components ($\hat{a}$ and χ) in the waveform. The SNR for the three configurations ($D = 1$ Gpc) is SNR $= (22.2, 24.8, 25.2)$, but the errors are all normalized to the fiducial value SNR $= 30$. For clarity, we present the $\log_{10}$ of the errors on $\ln M$, $\ln \mu$, $\hat{r}_0$, ϕ_0, and $\ln D$. For example, an entry "-4" for $\ln M$ ($\hat{r}_0$) means that the relative (absolute) error on M ($\hat{r}_0$) is 10^{-4}.

ℓ	$\ln M$	$\ln \mu$	$\hat{a}$	$\hat{r}_0$	ϕ_0	$\ln D$	$\Delta\Omega_S$	$\Delta\Omega_K$
2	-3.24	-3.53	-4.15	-4.45	0.48	-0.33	7.9×10^{-4}	2.5
2+3	-3.25	-3.54	-4.16	-4.46	-0.52	-1.34	7.3×10^{-4}	1.3×10^{-2}
2+3+4	-3.25	-3.55	-4.16	-4.46	-0.53	-1.35	7.2×10^{-4}	1.1×10^{-2}

Table 5.4: Same as Table 5.3 but assuming a spinning primary with $\hat{a} = 0.9$ and including $\hat{a}$ in the waveform parameters. In this case the SNR of the three configurations is SNR $= 92.2, 94.7, 95$, but we again normalize the errors to the fiducial value SNR $= 30$.

5.3.5 Results: Including the spin of the secondary

We now move to a more comprehensive analysis, by including the secondary spin in the waveform parameters. We shall present two cases: with and without imposing a Gaussian prior on χ. We start by neglecting the spin of the primary

in the waveform parameters and injecting $\hat{a} = 0$. The results of the Fisher-matrix error analysis are presented in Tables 5.5 and 5.6, which are the extension of Table 5.3 to the case of a spinning secondary.

ℓ	prior	$\ln M$	$\ln \mu$	χ	$\hat{r}_0$	ϕ_0
2	no	-2.95	-3.66	2.51	-4.18	0.55
	yes	-4.62	-4.19	-0.13	-4.96	0.55
2+3	no	-2.97	-3.67	2.50	-4.19	-0.64
	yes	-4.63	-4.22	-0.082	-4.97	-0.66
2+3+4	no	-2.97	-3.67	2.50	-4.19	-0.65
	yes	-4.63	-4.22	-0.076	-4.97	-0.67

Table 5.5: Same as Table 5.3 but including a spinning secondary with $\chi = 1$ and also considering the case in which a Gaussian prior on χ (with $\sigma_\chi = 1$) is enforced.

ℓ	prior	$\ln D$	$\Delta\Omega_S$	$\Delta\Omega_K$
2	no	-0.27	4.4×10^{-3}	1.6
	yes	-0.27	3.1×10^{-3}	1.5
2+3	no	-1.46	3.8×10^{-3}	8.6×10^{-3}
	yes	-1.46	2.4×10^{-3}	7.9×10^{-3}
2+3+4	no	-1.46	3.7×10^{-3}	7.9×10^{-3}
	yes	-1.46	2.4×10^{-3}	7.3×10^{-3}

Table 5.6: Same as Table 5.3 but including a spinning secondary with $\chi = 1$ and also considering the case in which a Gaussian prior on χ (with $\sigma_\chi = 1$) is enforced. Here we show the error on the distance and sky localization $\Delta\Omega_S$ and $\Delta\Omega_K$ on the primary spin and source, respectively

By comparing Tables 5.5, 5.6 with Table 5.3 we observe some interesting features. First of all, in the case in which a prior on the secondary spin is not imposed the relative error on χ is around 30000%, confirming that this parameter is not measurable [112, 113]. Nonetheless, in this case the errors on both masses deteriorate significantly (albeit they remain excellent in absolute terms). This issue is due to nonnegligible correlations between χ and the masses. Indeed, we find that all the intrinsic parameters are strongly correlated with χ. The correlation (in absolute value) is typically ≈ 0.99 and never less than 0.95. Therefore, large variations in χ as those shown in Table 5.5 can correlate with a small change in the total mass or in the mass ratio.
This issue can be fixed by imposing a prior on the secondary spin, in such a way that also its errors cannot become too large. As shown in Table 5.5,

imposing a Gaussian prior on χ with standard deviation $\sigma_\chi = 1$ reduces the errors on this parameter, but the confidence interval is as large as the prior range, again confirming that this parameter is not measurable. (In other words, the measurement errors are dominated by the priors.) Nonetheless, adding a prior on χ restores the accuracy in the measurements of the other intrinsic parameters, which become very similar to the case in which χ is neglected in the waveform (compare Table 5.5 with prior to Table 5.3). We also find that, including a prior on χ, the correlations between χ and the other parameters are much smaller.
From Table 5.6 we also observe that the role of $\ell > 2$ multipoles is not affected by the secondary spin: also in this case the inclusion of the $\ell = 3$ multipole improves the errors on the distance and on the orbital angular momentum solid angle by one and two orders of magnitude, respectively.
Finally, we are now in a position to present the complete analysis by including both the spin of the primary and of the secondary. A summary of our results are presented in Table 5.7 for the cases with $\hat{a} = 0.9$ and $\hat{a} = 0.99$, and considering both $\mu = 10M_\odot$ and $\mu = 100M_\odot$. In this analysis we only include the quadrupole ($\ell = 2$) since anyway the higher multipoles do not affect the errors on the intrinsic parameters.

$\tilde{a}_{\rm injected}$	$\mu/M_\odot$	prior	$\ln M$	$\ln \mu$	$\hat{a}$	χ	$\hat{r}_0$	ϕ_0
0.9	10	no	-2.26	-2.41	-2.66	2.85	-3.88	0.48
		yes	-3.24	-3.53	-4.14	0.48	-4.45	0.48
	100	no	-2.20	-2.39	-2.78	1.66	-4.14	-0.015
		yes	-3.30	-3.52	-4.32	0.064	-4.93	-0.024
0.99	10	no	-2.81	-2.96	-4.55	1.98	-3.89	0.47
		yes	-3.51	-3.76	-4.67	0.52	-4.32	0.47
	100	no	-2.14	-2.33	-3.39	1.21	-3.75	-0.12
		yes	-3.01	-3.22	-4.03	0.11	-4.50	-0.12

Table 5.7: Fisher-matrix errors on the EMRI parameters including both binary components spin in the waveform and including a spinning SCO with $\chi = 1$. We include only the quadrupole ($\ell = 2$) in the signal and consider two choices of the mass ratios and two values of the SMBH spin, with and without imposing a Gaussian prior on χ. In these configurations, the SNR for $\mu = 10M_\odot(100M_\odot)$ is SNR $= 92.2$ (SNR $= 174$) when $\hat{a} = 0.9$ and SNR $= 100$ (SNR $= 195$) when $\hat{a} = 0.99$. However, also in this table the results have been rescaled to have SNR $= 30$ (SNR $= 150$) when $\mu = 10M_\odot(100M_\odot)$, regardless of the primary spin.

In this general case we observe the same features of the previous analyses. In particular, the secondary spin is not measurable but its inclusion can significantly deteriorate the accuracy in the measurements of the masses, unless a prior on

χ is enforced. Even in an extreme case ($\hat{a} = 0.99$, $\mu = 100 M_\odot$) the relative error on χ is larger than 100% for SNR < 2433. We find again that including the SCO spin with a prior yields the same errors as in the case in which χ is neglected in the waveform parameters.
Strictly speaking, it is not possible to rescale the covariance matrix of the posterior by a fiducial SNR when a prior is introduced because Γ_0 does not depend on the distance D. However, since the error on χ is largely dominated by the prior, our numerical results are practically unaffected for the fiducial SNRs we used. Finally, it is worth noticing that, by rescaling only the likelihood covariance matrix, the posterior variance of χ would remain close to the prior variance even if the fiducial SNR were to be increased.

Chapter 6

Conclusions and outlook

My research focused on the extreme-mass-ratio inspiral of a spinning test-particle in Kerr spacetime, providing original contributions to source modeling and parameter estimation for the forthcoming LISA observatory. I summarize the main results of my work in the following.

- Using the Teukolsky formalism, I computed the GW fluxes of a spinning point particle on circular, equatorial motion with spins (anti-)aligned around the Kerr background. My computations included all linear and higher order terms in σ due to the secondary spin. I then expanded the GW fluxes in σ, recovering the linear order corrections with two methods: (i) numerically, with polynomial fitting and (ii) with a semi-analytically approach based on fully-linearized Teukolsky equations. Both methods are novel for the Kerr spacetime and agreed with previous results in the literature for Schwarzschild BH primaries. My work also provided original, technical results for the orbital dynamics of spinning particles on equatorial orbits, and for the solutions of the Teukolsky equations, specifically a new exact formulation of the source term for spinning particles, and new accurate boundary conditions for the numerical integration.

- My second contribution concerns the detectability of the EMRIs secondary spin by future space-borne detectors. I focused on circular equatorial motion around a Kerr BH and evolved the adiabatic inspiral through the asymptotic GW fluxes that include spin-induced corrections at all order in σ. I then numerically extracted the post-adiabatic contributions to the dominant GW phase at $\mathcal{O}(\sigma)$. Such terms represent novel results in literature. I derived a criterion for the minimum spin of the SCO resolvable by LISA based on the phase difference between waveforms that describe spinning and spinless particles. This method suggests that the secondary spin is potentially measurable at $5-25\%$ level of accuracy, depending on

its magnitude, as well as on the value of the intrinsic angular momentum of the primary.

I showed that measuring the spin of SCO could test the nature of the secondary in a theory-agnostic fashion. Indeed, the EMRI dynamics depends only on the first two multipoles of the secondary, its mass and spins, whereas the contribution of higher order multipoles is expected to be negligible. In particular, I demonstrated that an EMRI detection could potentially distinguish whether the SCO is a fast spinning BH or a slowly-spinning neutron star, or whether the SCO satisfies the Kerr bound or is a superspinar.

In a follow-up study, I improved upon my previous analysis by performing an accurate parameter estimation of the secondary spin with a Fisher matrix approach. I computed the waveform with the Teukolsky formalism to leading order in an adiabatic expansion, taking into account the motion of the LISA constellation, higher harmonics, and also including the leading correction from the spin of the SCO in the post-adiabatic approximation. I employed accurate asymptotic fluxes with semi-analytic linear order corrections to the secondary. This parameter estimation is the first to employ full-relativistic Teukolsky-based waveforms including LISA's antenna pattern functions on a Kerr background.

My analysis confirmed the results of Refs. [112, 113] which, using approximated waveforms, found that the spin of a SCO for EMRIs with (anti-)aligned spins on quasi-circular orbits is not measurable, although it produces a non-negligible dephasing. This is due to correlations that exist between the secondary spin and the other intrinsic parameters.

Because of these correlations, even if the secondary spin is not measurable, its inclusion in the waveform model can deteriorate the accuracy on the measurements of other parameters by orders of magnitude, unless a physically-motivated prior on the SCO spin is imposed. In the latter case, I found that the Fisher-matrix errors are identical to those obtained neglecting the secondary spin in the waveform parameters. This further suggests that, for the orbital configurations I have considered, the spin of a SCO in EMRIs can be neglected for parameter estimation.

Finally, I found that including higher harmonics in the GW signal improves the errors on the luminosity distance by an order of magnitude and those on the binary orbital angular-momentum angles by two orders of magnitude, relative to the quadrupole-only case. This is particularly relevant to identify the environment where EMRIs form [232, 233], for possible applications of multi-messenger astronomy with EMRIs [234] and for prospects to use

EMRIs as standard sirens [235].

The work done in this thesis can be extended/improved in several ways.

- An obvious extension of my work is to consider eccentricity and nonequatorial orbits, as well as spin misalignment (which introduce precession [94, 99, 236]). When the test-particle move away from the equatorial plane, the spins of the binary can not stay aligned, hence spin-precession occurs, which may break the degeneracies of the secondary spin with other parameters.

  However, the MPD equations are challenging to solve for generic motion since a spinning particle in Kerr background is a non-integrable dynamical system, and chaotic motion may ensue [57, 163, 199]. Nonetheless, given the fact that $\sigma \ll 1$ in EMRI, it is sufficient to consider the linear-in-spin approximation of the MPD equations, which are simpler. At least for the Tulczyjew-Dixon supplementary spin condition, integrability approximately holds at $\mathcal{O}(\sigma)$ thanks to approximate conserved quantities [56]. Being non separable, the spin-perturbed equations of motion for the trajectories remain still difficult to solve [237].

  Furthermore, the lack of a Carter constant for spinning particles poses conceptual problems for the adiabatic evolution of off-equatorial orbits. A Carter-like constant conserved at $\mathcal{O}(\sigma)$ order still exists [161, 162], but there are no rigorous flux-balance law for this approximately conserved quantity [53].

- Finally, my analysis did not include all the next-to-leading order terms in an adiabatic expansion, in particular it lacks the leading-order conservative self-force corrections [54, 55, 95, 104] and the dissipative corrections sourced by second order metric perturbations [76, 77]. A complete account of dissipative effects in the case of a spinning SCO would also require to consider the spin evolution due to self-force effects, which is a more challenging problem [53]. It would be interesting to include all the aforementioned post-adiabatic terms and study how these affect the detectability of the smaller companion spin. Indeed, given the fact that the secondary spin is a small effect, a faithful measurement requires having all first-order post-adiabatic effects under control.

A complete model of a spinning particle in EMRI is one of the key deliverables of the LISA Science Working Groups. My work constitutes an important part of this on-going program aimed to study gravitational waveforms with spinning SCO in Kerr for generic orbits, spin orientation [238] and including self-force effects [54].

Appendix A

Sasaki-Nakamura equation

In this and in the following appendix we provide further technical details on the formalisms that we use in chapter 4, section 4.2 to compute the GW fluxes. The homogeneous Teukolsky equation is an example of stiff differential problem, with the solutions (4.1.7)-(4.1.8) rapidly diverging at infinity due to the long-range character of the potential. High accuracy solutions require therefore time-consuming numerical integrations. A substantial improvement in this direction has been achieved by Sasaki and Nakamura, finding a suitable transformation which maps the homogeneous Teukolsky equation to an equivalent form with a short-range potential that is easier to solve numerically [180]. The original form of the Sasaki-Nakamura (SN) equation, which we use here, is valid only for gravitational perturbation with helicity $s = -2$. Later on it was generalize to scalar and vector radiation in Ref. [239]. The SN equation is given by (we remind that hatted quantities are dimensionless)

$$\left[f(\hat{r})^2\frac{\mathrm{d}^2}{\mathrm{d}\hat{r}^2} + f(\hat{r})\left(\frac{\mathrm{d}f(\hat{r})}{\mathrm{d}\hat{r}} - F(\hat{r})\right)\frac{\mathrm{d}}{\mathrm{d}\hat{r}} - U(\hat{r})\right]X_{\ell m\hat{\omega}} = 0\,, \tag{A.0.1}$$

with $f(\hat{r}) = \frac{\mathrm{d}\hat{r}}{\mathrm{d}\hat{r}^*} = \frac{\Delta}{\hat{r}^2+\hat{a}^2}$. The coefficient $F(\hat{r})$ is defined as

$$F(\hat{r}) = \frac{\eta(\hat{r})_{,\hat{r}}}{\eta(\hat{r})}\frac{\Delta}{\hat{r}^2+\hat{a}^2}\,, \tag{A.0.2}$$

where $_{,\hat{r}}$ denotes the derivative with respect to $\hat{r}$ and

$$\eta(\hat{r}) = c_0 + \frac{c_1}{\hat{r}} + \frac{c_2}{\hat{r}^2} + \frac{c_3}{\hat{r}^3} + \frac{c_4}{\hat{r}^4}\,, \tag{A.0.3}$$

with

$$c_0 = -12i\hat{\omega} + {}_{-2}\lambda_{\ell m\hat{\omega}}({}_{-2}\lambda_{\ell m\hat{\omega}} + 2) - 12\hat{a}\hat{\omega}(\hat{a}\hat{\omega} - m)\,, \tag{A.0.4}$$

$$c_1 = 8i\hat{a}[3\hat{a}\hat{\omega} - {}_{-2}\lambda_{\ell m\hat{\omega}}(\hat{a}\hat{\omega} - m)]\,, \tag{A.0.5}$$

$$c_2 = -24i\hat{a}(\hat{a}\hat{\omega} - m) + 12\hat{a}^2[1 - 2(\hat{a}\hat{\omega} - m)^2]\,, \tag{A.0.6}$$

$$c_3 = 24i\hat{a}^3(\hat{a}\hat{\omega} - m) - 24\hat{a}^2\,, \tag{A.0.7}$$

$$c_4 = 12\hat{a}^4\,. \tag{A.0.8}$$

The function $U(\hat{r})$ in Eq. (A.0.1) reads

$$U(\hat{r}) = \frac{\Delta U_1(\hat{r})}{(\hat{r}^2 + \hat{a}^2)^2} + G(\hat{r})^2 + \frac{\Delta G(\hat{r})_{,\hat{r}}}{\hat{r}^2 + \hat{a}^2} - F(\hat{r})G(\hat{r})\,, \tag{A.0.9}$$

where

$$G(\hat{r}) = -\frac{2(\hat{r} - 1)}{\hat{r}^2 + \hat{a}^2} + \frac{\hat{r}\Delta}{(\hat{r}^2 + \hat{a}^2)^2}\,, \tag{A.0.10}$$

$$U_1(\hat{r}) = V(\hat{r}) + \frac{\Delta^2}{\beta}\left[\left(2\alpha + \frac{\beta_{,\hat{r}}}{\Delta}\right)_{,\hat{r}} - \frac{\eta(\hat{r})_{,\hat{r}}}{\eta(\hat{r})}\left(\alpha + \frac{\beta_{,\hat{r}}}{\Delta}\right)\right]\,, \tag{A.0.11}$$

$$\alpha = -iK(\hat{r})\frac{\beta}{\Delta^2} + 3iK(\hat{r})_{,\hat{r}} + {}_{-2}\lambda_{\ell m\hat{\omega}} + \frac{6\Delta}{\hat{r}^2}\,, \tag{A.0.12}$$

$$\beta = 2\Delta\Big[- iK(\hat{r}) + \hat{r} - 1 - \frac{2\Delta}{\hat{r}}\Big]\,. \tag{A.0.13}$$

The two functions $K(\hat{r})$ and $V(\hat{r})$ are the same introduced for the Teukolsky radial equation (4.1.4).
The SN equation admits two linearly independent solutions, $X^{\rm in}_{\ell m\hat{\omega}}$ and $X^{\rm up}_{\ell m\hat{\omega}}$, which behave asymptotically as

$$X^{\rm in}_{\ell m\hat{\omega}} \sim \begin{cases} e^{-i\hat{\kappa}\hat{r}^*} & \hat{r} \to \hat{r}_+ \\ A^{\rm out}_{\ell m\hat{\omega}} e^{i\hat{\omega}\hat{r}^*} + A^{\rm in}_{\ell m\hat{\omega}} e^{-i\hat{\omega}\hat{r}^*} & \hat{r} \to \infty \end{cases}\,, \tag{A.0.14}$$

$$X^{\rm up}_{\ell m\hat{\omega}} \sim \begin{cases} C^{\rm out}_{\ell m\hat{\omega}} e^{i\hat{\kappa}\hat{r}^*} + C^{\rm in}_{\ell m\hat{\omega}} e^{-i\hat{\kappa}\hat{r}^*} & r \to r_+ \\ e^{i\hat{\omega}\hat{r}^*} & \hat{r} \to \infty \end{cases}\,. \tag{A.0.15}$$

The solutions of the Teukolsky and SN equations are related by:

$$R^{\rm in,up}_{\ell m\hat{\omega}}(\hat{r}) = \frac{1}{\eta}\left[\left(\alpha + \frac{\beta_{,\hat{r}}}{\Delta}\right)Y^{\rm in,up}_{\ell m\hat{\omega}} - \frac{\beta}{\Delta}Y^{\rm in,up}_{\ell m\hat{\omega},\hat{r}}\right]\,, \tag{A.0.16}$$

$$Y^{\rm in,up}_{\ell m\hat{\omega}} = \frac{\Delta}{\sqrt{\hat{r}^2 + \hat{a}^2}} X^{\rm in,up}_{\ell m\hat{\omega}}\,. \tag{A.0.17}$$

With the above normalization of the solutions $X^{\rm in}_{\ell m\hat{\omega}}$ $X^{\rm up}_{\ell m\hat{\omega}}$, these transformations allow to fix the arbitrary constants $D^{\rm tran}_{\ell m\hat{\omega}}$ and $B^{\rm tran}_{\ell m\omega}$ [cf. Eq. (4.1.16)] as [172]:

$$D^{\rm tran}_{\ell m\hat{\omega}} = -\frac{4\hat{\omega}^2}{c_0}\,, \qquad B^{\rm tran}_{\ell m\hat{\omega}} = \frac{1}{d_{\ell m\hat{\omega}}}\,, \tag{A.0.18}$$

where

$$\begin{aligned} d_{\ell m\hat{\omega}} = 4\sqrt{2\hat{r}_+}[&(2-6i\hat{\omega}-4\hat{\omega}^2)\hat{r}_+^2 + (3i\hat{a}m - 4 + 4\hat{a}m\hat{\omega} + 6i\hat{\omega})\hat{r}_+ \\ &- \hat{a}^2m^2 - 3i\hat{a}m + 2]\,, \end{aligned} \tag{A.0.19}$$

and the coefficient c_0 is given in Eq. (A.0.4).
The numerical values of $X^{\rm in}_{\ell m\hat{\omega}}$ (resp. $X^{\rm up}_{\ell m\hat{\omega}}$) are obtained by integrating Eq. (A.0.1) from $\hat{r}_+$ (resp. infinity) up to infinity (resp. $\hat{r}_+$) using the boundary conditions (A.0.14) (resp. (A.0.15)). In this work we have derived the boundary conditions for the homogeneous SN equation in terms of explicit recursion relations which can be truncated at arbitrary order (see Sec. A.1). We finally transform back $X^{\rm in}_{\ell m\hat{\omega}}$, $X^{\rm up}_{\ell m\hat{\omega}}$ to the Teukolsky solutions using Eq. (A.0.16). The amplitude $B^{\rm in}_{\ell m\hat{\omega}}$ can be obtained from the Wronskian $W_{\hat{r}}$ at a given orbital separation.

A.1 Boundary conditions for the SN equation

We have derived accurate boundary conditions by looking for series expansions of the master equation at the outer horizon $\hat{r}_+$ and at infinity. To this aim we have studied the singularities on the real axis of Eq. (A.0.1), which can be recast in the form

$$\Delta^2\frac{d^2X_{\ell m\hat{\omega}}}{d\hat{r}^2} + \Delta\overline{F}(\hat{r})\frac{dX_{\ell m\hat{\omega}}}{d\hat{r}} + \overline{U}(\hat{r})X_{\ell m\hat{\omega}} = 0\,, \tag{A.1.1}$$

where

$$\overline{F}(\hat{r}) = (\hat{r}^2+\hat{a}^2)\left(\frac{{\rm d}f(\hat{r})}{{\rm d}\hat{r}} - F(\hat{r})\right)\,, \tag{A.1.2}$$

$$\overline{U}(\hat{r}) = -(\hat{r}^2+\hat{a}^2)^2U(\hat{r})\,. \tag{A.1.3}$$

Moreover

$$F(\hat{r}_\pm) = 0\,, \qquad F(\hat{r}) \xrightarrow[\hat{r}\to\infty]{} 0\,, \tag{A.1.4}$$

$$U(\hat{r}_+) = -\hat{\kappa}^2\,, \qquad U(\hat{r}) \xrightarrow[\hat{r}\to\infty]{} -\hat{\omega}^2\,. \tag{A.1.5}$$

Since the functions $\overline{F}(\hat{r})$ and $\overline{U}(\hat{r})$ are analytic on the positive real axis, it turns out that the Eq. (A.0.1) has three singularities: two at the horizons $\hat{r} = \hat{r}_-$ and $\hat{r} = \hat{r}_+$,

both of which are regular singularities, and one at $\hat{r} = \infty$ which is an irregular singularity of rank 1. By Fuchs theorem, the solutions of the SN equation around $\hat{r}_+$ can be written as Frobenius series, with radius of convergence

$$\hat{r}_+ - \hat{r}_- = 2\sqrt{1-\hat{a}^2}\,. \tag{A.1.6}$$

For $\hat{r} = \infty$ or $\hat{a} = 1$ (for which $\hat{r}_+ = \hat{r}_-$) the boundary conditions can be written in terms of asymptotic expansions.

A.1.1 Boundary condition at the horizon

To compute the boundary conditions at the outer horizon $\hat{r}_+$, it is convenient to recast the SN equation as

$$(\hat{r}-\hat{r}_+)^2\frac{d^2X_{\ell m\hat{\omega}}}{d\hat{r}^2} + (\hat{r}-\hat{r}_+)p_H(\hat{r})\frac{dX_{\ell m\omega}}{d\hat{r}} + q_H(\hat{r})X_{\ell m\hat{\omega}} = 0 \tag{A.1.7}$$

where

$$p_H(\hat{r}) = \left(\frac{\hat{r}^2+\hat{a}^2}{\hat{r}-\hat{r}_-}\right)\left[\frac{\mathrm{d}f(\hat{r})}{\mathrm{d}\hat{r}} - F(\hat{r})\right], \tag{A.1.8}$$

$$q_H(\hat{r}) = -\left(\frac{\hat{r}^2+\hat{a}^2}{\hat{r}-\hat{r}_-}\right)^2 U(\hat{r})\,. \tag{A.1.9}$$

Following the Frobenius method we look for a power series solution of the form

$$X_{\ell m\hat{\omega}} = (\hat{r}-\hat{r}_+)^d \sum_{n=0}^{\infty} a_n(\hat{r}-\hat{r}_+)^n\,, \tag{A.1.10}$$

where d is one of the solutions of the indicial equation

$$I(d) = d(d-1) + p_H(\hat{r}_+)d + q_H(\hat{r}_+) = 0\,. \tag{A.1.11}$$

For Eq. (A.0.1), the latter corresponds to

$$I(d) = d^2 + \kappa^2\left(\frac{2\hat{r}_+}{\hat{r}_+-\hat{r}_-}\right)^2 = 0\,, \qquad \hat{\kappa} = \hat{\omega} - \frac{m\hat{a}}{2\hat{r}_+}\,. \tag{A.1.12}$$

Given (d_1, d_2) two solutions of the above equation, their difference $d_1 - d_2$ is neither zero nor an integer. We have therefore two linearly independent solutions such that

$$X_{\ell m\hat{\omega}} = \exp\left\{\pm i\hat{\kappa}\frac{2\hat{r}_+}{\hat{r}_+-\hat{r}_-}\log(\hat{r}-\hat{r}_+)\right\}\sum_{n=0}^{\infty} a_n(r-r_+)^n\,. \tag{A.1.13}$$

The recursion relation for the coefficients a_n is (setting $a_0 = 1$)

$$a_n = -\frac{1}{I(d+n)} \sum_{k=0}^{n-1} \frac{(k+d)p_H^{(n-k)}(\hat{r}_+) + q_H^{(n-k)}(r_+)}{(n-k)!} a_k \,, \tag{A.1.14}$$

where $p_H^{(k)}(\hat{r}_+)$ and $q_H^{(k)}(\hat{r}_+)$ are the k-th derivatives of the coefficients $p_H(\hat{r})$ and $q_H(\hat{r})$ with respect to $\hat{r}$, and calculated at $\hat{r}_+$. For $\hat{a} \leq 0.9$, the boundary conditions at the horizon have been calculated at $\hat{r}_{\rm in} = \hat{r}_+ + \epsilon$ with $\epsilon = 10^{-3}$, while for higher spins we have fixed $\epsilon = 10^{-5}$. To increase precision, we compute the series coefficients up to $n = 10$.

A.1.2 Boundary condition at infinity

Ordinary differential equations with irregular singularities of rank 1, like the SN equation, admit general expressions for asymptotic expansions around such singularities (see Refs. [240, 241] and especially Ref. [242] for more details). To calculate the boundary conditions at infinity we rewrite the SN equation as

$$\frac{d^2 X_{\ell m\hat{\omega}}}{d\hat{r}^2} + p_\infty(\hat{r}) \frac{dX_{\ell m\hat{\omega}}}{d\hat{r}} + q_\infty(\hat{r}) X_{\ell m\hat{\omega}} = 0 \,, \tag{A.1.15}$$

where

$$p_\infty(\hat{r}) = \frac{(\hat{r}^2 + \hat{a}^2)}{\Delta} \left[\frac{\mathrm{d}f(\hat{r})}{\mathrm{d}\hat{r}} - F(\hat{r}) \right] , \tag{A.1.16}$$

$$q_\infty(\hat{r}) = -\left(\frac{\hat{r}^2 + \hat{a}^2}{\Delta} \right)^2 U(\hat{r}) \,. \tag{A.1.17}$$

The functions $p_\infty(\hat{r})$ and $q_\infty(\hat{r})$ are analytic on the positive real axis, so the series

$$p_\infty(\hat{r}) = \sum_{n=0}^{\infty} \frac{1}{n!} \frac{p_\infty^{(n)}}{\hat{r}^n} \,, \qquad q_\infty(\hat{r}) = \sum_{n=0}^{\infty} \frac{1}{n!} \frac{q_\infty^{(n)}}{\hat{r}^n} \,,$$

converge, with $p_\infty^{(n)}$ and $q_\infty^{(n)}$ being the n-th derivatives of the coefficients p_∞ and q_∞ with respect to $\hat{r}$. If at least one of $p_\infty^{(0)}$, $q_\infty^{(0)}$ or $q_\infty^{(1)}$ is nonzero, the formal solution is given by

$$X_{\ell m\hat{\omega}} = e^{\gamma\hat{r}} \hat{r}^{\xi} \sum_{n=0}^{\infty} \frac{b_n}{\hat{r}^n} \,, \tag{A.1.18}$$

where γ is one of the solutions of the characteristic equation

$$\gamma^2 + p_\infty^{(0)} \gamma + q_\infty^{(0)} = 0 \,, \tag{A.1.19}$$

while

$$\xi = -\frac{p_\infty^{(1)}\gamma + q_\infty^{(1)}}{p_\infty^{(0)} + 2\gamma} \,. \tag{A.1.20}$$

For the SN equation

$$p_\infty^{(0)} = 0 = p_\infty^{(1)} \,, \qquad q_\infty^{(0)} = \omega^2 \,, \qquad q_\infty^{(1)} = 4\hat{\omega}^2 \,, \tag{A.1.21}$$

$$\gamma^2 + \hat{\omega}^2 = 0 \,, \qquad \xi = -\frac{q_\infty^{(1)}}{2\gamma} = \pm 2i\hat{\omega} \,. \tag{A.1.22}$$

Therefore, we have two series solutions

$$X_{\ell m\hat{\omega}} = \exp\{\pm i\hat{\omega}[\hat{r} + 2\log(\hat{r})]\} \sum_{n=0}^{\infty} \frac{b_n}{\hat{r}^n} \,. \tag{A.1.23}$$

The general recursion relation for the coefficients b_n is (we set again $b_0 = 1$)

$$\begin{aligned}(p_\infty^{(0)} + 2\gamma) n b_n = (n-\xi)(n-1-\xi) b_{n-1} + \\ + \sum_{k=1}^{n} \left[\gamma p_\infty^{(k+1)} + q_\infty^{(k+1)} - (n-k-\xi) p_\infty^{(k)}\right] b_{n-k} \,.\end{aligned} \tag{A.1.24}$$

It can be proved that the series solutions constructed in this way diverge, and they have to be considered as asymptotic expansions. However, these solutions are unique and linearly independent. We computed the series coefficients up to $n = 13$.

A.1.3 Cross check of the boundary conditions with Ref. [1]

We compared our boundary conditions with the ones used in Ref. [1], which are in form

$$e^{\pm i\hat{\kappa}\hat{r}^*} \sum_{n=0}^{\infty} a_n^{\mathrm{H}} (\hat{r} - \hat{r}_+)^n \,, \tag{A.1.25}$$

$$e^{\pm i\hat{\omega}\hat{r}^*} \sum_{n=0}^{\infty} a_n^{\infty} \frac{1}{(\hat{\omega}\hat{r})^n} \,. \tag{A.1.26}$$

First, we notice that the tortoise coordinate $\hat{r}^*(\hat{r})$ at the boundaries can be written as

$$\hat{r}^*(\hat{r}) \sim \hat{r} + 2\ln(\hat{r}) - 2\ln(2) \,, \tag{A.1.27}$$

$$\hat{r}^*(\hat{r}) \sim \frac{2\hat{r}_+}{\hat{r}_+ - \hat{r}_-} \ln(\hat{r} - \hat{r}_+) + \delta r^*(r_+) \,, \tag{A.1.28}$$

at $\hat{r} \to \infty$ and $\hat{r} \to \hat{r}_+$, respectively, and where we defined

$$\delta\hat{r}^*(\hat{r}_+) \equiv -2\ln(2) - \frac{2\hat{r}_-}{\hat{r}_+ - \hat{r}_-}\ln(\hat{r}_+ - \hat{r}_-) + \hat{r}_+ \,. \tag{A.1.29}$$

If we multiply Eq. (A.1.13) by the phase factor $\exp\{\pm i\hat{\kappa}\delta\hat{r}^*(\hat{r}_+)\}$ and Eq. (A.1.23) by $\exp\{\pm i\hat{\omega}[-2\ln(2)]\}$, our boundary conditions have the same modulus and phase as those in Ref. [1] for all the values of the parameters space we have considered, up to numerical error. In the worst case, for $\hat{a} = 0.995$ and $\ell = 20$ at the ISCO, the fractional difference in both modulus and phase is at most of one part in 10^{10}, and typically much smaller.
Since the solutions by means of series expansion of an ordinary differential equation are uniquely determined a part for a constant complex factor, the boundary conditions (A.1.13) and (A.1.23) are consistent with the ones of Ref. [1].

Appendix B

Teukolsky equation in hyperboloidal-slicing coordinates

The coefficients $\tilde{F}(\hat{r})$ and $\tilde{U}(\hat{r})$ of Eq. (4.3.14) are given by

$$\tilde{F}(\hat{r};H) = \frac{2}{\hat{r}^2+\hat{a}^2}\left(\hat{r}^2-\hat{a}^2-\tilde{G}(\hat{r};H)\right), \tag{B.0.1}$$

$$\tilde{G}(\hat{r};H) = (\hat{r}^2+\hat{a}^2)[s(\hat{r}-1)-i((\hat{r}^2+\hat{a}^2)\hat{\omega}H+m\hat{a})]+\frac{\hat{a}^2\Delta}{\hat{r}}, \tag{B.0.2}$$

$$\begin{aligned}\tilde{U}(\hat{r};H) = {} & 2is\hat{\omega}[\hat{r}\Delta(1-H)-(\hat{r}^2-\hat{a}^2)(1+H)]+\\ & +\frac{\Delta}{\hat{r}^2}[2\hat{a}^2-\hat{r}^2\,{}_s\lambda_{\ell m\hat{\omega}}-2\hat{r}(s+1)]+\\ & -2m\hat{a}\hat{\omega}(\hat{r}^2+\hat{a}^2)(1+H)-2i\hat{a}\frac{\Delta}{\hat{r}}(m+\hat{a}\hat{\omega}H),\end{aligned} \tag{B.0.3}$$

where $H=-1\,(+1)$ for the linearly independent solution ${}_s\psi^{\rm in}_{\ell m\omega}({}_s\psi^{\rm up}_{\ell m\omega})$. This is the same convention adopted in the *Teukolsky* package of the Black Hole Perturbation Toolkit [119]. Notice that

$$\tilde{U}(\hat{r}_+;-1)=0\,, \tag{B.0.4}$$

$$\frac{\tilde{U}(\hat{r}\to\infty;1)}{\Delta^2}\to-\frac{{}_s\lambda_{\ell m\hat{\omega}}+4am\hat{\omega}+4is\hat{\omega}}{\hat{r}^2}\,, \tag{B.0.5}$$

$$\frac{\tilde{F}(\hat{r}\to\infty;1)}{\Delta}\to 2i\hat{\omega}\,. \tag{B.0.6}$$

It is easy to show that the ordinary differential equation (4.3.14) has three singularities on the real positive axis: two at the horizons $\hat{r}=\hat{r}_-$ and $\hat{r}=\hat{r}_+$, both of which are regular singularities, and one at $\hat{r}=\infty$ which is an irregular singularity of rank 1. Despite having different coefficients, the radial Teukolsky equation,

the Sasaki-Nakamura equation, and Eq. (4.3.14) have the same singularities. Therefore, both the Sasaki-Nakamura transformation and transformation (4.3.12) preserve the singularity structure of the radial Teukolsky equation. We compute accurate boundary conditions at the outer horizon $\hat{r}_+$ and at infinity through suitable series expansions, as done in Ref. [118]. The Fuchs theorem guarantees that the solutions of (4.3.14) around $\hat{r}_+$ can be written as Frobenius series, with radius of convergence

$$\hat{r}_+ - \hat{r}_- = 2\sqrt{1-\hat{a}^2}\,. \tag{B.0.7}$$

At infinity or when $\hat{a} = 1$ (for which $\hat{r}_+ = \hat{r}_-$), the boundary conditions can be computed accurately as asymptotic expansions.

B.1 Boundary conditions for the Teukolsky equation in hyperboloidal-slicing coordinates

B.1.1 Boundary condition at the horizon

To compute the boundary conditions at the outer horizon $\hat{r}_+$, it is convenient to rewrite Eq. (4.3.14) as

$$(\hat{r}-\hat{r}_+)^2 \frac{d^2\,{}_s\psi^{\rm in}_{\ell m\omega}}{d\hat{r}^2} + (\hat{r}-\hat{r}_+)p_H(\hat{r})\frac{d\,{}_s\psi^{\rm in}_{\ell m\omega}}{d\hat{r}} + q_H(\hat{r})\,{}_s\psi^{\rm in}_{\ell m\omega} = 0\,, \tag{B.1.1}$$

where

$$p_H(\hat{r}) = \frac{\tilde{F}(\hat{r};-1)}{\hat{r}-\hat{r}_-}\,, \qquad q_H(\hat{r}) = \frac{\tilde{U}(\hat{r};-1)}{(\hat{r}-\hat{r}_-)^2}\,. \tag{B.1.2}$$

We seek for a Frobenius power series solution of the form

$${}_s\psi^{\rm in}_{\ell m\omega} = (\hat{r}-\hat{r}_+)^d \sum_{n=0}^{\infty} a_n (\hat{r}-\hat{r}_+)^n\,, \tag{B.1.3}$$

where the index d is a solution of the indicial equation

$$I(d) = d(d-1) + p_H(\hat{r}_+)d + q_H(\hat{r}_+) = 0\,. \tag{B.1.4}$$

For Eq. (4.3.14), the latter is given by

$$I(d) = d(d-c_H) = 0\,, \qquad c_H = \frac{4i\hat{r}_+}{\hat{r}_+-\hat{r}_-}\kappa + s\,, \tag{B.1.5}$$

and $\kappa = \hat{\omega} - m\hat{a}/(2\hat{r}_+)$. Near the outer horizon $\hat{r}_+$, the radial solution ${}_sR^{\rm in}_{\ell m\hat{\omega}}$ has the following asymptotic behavior

$$ {}_sR^{\rm in}_{\ell m\hat{\omega}} \sim \Delta^{-s} e^{-i\hat{\kappa}\hat{r}^*} \qquad \hat{r} \to \hat{r}_+ \,, \tag{B.1.6} $$

Thus, only $d = 0$ is a physical solution of the indicial equation. Moreover, we notice that the ansatz (4.3.12) for the ${}_sR^{\rm in}_{\ell m\hat{\omega}}$ solution can be rewritten as

$$ {}_sR^{\rm in}_{\ell m\hat{\omega}}(\hat{r}) = \hat{r}^{-1}\Delta^{-s} e^{-i\kappa\hat{r}^*} e^{-i\delta_H(\hat{r})}\, {}_s\psi^{\rm in}_{\ell m\omega} \,, \tag{B.1.7} $$

$$ \delta_H(\hat{r}) \equiv \frac{am}{\hat{r}_+}\left[\frac{\hat{r}}{2} + \ln\left(\frac{\hat{r}-\hat{r}_-}{2}\right)\right]. \tag{B.1.8} $$

Therefore, to ensure the correct physical behavior of $R^{\rm in}_{\ell m\hat{\omega}}(\hat{r})$ at the outer horizon, we fix $d = 0$ and write the Frobenius series (B.1.3) as

$$ {}_s\psi^{\rm in}_{\ell m\omega} = \hat{r}_+ e^{i\delta_H(\hat{r}_+)} \sum_{n=0}^{\infty} a_n (\hat{r}-\hat{r}_+)^n \,. \tag{B.1.9} $$

The recursion relation for the coefficients a_n is (setting $a_0 = 1$)

$$ a_n = -\frac{1}{I(n)} \sum_{k=0}^{n-1} \left(k\, p_H^{(n-k)}(\hat{r}_+) + q_H^{(n-k)}(\hat{r}_+) \right) a_k \,, \tag{B.1.10} $$

where $p_H^{(k)}(\hat{r}_+)$ and $q_H^{(k)}(\hat{r}_+)$ are the k-th derivatives of the coefficients $p_H(\hat{r})$ and $q_H(\hat{r})$ with respect to $\hat{r}$, and calculated at $\hat{r}_+$. Their general expression are given by

$$ p_H^{(n)}(\hat{r}_+) = \begin{cases} 1 - c_H & n = 0 \,, \\ (\rho_H^2 \hat{r}_+)^{-1}[-2\hat{r}_-^2 + \hat{a}^2(3 + 2s + 4i\hat{r}_+\hat{\omega}) + \hat{r}_+(\mathfrak{p}_H - \hat{r}_+)] & n = 1 \,, \\ 2(-\hat{r}_+)^{-n} - \rho_H^{-n} + \rho_H^{-n-1}[2s\hat{r}_- + 2i(\hat{r}_+^2 + \hat{r}_-^2)\hat{\omega} + \mathfrak{p}_H] & n > 1 \,, \end{cases} \tag{B.1.11} $$

$$ q_H^{(n)}(\hat{r}_+) = \begin{cases} 0 & n = 0 \,, \\ \rho_H^{-1}\mathfrak{q}_H(1) & n = 1 \,, \\ 2(n-1)(-\hat{r}_+)^{-n} + \rho_H^{-n}\mathfrak{q}_H(n)\, {}_2F_1\left(1, 1-n; 2; \frac{\hat{r}_-}{\hat{r}_+}\right) & n > 1 \,, \end{cases} \tag{B.1.12} $$

where ${}_2F_1(1, 1-n; 2; \hat{r}_-/\hat{r}_+)$ is the hypergeometric function ${}_2F_1(a, b; c; z)$ and

$$ \begin{aligned} \rho_H &\equiv (\hat{r}_- - \hat{r}_+) \,, \\ \mathfrak{p}_H &\equiv 2i(is - \hat{a}m + \hat{a}^2\hat{\omega} - \hat{r}_+^2\omega) \,, \\ \mathfrak{q}_H(n) &\equiv \frac{n}{\hat{r}_+}[2i\hat{a}m + 2(s-1) - 2i\hat{a}^2\hat{\omega}] + (2 + {}_s\lambda_{\ell m\hat{\omega}} - 4i\hat{r}_- s\hat{\omega}) \,. \end{aligned} $$

.

B.1.2 Boundary condition at infinity

General expressions for series solutions around irregular singularities are also available in the literature [240–242]. However, unlike the regular case, these solutions are not convergent, and have to be considered as asymptotic expansions. To calculate the boundary conditions at infinity, we rewrite Eq. (4.3.14) as

$$\frac{d^2{}_s\psi^{\rm up}_{\ell m\omega}}{d\hat{r}^2} + p_\infty(\hat{r})\frac{d_s\psi^{\rm up}_{\ell m\omega}}{d\hat{r}} + q_\infty(\hat{r})_s\psi^{\rm up}_{\ell m\omega} = 0\,, \tag{B.1.13}$$

where

$$p_\infty(\hat{r}) = \frac{\tilde{F}(\hat{r};1)}{\Delta}\,, \qquad q_\infty(\hat{r}) = \frac{\tilde{U}(\hat{r};1)}{\Delta^2}\,. \tag{B.1.14}$$

The functions $p_\infty(\hat{r})$ and $q_\infty(\hat{r})$ are analytic on the positive real axis, so the series

$$p_\infty(\hat{r}) = \sum_{n=0}^{\infty}\frac{1}{n!}\frac{p_\infty^{(n)}}{\hat{r}^n}\,, \qquad q_\infty(\hat{r}) = \sum_{n=0}^{\infty}\frac{1}{n!}\frac{q_\infty^{(n)}}{\hat{r}^n}\,,$$

converge, with $p_\infty^{(n)}$ and $q_\infty^{(n)}$ being the n-th derivatives of the coefficients p_∞ and q_∞ with respect to $\hat{r}$. In the case of irregular singularities of rank 1, the formal solution is given by

$${}_s\psi^{\rm up}_{\ell m\omega} = e^{\gamma\hat{r}}\hat{r}^\xi\sum_{n=0}^{\infty}\frac{b_n}{\hat{r}^n}\,, \tag{B.1.15}$$

provided that at least one of $p_\infty^{(0)}$, $q_\infty^{(0)}$ or $q_\infty^{(1)}$ is nonzero. The exponent γ is one of the solutions of the characteristic equation

$$\gamma^2 + p_\infty^{(0)}\gamma + q_\infty^{(0)} = 0\,, \tag{B.1.16}$$

while

$$\xi = -\frac{p_\infty^{(1)}\gamma + q_\infty^{(1)}}{p_\infty^{(0)} + 2\gamma}\,. \tag{B.1.17}$$

For Eq. (4.3.14) we have:

$$q_\infty^{(0)} = 0 = q_\infty^{(1)}\,, \qquad p_\infty^{(0)} = 2i\hat{\omega}\,, \qquad p_\infty^{(1)} = 4i\hat{\omega} - 2s\,, \tag{B.1.18}$$

$$\gamma(\gamma + 2i\hat{\omega}) = 0\,, \qquad \xi = -\frac{\gamma(2i\hat{\omega} - s)}{\gamma + i\hat{\omega}}\,. \tag{B.1.19}$$

When $\hat{r}\to\infty$, the radial solution ${}_sR^{\rm up}_{\ell m\hat{\omega}}$ has the following asymptotic behavior

$${}_sR^{\rm up}_{\ell m\hat{\omega}} \sim r^{-(2s+1)}e^{i\hat{\omega}\hat{r}^*} \qquad \hat{r}\to\infty\,. \tag{B.1.20}$$

Thus, only $\gamma = 0$ is a physical solution of the characteristic equation, and we can write

$$ {}_s\psi^{\rm up}_{\ell m\omega} = \sum_{n=0}^{\infty} \frac{b_n}{\hat{r}^n} \,. \tag{B.1.21} $$

The general recursion relation for the coefficients b_n is (we set again $b_0 = 1$):

$$ \begin{aligned} (p^{(0)}_\infty + 2\gamma) n b_n = (n-\xi)(n-1-\xi) b_{n-1} + \\ + \sum_{k=1}^{n} \left[\gamma p^{(k+1)}_\infty + q^{(k+1)}_\infty - (n-k-\xi) p^{(k)}_\infty \right] b_{n-k} \,. \end{aligned} \tag{B.1.22} $$

In our case, we can write

$$ b_n = \frac{n-1}{2i\hat{\omega}} b_{n-1} + \frac{1}{2i\hat{\omega} n} \sum_{k=1}^{n} \left[q^{(k+1)}_\infty - (n-k) p^{(k)}_\infty \right] b_{n-k} \,, \tag{B.1.23} $$

where

$$ p^{(n)}_\infty = \begin{cases} 2i\hat{\omega} & n = 0 \,, \\ 4i\hat{\omega} - 2s & n = 1 \,, \\ \hat{r}_-^{n-1} + \hat{r}_+^{n-1} + P_- - P_+ & n > 1 \,, \end{cases} \tag{B.1.24} $$

$$ P_\pm = \frac{2\hat{r}_\pm^{n-1}}{\rho_H} [(1-\hat{r}_\pm)s + i(\hat{a}m + (\hat{r}_\pm^2 + \hat{a}^2)\hat{\omega})] \,, \tag{B.1.25} $$

and

$$ q^{(n)}_\infty = \begin{cases} 0 & n = 0, 1 \,, \\ -(4\hat{a}m\hat{\omega} + 4is\hat{\omega} + {}_s\lambda_{\ell m\hat{\omega}}) & n = 2 \,, \\ \frac{2}{\rho_H} Q_1 + \frac{4\hat{\omega}}{\rho_H^3} Q_2 & n > 2 \,, \end{cases} \tag{B.1.26} $$

with

$$ \begin{aligned} Q_1 = \hat{r}_-^{n-2}\hat{r}_+ - \hat{r}_-\hat{r}_+^{n-2} - \frac{1}{2}(\hat{r}_-^{n-1} - \hat{r}_+^{n-1})\, {}_s\lambda_{\ell m\hat{\omega}} + \\ - (i\hat{a}m + s + 1 + i\hat{a}^2\hat{\omega})(\hat{r}_-^{n-2} - \hat{r}_+^{n-2}) \,, \end{aligned} \tag{B.1.27} $$

$$ \begin{aligned} Q_2 = is\hat{a}^2[\rho_H(n-1)(\hat{r}_-^{n-2} + \hat{r}_+^{n-2}) - 2(\hat{r}_-^{n-1} - \hat{r}_+^{n-1})] + \\ + (is + \hat{a}m)[\hat{r}_-^n(2 - n\rho_H) - \hat{r}_+^n(2 + n\rho_H)] + \\ + \hat{a}^3 m[\rho_H(1-n)(\hat{r}_-^{n-2} + \hat{r}_+^{n-2}) + 2(\hat{r}_-^{n-1} - \hat{r}_+^{n-1})] - \frac{i}{2}\rho_H^2\hat{a}^2(\hat{r}_-^{n-2} - \hat{r}_+^{n-2}) \,. \end{aligned} \tag{B.1.28} $$

Appendix C

Teukolsky source term

C.1 Spinning particle on a general bound orbit

The source term of the Teukolsky equation for graviational perturbation reads

$$ {}_{-2}\mathcal{T}_{\ell m\hat{\omega}} = 4\int \mathrm{d}\hat{t}\mathrm{d}\theta \sin\theta \mathrm{d}\phi \frac{\left(B_2' + B_2'^{*}\right)}{\bar{\rho}\rho^5} {}_{-2}S^{\hat{a}\hat{\omega}}_{\ell m} e^{-i(m\phi+\hat{\omega}\hat{t})} \,, \tag{C.1.1} $$

where the functions B_2' and $B_2'^{*}$ are defined as

$$ B_2' = -\frac{1}{2}\rho^8\bar{\rho}\mathcal{L}_{-1}\left[\frac{1}{\rho^4}\mathcal{L}_0\left[\frac{T_{nn}}{\rho^2\bar{\rho}}\right]\right] - \frac{1}{2\sqrt{2}}\Delta^2\rho^8\bar{\rho}\mathcal{L}_{-1}\left[\frac{\bar{\rho}^2}{\rho^4}J_+\left[\frac{T_{\overline{m}n}}{\Delta\rho^2\bar{\rho}^2}\right]\right] \,, \tag{C.1.2} $$

$$ B_2'^{*} = -\frac{1}{4}\Delta^2\rho^8\bar{\rho}J_+\left[\frac{1}{\rho^4}J_+\left[\frac{\bar{\rho}}{\rho^2}T_{\overline{m}\overline{m}}\right]\right] - \frac{1}{2\sqrt{2}}\Delta^2\rho^8\bar{\rho}J_+\left[\frac{\bar{\rho}^2}{\Delta\rho^4}\mathcal{L}_{-1}\left[\frac{T_{\overline{m}n}}{\rho^2\bar{\rho}^2}\right]\right] \,, \tag{C.1.3} $$

with $J_+ = \frac{\partial}{\partial\hat{r}} + \frac{iK}{\Delta}$ and

$$ \rho = \frac{1}{\hat{r} - i\hat{a}\cos(\theta)} \,, \qquad \bar{\rho} = \frac{1}{\hat{r} + i\hat{a}\cos(\theta)} \,, \tag{C.1.4} $$

$$ \mathcal{L}_p = \frac{\partial}{\partial\theta} + \frac{m}{\sin(\theta)} - \hat{a}\hat{\omega}\sin(\theta) + p\cot(\theta) \quad \,, \tag{C.1.5} $$

$$ \mathcal{L}_p^{\dagger} = \frac{\partial}{\partial\theta} - \frac{m}{\sin(\theta)} + \hat{a}\hat{\omega}\sin\theta + p\cot(\theta) \quad . \tag{C.1.6} $$

The components T_{nn}, $T_{\overline{m}n}$, and $T_{\overline{m}\overline{m}}$ are the projections of the stress-energy tensor with respect to the Newman-Penrose (NP) tetrad:

$$ l^\mu = \sqrt{\frac{\Sigma}{\Delta}}\left(e^\mu_{(0)} + e^\mu_{(1)}\right) \,, \quad n^\mu = \frac{1}{2}\sqrt{\frac{\Delta}{\Sigma}}\left(e^\mu_{(0)} - e^\mu_{(1)}\right) \,, \tag{C.1.7} $$

$$ m^\mu = \bar{\rho}\sqrt{\frac{\Sigma}{2}}\left(e^\mu_{(2)} + ie^\mu_{(3)}\right) \,, \; \overline{m}^\mu = \rho\sqrt{\frac{\Sigma}{2}}\left(e^\mu_{(2)} - ie^\mu_{(3)}\right) \,, \tag{C.1.8} $$

where, for example, $T_{nn} = n^\mu n^\nu T_{\mu\nu}$ [96]. Henceforth we use the notation $S^c_{\ell m}$ instead of ${}_{-2}S^{\hat{a}\hat{\omega}}_{\ell m}$ for the spin-weighted spheroidal harmonics to reduce clutter in the notation.
All θ-derivatives in $T_{nn}, T_{\overline{m}n}$ and $T_{\overline{m}\overline{m}}$ can be removed by repeated integrations by parts and by making use of the following identity

$$\int_0^\pi h(\theta)\mathcal{L}_p[g(\theta)]\sin(\theta)\mathrm{d}\theta = -\int_0^\pi g(\theta)\mathcal{L}_p^\dagger[h(\theta)]\sin(\theta)\mathrm{d}\theta\,, \tag{C.1.9}$$

with $h(\theta)$ and $g(\theta)$ regular functions. It is thus possible to write

$${}_{-2}\mathcal{T}_{\ell m\hat{\omega}} = \int \mathrm{d}t\mathrm{d}\theta\mathrm{d}\phi\Delta^2 e^{i(\hat{\omega}\hat{t}-m\phi)}\left(\mathcal{T}_{nn}+\mathcal{T}_{\overline{m}n}+\mathcal{T}_{\overline{m}\overline{m}}\right), \tag{C.1.10}$$

with

$$\mathcal{T}_{nn} = -\frac{2}{\Delta^2\rho^2\bar{\rho}}\mathcal{L}_1^\dagger\left[\frac{1}{\rho^4}\mathcal{L}_2^\dagger[\rho^3 S^c_{\ell m}]\right]\sin(\theta)T_{nn}\,, \tag{C.1.11}$$

$$\begin{aligned}\mathcal{T}_{\overline{m}n} = {}& \frac{4}{\sqrt{2}}\frac{\bar{\rho}}{\rho^2}\mathcal{L}_2^\dagger\left[S^c_{\ell m}\rho\bar{\rho}\right]J_+\left[\frac{T_{\overline{m}n}}{\Delta\rho^2\bar{\rho}^2}\right]\sin(\theta)+\\ &+\frac{2}{\sqrt{2}}\frac{1}{\rho^2\bar{\rho}^2\Delta}\mathcal{L}_2^\dagger\left[\rho^3 S^c_{\ell m}\frac{\mathrm{d}}{\mathrm{d}\hat{r}}\left(\frac{\bar{\rho}^2}{\rho^4}\right)\right]\sin(\theta)T_{\overline{m}n}\,,\end{aligned} \tag{C.1.12}$$

$$\mathcal{T}_{\overline{m}\overline{m}} = -\rho^3 S^c_{\ell m}J_+\left[\frac{1}{\rho^4}J_+\left[\frac{\bar{\rho}}{\rho^2}T_{\overline{m}\overline{m}}\right]\right]\sin(\theta)\,. \tag{C.1.13}$$

It is convenient to expand the previous terms in order to isolate the derivatives of the projected stress-energy tensor with respect to $\hat{r}$ and the derivative of $S^c_{\ell m}$ with respect to θ. After some algebra, we get

$$\mathcal{T}_{nn} = -\frac{2\sin(\theta)}{\Delta^2\rho^3\bar{\rho}}\left[\left(\mathcal{L}_1^\dagger - 2i\hat{a}\rho\sin(\theta)\right)\mathcal{L}_2^\dagger S^c_{\ell m}\right]T_{nn}\,, \tag{C.1.14}$$

$$\begin{aligned}\mathcal{T}_{\overline{m}n} = {}& \frac{4\sin(\theta)}{\sqrt{2}}\left\{\partial_{\hat{r}}\left[\left(\mathcal{L}_2^\dagger S^c_{\ell m}+i\hat{a}\sin(\theta)(\bar{\rho}-\rho)S^c_{\ell m}\right)\frac{T_{\overline{m}n}}{\rho^3\Delta}\right]\right.\\ &\left.+\left[\left(\frac{iK}{\Delta}+\rho+\bar{\rho}\right)\mathcal{L}_2^\dagger S^c_{\ell m}-\hat{a}\sin(\theta)\frac{K}{\Delta}(\bar{\rho}-\rho)S^c_{\ell m}\right]\frac{T_{\overline{m}n}}{\rho^3\Delta}\right\},\end{aligned} \tag{C.1.15}$$

$$\begin{aligned}\mathcal{T}_{\overline{m}\overline{m}} = {}& \left\{-\partial_{\hat{r}}^2\left(\frac{\bar{\rho}}{\rho^3}T_{\overline{m}\overline{m}}\right)-2\partial_{\hat{r}}\left(\left(\frac{\bar{\rho}}{\rho^2}+\frac{\bar{\rho}}{\rho^3}\frac{iK}{\Delta}\right)T_{\overline{m}\overline{m}}\right)\right.\\ &\left.+\frac{\bar{\rho}}{\rho^3}\left(\frac{\mathrm{d}}{\mathrm{d}\hat{r}}\left(\frac{iK}{\Delta}\right)-2\rho\frac{iK}{\Delta}+\frac{K^2}{\Delta^2}\right)T_{\overline{m}\overline{m}}\right\}\sin(\theta)S^c_{\ell m}\,.\end{aligned} \tag{C.1.16}$$

The stress-energy tensor for a spinning object is given by [99]

$$T^{\mu\nu} = q\int \mathrm{d}\hat{\lambda}\left[\frac{\delta^{(4)}_{x,z(\lambda)}}{\sqrt{-g}}u^{(\mu}v^{\nu)} - \nabla_\sigma\left(S^{\sigma(\mu}v^{\nu)}\frac{\delta^{(4)}_{x,z(\lambda)}}{\sqrt{-g}}\right)\right], \tag{C.1.17}$$

where $\delta^{(4)}_{x,z(\lambda)} \equiv \prod_{\nu=0}^{4}\delta\big(x^\nu - z^\nu(\hat{\lambda})\big)$ and indices within parenthesis denote symmetrization. The tetrad components are [99]

$$T^{(a)(b)} = q\int\frac{\mathrm{d}\hat{\lambda}}{\sqrt{-g}}\left[u^{((a}v^{(b))}\delta^{(4)}_{x,z(\lambda)} - e^{\big((a)}{}_\nu\, e^{(b)\big)}{}_\rho\nabla_\sigma\Big(S^{\sigma\nu}v^\rho\delta^{(4)}_{x,z(\lambda)}\Big)\right]. \tag{C.1.18}$$

The above equation can be written as

$$\begin{aligned}T^{(a)(b)} = q\int\frac{\mathrm{d}\hat{\lambda}}{\sqrt{-g}}\Big[\delta^{(4)}_{x,z(\lambda)}\Big(&u^{\big((a}v^{(b)\big)} + \omega_{(d)(c)}{}^{\big((a}v^{(b)\big)}S^{(d)(c)}\\ &-\omega_{(d)(c)}{}^{\big((a}S^{(b)\big)(d)}v^{(c)}\Big) - \partial_\sigma\Big(S^{\big((a}v^{(b)\big)}\delta^{(4)}_{x,z(\lambda)}\Big)\Big].\end{aligned} \tag{C.1.19}$$

For bound orbits, it is useful to rewrite the energy-momentum tensor as

$$T^{(a)(b)} = \frac{1}{\sqrt{-g}}\delta^{(3)}_{\underline{x},\underline{x}(\hat{t})}\Big(\mathcal{P}^{(a)(b)} - \mathcal{S}^{t(a)(b)}\partial_{\hat{t}}\Big) + \frac{1}{\sqrt{-g}}\partial_i\Big(\mathcal{S}^{i(a)(b)}\delta^{(3)}_{\underline{x},\underline{x}(t)}\Big), \tag{C.1.20}$$

where $i = \{r,\theta,\phi\}$, $\delta^{(3)}_{\underline{x},\underline{x}(t)} = \delta\big(\hat{r}-\hat{r}(\hat{t})\big)\delta\big(\theta-\theta(t)\big)\delta\big(\phi-\phi(\hat{t})\big)$, and we defined

$$\mathcal{P}^{(a)(b)} := q\left|\frac{\mathrm{d}\hat{t}}{\mathrm{d}\hat{\lambda}}\right|^{-1}\Big(u^{\big((a}v^{(b)\big)} + \omega_{(d)(c)}{}^{\big((a}v^{(b)\big)}S^{(d)(c)} - \omega_{(d)(c)}{}^{\big((a}S^{(b)\big)(d)}v^{(c)}\Big), \tag{C.1.21}$$

$$\mathcal{S}^{\sigma(a)(b)} := -q\left|\frac{\mathrm{d}\hat{t}}{\mathrm{d}\hat{\lambda}}\right|^{-1}S^{\sigma\big((a}v^{(b)\big)}. \tag{C.1.22}$$

To rewrite the stress-energy tensor we used the well-known property of the derivative of a Dirac delta:

$$\int_{-\infty}^{\infty}\mathrm{d}x h(x)\frac{\mathrm{d}}{\mathrm{d}x}\delta(x-x_0) = -\left.\frac{\mathrm{d}h}{\mathrm{d}x}\right|_{x=x_0}. \tag{C.1.23}$$

In this way, the stress-energy tensor can be interpreted as a linear differential operator that acts on the smooth functions inside of the Teukolsky source term.

We now need to project T^{ab} with respect to the NP null tetrad. In the following, we will employ a reduced version of the NP tetrad:

$$\tilde{l}^{\mu} = \left(e^{\mu}_{(0)} + e^{\mu}_{(1)}\right), \qquad \tilde{n}^{\mu} = \frac{1}{2}\left(e^{\mu}_{(0)} - e^{\mu}_{(1)}\right), \tag{C.1.24}$$

$$\tilde{m}^{\mu} = \frac{1}{\sqrt{2}}\left(e^{\mu}_{(2)} + ie^{\mu}_{(3)}\right), \quad \tilde{k}^{\mu} = \frac{1}{\sqrt{2}}\left(e^{\mu}_{(2)} - ie^{\mu}_{(3)}\right), \tag{C.1.25}$$

where $\tilde{k}^{\mu}$ is the complex conjugate of $\tilde{m}^{\mu}$. Taking into account that the $\hat{t}$ and ϕ coordinates in the Teukolsky source term are only present in the exponential, and using the definitions $T_{nn} = n^{\mu}n^{\nu}e_{\mu(a)}e_{\nu(b)}T^{(a)(b)}$ and so on, the projected components read

$$T_{nn} = \delta^{(3)}_{\underline{x},\underline{x}(t)}\mathcal{D}_{\tilde{n}\tilde{n}}[N_{nn}\,\cdot] + \partial_{\hat{r}}\left(\mathcal{S}^{r}_{\tilde{n}\tilde{n}}\delta^{(3)}_{\underline{x},\underline{x}(t)}\right)N_{nn}\,, \tag{C.1.26}$$

$$T_{\overline{m}n} = \delta^{(3)}_{\underline{x},\underline{x}(t)}\mathcal{D}_{\tilde{k}\tilde{n}}[N_{\overline{m}n}\,\cdot] + \partial_{\hat{r}}\left(\mathcal{S}^{r}_{\tilde{k}\tilde{n}}\delta^{(3)}_{\underline{x},\underline{x}(t)}\right)N_{\overline{m}n}\,, \tag{C.1.27}$$

$$T_{\overline{m}\overline{m}} = \delta^{(3)}_{\underline{x},\underline{x}(t)}\mathcal{D}_{\tilde{k}\tilde{k}}[N_{\overline{m}\overline{m}}\,\cdot] + \partial_{\hat{r}}\left(\mathcal{S}^{r}_{\tilde{k}\tilde{k}}\delta^{(3)}_{\underline{x},\underline{x}(t)}\right)N_{\overline{m}\overline{m}}\,, \tag{C.1.28}$$

with

$$N_{nn} = \frac{\Delta}{\sqrt{-g}\Sigma}, \quad N_{\overline{m}n} = \frac{\sqrt{\Delta}\rho}{\sqrt{-g}}, \quad N_{\overline{m}\overline{m}} = \frac{\Sigma\rho^2}{\sqrt{-g}}, \tag{C.1.29}$$

and where we define the following linear operators acting on a generic smooth function $h(\hat{r},\theta)$:

$$\mathcal{D}_{\tilde{n}\tilde{n}}[N_{nn}h(\hat{r},\theta)] \equiv \left(\mathcal{P}_{\tilde{n}\tilde{n}} - i\hat{\omega}\mathcal{S}^{t}_{\tilde{n}\tilde{n}} + im\mathcal{S}^{\phi}_{\tilde{n}\tilde{n}} - \mathcal{S}^{\theta}_{\tilde{n}\tilde{n}}\partial_{\theta}\right)\left(\frac{\Delta}{\sqrt{-g}\Sigma}h(\hat{r},\theta)\right), \tag{C.1.30}$$

$$\mathcal{D}_{\tilde{k}\tilde{n}}\left[N_{\tilde{k}\tilde{n}}h(\hat{r},\theta)\right] \equiv \left(\mathcal{P}_{\tilde{k}\tilde{n}} - i\hat{\omega}\mathcal{S}^{t}_{\tilde{k}\tilde{n}} + im\mathcal{S}^{\phi}_{\tilde{k}\tilde{n}} - \mathcal{S}^{\theta}_{\tilde{k}\tilde{n}}\partial_{\theta}\right)\left(\frac{\sqrt{\Delta}\rho}{\sqrt{-g}}h(\hat{r},\theta)\right), \tag{C.1.31}$$

$$\mathcal{D}_{\tilde{k}\tilde{k}}[N_{\overline{m}\overline{m}}h(\hat{r},\theta)] \equiv \left(\mathcal{P}_{\tilde{k}\tilde{k}} - i\omega\mathcal{S}^{t}_{\tilde{k}\tilde{k}} + im\mathcal{S}^{\phi}_{\tilde{k}\tilde{k}} - \mathcal{S}^{\theta}_{\tilde{k}\tilde{k}}\partial_{\theta}\right)\left(\frac{\Sigma\rho^2}{\sqrt{-g}}h(\hat{r},\theta)\right). \tag{C.1.32}$$

Using the relations (C.1.26), (C.1.27) and (C.1.28), we can now rewrite the terms $\mathcal{T}_{nn}$, $\mathcal{T}_{\overline{m}n}$ and $\mathcal{T}_{\overline{m}\overline{m}}$, obtaining

$$\mathcal{T}_{nn} = \left[\delta^{(3)}_{\underline{x},\underline{x}(t)}\mathcal{D}_{\tilde{n}\tilde{n}} + \partial_{\hat{r}}\left(\mathcal{S}^{r}_{\tilde{n}\tilde{n}}\delta^{(3)}_{\underline{x},\underline{x}(t)}\right)\right]f^{(0)}_{nn}\,, \tag{C.1.33}$$

$$f^{(0)}_{nn} := -\frac{2}{\Delta}\frac{\bar{\rho}}{\rho}\left(\mathcal{L}^{\dagger}_{1} - 2i\hat{a}\rho\sin(\theta)\right)\mathcal{L}^{\dagger}_{2}S^{c}_{\ell m}\,, \tag{C.1.34}$$

$$\mathcal{T}_{\overline{m}n} = \left[\delta^{(3)}_{\underline{x},\underline{x}(t)}\mathcal{D}_{\tilde{k}\tilde{n}} + \partial_{\hat{r}}\left(\mathcal{S}^{r}_{\tilde{k}\tilde{n}}\delta^{(3)}_{\underline{x},\underline{x}(t)}\right)\right] f^{(0)}_{\overline{m}n} + \partial_{\hat{r}}\left[\left(\delta^{(3)}_{\underline{x},\underline{x}(t)}\mathcal{D}_{\tilde{k}\tilde{n}} + \partial_{r}\left(\mathcal{S}^{r}_{\tilde{k}\tilde{n}}\delta^{(3)}_{\underline{x},\underline{x}(t)}\right)\right) f^{(1)}_{\overline{m}n}\right] , \tag{C.1.35}$$

$$f^{(0)}_{\overline{m}n} := \frac{4}{\sqrt{2}}\frac{\bar{\rho}}{\rho\sqrt{\Delta}}\left(\left(\frac{iK}{\Delta} + \rho + \bar{\rho}\right)\mathcal{L}_2^{\dagger}S^{c}_{\ell m} - \hat{a}\sin(\theta)\frac{K}{\Delta}(\bar{\rho} - \rho)S^{c}_{\ell m}\right) , \tag{C.1.36}$$

$$f^{(1)}_{\overline{m}n} := \frac{4}{\sqrt{2}}\frac{\bar{\rho}}{\rho\sqrt{\Delta}}\left(\mathcal{L}_2^{\dagger}S^{c}_{\ell m} + i\hat{a}\sin(\theta)(\bar{\rho} - \rho)\right) , \tag{C.1.37}$$

$$\begin{aligned}\mathcal{T}_{\overline{m}\overline{m}} = &\left[\delta^{(3)}_{\underline{x},\underline{x}(t)}\mathcal{D}_{\tilde{k}\tilde{k}} + \partial_{\hat{r}}\left(\mathcal{S}^{r}_{\tilde{k}\tilde{k}}\delta^{(3)}_{\underline{x},\underline{x}(t)}\right)\right] f^{(0)}_{\overline{m}\overline{m}} + \partial_{\hat{r}}\left[\left(\delta_{r,r(t)}\mathcal{D}_{\tilde{k}\tilde{k}} + \partial_{\hat{r}}\left(\mathcal{S}^{r}_{\tilde{k}\tilde{k}}\right)\right) f^{(1)}_{\overline{m}\overline{m}}\right] + \\ &+ \partial^2_{\hat{r}}\left[\left(\delta_{r,r(t)}\mathcal{D}_{\tilde{k}\tilde{k}} + \partial_{\hat{r}}\left(\mathcal{S}^{r}_{\tilde{k}\tilde{k}}\delta_{r,r(t)}\right)\right) f^{(2)}_{\overline{m}\overline{m}}\right] ,\end{aligned} \tag{C.1.38}$$

$$f^{(0)}_{\overline{m}\overline{m}} := \frac{\bar{\rho}}{\rho}\left(\frac{\mathrm{d}}{\mathrm{d}\hat{r}}\left(\frac{iK}{\Delta}\right) - 2\rho\frac{iK}{\Delta} + \frac{K^2}{\Delta^2}\right) S^{c}_{\ell m} , \tag{C.1.39}$$

$$f^{(1)}_{\overline{m}\overline{m}} := -2\frac{\bar{\rho}}{\rho}\left(\rho + \frac{iK}{\Delta}\right) S^{c}_{\ell m} , \tag{C.1.40}$$

$$f^{(2)}_{\overline{m}\overline{m}} := -\frac{\bar{\rho}}{\rho}S^{c}_{\ell m} . \tag{C.1.41}$$

We now have all the necessary ingredients to rewrite the inhomogeneous solutions of the Teukolsky equation in a form suitable to exploit the possible quasi-periodicities in the bound orbits. First of all, by plugging the terms (C.1.33), (C.1.35) and (C.1.38) into Eq. (C.1.10), integrating over the angles and using the $\delta(\theta - \theta(\hat{t}))\delta(\phi - \phi(\hat{t}))$ function, the Teukolsky source term becomes

$$\begin{aligned}\mathcal{T}_{\ell m\hat{\omega}} = &\int_{-\infty}^{\infty}\mathrm{d}\hat{t}\, e^{i(\hat{\omega}\hat{t} - m\phi(\hat{t}))}\Delta^2\Big\{\mathcal{T}^{(0)}_{\mathcal{D}}\delta_{r,r(t)} + \partial_{\hat{r}}\left(\mathcal{T}^{(0)}_{\mathcal{D}}\delta_{r,r(t)}\right) + \partial^2_{\hat{r}}\left(\mathcal{T}^{(0)}_{\mathcal{D}}\delta_{r,r(t)}\right) + \\ &+ \mathcal{T}^{(0)}_{\mathcal{S}^r} + \partial_{\hat{r}}\mathcal{T}^{(1)}_{\mathcal{S}^r} + \partial^2_{\hat{r}}\mathcal{T}^{(2)}_{\mathcal{S}^r}\Big\}\Big|_{\theta=\theta(\hat{t})} ,\end{aligned} \tag{C.1.42}$$

when $\delta_{r,r(t)} := \delta(\hat{r} - \hat{r}(\hat{t}))$, and we have rearranged the previous terms, defining

$$\mathcal{T}^{(0)}_{\mathcal{D}} = \mathcal{D}_{\tilde{n}\tilde{n}}f^{(0)}_{nn} + \mathcal{D}_{\tilde{k}\tilde{n}}f^{(0)}_{\overline{m}n} + \mathcal{D}_{\tilde{k}\tilde{k}}f^{(0)}_{\overline{m}\overline{m}} , \tag{C.1.43}$$

$$\mathcal{T}^{(1)}_{\mathcal{D}} = \mathcal{D}_{\tilde{k}\tilde{n}}f^{(1)}_{\overline{m}n} + \mathcal{D}_{\tilde{k}\tilde{k}}f^{(1)}_{\overline{m}\overline{m}} , \tag{C.1.44}$$

$$\mathcal{T}^{(2)}_{\mathcal{D}} = \mathcal{D}_{\tilde{k}\tilde{k}}f^{(2)}_{\overline{m}\overline{m}} , \tag{C.1.45}$$

and

$$\mathcal{T}^{(0)}_{\mathcal{S}^r} = \partial_{\hat{r}}\left[\mathcal{S}^r_{\tilde{n}\tilde{n}}\delta_{r,r(t)}\right] f^{(0)}_{nn} + \partial_{\hat{r}}\left[\mathcal{S}^r_{\tilde{k}\tilde{n}}\delta_{r,r(t)}\right] f^{(0)}_{\overline{mn}} + \partial_{\hat{r}}\left[\mathcal{S}^r_{\tilde{k}\tilde{k}}\delta_{r,r(t)}\right] f^{(0)}_{\overline{mm}}\,, \tag{C.1.46}$$

$$\mathcal{T}^{(1)}_{\mathcal{S}^r} = \partial_{\hat{r}}\left[\mathcal{S}^r_{\tilde{k}\tilde{n}}\delta_{r,r(t)}\right] f^{(1)}_{\overline{mn}} + \partial_{\hat{r}}\left[\mathcal{S}^r_{\tilde{k}\tilde{k}}\delta_{r,r(t)}\right] f^{(1)}_{\overline{mm}}\,, \tag{C.1.47}$$

$$\mathcal{T}^{(2)}_{\mathcal{S}^r} = \partial_{\hat{r}}\left[\mathcal{S}^r_{\tilde{k}\tilde{k}}\delta_{r,r(t)}\right] f^{(2)}_{\overline{mm}}\,. \tag{C.1.48}$$

To obtain the asymptotic fluxes, we need to calculate the amplitudes (4.1.14) and (4.1.15), namely

$$ {}_{-2}Z^{H,\infty}_{\ell m\hat{\omega}} = C^{H,\infty}_{\ell m\hat{\omega}} \int_{\hat{r}_+}^{\infty} \mathrm{d}\hat{r}' \frac{{}_{-2}R^{\mathrm{in,up}}_{\ell m\hat{\omega}}(\hat{r}')}{\Delta^2}\, {}_{-2}\mathcal{T}_{\ell m\hat{\omega}}(\hat{r}')\,. \tag{C.1.49}$$

By changing the order of integration between $\hat{r}'$ and $\hat{t}$, we get

$$\begin{aligned} {}_{-2}Z^{H,\infty}_{\ell m\hat{\omega}} = C^{H,\infty}_{\ell m\hat{\omega}} \int_{-\infty}^{\infty} \Bigg[&\left(\mathcal{T}^{(0)}_{\mathcal{D}} - \mathcal{T}^{(1)}_{\mathcal{D}}\frac{\mathrm{d}}{\mathrm{d}\hat{r}} + \mathcal{T}^{(2)}_{\mathcal{D}}\frac{\mathrm{d}^2}{\mathrm{d}\hat{r}^2}\right) {}_{-2}R^{\mathrm{in,up}}_{\ell m\hat{\omega}} \\ &+ \int_{\hat{r}_+}^{\infty} \mathrm{d}\hat{r} \left(\mathcal{T}^{(0)}_{\mathcal{S}^r} + \partial_{\hat{r}}\mathcal{T}^{(1)}_{\mathcal{S}^r} + \partial^2_{\hat{r}}\mathcal{T}^{(2)}_{\mathcal{S}^r}\right) {}_{-2}R^{\mathrm{in,up}}_{\ell m\hat{\omega}} \Bigg] e^{i(\hat{\omega}\hat{t} - m\phi(\hat{t}))}\mathrm{d}\hat{t}\,, \end{aligned} \tag{C.1.50}$$

which is calculated at $\theta = \theta(\hat{t})$. In the integral on the first line we have used the $\delta(\hat{r} - \hat{r}(\hat{t}))$ function. The double integral on the second line can be simplified with multiple integrations by parts, obtaining the general expression

$$\begin{aligned} {}_{-2}Z^{H,\infty}_{\ell m\hat{\omega}} = C^{H,\infty}_{\ell m\hat{\omega}} \int_{-\infty}^{\infty} \mathrm{d}\hat{t} e^{i(\hat{\omega}\hat{t} - m\phi(\hat{t}))} \Bigg(&A_0 - (A_1 + B_1)\frac{\mathrm{d}}{\mathrm{d}\hat{r}} \\ &+ (A_2 + B_2)\frac{\mathrm{d}^2}{\mathrm{d}\hat{r}^2} - B_3\frac{\mathrm{d}^3}{\mathrm{d}\hat{r}^3}\Bigg) {}_{-2}R^{\mathrm{in,up}}_{\ell m\hat{\omega}}\Big|_{\theta=\theta(\hat{t}),\hat{r}=\hat{r}(\hat{t})} \end{aligned} \tag{C.1.51}$$

where

$$A_0 := O_{\tilde{n}\tilde{n}} f^{(0)}_{nn} + O_{\tilde{k}\tilde{n}} f^{(0)}_{\overline{mn}} + O_{\tilde{k}\tilde{k}} f^{(0)}_{\overline{mm}}\,, \tag{C.1.52}$$

$$A_1 := O_{\tilde{k}\tilde{n}} f^{(1)}_{\overline{mn}} + O_{\tilde{k}\tilde{k}} f^{(1)}_{\overline{mm}}\,, \tag{C.1.53}$$

$$A_2 := O_{\tilde{k}\tilde{k}} f^{(2)}_{\overline{mm}}\,, \tag{C.1.54}$$

and

$$B_1 := \mathcal{S}^r_{\tilde{n}\tilde{n}} f^{(0)}_{nn} + \mathcal{S}^r_{\tilde{k}\tilde{n}} f^{(0)}_{\overline{mn}} + \mathcal{S}^r_{\tilde{k}\tilde{k}} f^{(0)}_{\overline{mm}}\,, \tag{C.1.55}$$

$$B_2 := \mathcal{S}^r_{\tilde{k}\tilde{n}} f^{(1)}_{\overline{mn}} + \mathcal{S}^r_{\tilde{k}\tilde{k}} f^{(1)}_{\overline{mm}}\,, \tag{C.1.56}$$

$$B_3 := \mathcal{S}^r_{\tilde{k}\tilde{k}} f^{(2)}_{\overline{mm}}\,, \tag{C.1.57}$$

with the operators $O_{\tilde{n}\tilde{n}}, O_{\tilde{k}\tilde{n}}, O_{\tilde{k}\tilde{k}}$ being defined as

$$O_{\tilde{n}\tilde{n}} := \mathcal{P}_{\tilde{n}\tilde{n}} - i\hat{\omega}\mathcal{S}^{t}_{\tilde{n}\tilde{n}} + im\mathcal{S}^{\phi}_{\tilde{n}\tilde{n}} - \mathcal{S}^{\theta}_{\tilde{n}\tilde{n}}\partial_{\theta} - \mathcal{S}^{r}_{\tilde{n}\tilde{n}}\partial_{\hat{r}}\,, \tag{C.1.58}$$

$$O_{\tilde{k}\tilde{n}} := \mathcal{P}_{\tilde{k}\tilde{n}} - i\hat{\omega}\mathcal{S}^{t}_{\tilde{k}\tilde{n}} + im\mathcal{S}^{\phi}_{\tilde{k}\tilde{n}} - \mathcal{S}^{\theta}_{\tilde{k}\tilde{n}}\partial_{\theta} - \mathcal{S}^{r}_{\tilde{k}\tilde{n}}\partial_{\hat{r}}\,, \tag{C.1.59}$$

$$O_{\tilde{k}\tilde{k}} := \mathcal{P}_{\tilde{k}\tilde{k}} - i\hat{\omega}\mathcal{S}^{t}_{\tilde{k}\tilde{k}} + im\mathcal{S}^{\phi}_{\tilde{k}\tilde{k}} - \mathcal{S}^{\theta}_{\tilde{k}\tilde{k}}\partial_{\theta} - \mathcal{S}^{r}_{\tilde{k}\tilde{k}}\partial_{\hat{r}}\,, \tag{C.1.60}$$

and $\mathcal{P}_{\tilde{n}\tilde{n}} = \tilde{n}^{\mu}\tilde{n}^{\nu}e_{\mu(a)}e_{\nu(b)}\mathcal{P}^{(a)(b)}$, while $\mathcal{S}^{\sigma}_{\tilde{n}\tilde{n}} = \tilde{n}^{\mu}\tilde{n}^{\nu}e_{\mu(a)}e_{\nu(b)}\mathcal{S}^{\sigma(a)(b)}$ and so on. The terms $f^{(i)}_{nn}$, $f^{(i)}_{\bar{m}n}$, $f^{(i)}_{\bar{m}\bar{m}}$ (with $i = 0,1,2$) are defined in Eqs. (C.1.34)–(C.1.41). We remark that Eq. (C.1.51) is general: it is valid for any bound orbit for a spinning test particle in Kerr spacetime.

C.1.1 Circular equatorial orbits

On the equatorial plane, $\theta = \pi/2$, the Teukolsky source term drastically simplifies. First of all, some terms of the previous equations vanish, namely

$$\mathcal{S}^{\theta}_{\tilde{n}\tilde{n}} = \mathcal{S}^{\theta}_{\tilde{k}\tilde{n}} = \mathcal{S}^{\theta}_{\tilde{k}\tilde{k}} = 0\,, \tag{C.1.61}$$

for $\theta = \pi/2$. Furthermore, we can write

$$f^{(0)}_{nn} = -4\frac{\hat{S}(r)}{\Delta}\,, \tag{C.1.62}$$

$$f^{(0)}_{\bar{m}n} = \frac{4}{\sqrt{2}}\frac{\tilde{S}}{\sqrt{\Delta}}\left(\frac{iK}{\Delta} + \frac{2}{\hat{r}}\right)\,, \tag{C.1.63}$$

$$f^{(1)}_{\bar{m}n} = \frac{4}{\sqrt{2}}\frac{\tilde{S}}{\sqrt{\Delta}}\,, \tag{C.1.64}$$

where we applied the angular Teukolsky equation, with

$$\tilde{S} := \left.\frac{\mathrm{d}S^{c}_{\ell m}}{\mathrm{d}\theta}\right|_{\theta=\pi/2} + (\hat{a}\hat{\omega} - m)S^{c}_{\ell m}(\pi/2)\,, \tag{C.1.65}$$

$$\hat{S}(\hat{r}) := \left(\hat{a}\hat{\omega} - m - i\frac{\hat{a}}{\hat{r}}\right)\tilde{S} - \frac{{}_{-2}\lambda_{\ell m\hat{\omega}}}{2}S^{c}_{\ell m}(\pi/2)\,. \tag{C.1.66}$$

Moreover

$$f^{(0)}_{\bar{m}\bar{m}} = \left(\frac{\mathrm{d}}{\mathrm{d}\hat{r}}\left(\frac{iK}{\Delta}\right) - \frac{2}{\hat{r}}\frac{iK}{\Delta} + \frac{K^2}{\Delta^2}\right)S^{c}_{\ell m}(\pi/2)\,, \tag{C.1.67}$$

$$f^{(1)}_{\bar{m}\bar{m}} = -2\left(\frac{1}{\hat{r}} + \frac{iK}{\Delta}\right)S^{c}_{\ell m}(\pi/2)\,, \tag{C.1.68}$$

$$f^{(2)}_{\bar{m}\bar{m}} = -S^{c}_{\ell m}(\pi/2)\,. \tag{C.1.69}$$

Finally, for a circular equatorial orbit the projected components of $\mathcal{P}^{(a)(b)}$ and $\mathcal{S}^{\sigma(a)(b)}$ onto the reduced NP basis are

$$\mathcal{P}_{\tilde{n}\tilde{n}} = -\frac{q}{4}\frac{P_\sigma}{\Sigma_\sigma\Gamma_+}\left(\mathfrak{r}_\sigma\Delta\hat{x}\sigma - \hat{r}\Sigma_\sigma\left[2\hat{x}\sigma(\hat{r}-\hat{a}^2) + P_\sigma(\hat{r}^2-\sigma\hat{a})\right]\right)\,, \tag{C.1.70}$$

$$\mathcal{P}_{\tilde{k}\tilde{n}} = \frac{iq}{4\sqrt{2}}\frac{\sqrt{\Delta}}{\Sigma_\sigma\Gamma_+}\Big(\hat{x}\mathfrak{r}_\sigma\left[\hat{x}\sigma(\hat{r}-\hat{a}^2) + P_\sigma(\hat{r}^2+\hat{a}\sigma)\right] + \\ +\hat{r}P_\sigma\Sigma_\sigma\left[\hat{r}^2\hat{x} + \sigma(3\hat{x}\hat{a}+P_\sigma)\right]\Big)\,, \tag{C.1.71}$$

$$\mathcal{P}_{\tilde{k}\tilde{k}} = \frac{q}{2}\frac{1}{\Sigma_\sigma\Gamma_-}\left\{\hat{x}\Delta\left[\sigma(P_\sigma+2\hat{x}\hat{a}) + \hat{x}\hat{r}^2\right]\mathfrak{r}_\sigma + \hat{a}\sigma\hat{r}\Sigma_\sigma P_\sigma^2\right\}\,, \tag{C.1.72}$$

with

$$\hat{x} := \tilde{J}_z - (\hat{a}+\sigma)\tilde{E}\,,$$
$$\Gamma_\pm := 3\hat{x}\hat{a}\sigma^2\Delta \pm \hat{r}\Sigma_\sigma\left[P_\sigma(\hat{r}^2+\hat{a}^2) + \hat{x}\hat{a}\Delta\right]\,,$$
$$\mathfrak{r}_\sigma := \hat{r}^3 + 2\sigma^2\,,$$

and

$$\mathcal{S}^\nu_{\tilde{n}\tilde{n}} = \frac{1}{4}q\sigma\hat{r}^2P_\sigma\left(\frac{\hat{a}P_\sigma + \hat{x}(\hat{r}^2+\hat{a}^2)}{\Gamma_+},\, -\frac{\Delta\hat{x}}{\Gamma_-},\, 0,\, -\frac{\hat{a}\hat{x}+P_\sigma}{\Gamma_-}\right)\,, \tag{C.1.73}$$

$$\mathcal{S}^\nu_{\tilde{k}\tilde{n}} = \frac{iq\sigma}{4\sqrt{2}}\frac{\hat{r}\hat{x}\sqrt{\Delta}}{\Sigma_\sigma\Gamma_+}\left(\mathfrak{r}_\sigma\left[\hat{a}P_\sigma + \hat{x}(\hat{r}^2+\hat{a}^2)\right],\, \hat{x}\Delta\mathfrak{r}_\sigma + \frac{\hat{r}}{\hat{x}}\Sigma_\sigma P_\sigma^2,\, 0,\, (\hat{a}\hat{x}+P_\sigma)\mathfrak{r}_\sigma\right)\,, \tag{C.1.74}$$

$$\mathcal{S}^\nu_{\tilde{k}\tilde{k}} = \frac{1}{2}q\sigma\frac{\hat{r}P_\sigma}{\Sigma_\sigma\Gamma_+}(0,\, \Delta\hat{x}\mathfrak{r}_\sigma,\, 0,\, 0)\,. \tag{C.1.75}$$

In Ref. [99] the Teukolsky source was calculated at first order in the spin. Our results for the source term are general and, when truncated at $\mathcal{O}(\sigma)$, agree with those in Ref. [99], except for a factor $1/\sqrt{2}$ in their $\tilde{Z}^{\bar{m}\bar{m}}_{lm\omega}$ term. This is probably a typo in their source term, since with our source term we can reproduce previous results for the fluxes of a nonspinning particle (see also Appendix E).

Appendix D

Linearization in the secondary spin of the Teukolsky equations

D.1 Linearization of the angular Teukolsky equation

For the study of the eigenvalues and eigenfunctions of Eq. (4.1.2), it is convenient to perform a change of variable defining $x = \cos\theta$, obtaining

$$\mathcal{H}|S\rangle = -\,{}_s\lambda_{\ell m\hat{\omega}}|S\rangle\,, \quad |S\rangle \equiv {}_sS^c_{\ell m}\,, \quad \mathcal{H} = \mathcal{K} + \mathcal{V}\,, \tag{D.1.1}$$

with

$$\mathcal{K} \equiv \frac{\mathrm{d}}{\mathrm{d}x}\left((1-x^2)\frac{\mathrm{d}}{\mathrm{d}x}\right), \tag{D.1.2}$$

$$\mathcal{V} \equiv cx(cx-2s) - c^2 + s + 2mc - \frac{(m+sx)^2}{1-x^2}\,, \tag{D.1.3}$$

We consider here only the case in which $c \in \mathbb{R}$. Physical solutions of (D.1.3) must be regular in the interval $[-1,1]$, which entails that ℓ and m must be integers with $|m| \leq \ell$. The solutions to Eq. (D.1.3) can be written as a series expansion around the singular points $x = \pm 1$ [243, 244]:

$${}_sS^c_{\ell m} = \frac{e^{cx}}{\sqrt{\mathcal{N}}}(1+x)^{k_-}(1-x)^{k_+}\sum_{n=0}^{\infty} d_n(1+x)^n\,, \tag{D.1.4}$$

where $k_\pm = |m \pm 2|/2$ and the coefficients d_n are given by the three-term recursion relations

$$\alpha_0 d_1 + \beta_0 d_0 = 0\,, \tag{D.1.5}$$

$$\alpha_n d_{n+1} + \beta_n d_n + \gamma_n d_{n-1} = 0 \qquad n = 1, 2\ldots \tag{D.1.6}$$

with

$$\alpha_n = -2(n+1)(n+2k_- +1)\,, \tag{D.1.7}$$
$$\beta_n = n(n+1) + 2n(k_s+1-2c) - 2c(2k_- +s+1) + \\ + k_s(k_s+1) - s(s+1) - {}_s\lambda_{\ell m\hat{\omega}} - 2mc\,, \tag{D.1.8}$$
$$\gamma_n = 2c(n+k_s+s)\,, \tag{D.1.9}$$

and $k_s = k_+ + k_-$. The normalization constant $\mathcal{N}$ can be written analytically as

$$\mathcal{N} \equiv \int_{-1}^{1} ({}_sS^c_{\ell m}(x))^2 \mathrm{d}x = (2\pi)2^{1+2k_s} e^{-2c}\Gamma(1+2k_+)\mathfrak{N}\,, \tag{D.1.10}$$

where

$$\mathfrak{N} \equiv \sum_{n=0}^{\infty} \frac{\Gamma(1+2k_- +n)}{\Gamma(2+2k_s+n)} 2^n F(n,n;c) \sum_{i=0}^{n} d_i d_{n-i}\,, \tag{D.1.11}$$
$$F(n,n;c) := {}_1F_1(1+2k_- +n, 2+2k_s+n; 4c)\,, \tag{D.1.12}$$

while $\Gamma(z)$ is the Euler gamma function and ${}_1F_1(a,b;z)$ is the Kummer confluent hypergeometric function. To ensure the convergence of the series (D.1.4) at $x = \pm 1$, the eigenvalue ${}_s\lambda_{\ell m\hat{\omega}}$ must satisfy the implicit continued fraction

$$0 = \beta_0 - \frac{\alpha_0\gamma_1}{\beta_1 -}\frac{\alpha_1\gamma_2}{\beta_2 -}\frac{\alpha_2\gamma_3}{\beta_3 -}\ldots \tag{D.1.13}$$

With the requirement of regularity at the boundaries $[-1,1]$, Eq. (D.1.3) defines a Sturm-Liouville eigenvalue problem. In particular, the eigenvalue problem is singular because the coefficient $(1-x^2)$ vanishes at the boundaries. Nevertheless, it can be shown that Eq. (D.1.3) still satisfies many of the properties of a regular Sturm-Liouville problem, namely (see [245] and references therein):

- the operator $\mathcal{H}$ is Hermitian, i.e. $\langle v|\mathcal{H}|w\rangle = \langle w|\mathcal{H}|v\rangle$ for any vector v, w;
- given a set s, m, c, the functions ${}_sS^c_{\ell m}(\theta)$ form a (strong) complete, orthogonal set on $[-1,1]$, labeled by the additional integer ℓ (see [246]);
- each eigenvalue ${}_s\lambda_{\ell m\hat{\omega}}$ has (up to a constant) a unique eigenfunction for any set s, m, c.

Thus, we can conveniently treat the secondary spin σ as a small perturbation of an Hermitian operator and compute the linear corrections in σ to ${}_s\lambda_{\ell m\hat{\omega}}$ using

the same techniques of nondegenerate perturbations of a quantum mechanical system [247]. To linear order in σ, we obtain

$$\mathcal{H}^0|S^0\rangle = -{}_s\lambda^0_{\ell m}|S^0\rangle\,, \tag{D.1.14}$$
$$\mathcal{H}^0|S^1\rangle + \mathcal{V}^1|S^0\rangle = -{}_s\lambda^0_{\ell m}|S^1\rangle - {}_s\lambda^1_{\ell m}|S^0\rangle\,, \tag{D.1.15}$$
$$\mathcal{H}^0 = \mathcal{K} + \mathcal{V}^0\,, \tag{D.1.16}$$
$$\mathcal{V}^1 = 2c^1(c^0x^2 - sx + m - c^0)\,, \tag{D.1.17}$$

where $\mathcal{V}^0$ is simply given by $\mathcal{H}$ with $c \leftrightarrow c^0$, ${}_sS^0_{\ell m} \equiv |S^0\rangle$, ${}_sS^1_{\ell m} \equiv |S^1\rangle$ and

$$\begin{aligned} {}_s\lambda^1_{\ell m} &= \langle S^0|\mathcal{V}^1|S^0\rangle \equiv \int_{-1}^{1} {}_sS^0_{\ell m}\mathcal{V}^1\,{}_sS^0_{\ell m}\mathrm{d}x \\ &= -\frac{c^1}{\mathfrak{N}^0}\sum_{n=0}^{\infty}\Xi(n)\Big[\Upsilon(n)F(n,n+1;c^0) - \Pi(n)F(n,n;c^0)\Big]\sum_{i=0}^{n} d^0_i d^0_{n-i}\,, \end{aligned} \tag{D.1.18}$$

with

$$\Xi(n) \equiv 2^{n+1}\frac{\Gamma(1+2k_- + n)}{\Gamma(3+k_s+n)}\,, \tag{D.1.19}$$
$$\Upsilon(n) \equiv (1+2k_+)(2+2k_s+n+2s)\,, \tag{D.1.20}$$
$$\Pi(n) \equiv (2+2k_s+n)(1+2k_+ - m + s)\,. \tag{D.1.21}$$

The term $\mathfrak{N}^0$ is given by $\mathfrak{N}$ with $c \leftrightarrow c^0$. We computed the 0th order eigenvalue ${}_s\lambda^0_{\ell m}$, the corresponding eigenfunctions ${}_sS^0_{\ell m}$ and the coefficients d^0_n using the routines of the *SpinWeightedSpheroidalHarmonics* MATHEMATICA package of [119]. Once the correction to the eigenvalue ${}_s\lambda^1_{\ell m}$ is known, we can evaluate the correction to the eigenfunction ${}_sS^1_{\ell m}$ by expanding in σ the Leaver series (D.1.4), obtaining

$${}_sS^1_{\ell m} = \frac{e^{c^0x}}{\sqrt{\mathcal{N}^0}}(1+x)^{k_-}(1-x)^{k_+}\sum_{n=0}^{\infty}(1+x)^n\left[d^1_n + d^0_n\Big((1+x) - \frac{\mathfrak{N}^1}{2\mathfrak{N}^0}\Big)\right], \tag{D.1.22}$$

where the three-term recursion relation for the correction d^1_n is given by, for $n = 1, 2\ldots$

$$d^1_0 = 0 \qquad \alpha_0 d^1_1 + \beta^1_0 d^0_0 = 0\,, \tag{D.1.23}$$
$$\alpha_n d^1_{n+1} + \beta^0_n d^1_n + \beta^1_n d^0_n + \gamma^0_n d^1_{n-1} + \gamma^1_n d^1_{n-1} = 0\,, \tag{D.1.24}$$

with

$$\beta_n^1 = -2c^1(1+2k_- + m + 2n + s) - {}_s\lambda_{\ell m}^1\,, \tag{D.1.25}$$
$$\gamma_n^1 = 2c^1(k_s + s + n)\,, \tag{D.1.26}$$

and

$$\mathfrak{N}^1 \equiv \sum_{n=0}^{\infty} \frac{2^{n+1}\Gamma(1+2k_+ + n)}{\Gamma(2+2k_s+n)} \Big[F(n,n;c^0) \sum_{i=0}^{n} d_i^0 d_{n-i}^1 + \\ + 2\frac{1+2k_- + n}{2+2k_s+n} F(n+1,n+1;c^0) \sum_{i=0}^{n} d_i^0 d_{n-i}^0 \Big]\,. \tag{D.1.27}$$

D.1.1 Linearization of the radial Teukolsky equation

The linear corrections in σ, ${}_sR_{\ell m}^{\text{in},1}$ and ${}_sR_{\ell m}^{\text{up},1}$, were obtained by expanding the ansatz (4.3.12) as follows. Let us first define

$$N_{\mp}^0 = \hat{r}^{-1}\Delta^{-s} e^{\mp i\hat{\omega}^0 \hat{r}^*} e^{im\tilde{\phi}}\,, \tag{D.1.28}$$
$$D_{\mp}^0 = -\frac{N_{\mp}^0}{\Delta}\Big(\frac{\Delta}{\hat{r}} + 2s(\hat{r}-1) \pm i(\hat{r}^2+\hat{a}^2)\hat{\omega}^0 + i\hat{a}m\Big)\,, \tag{D.1.29}$$
$$D_{\mp}^1 = \mp i\omega^1\Big(\frac{\hat{r}^2+\hat{a}^2}{\Delta}N_{\mp}^0 + \hat{r}^* D_{\mp}^0\Big)\,, \tag{D.1.30}$$

It is possible then to write

$${}_sR_{\ell m}^{\alpha,0} = N_{\mp}^0\, {}_s\psi_{\ell m}^{\alpha,0}\,, \tag{D.1.31}$$
$${}_sR_{\ell m}^{\alpha,1} = N_{\mp}^0({}_s\psi_{\ell m}^{\alpha,1} \mp i\hat{\omega}^1\hat{r}^*\, {}_s\psi_{\ell m}^{\alpha,0})\,, \tag{D.1.32}$$
$$\frac{\mathrm{d}\, {}_sR_{\ell m}^{\alpha,0}}{\mathrm{d}\hat{r}} = {}_s\psi_{\ell m}^{\alpha,0} D_{\mp}^0 + N_{\mp}^0 \frac{\mathrm{d}\, {}_s\psi_{\ell m}^{\alpha,0}}{\mathrm{d}\hat{r}}\,, \tag{D.1.33}$$
$$\frac{\mathrm{d}\, {}_sR_{\ell m}^{\alpha,1}}{\mathrm{d}\hat{r}} = {}_s\psi_{\ell m}^{\alpha,1} D_{\mp}^0 + {}_s\psi_{\ell m}^{\alpha,0} D_{\mp}^1 + N_{\mp}^0\Big(\frac{\mathrm{d}\, {}_s\psi_{\ell m}^{\alpha,1}}{\mathrm{d}\hat{r}} \mp i\hat{\omega}^1\hat{r}^* \frac{\mathrm{d}\, {}_s\psi_{\ell m}^{\alpha,0}}{\mathrm{d}\hat{r}}\Big)\,, \tag{D.1.34}$$

where $\alpha = \text{in}\,(\text{up})$ for the minus (plus) sign. Finally, we computed the linear corrections ${}_s\psi_{\ell m}^{\text{in},0}$, ${}_s\psi_{\ell m}^{\text{in},1}$ and ${}_s\psi_{\ell m}^{\text{up},0}$, ${}_s\psi_{\ell m}^{\text{up},1}$ as solutions of a system of ordinary differential equations obtained by expanding Eq. (4.3.14) and the related boundary conditions in σ.

For the solutions ${}_s\psi^{\text{in},0}_{\ell m}$, ${}_s\psi^{\text{in},1}_{\ell m}$, the system of differential equations is

$$\frac{d^2\,{}_s\psi^{\text{in},0}_{\ell m}}{d\hat{r}^2}+\frac{p^0_H(\hat{r})}{\hat{r}-\hat{r}_+}\frac{d\,{}_s\psi^{\text{in},0}_{\ell m}}{d\hat{r}}+\frac{q^0_H(\hat{r})}{(\hat{r}-\hat{r}_+)^2}\,{}_s\psi^{\text{in},0}_{\ell m}=0\,, \tag{D.1.35}$$

$$\frac{d^2\,{}_s\psi^{\text{in},1}_{\ell m}}{d\hat{r}^2}+\frac{p^0_H(\hat{r})}{\hat{r}-\hat{r}_+}\frac{d\,{}_s\psi^{\text{in},1}_{\ell m}}{d\hat{r}}+\frac{p^1_H(\hat{r})}{\hat{r}-\hat{r}_+}\frac{d\,{}_s\psi^{\text{in},0}_{\ell m}}{d\hat{r}}+ \\ +\frac{q^0_H(\hat{r})}{(\hat{r}-\hat{r}_+)^2}\,{}_s\psi^{\text{in},1}_{\ell m}+\frac{q^1_H(\hat{r})}{(\hat{r}-\hat{r}_+)^2}\,{}_s\psi^{\text{in},0}_{\ell m}=0\,, \tag{D.1.36}$$

where

$$p^1_H(\hat{r})=-\frac{2\tilde{G}^1(\hat{r};-1)}{(\hat{r}-\hat{r}_-)(\hat{r}^2+\hat{a}^2)}\qquad q^1_H(\hat{r})=\frac{\tilde{U}^1(\hat{r};-1)}{(\hat{r}-\hat{r}_-)^2}\,, \tag{D.1.37}$$

$$\tilde{G}^1(\hat{r};-1)=i(\hat{r}^2+\hat{a}^2)^2\hat{\omega}^1\,, \tag{D.1.38}$$

$$\tilde{U}^1(\hat{r};-1)=\Delta\Big[-{}_s\lambda^1_{\ell m}+2i\hat{\omega}^1\Big(\frac{\hat{a}^2}{\hat{r}}+2\hat{r}s\Big)\Big]\,, \tag{D.1.39}$$

and the boundary conditions for ${}_s\psi^{\text{in},1}_{\ell m}$ are

$${}_s\psi^{\text{in},1}_{\ell m}(\hat{r})=\hat{r}_+e^{i\delta_H(\hat{r}_+)}\sum_{n=0}^{\infty}a^1_n(\hat{r}-\hat{r}_+)^n\,. \tag{D.1.40}$$

The recursion relation for the coefficients a^1_n is (setting $a^1_0=0$)

$$a^1_n=-\sum_{k=0}^{n-1}\Big(kp^{(n-k),1}_H(\hat{r}_+)+q^{(n-k),1}_H(\hat{r}_+)\Big)\frac{a^0_k}{I(n)}+ \\ -\sum_{k=0}^{n-1}\Big(kp^{(n-k),0}_H(\hat{r}_+)+q^{(n-k),0}_H(\hat{r}_+)\Big)\frac{a^1_k}{I(n)}-\frac{c^1_Ha^0_n}{n-c^0_H}\,, \tag{D.1.41}$$

where $c^1_H=\frac{4i\hat{r}_+}{\hat{r}_+-\hat{r}_-}\hat{\omega}^1$ and

$$p^{(n),1}_H(\hat{r}_+)=\begin{cases}-c^1_H & n=0\,,\\ -2i(\hat{r}^2_+-3\hat{a}^2)\hat{\omega}^1\rho^{-2}_H & n=1\,,\\ 2i(\hat{a}^2+\hat{r}^2_-)\rho^{-1-n}_H\hat{\omega}^1 & n>1\,,\end{cases} \tag{D.1.42}$$

$$q^{(n),1}_H(\hat{r}_+)=\begin{cases}0 & n=0\,,\\ \frac{\hat{r}_+({}_s\lambda^1_{\ell m}-4i\hat{r}_+s\hat{\omega}^1)-2i\hat{a}^2\hat{\omega}^1}{\hat{r}_+\rho_H} & n=1\,,\\ \frac{\rho^{-n}_H}{\hat{r}_+}\Big[\hat{r}_+\,{}_s\lambda^1_{\ell m}-4i\hat{a}^2\hat{\omega}^1s-n2i\hat{a}^2\hat{\omega}^1\,{}_2F_1\Big(1,1-n;2;\frac{\hat{r}_-}{\hat{r}_+}\Big)\Big] & n>1\,,\end{cases} \tag{D.1.43}$$

The coefficients $q_H^0(\hat{r}), p_H^0(\hat{r}), a_n^0$ and the boundary conditions for ${}_s\psi_{\ell m}^{\text{in},0}$ are given in Appendix B.1 with $\omega \leftrightarrow \omega^0, {}_s\lambda_{\ell m\hat{\omega}} \leftrightarrow {}_s\lambda_{\ell m}^0$.
For the solutions ${}_s\psi_{\ell m}^{\text{up},0}, {}_s\psi_{\ell m}^{\text{up},1}$, the system of differential equations is

$$\frac{d^2\,{}_s\psi_{\ell m}^{\text{up},0}}{d\hat{r}^2} + p_\infty^0(\hat{r})\frac{d\,{}_s\psi_{\ell m}^{\text{up},0}}{d\hat{r}} + q_\infty^0(\hat{r})\psi^{\text{up},0} = 0\,, \tag{D.1.44}$$

$$\frac{d^2\,{}_s\psi_{\ell m}^{\text{up},1}}{d\hat{r}^2} + p_\infty^0(\hat{r})\frac{d\,{}_s\psi_{\ell m}^{\text{up},1}}{d\hat{r}} + p_\infty^1(\hat{r})\frac{d\,{}_s\psi_{\ell m}^{\text{in},0}}{d\hat{r}} + q_\infty^0(\hat{r})\,{}_s\psi_{\ell m}^{\text{up},1} + q_\infty^1(\hat{r})\,{}_s\psi_{\ell m}^{\text{up},0} = 0\,, \tag{D.1.45}$$

where

$$p_\infty^1(\hat{r}) = -\frac{2\tilde{G}^1(\hat{r};1)}{\Delta(\hat{r}^2+\hat{a}^2)} \qquad q_\infty^1(\hat{r}) = \frac{\tilde{U}^1(\hat{r};1)}{\Delta^2}\,, \tag{D.1.46}$$

$$\tilde{G}^1(\hat{r};1) = -i(\hat{r}^2+\hat{a}^2)^2\hat{\omega}^1\,, \tag{D.1.47}$$

$$\tilde{U}^1(\hat{r};1) = -4\hat{\omega}^1[m\hat{a}(\hat{r}^2+\hat{a}^2) + i(\hat{r}^2-\hat{a}^2)s] - \Delta\Big({}_s\lambda_{\ell m}^1 + 2i\hat{\omega}^1\frac{\hat{a}^2}{\hat{r}}\Big)\,. \tag{D.1.48}$$

and the boundary conditions for ${}_s\psi_{\ell m}^{\text{up},1}$ are

$${}_s\psi_{\ell m}^{\text{up},1}(\hat{r}) = \sum_{n=0}^{\infty}\frac{b_n^1}{\hat{r}^n}\,. \tag{D.1.49}$$

The recursion relation for the coefficients b_n^1 is (setting $b_0^1 = 0$)

$$b_n^1 = \frac{n-1}{2i\hat{\omega}^0}b_{n-1}^1 + \sum_{k=1}^{n}\Big[q_\infty^{(k+1),0} - (n-k)p_\infty^{(k),0}\Big]\frac{b_k^1}{2i\hat{\omega}^0 n} + \\ + \sum_{k=1}^{n}\Big[q_\infty^{(k+1),1} - (n-k)p_\infty^{(k),1}\Big]\frac{b_k^1}{2i\hat{\omega}^0 n} - \frac{\hat{\omega}^1}{\hat{\omega}^0}b_n^0\,, \tag{D.1.50}$$

where

$$p_\infty^{(n),1} = \begin{cases} 2i\hat{\omega}^1 & n=0\,, \\ 4i\hat{\omega}^1 & n=1\,, \\ (4i(\hat{r}_-^n - \hat{r}_+^n)\hat{\omega}^1\rho_H^{-1} & n>1\,, \end{cases} \tag{D.1.51}$$

$$q_\infty^{(n),1} = \begin{cases} 0 & n=0,1\,, \\ -{}_s\lambda_{\ell m}^1 - 4(\hat{a}\hat{m}+is)\hat{\omega}^1 & n=2\,, \\ \frac{2}{\rho_H}Q_1^1 + \frac{4\hat{\omega}^1}{\rho_H^3}Q_2 & n>2\,, \end{cases} \tag{D.1.52}$$

with

$$Q_1^1 = -\frac{1}{2}(\hat{r}_-^{n-1} - \hat{r}_+^{n-1})\,{}_s\lambda_{\ell m}^1\,. \tag{D.1.53}$$

The coefficients $q_\infty^0(\hat{r})$, $p_\infty^0(\hat{r})$, b_n^0 and the boundary conditions for ${}_s\psi_{\ell m}^{\mathrm{up},0}$ are given in Appendix B.1 with $\omega \leftrightarrow \omega^0$, ${}_s\lambda_{\ell m\hat{\omega}} \leftrightarrow {}_s\lambda_{\ell m}^0$.

D.1.2 Linearization of the source

From Eq. (4.1.23), the amplitudes ${}_{-2}Z_{\ell m\hat{\omega}}^{H,\infty}$ can be written as

$$\begin{aligned}{}_{-2}Z_{\ell m\hat{\omega}}^{H,\infty} = \frac{2\pi}{W_{\hat{r}}}\Bigg(&A_0 - (A_1+B_1)\frac{\mathrm{d}}{\mathrm{d}\hat{r}} + \\ &+ (A_2+B_2)\frac{\mathrm{d}^2}{\mathrm{d}\hat{r}^2} - B_3\frac{\mathrm{d}^3}{\mathrm{d}\hat{r}^3}\Bigg)\,{}_{-2}R_{\ell m\hat{\omega}}^{\mathrm{in,up}}\Big|_{\theta=\pi/2,\hat{r}=\hat{r}_0}\,,\end{aligned} \tag{D.1.54}$$

where we set $B_{\ell m\hat{\omega}}^{\mathrm{tran}} = D_{\ell m\hat{\omega}}^{\mathrm{tran}} = 1$, which implies $C_{\ell m\hat{\omega}}^H \equiv C_{\ell m\hat{\omega}}^\infty$. In order to write the linearized amplitudes ${}_{-2}Z_{\ell m\hat{\omega}}^{H,\infty}$ in the parameter σ, it is convenient first to recast them as function of only ${}_{-2}R_{\ell m\hat{\omega}}^{\mathrm{in}}$, ${}_{-2}R_{\ell m\hat{\omega}}^{\mathrm{up}}$ and its first derivative. Taking advantage of the analyticity of the radial solutions in the positive real axis (except at the inner and outer horizons), second and higher order derivatives can be written solely in terms of ${}_{-2}R_{\ell m\hat{\omega}}^{\mathrm{in,up}}$ and its first derivative. Thus, we can write Eq. (D.1.54) as

$${}_{-2}Z_{\ell m\hat{\omega}}^{H,\infty} = \frac{2\pi}{W_{\hat{r}}}\left(X(\hat{r})\,{}_{-2}R_{\ell m\hat{\omega}}^{\mathrm{in,up}} + Y(\hat{r})\frac{\mathrm{d}\,{}_{-2}R_{\ell m\hat{\omega}}^{\mathrm{in,up}}}{\mathrm{d}\hat{r}}\right), \tag{D.1.55}$$

where $V(\hat{r})$ is the Teukolsky potential of Eq. (4.1.4), while

$$X(\hat{r}) \equiv A_0 + \frac{V(\hat{r})}{\Delta}C_2 - \frac{B_3}{\Delta}\frac{\mathrm{d}V(\hat{r})}{\mathrm{d}\hat{r}}\,, \tag{D.1.56}$$

$$Y(\hat{r}) \equiv -C_1 + \frac{2(\hat{r}-1)}{\Delta}C_2 - \frac{B_3}{\Delta}(2+V(\hat{r}))\,, \tag{D.1.57}$$

$$C_1 \equiv A_1 + B_1\,, \quad C_2 \equiv A_2 + B_2\,. \tag{D.1.58}$$

After expanding Eq. (D.1.55) in the parameter σ, we can write the 0th order term as

$${}_{-2}Z_{\ell m}^{\beta,0} = \frac{2\pi}{W_{\hat{r}}^0}\left(X^0(\hat{r})\,{}_{-2}R_{\ell m}^{\alpha,0} + Y^0(\hat{r})\frac{\mathrm{d}\,{}_{-2}R_{\ell m}^{\alpha,0}}{\mathrm{d}\hat{r}}\right), \tag{D.1.59}$$

where $\beta = H(\infty)$ when $\alpha = \text{in(up)}$, while

$$X^0(\hat{r}) \equiv A_0^0 + \frac{V(\hat{r})}{\Delta} C_2^0 \,, \tag{D.1.60}$$

$$Y^0(\hat{r}) \equiv -C_1^0 + \frac{2(\hat{r}-1)}{\Delta} C_2^0 \,, \tag{D.1.61}$$

$$V(\hat{r}) = -\frac{(K^0)^2 + 4i(\hat{r}-1)K^0}{\Delta} + 8i\hat{\omega}^0\hat{r} + {}_{-2}\lambda_{\ell m}^0 \,, \tag{D.1.62}$$

$$K^0 = (\hat{r}^2 + \hat{a}^2)\hat{\omega}^0 - \hat{a}m \,, \tag{D.1.63}$$

$$W_{\hat{r}}^0 \equiv \frac{1}{\Delta}\left({}_{-2}R_{\ell m}^{\text{in},0} \frac{\mathrm{d}\, {}_{-2}R_{\ell m}^{\text{up},0}}{\mathrm{d}\hat{r}} - {}_{-2}R_{\ell m}^{\text{up},0} \frac{\mathrm{d}\, {}_{-2}R_{\ell m}^{\text{in},0}}{\mathrm{d}\hat{r}} \right) . \tag{D.1.64}$$

Before writing the 0th order source terms A_0^0, C_1^0, C_2^0, we need to define the following auxiliary quantities:

$$S^0 \equiv {}_{-2}S_{\ell m}^0(\pi/2, c^0) \,, \tag{D.1.65}$$

$$\tilde{S}^0 = \frac{\mathrm{d}S^0}{\mathrm{d}\theta} - mS^0 + c^0 S^0 \,, \tag{D.1.66}$$

$$\mathcal{S}^0 = -\frac{1}{2} S^0 \, {}_{-2}\lambda_{\ell m}^0 + \tilde{S}^0\left(c^0 - m - \frac{i\hat{a}}{\hat{r}}\right) , \tag{D.1.67}$$

and

$$\mathcal{J}_z^0 = \tilde{J}_z^0 - \tilde{E}^0\hat{a} \,, \tag{D.1.68}$$

$$P_\sigma^0 = -J_z^0\hat{a} + \tilde{E}^0(\hat{r}^2 + \hat{a}^2) \,, \tag{D.1.69}$$

$$\Gamma^0 \equiv P_\sigma^0(\hat{r}^2 + \hat{a}^2) + \hat{a}\Delta\mathcal{J}_z^0 \,. \tag{D.1.70}$$

The 0th order source terms can then be written as

$$A_0^0 = -\frac{1}{2\hat{r}\Gamma^0\Delta}\left[{}_1A_0^0 + {}_2A_0^0 + (\mathcal{J}_z^0)^2 S^0({}_3A_0^0 + {}_4A_0^0)\right] , \tag{D.1.71}$$

$$C_1^0 = \frac{\mathcal{J}_z^0}{\hat{r}\Gamma^0}\left[i\hat{r}P_\sigma^0\tilde{S}^0 + S^0\mathcal{J}_z^0(\Delta + i\hat{r}^3\omega^0 + i\hat{a}\hat{r}(c^0 - m))\right] , \tag{D.1.72}$$

$$C_2^0 = \frac{S^0(\mathcal{J}_z^0)^2\Delta}{2\Gamma^0} \,, \tag{D.1.73}$$

where

$${}_1A_0^0 = 2\hat{r}(P_\sigma^0)^2\mathcal{S}^0 \,, \tag{D.1.74}$$

$${}_2A_0^0 = 2P_\sigma^0\mathcal{S}^0\mathcal{J}_z^0[(4i - m\hat{a})\hat{r} + (\hat{r}^2 + \hat{a}^2)(\hat{r}\hat{\omega}^0 - 2i)] \,, \tag{D.1.75}$$

$${}_3A_0^0 = 2i(3\hat{a}^2\hat{r} + \hat{r}^3)\hat{\omega}^0 + (\hat{r}^2 + \hat{a}^2)^2(\hat{r}\hat{\omega}^0 - 2i)\hat{\omega}^0 \,, \tag{D.1.76}$$

$${}_4A_0^0 = m\hat{a}^2\hat{r} - 2m\hat{a}[\hat{a}^2(\hat{r}\hat{\omega}^0 - i) + \hat{r}(3i - 2i\hat{r} + \hat{\omega}^0\hat{r}^2)] \,. \tag{D.1.77}$$

The 1th order correction $Z^{\beta,1}_{\ell m}$ is given by

$$ {}_{-2}Z^{\beta,1}_{\ell m} = \frac{2\pi}{W^0_{\hat{r}}}\left(X^1(\hat{r})\,{}_{-2}R^{\alpha,0}_{\ell m} + Y^1(\hat{r})\frac{\mathrm{d}\,{}_{-2}R^{\alpha,0}_{\ell m}}{\mathrm{d}\hat{r}} + X^0(\hat{r})\,{}_{-2}R^{\alpha,1}_{\ell m} + Y^0(\hat{r})\frac{\mathrm{d}\,{}_{-2}R^{\alpha,1}_{\ell m}}{\mathrm{d}\hat{r}}\right) + $$
$$ - \frac{W^1_{\hat{r}}}{W^0_{\hat{r}}}\,{}_{-2}Z^{\beta,0}_{\ell m}\,, \tag{D.1.78} $$

where again $\beta = H(\infty)$ when $\alpha = \mathrm{in(up)}$, while

$$ X^1(\hat{r}) \equiv A^1_0 + \frac{1}{\Delta}\left(V^1(\hat{r})C^0_2 + V^0(\hat{r})C^1_2 - \frac{\mathrm{d}V^0(\hat{r})}{\mathrm{d}\hat{r}}B^1_3\right), \tag{D.1.79} $$

$$ Y^1(\hat{r}) \equiv -C^1_1 + \frac{2(\hat{r}-1)}{\Delta}C^1_2 - \frac{2+V^0(\hat{r})}{\Delta}B^1_3\,, \tag{D.1.80} $$

$$ V^1(\hat{r}) = -\frac{2K^0 + 4i(\hat{r}-1)}{\Delta}K^1 + 8i\hat{\omega}^1\hat{r} + {}_{-2}\lambda^1_{\ell m}\,, \tag{D.1.81} $$

$$ K^1 = (\hat{r}^2 + \hat{a}^2)\hat{\omega}^1\,, \tag{D.1.82} $$

$$ W^1_{\hat{r}} \equiv \frac{1}{\Delta}\left({}_{-2}R^{\mathrm{in},0}_{\ell m}\frac{\mathrm{d}\,{}_{-2}R^{\mathrm{up},1}_{\ell m}}{\mathrm{d}\hat{r}} + {}_{-2}R^{\mathrm{in},1}_{\ell m}\frac{\mathrm{d}\,{}_{-2}R^{\mathrm{up},0}_{\ell m}}{\mathrm{d}\hat{r}}\right) + $$
$$ - \frac{1}{\Delta}\left({}_{-2}R^{\mathrm{up},0}_{\ell m}\frac{\mathrm{d}\,{}_{-2}R^{\mathrm{in},1}_{\ell m}}{\mathrm{d}\hat{r}} + {}_{-2}R^{\mathrm{up},1}_{\ell m}\frac{\mathrm{d}\,{}_{-2}R^{\mathrm{in},0}_{\ell m}}{\mathrm{d}\hat{r}}\right). \tag{D.1.83} $$

The 1th order source terms $A^1_0, C^1_1, C^1_2, A^1_3$ are quite cumbersome, and they are provided in a supplemental MATHEMATICA notebook [177].
Once the amplitudes ${}_{-2}Z^{\beta,0}_{\ell m}, {}_{-2}Z^{\beta,1}_{\ell m}$ with $\beta = (H,\infty)$ are known, it is possible to compute the corrections to the fluxes of Eqs. (4.3.17) and (4.3.18) as follows

$$ I^0_{\ell m}(\hat{r},\hat{\omega}^0) = \frac{\left|\,{}_{-2}Z^{H,0}_{\ell m}\right|^2}{2\pi(\hat{\omega}^0)^2}\,, \tag{D.1.84} $$

$$ I^1_{\ell m}(\hat{r},\hat{\omega}^0,\hat{\omega}^1) = \left(\frac{{}_{-2}Z^{H,0}_{\ell m}\;{}_{-2}\bar{Z}^{H,1}_{\ell m}}{2\pi(\hat{\omega}^0)^2} + \text{c.c.} - 2\frac{\hat{\omega}^1}{\hat{\omega}^0}I^0_{\ell m}(\hat{r},\hat{\omega}^0)\right), \tag{D.1.85} $$

$$ H^0_{\ell m}(\hat{r},\hat{\omega}^0) = \frac{\tilde{\alpha}^0_{\ell m}}{2\pi}\left|\,{}_{-2}Z^{\infty,0}_{\ell m}\right|^2, \tag{D.1.86} $$

$$ H^1_{\ell m}(\hat{r},\hat{\omega}^0,\hat{\omega}^1) = \frac{\tilde{\alpha}^0_{\ell m}}{2\pi}\left({}_{-2}Z^{\infty,0}_{\ell m}\;{}_{-2}\bar{Z}^{\infty,1}_{\ell m} + \text{c.c.}\right) + \frac{\tilde{\alpha}^1_{\ell m}}{2\pi}\left|\,{}_{-2}Z^{\infty,0}_{\ell m}\right|^2, \tag{D.1.87} $$

where c.c. stands for complex conjugation, and

$$\tilde{\alpha}^0_{\ell m} = \frac{1}{\mathcal{D}^0}\left[256(2\hat{r}_+)^5\hat{\kappa}^0((\hat{\kappa}^0)^2+4\epsilon^2)((\hat{\kappa}_0)^2+16\epsilon^2)\hat{\omega}^0\right], \tag{D.1.88}$$

$$\begin{aligned}\tilde{\alpha}^1_{\ell m} = &-\frac{\mathcal{D}^1}{\mathcal{D}^0}\tilde{\alpha}^0_{\ell m} + \frac{256(2\hat{r}_+)^5}{\mathcal{C}^0_{\ell m}}\hat{\omega}^1\left[64\epsilon^4(\kappa^0+\omega^0)+\right.\\ &\left.+20(\epsilon\kappa^0)^2(\kappa^0+3\omega^0)+(\kappa^0)^4(\kappa^0+5\omega^0)\right],\end{aligned} \tag{D.1.89}$$

with $\epsilon = \sqrt{1-\hat{a}^2}/(4\hat{r}_+)$, $\hat{\kappa}^0 = \hat{\omega}^0 - \hat{a}m/(2\hat{r}_+)$ and

$$\begin{aligned}\mathcal{D}^0 = &[({}_s\lambda^0_{\ell m}+2)^2+4c^0(m-c^0)][({}_s\lambda^0_{\ell m})^2+36c^0(m-c^0)]\\ &+(2\,{}_s\lambda^0_{\ell m}+3)[96(c^0)^2-48mc^0]+144(\hat{\omega}^0)^2(1-\hat{a}^2),\end{aligned} \tag{D.1.90}$$

$$\begin{aligned}\mathcal{D}^1 = &4\{({}_s\lambda^0_{\ell m})^3\,{}_s\lambda^1_{\ell m}+({}_s\lambda^0_{\ell m})^2[3\,{}_s\lambda^1_{\ell m}+10(m-2c^0)c^1]+\\ &+2\,{}_s\lambda^0_{\ell m}[{}_s\lambda^1_{\ell m}+10\,{}_s\lambda^1_{\ell m}c^0(m-c^0)+6c^1(m+2c^0)]+\\ &+72\hat{\omega}^0\hat{\omega}^1[1+\hat{a}^2(m-2c^0)(m-c^0)]+12c^0\,{}_s\lambda^1_{\ell m}(m+c^0)\}.\end{aligned} \tag{D.1.91}$$

Appendix E

Comparisons of the GW fluxes with previous work

We have tested our code by comparing the GW fluxes against results already published in the literature. In this section we provide a detailed comparison in order to assess the accuracy of our method.

E.1 Comparison with Harms *et al.*

The GW fluxes at infinity for a spinning particle have been calculated in Ref. [110] by solving the Teukolsky equation in the time domain and assuming $q = 1$, so that $\sigma = q\chi$ is not small when $\chi = \mathcal{O}(1)$. To make the comparison, we also set $q = 1$. We remark that we use the same spin supplementary conditions and the same orbital dynamics as in Ref. [110].
Tables E.1–E.3 show the relative percentage difference between our results and those listed in Table II, III, and IV of Ref. [110] for the $\ell = 2, 3$ modes. The fluxes are normalized with respect to the leading Post-Newtonian order. Here the normalized fluxes are denoted as follows:

$$\hat{\mathcal{F}}^{\infty}_{\ell m} = \mathcal{F}^{\infty}_{\ell m}/k_{\ell m}\,, \tag{E.1.1}$$

where

$$k_{22} = \frac{32}{5}|\widehat{\Omega}|^{\frac{10}{3}}\,,\; k_{21} = \frac{8}{45}|\widehat{\Omega}|^{\frac{12}{3}}\,,\; k_{33} = \frac{243}{28}|\widehat{\Omega}|^{\frac{12}{3}} \tag{E.1.2}$$

and $\mathcal{F}^{\infty}_{\ell m}$ includes only the fluxes at infinity, assuming $q = 1$, and therefore $\sigma = \chi$. Moreover, we define

$$\Delta_{\ell m} = 100\left|1 - \hat{\mathcal{F}}^{\infty}_{\ell m}/\hat{F}_{S\ell m}\right|\,, \tag{E.1.3}$$

where $\hat{F}_{S\ell m}$ given in [110]. Note that Ref. [110] assumed $\hat{J}_z > 0$, distinguishing prograde and retrograde orbits on the base of the sign of $\hat{a}$. In our work we

consider the opposite convention: we fix $\hat{a} \geq 0$, while $\hat{J}_z$ is positive (negative) for corotating (counter-rotating) orbits. Therefore, for retrograde orbits we compare our fluxes for $\sigma > 0$ with the results $\sigma < 0$ of Ref. [110] and vice versa.
Tables E.1-E.3 show that our results are in good agreement with those of Ref. [110], with relative errors of the order of the percent or below for all the considered configurations. For the $\ell = m = 2$ and $\ell = m = 3$ modes the fractional difference is always less than 0.5%.
This picture does not change for Δ_{21} except for fast spinning bodies with $\hat{a} = 0.9$: in this case retrograde and prograde orbits lead to maximum discrepancies of 1.3% and 16%, respectively. We believe that the last value may be given by numerical rounding, since the corresponding flux is given in Ref. [110] with only one significant figure.
Finally, in Fig. E.1 we plot $\hat{\mathcal{F}}_{22}$ for prograde orbits with $\hat{a} = 0.9$ and $\hat{r} = 3$ as a function of χ. Owing to the fact that $q = 1$ (and therefore σ is not small), the fluxes depend on the spin of the secondary in a nonlinear fashion when $\chi = \mathcal{O}(1)$.

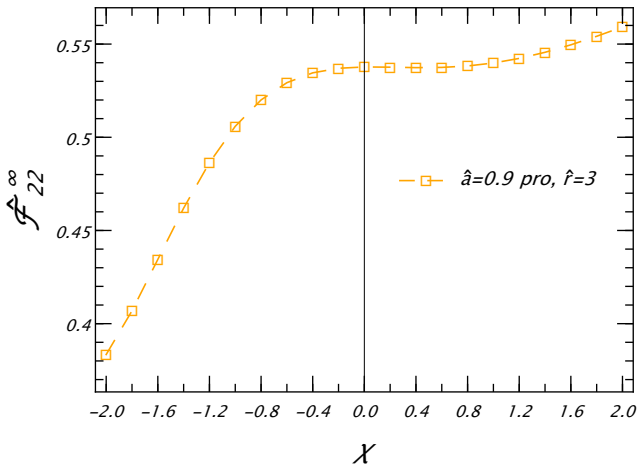

Figure E.1: Fluxes $\hat{\mathcal{F}}^{\infty}_{22}$ for the $\ell = m = 2$ modes as a function of σ for $\hat{a} = 0.9$, prograde orbits and $\hat{r} = 3$. Notice the nonlinear dependence of the fluxes on σ for the extreme case $q = 1$.

$\hat{a} = 0$

$\hat{r}$	σ	$\hat{\mathcal{F}}^{\infty}_{22}$	$\Delta_{22}[\%]$	$\hat{\mathcal{F}}^{\infty}_{21}$	$\Delta_{21}[\%]$	$\hat{\mathcal{F}}^{\infty}_{33}$	$\Delta_{33}[\%]$
4	−0.9	2.2135	0.2	2.1607	0.4	2.4238	0.3
	−0.5	1.7954	0.2	2.3052	0.4	1.8302	0.3
	0.5	1.0422	0.3	2.1033	0.5	0.8709	0.4
	0.9	0.8538	0.3	2.0157	0.5	0.6549	0.4
5	−0.9	1.2143	0.2	0.9541	0.5	1.2187	0.3
	−0.5	1.1143	0.2	1.2514	0.5	1.0605	0.3
	0.5	0.8703	0.2	1.7777	0.5	0.7181	0.3
	0.9	0.7849	0.2	1.9312	0.5	0.6110	0.4
6	−0.9	1.0137	0.2	0.7042	0.5	0.9780	0.3
	−0.5	0.9610	0.2	0.9837	0.5	0.8881	0.3
	0.5	0.8249	0.2	1.6424	0.5	0.6837	0.3
	0.9	0.7727	0.2	1.8835	0.5	0.6132	0.3
8	−0.9	0.9042	0.2	0.5629	0.5	0.8430	0.3
	−0.5	0.8778	0.2	0.8124	0.5	0.7955	0.3
	0.5	0.8093	0.2	1.5136	0.5	0.6837	0.3
	0.9	0.7818	0.2	1.8115	0.5	0.6424	0.3
10	−0.9	0.8779	0.2	0.5292	0.5	0.8110	0.3
	−0.5	0.8608	0.2	0.7602	0.5	0.7792	0.3
	0.5	0.8166	0.2	1.4464	0.5	0.7030	0.3
	0.9	0.7987	0.2	1.7537	0.5	0.6741	0.3
20	−0.9	0.8875	0.2	0.5560	0.4	0.8290	0.3
	−0.5	0.8820	0.2	0.7426	0.4	0.8179	0.3
	0.5	0.8680	0.2	1.3100	0.4	0.7907	0.3
	0.9	0.8623	0.2	1.5745	0.4	0.7799	0.3

Table E.1: Normalized fluxes and fractional differences [Eq. (E.1.1)] between our results and those obtained in Table II of Ref. [110] for $\hat{a} = 0$, and different values of $\hat{r}$. Note that we set $q = 1$ to agree with Ref. [110].

$\hat{a} = 0.9$ retrograde orbits

$\hat{r}$	σ	$\hat{\mathcal{F}}^{\infty}_{22}$	$\Delta_{22}[\%]$	$\hat{\mathcal{F}}^{\infty}_{21}$	$\Delta_{21}[\%]$	$\hat{\mathcal{F}}^{\infty}_{33}$	$\Delta_{33}[\%]$
5	-0.9	1.2361	0.2	5.6616	0.4	1.0827	0.3
	-0.5	1.6251	0.2	6.6959	0.4	1.5729	0.3
	0.5	3.3150	0.2	10.789	0.3	3.9783	0.3
	0.9	4.4462	0.2	13.255	0.3	5.7567	0.3
6	-0.9	1.0335	0.2	4.6842	0.4	0.8937	0.3
	-0.5	1.2023	0.2	4.8148	0.4	1.1143	0.3
	0.5	1.7181	0.2	4.8963	0.4	1.8635	0.3
	0.9	1.9563	0.2	4.7277	0.3	2.2404	0.3
8	-0.9	0.9123	0.2	3.7900	0.4	0.7911	0.3
	-0.5	0.9784	0.2	3.5167	0.4	0.8842	0.3
	0.5	1.1510	0.2	2.6978	0.4	1.1499	0.3
	0.9	1.2208	0.2	2.3159	0.3	1.2679	0.3
10	-0.9	0.8816	0.2	3.3399	0.4	0.7727	0.3
	-0.5	0.9193	0.2	2.9873	0.4	0.8286	0.3
	0.5	1.0142	0.2	2.0862	0.4	0.9799	0.3
	0.9	1.0519	0.2	1.7269	0.3	1.0446	0.3
20	-0.9	0.8875	0.3	2.4826	0.7	0.8130	1.2
	-0.5	0.8969	0.1	2.1581	0.6	0.8290	0.4
	0.5	0.9202	0.2	1.4249	0.3	0.8699	0.0
	0.9	0.9294	0.2	1.1662	1.3	0.8866	0.3

Table E.2: Normalized fluxes and fractional differences with the fluxes in Table III of Ref. [110] in the case $\hat{a} = 0.9$, retrogade orbits. The fluxes $\hat{\mathcal{F}}^{\infty}_{\ell m}$ with $\sigma < 0$ have to be compared with the fluxes $\hat{F}_{S\ell m}$ with $\sigma > 0$ and vice versa.

$\hat{a} = 0.9$ prograde orbits

$\hat{r}$	σ	$\hat{\mathcal{F}}_{22}^{\infty}$	$\Delta_{22}[\%]$	$\hat{\mathcal{F}}_{21}$	$\Delta_{21}[\%]$	$\hat{\mathcal{F}}_{33}$	$\Delta_{33}[\%]$
4	-0.9	0.6037	0.2	3.3×10^{-4}	16	0.5052	0.3
	-0.5	0.6077	0.2	0.0315	1.3	0.4888	0.3
	0.5	0.6038	0.2	0.3081	0.7	0.4458	0.3
	0.9	0.6015	0.2	0.4651	0.7	0.4314	0.3
6	-0.9	0.6900	0.2	0.0093	$*$	0.5826	0.3
	-0.5	0.6880	0.2	0.0737	$*$	0.5671	0.3
	0.5	0.6792	0.2	0.4314	$*$	0.5294	0.3
	0.9	0.6750	0.2	0.6330	0.7	0.5154	0.3
8	-0.9	0.7384	0.2	0.0324	1.2	0.6357	0.3
	-0.5	0.7354	0.2	0.1164	$*$	0.6223	0.3
	0.5	0.7261	0.2	0.5092	$*$	05899	0.3
	0.9	0.7221	0.2	0.7264	0.7	0.5776	0.3
10	-0.9	0.7716	0.2	0.0596	1.1	0.6755	0.3
	-0.5	0.7685	0.2	0.1558	$*$	0.6640	0.3
	0.5	0.7598	0.2	0.5633	$*$	0.6361	0.3
	0.9	0.7560	0.2	0.7842	0.6	0.6253	0.3
20	-0.9	0.8558	0.1	0.1848	1.0	0.7862	0.00
	-0.5	0.8537	0.2	0.2998	1.7	0.7800	0.01
	0.5	0.8481	0.2	0.6982	0.3	0.7646	0.2
	0.9	0.8458	0.2	0.8998	1.9	0.7586	0.1

Table E.3: Normalized fluxes compared against the fluxes shown in Table IV of Ref. [110] for $\hat{a} = 0.9$ and prograde orbits. The $*$ indicates fluxes not calculated in Ref. [110].

E.2 Comparison with Taracchini *et al.*

Reference [248] computed high-precision GW fluxes for nonspinning particles orbiting around Schwarzschild and Kerr BHs solving the Teukolsky equation in the frequency domain. We have checked our code against both their set-up. The relative errors are shown in Tables E.4-E.7 for the values of the GW fluxes computed at the ISCO and at a different orbital separations $\hat{r}$, as a function of the primary spin. Note that in Ref. [248] the sum over the harmonic index ℓ was truncated at a certain value $\ell_{\rm max}$ such that the fractional error between the flux at $\ell_{\rm max}$ and $\ell_{\rm max}-1$ was less than 10^{-14}. To achieve this accuracy the required $\ell_{\rm max}$ is in general very large: at the ISCO, for example, $\ell_{\rm max}=30$ for $\hat{a}=0$, and $\ell_{\rm max}=66$ for $\hat{a}=0.99$. In our calculations we fixed $\ell_{\rm max}=20$. Nonetheless, the agreement between our results and those computed in Ref. [248] is extremely good. Even for the fastest spinning BH considered (with $\hat{a}=0.9$), we find a relative difference smaller than 10^{-5}.

$\hat{a}$	ISCO	$\mathcal{F}^0$	$\Delta^{\rm rel}(\mathcal{F}^0)$
0.1	5.669	1.203797640×10^{-3}	8.5×10^{-11}
0.3	4.979	2.10037308×10^{-3}	1.4×10^{-9}
0.5	4.233	4.11717449×10^{-3}	6.9×10^{-10}
0.8	2.907	1.71190×10^{-2}	4.4×10^{-7}
0.9	2.321	3.5223×10^{-2}	5.4×10^{-6}

Table E.4: Fluxes for a nonspinning objects around Kerr BHs $\mathcal{F}^0$ at the ISCO and fractional difference $\Delta^{\rm rel}(\mathcal{F}^0)$ compared to the results of Ref. [248].

	$\hat{a}=0$		$\hat{a}=0.3$	
$\hat{r}$	$\mathcal{F}^0$	$\Delta^{\rm rel}(\mathcal{F}^0)$	$\mathcal{F}^0$	$\Delta^{\rm rel}(\mathcal{F}^0)$
10	$6.15163167846\times10^{-5}$	1.8×10^{-13}	$5.72185605812\times10^{-5}$	1.1×10^{-12}
8	$1.9610454858336\times10^{-4}$	1.6×10^{-14}	$1.757401400491\times10^{-4}$	2.4×10^{-14}
6	9.40339356×10^{-4}	3.8×10^{-11}	$7.7105423521\times10^{-4}$	1.2×10^{-11}

Table E.5: Same as Table E.4 but for generic orbital separation different from the ISCO, and focusing on $\hat{a}=(0,0.3)$.

$\hat{a} = 0.5$		
$\hat{r}$	$\mathcal{F}^0$	$\Delta^{\rm rel}(\mathcal{F}^0)$
10	$5.4706016232 \times 10^{-5}$	3.0×10^{-12}
8	$1.64390512713 \times 10^{-4}$	7.2×10^{-13}
6	$6.8651481394 \times 10^{-4}$	7.1×10^{-12}

Table E.6: Same as Table E.4 but for generic orbital separation different from the ISCO, and focusing on $\hat{a} = 0.5$.

	$\hat{a} = 0.8$		$\hat{a} = 0.9$	
$\hat{r}$	$\mathcal{F}$	$\Delta^{\rm rel}(\mathcal{F})$	$\mathcal{F}$	$\Delta^{\rm rel}(\mathcal{F})$
10	$5.13763911701 \times 10^{-5}$	4.3×10^{-13}	$5.0368602531 \times 10^{-5}$	1.4×10^{-12}
8	$1.49973726131 \times 10^{-4}$	2.6×10^{-13}	$1.4574909234 \times 10^{-4}$	9.5×10^{-13}
6	$5.8851295900 \times 10^{-4}$	2.7×10^{-12}	$5.6168859157 \times 10^{-4}$	1.5×10^{-12}
4	3.9084751×10^{-3}	2.2×10^{-9}	$3.53976293 \times 10^{-3}$	1.4×10^{-9}

Table E.7: Fluxes for a non spinning object $\mathcal{F}^0$ and fractional difference $\Delta^{\rm rel}(\mathcal{F}^0)$ with respect to the fluxes listed in Ref. [248] for fast rotating BHs with $\hat{a} = (0.8, 09)$.

E.3 Comparison with Gralla *et al.*

Finally, we tested our code in the case of a nonspinning secondary and fast spinning primary BHs with $\hat{a} > 0.9$. In this case we use the data obtained in Ref. [178] using the Teukolsky formalism in the frequency domain and assuming $\ell_{\rm max} = 30$ [178]. The comparison is shown in Table E.8 for $\hat{a} = 0.99$ and $\hat{a} = 0.995$ for orbital radii equal to and larger than the ISCO. The discrepancy between our results and those of Ref. [178] increases for larger spins and smaller orbital separation. However, in the worst case scenario, the fluxes differ at most by one part over 10^3.

	$\hat{a} = 0.990$		$\hat{a} = 0.995$	
$\hat{r}$	$\mathcal{F}$	$\Delta^{\rm rel}(\mathcal{F})$	$\mathcal{F}$	$\Delta^{\rm rel}(\mathcal{F})$
10	$4.9500572776 \times 10^{-5}$	2.7×10^{-12}	$4.9453383948 \times 10^{-5}$	3.4×10^{-12}
8	$1.4216152170 \times 10^{-4}$	1.5×10^{-11}	$1.419678387 \times 10^{-4}$	1.4×10^{-11}
6	$5.395577551 \times 10^{-4}$	6.6×10^{-11}	$5.38379633 \times 10^{-4}$	6.6×10^{-11}
4	$3.26013974 \times 10^{-3}$	1.3×10^{-9}	$3.24583765 \times 10^{-3}$	1.3×10^{-9}
2	4.301×10^{-2}	1.1×10^{-5}	4.221×10^{-2}	1.0×10^{-5}
ISCO	9.17×10^{-2}	5.0×10^{-4}	9.5×10^{-2}	1.0×10^{-3}

Table E.8: Fluxes for a nonspinning object $\mathcal{F}^0$ and fractional difference $\Delta^{\rm rel}(\mathcal{F}^0)$ with respect to the fluxes listed in [119]. The ISCO is at $\hat{r} = 1.454$ and $\hat{r} = 1.341$ for $\hat{a} = 0.990$ and $\hat{a} = 0.995$ respectively.

Appendix F

Stability and convergence of the Fisher and covariance matrices

In this appendix we provide some details on our procedure to assess the stability and numerical convergence of the Fisher and covariant matrices.
This task is particularly delicate for EMRI waveforms, since the Fisher matrix is known to be ill-conditioned [188]. In the best configuration, the condition number was $\kappa \sim 10^{12}$, while in worst scenario (typically occurring in the presence of a spinning secondary), the condition number was as large as $\kappa \sim 10^{20}$. Moreover, all waveform derivatives were computed numerically, which is an ill-conditioned operation.
To ameliorate the ill-condition issues, we performed our computation with arbitrary-precision arithmetic, obtaining Fisher matrices with precision no less than 38-digit in all elements and for all configurations.
We validated our Fisher analysis by:

- testing the stability of the Fisher and covariance matrices under random perturbations;
- testing the convergence of the Fisher and covariance matrices under a change in the finite-difference parameter ϵ that regulates the accuracy of the numerical derivatives.

We check the stability of the Fisher and covariance matrices by perturbing each element with a deviation matrix F^{ij}. All elements of F^{ij} are drawn from a uniform distribution U, which depends on the configuration under exam. Then, we compute

$$\delta_{\text{stability}} \equiv \max_{ij}\left[\frac{\left((\Gamma+F)^{-1}-\Gamma^{-1}\right)^{ij}}{(\Gamma^{-1})^{ij}}\right] \tag{F.0.1}$$

By performing a case-by-case careful analysis and boosting the numerical precision of our codes, we find that for the *worst* cases in all configurations:

- the Fisher matrices converges within 2 orders of magnitudes in the ϵ parameters with relative deviations at the level of 0.03% (another worst case is a convergence within 3 orders of magnitude in ϵ with deviations at 0.2%);
- the inverse matrix without priors converges in 2 order of magnitude in ϵ with deviations at 14%, while the diagonal elements converge with deviations at 0.1%;
- the inverse with priors converges in 2 order of magnitude in ϵ with deviations at 3.8%;
- the inverse without priors is stable with $\delta_{\text{stability}} = 7.5\%$ and perturbations $U[-10^{-7}, 10^{-7}]$;
- the inverse with priors is stable with $\delta_{\text{stability}} = 4.1\%$ and perturbations $U[-10^{-6}, 10^{-6}]$.

Moreover, we noticed that, in order to achieve a convergent inverse with an accuracy of order $\mathcal{O}(1\%)$, it was necessary to compute a convergent Fisher matrix accurate at a the level of $\mathcal{O}(0.01\%)$.
Finally, it is worth noticing that, for some configurations in the presence of the secondary spin, we were unable to obtain a fully convergent covariance matrix: only the diagonal terms were convergent. Nonetheless, for all configurations presented in the main text the covariance matrix was found to be fully convergent.

Bibliography

[1] S. E. Gralla, A. P. Porfyriadis, and N. Warburton, "Particle on the Innermost Stable Circular Orbit of a Rapidly Spinning Black Hole," *Phys. Rev.* **D92** no. 6, (2015) 064029, arXiv:1506.08496 [gr-qc]. (Pages iv, 94, and 95)

[2] **LIGO Scientific, Virgo** Collaboration, B. P. Abbott *et al.*, "Observation of Gravitational Waves from a Binary Black Hole Merger," *Phys. Rev. Lett.* **116** no. 6, (2016) 061102, arXiv:1602.03837 [gr-qc]. (Page 1)

[3] **LIGO Scientific, VIRGO, KAGRA** Collaboration, R. Abbott *et al.*, "GWTC-3: Compact Binary Coalescences Observed by LIGO and Virgo During the Second Part of the Third Observing Run," arXiv:2111.03606 [gr-qc]. (Page 1)

[4] **LIGO Scientific, Virgo** Collaboration, R. Abbott *et al.*, "GWTC-2: Compact Binary Coalescences Observed by LIGO and Virgo During the First Half of the Third Observing Run," *Phys. Rev. X* **11** (2021) 021053, arXiv:2010.14527 [gr-qc]. (Page 1)

[5] **LIGO Scientific, Virgo** Collaboration, B. Abbott *et al.*, "GWTC-1: A Gravitational-Wave Transient Catalog of Compact Binary Mergers Observed by LIGO and Virgo during the First and Second Observing Runs," *Phys. Rev. X* **9** no. 3, (2019) 031040, arXiv:1811.12907 [astro-ph.HE]. (Page 1)

[6] **LIGO Scientific, VIRGO, KAGRA** Collaboration, R. Abbott *et al.*, "The population of merging compact binaries inferred using gravitational waves through GWTC-3," arXiv:2111.03634 [astro-ph.HE]. (Page 2)

[7] **LIGO Scientific, Virgo** Collaboration, B. P. Abbott *et al.*, "GW170817: Observation of Gravitational Waves from a Binary Neutron Star Inspiral," *Phys. Rev. Lett.* **119** no. 16, (2017) 161101, arXiv:1710.05832 [gr-qc]. (Page 2)

[8] B. Margalit and B. D. Metzger, "Constraining the Maximum Mass of Neutron Stars From Multi-Messenger Observations of GW170817," *Astrophys. J. Lett.* **850** no. 2, (2017) L19, arXiv:1710.05938 [astro-ph.HE]. (Page 2)

[9] M. R. Drout *et al.*, "Light Curves of the Neutron Star Merger GW170817/SSS17a: Implications for R-Process Nucleosynthesis," *Science* **358** (2017) 1570–1574, arXiv:1710.05443 [astro-ph.HE]. (Page 2)

[10] **LIGO Scientific, Virgo, Fermi-GBM, INTEGRAL** Collaboration, B. P. Abbott *et al.*, "Gravitational Waves and Gamma-rays from a Binary Neutron Star Merger: GW170817 and GRB 170817A," *Astrophys. J. Lett.* **848** no. 2, (2017) L13, arXiv:1710.05834 [astro-ph.HE]. (Page 2)

[11] **LIGO Scientific, Virgo, 1M2H, Dark Energy Camera GW-E, DES, DLT40, Las Cumbres Observatory, VINROUGE, MASTER** Collaboration, B. P. Abbott *et al.*, "A gravitational-wave standard siren measurement of the Hubble constant," *Nature* **551** no. 7678, (2017) 85–88, arXiv:1710.05835 [astro-ph.CO]. (Page 2)

[12] N. Yunes and X. Siemens, "Gravitational-Wave Tests of General Relativity with Ground-Based Detectors and Pulsar Timing-Arrays," *Living Rev. Rel.* **16** (2013) 9, arXiv:1304.3473 [gr-qc]. (Page 2)

[13] C. M. Will, "The Confrontation between General Relativity and Experiment," *Living Rev. Rel.* **17** (2014) 4, arXiv:1403.7377 [gr-qc]. (Pages 2 and 3)

[14] R. Penrose, "Gravitational collapse: The role of general relativity," *Riv. Nuovo Cim.* **1** (1969) 252–276. (Page 2)

[15] R. Penrose, "Gravitational collapse and space-time singularities," *Phys. Rev. Lett.* **14** (Jan, 1965) 57–59. https://link.aps.org/doi/10.1103/PhysRevLett.14.57. (Page 2)

[16] V. Cardoso, J. a. L. Costa, K. Destounis, P. Hintz, and A. Jansen, "Quasinormal modes and strong cosmic censorship," *Phys. Rev. Lett.* **120** (Jan, 2018) 031103. https://link.aps.org/doi/10.1103/PhysRevLett.120.031103. (Page 2)

[17] V. Cardoso and P. Pani, "Tests for the existence of black holes through gravitational wave echoes," *Nature Astron.* **1** no. 9, (2017) 586–591, arXiv:1709.01525 [gr-qc]. (Page 2)

[18] T. Clifton, P. G. Ferreira, A. Padilla, and C. Skordis, "Modified Gravity and Cosmology," *Phys. Rept.* **513** (2012) 1–189, arXiv:1106.2476 [astro-ph.CO]. (Page 3)

[19] D. Lovelock, "The four-dimensionality of space and the einstein tensor," *J. Math. Phys.* **13** (1972) 874–876. (Page 3)

[20] A. Joyce, B. Jain, J. Khoury, and M. Trodden, "Beyond the Cosmological Standard Model," *Phys. Rept.* **568** (2015) 1–98, arXiv:1407.0059 [astro-ph.CO]. (Page 3)

[21] L. Barack *et al.*, "Black holes, gravitational waves and fundamental physics: a roadmap," *Class. Quant. Grav.* **36** no. 14, (2019) 143001, arXiv:1806.05195 [gr-qc]. (Pages 3, 71, and 73)

[22] W. Israel, "Event horizons in static vacuum space-times," *Phys. Rev.* **164** (Dec, 1967) 1776–1779. https://link.aps.org/doi/10.1103/PhysRev.164.1776. (Page 3)

[23] B. Carter, "Axisymmetric Black Hole Has Only Two Degrees of Freedom," *Phys. Rev. Lett.* **26** (1971) 331–333. (Page 3)

[24] D. Robinson, "Four decades of black holes uniqueness theorems," in *Kerr Fest: Black Holes in Astrophysics, General Relativity and Quantum Gravity*. 8, 2004. (Page 3)

[25] P. T. Chrusciel, J. Lopes Costa, and M. Heusler, "Stationary Black Holes: Uniqueness and Beyond," *Living Rev. Rel.* **15** (2012) 7, arXiv:1205.6112 [gr-qc]. (Page 3)

[26] E. Berti, V. Cardoso, and A. O. Starinets, "Quasinormal modes of black holes and black branes," *Class. Quant. Grav.* **26** (2009) 163001, arXiv:arXiv:0905.2975 [gr-qc]. (Pages 3 and 8)

[27] V. Cardoso and L. Gualtieri, "Testing the black hole 'no-hair' hypothesis," *Class. Quant. Grav.* **33** no. 17, (2016) 174001, arXiv:1607.03133 [gr-qc]. (Page 3)

[28] **LIGO Scientific, VIRGO, KAGRA** Collaboration, R. Abbott *et al.*, "Tests of General Relativity with GWTC-3," arXiv:2112.06861 [gr-qc]. (Page 3)

[29] M. Punturo *et al.*, "The third generation of gravitational wave observatories and their science reach," *Class. Quant. Grav.* **27** (2010) 084007. (Page 3)

[30] M. Maggiore *et al.*, "Science Case for the Einstein Telescope," *JCAP* **03** (2020) 050, arXiv:1912.02622 [astro-ph.CO]. (Page 3)

[31] D. Reitze *et al.*, "Cosmic Explorer: The U.S. Contribution to Gravitational-Wave Astronomy beyond LIGO," *Bull. Am. Astron. Soc.* **51** no. 7, (2019) 035, arXiv:1907.04833 [astro-ph.IM]. (Page 3)

[32] **LISA** Collaboration, P. Amaro-Seoane *et al.*, "Laser Interferometer Space Antenna," arXiv:1702.00786 [astro-ph.IM]. (Page 4)

[33] S. Babak, J. Gair, A. Sesana, E. Barausse, C. F. Sopuerta, C. P. L. Berry, E. Berti, P. Amaro-Seoane, A. Petiteau, and A. Klein, "Science with the space-based interferometer LISA. V: Extreme mass-ratio inspirals," *Phys. Rev.* **D95** no. 10, (2017) 103012, arXiv:1703.09722 [gr-qc]. (Pages 4, 5, 15, 61, 69, and 82)

[34] C. P. L. Berry, S. A. Hughes, C. F. Sopuerta, A. J. K. Chua, A. Heffernan, K. Holley-Bockelmann, D. P. Mihaylov, M. C. Miller, and A. Sesana, "The unique potential of extreme mass-ratio inspirals for gravitational-wave astronomy," arXiv:1903.03686 [astro-ph.HE]. (Page 5)

[35] C. F. Sopuerta and N. Yunes, "Extreme and Intermediate-Mass Ratio Inspirals in Dynamical Chern-Simons Modified Gravity," *Phys. Rev.* **D80** (2009) 064006, arXiv:0904.4501 [gr-qc]. (Page 5)

[36] N. Yunes, P. Pani, and V. Cardoso, "Gravitational Waves from Quasicircular Extreme Mass-Ratio Inspirals as Probes of Scalar-Tensor Theories," *Phys. Rev.* **D85** (2012) 102003, arXiv:1112.3351 [gr-qc]. (Page 5)

[37] P. Pani, V. Cardoso, and L. Gualtieri, "Gravitational waves from extreme mass-ratio inspirals in Dynamical Chern-Simons gravity," *Phys. Rev.* **D83** (2011) 104048, arXiv:1104.1183 [gr-qc]. (Pages 5 and 73)

[38] E. Barausse, N. Yunes, and K. Chamberlain, "Theory-Agnostic Constraints on Black-Hole Dipole Radiation with Multiband Gravitational-Wave Astrophysics," *Phys. Rev. Lett.* **116** no. 24, (2016) 241104, arXiv:1603.04075 [gr-qc]. (Page 5)

[39] K. Chamberlain and N. Yunes, "Theoretical Physics Implications of Gravitational Wave Observation with Future Detectors," *Phys. Rev.* **D96** no. 8, (2017) 084039, arXiv:1704.08268 [gr-qc]. (Page 5)

[40] V. Cardoso, G. Castro, and A. Maselli, "Gravitational waves in massive gravity theories: waveforms, fluxes and constraints from extreme-mass-ratio mergers," *Phys. Rev. Lett.* **121** no. 25, (2018) 251103, arXiv:1809.00673 [gr-qc]. (Pages 5 and 73)

[41] L. Barack and C. Cutler, "Using LISA EMRI sources to test off-Kerr deviations in the geometry of massive black holes," *Phys. Rev.* **D75** (2007) 042003, arXiv:gr-qc/0612029 [gr-qc]. (Pages 5, 69, 76, and 82)

[42] P. Pani, E. Berti, V. Cardoso, Y. Chen, and R. Norte, "Gravitational-wave signatures of the absence of an event horizon. II. Extreme mass ratio inspirals in the spacetime of a thin-shell gravastar," *Phys. Rev.* **D81** (2010) 084011, arXiv:1001.3031 [gr-qc]. (Page 5)

[43] P. Pani and A. Maselli, "Love in Extrema Ratio," *Int. J. Mod. Phys.* **D28** no. 14, (2019) 1944001, arXiv:1905.03947 [gr-qc]. (Page 5)

[44] S. Datta, R. Brito, S. Bose, P. Pani, and S. A. Hughes, "Tidal heating as a discriminator for horizons in extreme mass ratio inspirals," *Phys. Rev.* **D101** no. 4, (2020) 044004, arXiv:1910.07841 [gr-qc]. (Page 5)

[45] J. R. Gair, M. Vallisneri, S. L. Larson, and J. G. Baker, "Testing General Relativity with Low-Frequency, Space-Based Gravitational-Wave Detectors," *Living Rev. Rel.* **16** (2013) 7, arXiv:1212.5575 [gr-qc]. (Page 5)

[46] E. Barausse *et al.*, "Prospects for Fundamental Physics with LISA," *Gen. Rel. Grav.* **52** no. 8, (2020) 81, arXiv:2001.09793 [gr-qc]. (Page 5)

[47] A. J. K. Chua, N. Korsakova, C. J. Moore, J. R. Gair, and S. Babak, "Gaussian processes for the interpolation and marginalization of waveform error in extreme-mass-ratio-inspiral parameter estimation," *Phys. Rev.* **D101** no. 4, (2020) 044027, arXiv:1912.11543 [astro-ph.IM]. (Pages 5 and 61)

[48] M. L. Katz, A. J. K. Chua, L. Speri, N. Warburton, and S. A. Hughes, "FastEMRIWaveforms: New tools for millihertz gravitational-wave data analysis," arXiv:2104.04582 [gr-qc]. (Pages 5, 15, 61, and 62)

[49] A. J. K. Chua, M. L. Katz, N. Warburton, and S. A. Hughes, "Rapid generation of fully relativistic extreme-mass-ratio-inspiral waveform templates for LISA data analysis," *Phys. Rev. Lett.* **126** no. 5, (2021) 051102, arXiv:2008.06071 [gr-qc]. (Pages 5 and 61)

[50] A. Pound and B. Wardell, "Black hole perturbation theory and gravitational self-force," arXiv:2101.04592 [gr-qc]. (Pages 5, 8, 12, 13, 14, 22, 23, and 60)

[51] L. Barack and A. Pound, "Self-force and radiation reaction in general relativity," *Rept. Prog. Phys.* **82** no. 1, (2019) 016904, arXiv:1805.10385 [gr-qc]. (Pages 5, 6, 8, and 22)

[52] A. Pound, "Motion of small objects in curved spacetimes: An introduction to gravitational self-force," *Fund. Theor. Phys.* **179** (2015) 399–486, arXiv:1506.06245 [gr-qc]. (Pages 6, 14, and 22)

[53] S. Akcay, S. R. Dolan, C. Kavanagh, J. Moxon, N. Warburton, and B. Wardell, "Dissipation in extreme-mass ratio binaries with a spinning secondary," *Phys. Rev. D* **102** no. 6, (2020) 064013, arXiv:1912.09461 [gr-qc]. (Pages 6, 14, 15, 52, 53, 54, 58, 63, and 88)

[54] J. Mathews, A. Pound, and B. Wardell, "Self-Force Calculations with a Spinning Secondary," arXiv:2112.13069 [gr-qc]. (Pages 6, 14, 42, 54, and 88)

[55] N. Warburton, T. Osburn, and C. R. Evans, "Evolution of small-mass-ratio binaries with a spinning secondary," *Phys. Rev.* **D96** no. 8, (2017) 084057, arXiv:1708.03720 [gr-qc]. (Pages 6, 14, 15, and 88)

[56] G. Lukes-Gerakopoulos and V. Witzany, "Non-linear effects in EMRI dynamics and their imprints on gravitational waves," arXiv:2103.06724 [gr-qc]. (Pages 6, 10, 14, 35, and 88)

[57] G. Lukes-Gerakopoulos, "Spinning particles moving around black holes: integrability and chaos," in *Proceedings, 14th Marcel Grossmann Meeting on Recent Developments in Theoretical and Experimental General Relativity, Astrophysics, and Relativistic Field Theories (MG14) (In 4 Volumes): Rome, Italy, July 12-18, 2015*, vol. 2, pp. 1960–1965. 2017. arXiv:1606.09430 [gr-qc]. (Pages 6, 35, and 88)

[58] T. Hinderer and E. E. Flanagan, "Two timescale analysis of extreme mass ratio inspirals in Kerr. I. Orbital Motion," *Phys. Rev.* **D78** (2008) 064028, arXiv:0805.3337 [gr-qc]. (Pages 6, 12, 13, and 62)

[59] F. Pretorius, "Evolution of binary black hole spacetimes," *Phys. Rev. Lett.* **95** (2005) 121101, arXiv:gr-qc/0507014. (Page 7)

[60] M. Campanelli, C. O. Lousto, P. Marronetti, and Y. Zlochower, "Accurate evolutions of orbiting black-hole binaries without excision," *Phys. Rev. Lett.* **96** (2006) 111101, arXiv:gr-qc/0511048. (Page 7)

[61] A. Ramos-Buades, S. Husa, G. Pratten, H. Estellés, C. García-Quirós, M. Mateu-Lucena, M. Colleoni, and R. Jaume, "First survey of spinning eccentric black hole mergers: Numerical relativity simulations, hybrid waveforms, and parameter estimation," *Phys. Rev. D* **101** no. 8, (2020) 083015, arXiv:1909.11011 [gr-qc]. (Page 7)

[62] J. Healy, C. O. Lousto, J. Lange, R. O'Shaughnessy, Y. Zlochower, and M. Campanelli, "Second RIT binary black hole simulations catalog and its application to gravitational waves parameter estimation," *Phys. Rev. D* **100** no. 2, (2019) 024021, arXiv:1901.02553 [gr-qc]. (Page 7)

[63] L. Blanchet, "Gravitational Radiation from Post-Newtonian Sources and Inspiralling Compact Binaries," *Living Rev. Rel.* **17** (2014) 2, arXiv:1310.1528 [gr-qc]. (Page 7)

[64] E. Poisson, A. Pound, and I. Vega, "The Motion of point particles in curved spacetime," *Living Rev. Rel.* **14** (2011) 7, arXiv:1102.0529 [gr-qc]. (Pages 8 and 22)

[65] A. Buonanno and T. Damour, "Effective one-body approach to general relativistic two-body dynamics," *Phys. Rev. D* **59** (1999) 084006, arXiv:gr-qc/9811091. (Page 8)

[66] T. Damour and A. Nagar, "The Effective One Body description of the Two-Body problem," *Fundam. Theor. Phys.* **162** (2011) 211–252, arXiv:0906.1769 [gr-qc]. (Page 8)

[67] S. Ossokine *et al.*, "Multipolar Effective-One-Body Waveforms for Precessing Binary Black Holes: Construction and Validation," *Phys. Rev. D* **102** no. 4, (2020) 044055, arXiv:2004.09442 [gr-qc]. (Page 8)

[68] A. Nagar *et al.*, "Time-domain effective-one-body gravitational waveforms for coalescing compact binaries with nonprecessing spins, tides and self-spin effects," *Phys. Rev. D* **98** no. 10, (2018) 104052, arXiv:1806.01772 [gr-qc]. (Page 8)

[69] L. Barack, T. Damour, and N. Sago, "Precession effect of the gravitational self-force in a Schwarzschild spacetime and the effective one-body formalism," *Phys. Rev. D* **82** (2010) 084036, arXiv:1008.0935 [gr-qc]. (Page 8)

[70] C. Kavanagh, A. C. Ottewill, and B. Wardell, "Analytical high-order post-Newtonian expansions for spinning extreme mass ratio binaries," *Phys. Rev. D* **93** no. 12, (2016) 124038, arXiv:1601.03394 [gr-qc]. (Page 8)

[71] S. Akcay, A. Le Tiec, L. Barack, N. Sago, and N. Warburton, "Comparison Between Self-Force and Post-Newtonian Dynamics: Beyond Circular Orbits," *Phys. Rev. D* **91** no. 12, (2015) 124014, arXiv:1503.01374 [gr-qc]. (Page 8)

[72] C. Kavanagh, D. Bini, T. Damour, S. Hopper, A. C. Ottewill, and B. Wardell, "Spin-orbit precession along eccentric orbits for extreme mass ratio black hole binaries and its effective-one-body transcription," *Phys. Rev. D* **96** no. 6, (2017) 064012, arXiv:1706.00459 [gr-qc]. (Page 8)

[73] A. Le Tiec, E. Barausse, and A. Buonanno, "Gravitational Self-Force Correction to the Binding Energy of Compact Binary Systems," *Phys. Rev. Lett.* **108** (2012) 131103, arXiv:1111.5609 [gr-qc]. (Page 9)

[74] A. Le Tiec *et al.*, "Periastron Advance in Spinning Black Hole Binaries: Gravitational Self-Force from Numerical Relativity," *Phys. Rev. D* **88** no. 12, (2013) 124027, arXiv:1309.0541 [gr-qc]. (Page 9)

[75] M. van de Meent and H. P. Pfeiffer, "Intermediate mass-ratio black hole binaries: Applicability of small mass-ratio perturbation theory," *Phys. Rev. Lett.* **125** no. 18, (2020) 181101, arXiv:2006.12036 [gr-qc]. (Page 9)

[76] N. Warburton, A. Pound, B. Wardell, J. Miller, and L. Durkan, "Gravitational-Wave Energy Flux for Compact Binaries through Second Order in the Mass Ratio," *Phys. Rev. Lett.* **127** no. 15, (2021) 151102, arXiv:2107.01298 [gr-qc]. (Pages 9, 21, and 88)

[77] B. Wardell, A. Pound, N. Warburton, J. Miller, L. Durkan, and A. Le Tiec, "Gravitational waveforms for compact binaries from second-order self-force theory," arXiv:2112.12265 [gr-qc]. (Pages 9, 21, and 88)

[78] A. Le Tiec, A. H. Mroue, L. Barack, A. Buonanno, H. P. Pfeiffer, N. Sago, and A. Taracchini, "Periastron Advance in Black Hole Binaries," *Phys. Rev. Lett.* **107** (2011) 141101, arXiv:1106.3278 [gr-qc]. (Page 9)

[79] B. Carter, "Global structure of the kerr family of gravitational fields," *Phys. Rev.* **174** no. 5, (10, 1968) 1559–1571. (Pages 9 and 10)

[80] V. Arnold, K. Vogtmann, and A. Weinstein, *Mathematical Methods of Classical Mechanics*. Graduate Texts in Mathematics. Springer New York, 2013. (Page 9)

[81] Y. Mino, "Perturbative approach to an orbital evolution around a supermassive black hole," *Phys. Rev. D* **67** (Apr, 2003) 084027. https://link.aps.org/doi/10.1103/PhysRevD.67.084027. (Page 10)

[82] E. E. Flanagan and T. Hinderer, "Transient resonances in the inspirals of point particles into black holes," *Phys. Rev. Lett.* **109** (2012) 071102, arXiv:1009.4923 [gr-qc]. (Page 10)

[83] J. Gair, N. Yunes, and C. M. Bender, "Resonances in Extreme Mass-Ratio Inspirals: Asymptotic and Hyperasymptotic Analysis," *J. Math. Phys.* **53** (2012) 032503, arXiv:1111.3605 [gr-qc]. (Page 10)

[84] E. E. Flanagan, S. A. Hughes, and U. Ruangsri, "Resonantly enhanced and diminished strong-field gravitational-wave fluxes," *Phys. Rev. D* **89** no. 8, (2014) 084028, arXiv:1208.3906 [gr-qc]. (Page 10)

[85] U. Ruangsri and S. A. Hughes, "Census of transient orbital resonances encountered during binary inspiral," *Phys. Rev. D* **89** no. 8, (2014) 084036, arXiv:1307.6483 [gr-qc]. (Page 10)

[86] M. van de Meent, "Conditions for Sustained Orbital Resonances in Extreme Mass Ratio Inspirals," *Phys. Rev. D* **89** no. 8, (2014) 084033, arXiv:1311.4457 [gr-qc]. (Page 10)

[87] C. P. L. Berry, R. H. Cole, P. Cañizares, and J. R. Gair, "Importance of transient resonances in extreme-mass-ratio inspirals," *Phys. Rev. D* **94** no. 12, (2016) 124042, arXiv:1608.08951 [gr-qc]. (Page 10)

[88] S. Isoyama, R. Fujita, H. Nakano, N. Sago, and T. Tanaka, ""Flux-balance formulae" for extreme mass-ratio inspirals," *PTEP* **2019** no. 1, (2019) 013E01, arXiv:1809.11118 [gr-qc]. (Page 10)

[89] Y. Mino, M. Sasaki, and T. Tanaka, "Gravitational radiation reaction to a particle motion," *Phys. Rev. D* **55** (1997) 3457–3476, arXiv:gr-qc/9606018. (Pages 11 and 21)

[90] T. C. Quinn and R. M. Wald, "An Axiomatic approach to electromagnetic and gravitational radiation reaction of particles in curved space-time," *Phys. Rev. D* **56** (1997) 3381–3394, arXiv:gr-qc/9610053. (Pages 11 and 21)

[91] S. L. Detweiler and B. F. Whiting, "Selfforce via a Green's function decomposition," *Phys. Rev. D* **67** (2003) 024025, arXiv:gr-qc/0202086. (Page 11)

[92] A. Pound, "Self-consistent gravitational self-force," *Phys. Rev. D* **81** (2010) 024023, arXiv:0907.5197 [gr-qc]. (Page 11)

[93] S. E. Gralla and R. M. Wald, "A Rigorous Derivation of Gravitational Self-force," *Class. Quant. Grav.* **25** (2008) 205009, arXiv:0806.3293 [gr-qc]. [Erratum: Class.Quant.Grav. 28, 159501 (2011)]. (Page 11)

[94] S. R. Dolan, N. Warburton, A. I. Harte, A. Le Tiec, B. Wardell, and L. Barack, "Gravitational self-torque and spin precession in compact binaries," *Phys. Rev.* **D89** no. 6, (2014) 064011, arXiv:1312.0775 [gr-qc]. (Pages 14, 15, and 88)

[95] L. M. Burko and G. Khanna, "Self-force gravitational waveforms for extreme and intermediate mass ratio inspirals. III: Spin-orbit coupling revisited," *Phys. Rev.* **D91** no. 10, (2015) 104017, arXiv:1503.05097 [gr-qc]. (Pages 14, 15, and 88)

[96] Y. Mino, M. Shibata, and T. Tanaka, "Gravitational waves induced by a spinning particle falling into a rotating black hole," *Phys. Rev.* **D53** (1996) 622–634. [Erratum: Phys. Rev.D59,047502(1999)]. (Pages 14, 34, and 102)

[97] M. Saijo, K.-i. Maeda, M. Shibata, and Y. Mino, "Gravitational waves from a spinning particle plunging into a Kerr black hole," *Phys. Rev.* **D58** (1998) 064005. (Pages 14, 35, 36, and 37)

[98] K. Tominaga, M. Saijo, and K.-i. Maeda, "Gravitational waves from a spinning particle scattered by a relativistic star: Axial mode case," *Phys. Rev.* **D63** (2001) 124012, arXiv:gr-qc/0009055 [gr-qc]. (Page 14)

[99] T. Tanaka, Y. Mino, M. Sasaki, and M. Shibata, "Gravitational waves from a spinning particle in circular orbits around a rotating black hole," *Phys. Rev.* **D54** (1996) 3762–3777, arXiv:gr-qc/9602038 [gr-qc]. (Pages 14, 30, 39, 64, 88, 103, and 108)

[100] A. Nagar, F. Messina, C. Kavanagh, G. Lukes-Gerakopoulos, N. Warburton, S. Bernuzzi, and E. Harms, "Factorization and resummation: A new paradigm to improve gravitational wave amplitudes. III: the spinning test-body terms," *Phys. Rev.* **D100** no. 10, (2019) 104056, arXiv:1907.12233 [gr-qc]. (Page 15)

[101] G. Lukes-Gerakopoulos, E. Harms, S. Bernuzzi, and A. Nagar, "Spinning test-body orbiting around a Kerr black hole: circular dynamics and gravitational-wave fluxes," *Phys. Rev.* **D96** no. 6, (2017) 064051, arXiv:1707.07537 [gr-qc]. (Pages 15 and 38)

[102] S. Akcay, D. Dempsey, and S. R. Dolan, "Spin-orbit precession for eccentric black hole binaries at first order in the mass ratio," *Class. Quant. Grav.* **34** no. 8, (2017) 084001, arXiv:1608.04811 [gr-qc]. (Page 15)

[103] S. Akcay, "Self-force correction to geodetic spin precession in Kerr spacetime," *Phys. Rev. D* **96** no. 4, (2017) 044024, arXiv:1705.03282 [gr-qc]. (Page 15)

[104] L. M. Burko, "Orbital evolution of a particle around a black hole. 2. Comparison of contributions of spin orbit coupling and the selfforce," *Phys. Rev. D* **69** (2004) 044011, arXiv:gr-qc/0308003. (Pages 15 and 88)

[105] B. Chen, G. Compère, Y. Liu, J. Long, and X. Zhang, "Spin and Quadrupole Couplings for High Spin Equatorial Intermediate Mass-ratio Coalescences," *Class. Quant. Grav.* **36** no. 24, (2019) 245011, arXiv:1901.05370 [gr-qc]. (Page 15)

[106] E. Barausse, A. Buonanno, S. A. Hughes, G. Khanna, S. O'Sullivan, and Y. Pan, "Modeling multipolar gravitational-wave emission from small mass-ratio mergers," *Phys. Rev. D* **85** (2012) 024046, arXiv:1110.3081 [gr-qc]. (Page 15)

[107] S. Bernuzzi, A. Nagar, and A. Zenginoglu, "Binary black hole coalescence in the extreme-mass-ratio limit: testing and improving the effective-one-body multipolar waveform," *Phys. Rev. D* **83** (2011) 064010, arXiv:1012.2456 [gr-qc]. (Page 15)

[108] S. Albanesi, A. Nagar, and S. Bernuzzi, "Effective one-body model for extreme-mass-ratio spinning binaries on eccentric equatorial orbits: Testing radiation reaction and waveform," *Phys. Rev. D* **104** no. 2, (2021) 024067, arXiv:2104.10559 [gr-qc]. (Page 15)

[109] N. Yunes, A. Buonanno, S. A. Hughes, Y. Pan, E. Barausse, M. Miller, and W. Throwe, "Extreme Mass-Ratio Inspirals in the Effective-One-Body Approach: Quasi-Circular, Equatorial Orbits around a Spinning Black Hole," *Phys. Rev. D* **83** (2011) 044044, arXiv:1009.6013 [gr-qc]. [Erratum: Phys.Rev.D 88, 109904 (2013)]. (Pages 15 and 69)

[110] E. Harms, G. Lukes-Gerakopoulos, S. Bernuzzi, and A. Nagar, "Asymptotic gravitational wave fluxes from a spinning particle in circular equatorial orbits around a rotating black hole," *Phys. Rev.* **D93** no. 4, (2016) 044015, arXiv:1510.05548 [gr-qc]. [Addendum: Phys. Rev.D100,no.12,129901(2019)]. (Pages 15, 40, 119, 120, 121, 122, and 123)

[111] E. Harms, G. Lukes-Gerakopoulos, S. Bernuzzi, and A. Nagar, "Spinning test body orbiting around a Schwarzschild black hole: Circular dynamics and gravitational-wave fluxes," *Phys. Rev.* **D94** no. 10, (2016) 104010, arXiv:1609.00356 [gr-qc]. (Pages 15 and 38)

[112] E. Huerta and J. R. Gair, "Importance of including small body spin effects in the modelling of extreme and intermediate mass-ratio inspirals," *Phys. Rev. D* **84** (2011) 064023, arXiv:1105.3567 [gr-qc]. (Pages 15, 61, 69, 75, 76, 81, 82, 83, and 87)

[113] E. A. Huerta, J. R. Gair, and D. A. Brown, "Importance of including small body spin effects in the modelling of intermediate mass-ratio inspirals. II Accurate parameter extraction of strong sources using higher-order spin effects," *Phys. Rev. D* **85** (2012) 064023, arXiv:1111.3243 [gr-qc]. (Pages 15, 61, 81, 82, 83, and 87)

[114] L. Barack and C. Cutler, "LISA capture sources: Approximate waveforms, signal-to-noise ratios, and parameter estimation accuracy," *Phys. Rev. D* **69** (2004) 082005, arXiv:gr-qc/0310125. (Pages 15 and 61)

[115] S. Babak, H. Fang, J. R. Gair, K. Glampedakis, and S. A. Hughes, "'Kludge' gravitational waveforms for a test-body orbiting a Kerr black hole," *Phys. Rev. D* **75** (2007) 024005, arXiv:gr-qc/0607007. [Erratum: Phys.Rev.D 77, 04990 (2008)]. (Pages 15 and 61)

[116] A. J. K. Chua, C. J. Moore, and J. R. Gair, "Augmented kludge waveforms for detecting extreme-mass-ratio inspirals," *Phys. Rev. D* **96** no. 4, (2017) 044005, arXiv:1705.04259 [gr-qc]. (Pages 15 and 61)

[117] L. Speri and J. R. Gair, "Assessing the impact of transient orbital resonances," arXiv:2103.06306 [gr-qc]. (Pages 15 and 61)

[118] G. A. Piovano, A. Maselli, and P. Pani, "Extreme mass ratio inspirals with spinning secondary: a detailed study of equatorial circular motion," *Phys. Rev. D* **102** no. 2, (2020) 024041, arXiv:2004.02654 [gr-qc]. (Pages 17, 28, 33, 37, 40, 42, 48, 58, 61, 62, 64, 66, and 97)

[119] "Black Hole Perturbation Toolkit." (bhptoolkit.org). (Pages 17, 49, 50, 51, 56, 96, 111, and 126)

[120] B. Wardell, "Self-force: Computational Strategies," *Fund. Theor. Phys.* **179** (2015) 487–522, arXiv:1501.07322 [gr-qc]. (Pages 22 and 60)

[121] "Kavli RISE Summer School on Gravitational Waves." (www.ctc.cam.ac.uk/activities/rise/). (Page 22)

[122] S. Akcay, "A Fast Frequency-Domain Algorithm for Gravitational Self-Force: I. Circular Orbits in Schwarzschild Spacetime," *Phys. Rev. D* **83** (2011) 124026, arXiv:1012.5860 [gr-qc]. (Page 22)

[123] S. R. Dolan and L. Barack, "Self-force via m-mode regularization and 2+1D evolution: III. Gravitational field on Schwarzschild spacetime," *Phys. Rev. D* **87** (2013) 084066, arXiv:1211.4586 [gr-qc]. (Page 22)

[124] S. Akcay, N. Warburton, and L. Barack, "Frequency-domain algorithm for the Lorenz-gauge gravitational self-force," *Phys. Rev. D* **88** no. 10, (2013) 104009, arXiv:1308.5223 [gr-qc]. (Page 22)

[125] S. Isoyama, L. Barack, S. R. Dolan, A. Le Tiec, H. Nakano, A. G. Shah, T. Tanaka, and N. Warburton, "Gravitational Self-Force Correction to the Innermost Stable Circular Equatorial Orbit of a Kerr Black Hole," *Phys. Rev. Lett.* **113** no. 16, (2014) 161101, arXiv:1404.6133 [gr-qc]. (Page 22)

[126] L. Barack and C. O. Lousto, "Perturbations of Schwarzschild black holes in the Lorenz gauge: Formulation and numerical implementation," *Phys. Rev. D* **72** (2005) 104026, arXiv:gr-qc/0510019. (Page 22)

[127] L. Barack and N. Sago, "Gravitational self-force on a particle in eccentric orbit around a Schwarzschild black hole," *Phys. Rev. D* **81** (2010) 084021, arXiv:1002.2386 [gr-qc]. (Page 22)

[128] L. Barack and N. Sago, "Gravitational self force on a particle in circular orbit around a Schwarzschild black hole," *Phys. Rev. D* **75** (2007) 064021, arXiv:gr-qc/0701069. (Page 22)

[129] T. Regge and J. A. Wheeler, "Stability of a Schwarzschild singularity," *Phys. Rev.* **108** (1957) 1063–1069. (Page 23)

[130] F. J. Zerilli, "Gravitational field of a particle falling in a schwarzschild geometry analyzed in tensor harmonics," *Phys. Rev. D* **2** (Nov, 1970) 2141–2160. https://link.aps.org/doi/10.1103/PhysRevD.2.2141. (Page 23)

[131] S. R. Dolan, C. Kavanagh, and B. Wardell, "Gravitational Perturbations of Rotating Black Holes in Lorenz Gauge," *Phys. Rev. Lett.* **128** no. 15, (2022) 151101, arXiv:2108.06344 [gr-qc]. (Page 23)

[132] S. Chandrasekhar and S. Chandrasekhar, *The Mathematical Theory of Black Holes*. International series of monographs on physics. Clarendon Press, 1998. https://books.google.it/books?id=LBOVcrzFfhsC. (Pages 24, 25, and 26)

[133] R. Penrose and W. Rindler, *Classification of curvature tensors*, vol. 2 of *Cambridge Monographs on Mathematical Physics*, p. 223–290. Cambridge University Press, 1986. (Page 24)

[134] A. Petrov, "Sci not," *Kazan State Univ* **114** (1954) 55. (Page 24)

[135] A. Petrov, *Einstein Spaces*. Pergamon Press, 1969. https://books.google.it/books?id=zeo2xgEACAAJ. (Page 24)

[136] E. Newman and R. Penrose, "An Approach to gravitational radiation by a method of spin coefficients," *J. Math. Phys.* **3** (1962) 566–578. (Page 25)

[137] S. A. Teukolsky, "Perturbations of a rotating black hole. 1. Fundamental equations for gravitational electromagnetic and neutrino field perturbations," *Astrophys. J.* **185** (1973) 635–647. (Pages 26 and 27)

[138] L. Barack and P. Giudice, "Time-domain metric reconstruction for self-force applications," *Phys. Rev. D* **95** no. 10, (2017) 104033, arXiv:1702.04204 [gr-qc]. (Page 27)

[139] C. Merlin, A. Ori, L. Barack, A. Pound, and M. van de Meent, "Completion of metric reconstruction for a particle orbiting a Kerr black hole," *Phys. Rev. D* **94** no. 10, (2016) 104066, arXiv:1609.01227 [gr-qc]. (Page 27)

[140] M. van de Meent, "Gravitational self-force on generic bound geodesics in Kerr spacetime," *Phys. Rev. D* **97** no. 10, (2018) 104033, arXiv:1711.09607 [gr-qc]. (Page 27)

[141] E. Poisson and C. M. Will, *Gravity: Newtonian, Post-Newtonian, Relativistic*. Cambridge University Press, 2014. (Page 29)

[142] J. D. Jackson, *Classical Electrodynamics*. Wiley, 1998. (Page 29)

[143] W. Tulczyjew, "Motion of multipole particles in general relativity theory," *Acta Phys. Pol.* **18** (1959) 393. (Pages 29 and 30)

[144] W. Dixon, "A covariant multipole formalism for extended test bodies in general relativity," *Il Nuovo Cimento* **34** no. 2, (Oct, 1964) 317–339. (Pages 29 and 30)

[145] W. G. Dixon, "Dynamics of extended bodies in general relativity. I. Momentum and angular momentum," *Proc. Roy. Soc. Lond.* **A314** (1970) 499–527. (Pages 29 and 30)

[146] W. G. Dixon, "Dynamics of extended bodies in general relativity. II. Moments of the charge-current vector," *Proc. Roy. Soc. Lond.* **A319** (1970) 509–547. (Pages 29 and 30)

[147] K. Kyrian and O. Semerak, "Spinning test particles in a Kerr field," *Mon. Not. Roy. Astron. Soc.* **382** (2007) 1922. (Pages 29 and 32)

[148] W. Dixon, "Extended bodies in general relativity; their description and motion," in *Isolated Gravitating Systems in General Relativity - Proceedings of the International School of Physics "Enrico Fermi"*. 1978. (Page 30)

[149] J. L. Synge, ed., *Relativity: The General theory*. North-Holland, 1960. (Page 30)

[150] M. Mathisson, "Neue mechanik materieller systemes," *Acta Phys. Polon.* **6** (1937) 163–2900. (Page 30)

[151] A. Papapetrou, "Spinning test particles in general relativity. 1.," *Proc. Roy. Soc. Lond.* **A209** (1951) 248–258. (Page 30)

[152] E. Corinaldesi and A. Papapetrou, "Spinning test particles in general relativity. 2.," *Proc. Roy. Soc. Lond.* **A209** (1951) 259–268. (Page 30)

[153] J. Steinhoff and D. Puetzfeld, "Multipolar equations of motion for extended test bodies in General Relativity," *Phys. Rev.* **D81** (2010) 044019, arXiv:0909.3756 [gr-qc]. (Page 30)

[154] O. Semerak, "Spinning test particles in a Kerr field. 1.," *Mon. Not. Roy. Astron. Soc.* **308** (1999) 863–875. (Page 30)

[155] J. Ehlers and E. Rudolph, "Dynamics of extended bodies in general relativity center-of-mass description and quasirigidity," *General Relativity and Gravitation* **8** no. 3, (Mar, 1977) 197–217. (Pages 31 and 32)

[156] F. Costa, C. A. R. Herdeiro, J. Natario, and M. Zilhao, "Mathisson's helical motions for a spinning particle: Are they unphysical?," *Phys. Rev.* **D85** (2012) 024001, arXiv:1109.1019 [gr-qc]. (Page 32)

[157] L. F. O. Costa and J. Natário, "Center of mass, spin supplementary conditions, and the momentum of spinning particles," *Fund. Theor. Phys.* **179** (2015) 215–258, arXiv:1410.6443 [gr-qc]. (Page 32)

[158] G. Lukes-Gerakopoulos, "Time parameterizations and spin supplementary conditions of the Mathisson-Papapetrou-Dixon equations," *Phys. Rev.* **D96** no. 10, (2017) 104023, arXiv:1709.08942 [gr-qc]. (Page 32)

[159] V. Witzany, J. Steinhoff, and G. Lukes-Gerakopoulos, "Hamiltonians and canonical coordinates for spinning particles in curved space-time," *Class. Quant. Grav.* **36** no. 7, (2019) 075003, arXiv:1808.06582 [gr-qc]. (Page 32)

[160] C. MøÎler, "Sur la dynamique des systèmes ayant un moment angulaire interne," *Annales de l'institut Henri Poincaré* **11** no. 5, (1949) 251–278. http://eudml.org/doc/79030. (Page 33)

[161] R. Rüdiger, "Conserved quantities of spinning test particles in general relativity. i," *Proceedings of the Royal Society of London. Series A, Mathematical and Physical Sciences* **375** no. 1761, (1981) 185–193. http://www.jstor.org/stable/2990231. (Pages 35 and 88)

[162] R. R. diger, "Conserved quantities of spinning test particles in general relativity. ii," *Proceedings of the Royal Society of London. Series A, Mathematical and Physical Sciences* **385** no. 1788, (1983) 229–239. http://www.jstor.org/stable/2397480. (Pages 35 and 88)

[163] O. Zelenka, G. Lukes-Gerakopoulos, V. Witzany, and O. Kopáček, "Growth of resonances and chaos for a spinning test particle in the Schwarzschild background," *Phys. Rev.* **D101** no. 2, (2020) 024037, arXiv:1911.00414 [gr-qc]. (Pages 35 and 88)

[164] J. Steinhoff and D. Puetzfeld, "Influence of internal structure on the motion of test bodies in extreme mass ratio situations," *Phys. Rev.* **D86** (2012) 044033, arXiv:1205.3926 [gr-qc]. (Page 36)

[165] V. Skoupý and G. Lukes-Gerakopoulos, "Spinning test body orbiting around a Kerr black hole: Eccentric equatorial orbits and their asymptotic gravitational-wave fluxes," *Phys. Rev. D* **103** no. 10, (2021) 104045, arXiv:2102.04819 [gr-qc]. (Page 37)

[166] P. I. Jefremov, O. Yu. Tsupko, and G. S. Bisnovatyi-Kogan, "Innermost stable circular orbits of spinning test particles in Schwarzschild and Kerr

space-times," *Phys. Rev.* **D91** no. 12, (2015) 124030, arXiv:1503.07060 [gr-qc]. (Pages 38 and 40)

[167] S. Suzuki and K.-i. Maeda, "Innermost stable circular orbit of a spinning particle in Kerr space-time," *Phys. Rev.* **D58** (1998) 023005, arXiv:gr-qc/9712095 [gr-qc]. (Page 39)

[168] J. M. Bardeen, W. H. Press, and S. A. Teukolsky, "Rotating Black Holes: Locally Nonrotating Frames, Energy Extraction, and Scalar Synchrotron Radiation," *The Astrophysical Journal* **178** (Dec, 1972) 347–370. (Page 41)

[169] G. A. Piovano, R. Brito, A. Maselli, and P. Pani, "Assessing the detectability of the secondary spin in extreme mass-ratio inspirals with fully relativistic numerical waveforms," *Phys. Rev. D* **104** no. 12, (2021) 124019, arXiv:2105.07083 [gr-qc]. (Pages 42, 43, 54, 62, 64, and 66)

[170] "Spheroidal Wave functions." (dlmf.nist.gov/30.2). (Page 44)

[171] R. A. Breuer, J. Ryan, M. P., and S. Waller, "Some Properties of Spin-Weighted Spheroidal Harmonics," *Proceedings of the Royal Society of London Series A* **358** no. 1692, (Dec., 1977) 71–86. (Page 44)

[172] Y. Mino, M. Sasaki, M. Shibata, H. Tagoshi, and T. Tanaka, "Black hole perturbation: Chapter 1," *Prog. Theor. Phys. Suppl.* **128** (1997) 1–121, arXiv:gr-qc/9712057 [gr-qc]. (Pages 45 and 91)

[173] S. A. Hughes, "The Evolution of circular, nonequatorial orbits of Kerr black holes due to gravitational wave emission," *Phys. Rev.* **D61** no. 8, (2000) 084004, arXiv:gr-qc/9910091 [gr-qc]. [Erratum: Phys. Rev.D63,no.4,049902(2001); Erratum: Phys. Rev.D65,no.6,069902(2002); Erratum: Phys. Rev.D67,no.8,089901(2003); Erratum: Phys. Rev.D78,no.10,109902(2008); Erratum: Phys. Rev.D90,no.10,109904(2014)]. (Page 48)

[174] S. Mano, H. Suzuki, and E. Takasugi, "Analytic solutions of the Teukolsky equation and their low frequency expansions," *Prog. Theor. Phys.* **95** (1996) 1079–1096, arXiv:gr-qc/9603020 [gr-qc]. (Page 49)

[175] R. Fujita and H. Tagoshi, "New numerical methods to evaluate homogeneous solutions of the Teukolsky equation," *Prog. Theor. Phys.* **112** (2004) 415–450, arXiv:gr-qc/0410018 [gr-qc]. (Pages 49 and 57)

[176] R. Fujita, W. Hikida, and H. Tagoshi, "An Efficient Numerical Method for Computing Gravitational Waves Induced by a Particle Moving on

Eccentric Inclined Orbits around a Kerr Black Hole," *Prog. Theor. Phys.* **121** (2009) 843–874, arXiv:0904.3810 [gr-qc]. (Pages 49 and 57)

[177] Data and relevant codes are publicly available at https://web.uniroma1.it/gmunu. (Pages 51 and 117)

[178] S. E. Gralla, S. A. Hughes, and N. Warburton, "Inspiral into Gargantua," *Class. Quant. Grav.* **33** no. 15, (2016) 155002, arXiv:1603.01221 [gr-qc]. (Pages 52, 53, and 126)

[179] V. Skoupý and G. Lukes-Gerakopoulos, "Adiabatic equatorial inspirals of a spinning body into a Kerr black hole," arXiv:2201.07044 [gr-qc]. (Page 54)

[180] M. Sasaki and T. Nakamura, "Gravitational Radiation From a Kerr Black Hole. 1. Formulation and a Method for Numerical Analysis," *Prog. Theor. Phys.* **67** (1982) 1788. (Pages 57 and 89)

[181] A. Zenginoglu, "A Geometric framework for black hole perturbations," *Phys. Rev. D* **83** (2011) 127502, arXiv:1102.2451 [gr-qc]. (Page 57)

[182] E. Harms, S. Bernuzzi, and B. Brügmann, "Numerical solution of the 2+1 Teukolsky equation on a hyperboloidal and horizon penetrating foliation of Kerr and application to late-time decays," *Class. Quant. Grav.* **30** (2013) 115013, arXiv:1301.1591 [gr-qc]. (Page 57)

[183] E. Harms, S. Bernuzzi, A. Nagar, and A. Zenginoglu, "A new gravitational wave generation algorithm for particle perturbations of the Kerr spacetime," *Class. Quant. Grav.* **31** no. 24, (2014) 245004, arXiv:1406.5983 [gr-qc]. (Page 57)

[184] S. A. Hughes, N. Warburton, G. Khanna, A. J. K. Chua, and M. L. Katz, "Adiabatic waveforms for extreme mass-ratio inspirals via multivoice decomposition in time and frequency," arXiv:2102.02713 [gr-qc]. (Page 61)

[185] M. Van De Meent and N. Warburton, "Fast Self-forced Inspirals," *Class. Quant. Grav.* **35** no. 14, (2018) 144003, arXiv:1802.05281 [gr-qc]. (Page 61)

[186] G. A. Piovano, A. Maselli, and P. Pani, "Model independent tests of the Kerr bound with extreme mass ratio inspirals," *Phys. Lett. B* **811** (2020) 135860, arXiv:2003.08448 [gr-qc]. (Pages 61, 62, 64, 66, and 72)

[187] L. Lindblom, B. J. Owen, and D. A. Brown, "Model Waveform Accuracy Standards for Gravitational Wave Data Analysis," *Phys. Rev.* **D78** (2008) 124020, arXiv:0809.3844 [gr-qc]. (Pages 61, 66, and 70)

[188] M. Vallisneri, "Use and abuse of the Fisher information matrix in the assessment of gravitational-wave parameter-estimation prospects," *Phys. Rev. D* **77** (2008) 042001, arXiv:gr-qc/0703086. (Pages 61, 78, and 127)

[189] S. A. Hughes, "Bound orbits of a slowly evolving black hole," *Phys. Rev.* **D100** no. 6, (2019) 064001, arXiv:1806.09022 [gr-qc]. (Page 62)

[190] A. Ori and K. S. Thorne, "The Transition from inspiral to plunge for a compact body in a circular equatorial orbit around a massive, spinning black hole," *Phys. Rev. D* **62** (2000) 124022, arXiv:gr-qc/0003032. (Pages 63, 67, and 76)

[191] O. Burke, J. R. Gair, and J. Simón, "Transition from Inspiral to Plunge: A Complete Near-Extremal Trajectory and Associated Waveform," *Phys. Rev. D* **101** no. 6, (2020) 064026, arXiv:1909.12846 [gr-qc]. (Pages 63 and 67)

[192] G. Compère, K. Fransen, and C. Jonas, "Transition from inspiral to plunge into a highly spinning black hole," *Class. Quant. Grav.* **37** no. 9, (2020) 095013, arXiv:1909.12848 [gr-qc]. (Pages 63 and 67)

[193] D. Kennefick, "Stability under radiation reaction of circular equatorial orbits around Kerr black holes," *Phys. Rev. D* **58** (1998) 064012, arXiv:gr-qc/9805102. (Page 64)

[194] D. Kennefick and A. Ori, "Radiation reaction induced evolution of circular orbits of particles around Kerr black holes," *Phys. Rev. D* **53** (1996) 4319–4326, arXiv:gr-qc/9512018. (Page 64)

[195] D. Bini and A. Geralico, "Deviation of quadrupolar bodies from geodesic motion in a Kerr spacetime," *Phys. Rev. D* **89** no. 4, (2014) 044013, arXiv:1311.7512 [gr-qc]. (Page 64)

[196] D. Bini and A. Geralico, "Spin-geodesic deviations in the Kerr spacetime," *Phys. Rev. D* **84** (2011) 104012, arXiv:1408.4952 [gr-qc]. (Page 64)

[197] B. Mashhoon and D. Singh, "Dynamics of Extended Spinning Masses in a Gravitational Field," *Phys. Rev. D* **74** (2006) 124006, arXiv:astro-ph/0608278. (Page 64)

[198] E. G. Gimon and P. Horava, "Astrophysical violations of the Kerr bound as a possible signature of string theory," *Phys. Lett.* **B672** (2009) 299–302, arXiv:0706.2873 [hep-th]. (Pages 65, 71, and 73)

[199] M. D. Hartl, "Dynamics of spinning test particles in Kerr space-time," *Phys. Rev.* **D67** (2003) 024005, arXiv:gr-qc/0210042 [gr-qc]. (Pages 66 and 88)

[200] S. D. Mathur, "Fuzzballs and the information paradox: A Summary and conjectures," arXiv:0810.4525 [hep-th]. (Page 71)

[201] S. Giusto, O. Lunin, S. D. Mathur, and D. Turton, "D1-D5-P microstates at the cap," *JHEP* **02** (2013) 050, arXiv:1211.0306 [hep-th]. (Page 71)

[202] I. Bena, A. Puhm, and B. Vercnocke, "Metastable Supertubes and non-extremal Black Hole Microstates," *JHEP* **04** (2012) 100, arXiv:1109.5180 [hep-th]. (Page 71)

[203] I. Bena, S. Giusto, R. Russo, M. Shigemori, and N. P. Warner, "Habemus Superstratum! A constructive proof of the existence of superstrata," *JHEP* **05** (2015) 110, arXiv:1503.01463 [hep-th]. (Page 71)

[204] M. Bianchi, D. Consoli, A. Grillo, and J. F. Morales, "The dark side of fuzzball geometries," *JHEP* **05** (2019) 126, arXiv:1811.02397 [hep-th]. (Page 71)

[205] V. Cardoso and P. Pani, "Testing the nature of dark compact objects: a status report," *Living Rev. Rel.* **22** no. 1, (2019) 4, arXiv:1904.05363 [gr-qc]. (Pages 71, 72, and 73)

[206] C. Bambi, "Testing the Kerr black hole hypothesis," *Mod. Phys. Lett.* **A26** (2011) 2453–2468, arXiv:1109.4256 [gr-qc]. (Page 71)

[207] E. Berti *et al.*, "Testing General Relativity with Present and Future Astrophysical Observations," *Class. Quant. Grav.* **32** (2015) 243001, arXiv:1501.07274 [gr-qc]. (Pages 71 and 73)

[208] K. Yagi and L. C. Stein, "Black Hole Based Tests of General Relativity," *Class. Quant. Grav.* **33** no. 5, (2016) 054001, arXiv:1602.02413 [gr-qc]. (Page 71)

[209] F. D. Ryan, "Spinning boson stars with large selfinteraction," *Phys. Rev.* **D55** (1997) 6081–6091. (Page 71)

[210] P. Pani, C. F. B. Macedo, L. C. B. Crispino, and V. Cardoso, "Slowly rotating black holes in alternative theories of gravity," *Phys. Rev.* **D84** (2011) 087501, arXiv:1109.3996 [gr-qc]. (Page 71)

[211] B. Kleihaus, J. Kunz, and E. Radu, "Rotating Black Holes in Dilatonic Einstein-Gauss-Bonnet Theory," *Phys. Rev. Lett.* **106** (2011) 151104, arXiv:1101.2868 [gr-qc]. (Page 71)

[212] C. A. R. Herdeiro and E. Radu, "Kerr black holes with scalar hair," *Phys. Rev. Lett.* **112** (2014) 221101, arXiv:1403.2757 [gr-qc]. (Page 71)

[213] D. Ayzenberg and N. Yunes, "Slowly-Rotating Black Holes in Einstein-Dilaton-Gauss-Bonnet Gravity: Quadratic Order in Spin Solutions," *Phys. Rev.* **D90** (2014) 044066, arXiv:1405.2133 [gr-qc]. [Erratum: Phys. Rev.D91,no.6,069905(2015)]. (Page 71)

[214] A. Maselli, P. Pani, L. Gualtieri, and V. Ferrari, "Rotating black holes in Einstein-Dilaton-Gauss-Bonnet gravity with finite coupling," *Phys. Rev.* **D92** no. 8, (2015) 083014, arXiv:1507.00680 [gr-qc]. (Page 71)

[215] E. Barausse, T. P. Sotiriou, and I. Vega, "Slowly rotating black holes in Einstein-æther theory," *Phys. Rev.* **D93** no. 4, (2016) 044044, arXiv:1512.05894 [gr-qc]. (Page 71)

[216] C. Herdeiro, E. Radu, and H. Rúnarsson, "Kerr black holes with Proca hair," *Class. Quant. Grav.* **33** no. 15, (2016) 154001, arXiv:1603.02687 [gr-qc]. (Page 71)

[217] P. V. P. Cunha, C. A. R. Herdeiro, and E. Radu, "Spontaneously Scalarized Kerr Black Holes in Extended Scalar-Tensor–Gauss-Bonnet Gravity," *Phys. Rev. Lett.* **123** no. 1, (2019) 011101, arXiv:1904.09997 [gr-qc]. (Page 71)

[218] A. Maselli, H. O. Silva, M. Minamitsuji, and E. Berti, "Slowly rotating black hole solutions in Horndeski gravity," *Phys. Rev.* **D92** no. 10, (2015) 104049, arXiv:1508.03044 [gr-qc]. (Page 71)

[219] P. Pani, E. Barausse, E. Berti, and V. Cardoso, "Gravitational instabilities of superspinars," *Phys. Rev.* **D82** (2010) 044009, arXiv:1006.1863 [gr-qc]. (Page 72)

[220] E. Maggio, P. Pani, and V. Ferrari, "Exotic Compact Objects and How to Quench their Ergoregion Instability," *Phys. Rev.* **D96** no. 10, (2017) 104047, arXiv:1703.03696 [gr-qc]. (Page 72)

[221] E. Maggio, V. Cardoso, S. R. Dolan, and P. Pani, "Ergoregion instability of exotic compact objects: electromagnetic and gravitational perturbations and the role of absorption," *Phys. Rev. D* **99** no. 6, (2019) 064007, arXiv:1807.08840 [gr-qc]. (Page 72)

[222] R. Roy, P. Kocherlakota, and P. S. Joshi, "Mode stability of a near-extremal Kerr superspinar," arXiv:1911.06169 [gr-qc]. (Page 72)

[223] J. W. Hessels, S. M. Ransom, I. H. Stairs, P. C. C. Freire, V. M. Kaspi, and F. Camilo, "A radio pulsar spinning at 716-hz," *Science* **311** (2006) 1901–1904, arXiv:astro-ph/0601337. (Page 72)

[224] R. N. Manchester, G. B. Hobbs, A. Teoh, and M. Hobbs, "The Australia Telescope National Facility pulsar catalogue," *Astron. J.* **129** (2005) 1993, arXiv:astro-ph/0412641. (Page 72)

[225] B. C. Bisscheroux, O. R. Pols, P. Kahabka, T. Belloni, and E. P. J. van den Heuvel, "The nature of the bright subdwarf HD 49798 and its X-ray pulsating companion.," *Astron.Astrophys.* **317** (Feb., 1997) 815–822. (Page 72)

[226] E. Barausse, V. Cardoso, and P. Pani, "Can environmental effects spoil precision gravitational-wave astrophysics?," *Phys. Rev. D* **89** no. 10, (2014) 104059, arXiv:1404.7149 [gr-qc]. (Page 73)

[227] A. Maselli, N. Franchini, L. Gualtieri, and T. P. Sotiriou, "Detecting scalar fields with Extreme Mass Ratio Inspirals," *Phys. Rev. Lett.* **125** no. 14, (2020) 141101, arXiv:2004.11895 [gr-qc]. (Page 73)

[228] E. Gourgoulhon, A. Le Tiec, F. H. Vincent, and N. Warburton, "Gravitational waves from bodies orbiting the Galactic Center black hole and their detectability by LISA," *Astron. Astrophys.* **627** (2019) A92, arXiv:1903.02049 [gr-qc]. (Page 75)

[229] T. Robson, N. J. Cornish, and C. Liu, "The construction and use of LISA sensitivity curves," *Class. Quant. Grav.* **36** no. 10, (2019) 105011, arXiv:1803.01944 [astro-ph.HE]. (Pages 75 and 79)

[230] E. Poisson and C. M. Will, "Gravitational waves from inspiraling compact binaries: Parameter estimation using second postNewtonian wave forms," *Phys. Rev. D* **52** (1995) 848–855, arXiv:gr-qc/9502040. (Page 78)

[231] A. Maselli, N. Franchini, L. Gualtieri, T. P. Sotiriou, S. Barsanti, and P. Pani, "Detecting fundamental fields with LISA observations of gravitational

waves from extreme mass-ratio inspirals," arXiv:2106.11325 [gr-qc]. (Pages 79 and 80)

[232] P. Amaro-Seoane, J. R. Gair, M. Freitag, M. Coleman Miller, I. Mandel, C. J. Cutler, and S. Babak, "Astrophysics, detection and science applications of intermediate- and extreme mass-ratio inspirals," *Class. Quant. Grav.* **24** (2007) R113–R169, arXiv:astro-ph/0703495. (Page 87)

[233] Z. Pan, Z. Lyu, and H. Yang, "Wet Extreme Mass Ratio Inspirals May Be More Common For Spaceborne Gravitational Wave Detection," arXiv:2104.01208 [astro-ph.HE]. (Page 87)

[234] S. McGee, A. Sesana, and A. Vecchio, "Linking gravitational waves and X-ray phenomena with joint LISA and Athena observations," *Nature Astron.* **4** no. 1, (2020) 26–31, arXiv:1811.00050 [astro-ph.HE]. (Page 87)

[235] D. Laghi, N. Tamanini, W. Del Pozzo, A. Sesana, J. Gair, and S. Babak, "Gravitational wave cosmology with extreme mass-ratio inspirals," arXiv:2102.01708 [astro-ph.CO]. (Page 88)

[236] U. Ruangsri, S. J. Vigeland, and S. A. Hughes, "Gyroscopes orbiting black holes: A frequency-domain approach to precession and spin-curvature coupling for spinning bodies on generic Kerr orbits," *Phys. Rev.* **D94** no. 4, (2016) 044008, arXiv:1512.00376 [gr-qc]. (Page 88)

[237] V. Witzany, "Hamilton-Jacobi equation for spinning particles near black holes," *Phys. Rev.* **D100** no. 10, (2019) 104030, arXiv:1903.03651 [gr-qc]. (Page 88)

[238] L. V. Drummond and S. A. Hughes, "Precisely computing bound orbits of spinning bodies around black holes II: Generic orbits," arXiv:2201.13335 [gr-qc]. (Page 88)

[239] S. A. Hughes, "Computing radiation from Kerr black holes: Generalization of the Sasaki-Nakamura equation," *Phys. Rev. D* **62** (2000) 044029, arXiv:gr-qc/0002043. [Erratum: Phys.Rev.D 67, 089902 (2003)]. (Page 89)

[240] F. W. J. Olver, "Asymptotic expansions of the coefficients in asymptotic series solutions of linear differential equations," *Methods Appl. Anal.* **1** no. 1, (1994) 1–13. (Pages 93 and 99)

[241] F. W. J. Olver, "Asymptotic solutions of linear ordinary differential equations at an irregular singularity of rank unity," *Methods Appl. Anal.* **4** no. 4, (1997) 375–403. (Pages 93 and 99)

[242] F. Olver, *Asymptotics and Special Functions*. Computer science and applied mathematics : a series of monographs and textbooks. Academic Press, 1974. (Pages 93 and 99)

[243] E. W. Leaver, "An Analytic representation for the quasi normal modes of Kerr black holes," *Proc. Roy. Soc. Lond. A* **402** (1985) 285–298. (Page 109)

[244] E. W. Leaver, "Solutions to a generalized spheroidal wave equation: Teukolsk's equations in general relativity, and the two-center problem in molecular quantum mechanics," *Journal of Mathematical Physics* **27** (1986) 1238–1265. (Page 109)

[245] R. S. Borissov and P. P. Fiziev, "Exact Solutions of Teukolsky Master Equation with Continuous Spectrum," *Bulg. J. Phys.* **37** (2010) 065–089, arXiv:0903.3617 [gr-qc]. (Page 110)

[246] J. Stewart, "On the Stability of Kerr's Space-Time," *Proceedings of the Royal Society of London. Series A, Mathematical and Physical Sciences* **344** (1975) 65–79. (Page 110)

[247] J. J. Sakurai and J. Napolitano, *Modern Quantum Mechanics*. 2nd. Addison-Wesley, 2010. (Page 111)

[248] A. Taracchini, A. Buonanno, S. A. Hughes, and G. Khanna, "Modeling the horizon-absorbed gravitational flux for equatorial-circular orbits in Kerr spacetime," *Phys. Rev.* **D88** (2013) 044001, arXiv:1305.2184 [gr-qc]. [Erratum: Phys. Rev.D88,no.10,109903(2013)]. (Pages 124 and 125)